UNIVERSITY OF CAPE TOWN
IYUNIVESITHI YASEKAPA • UNIVERSITEIT VAN KAAPSTAD

Stable algorithms for generalized thermoelasticity based on operator-splitting and time-discontinuous Galerkin finite element methods

by

Mebratu Fenta Wakeni

Thesis Presented for the Degree of

Doctor of Philosophy in Applied Mathematics

University of Cape Town

November, 2016

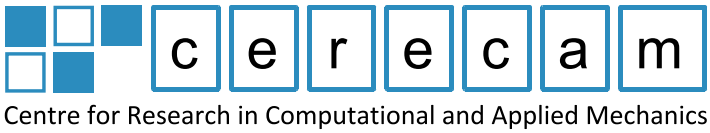

Stable algorithms for generalized thermoelasticity based on operator-splitting and time-discontinuous Galerkin finite element methods

Mebratu Fenta Wakeni

Abstract

This thesis deals with the theoretical and numerical analysis of coupled problems in thermoelasticity. Of particular interest are models that support propagation of thermal energy as waves, rather than the usual mechanism by diffusion. The thesis consists of two parts. The first deals with the non-classical, linear thermoelastic model first proposed and developed by Green and Naghdi in the years between 1991 and 1995, as a possible alternative that potentially removes the shortcomings of the standard Fourier based model. The non-classical theory incorporates three models: the classical model based on Fourier's law of heat conduction, resulting in a hyperbolic–parabolic coupled system; a non-classical theory of a fully-hyperbolic extension; and a combination of the two.

An efficient staggered time-stepping algorithm is proposed based on operator-splitting and the time–discontinuous Galerkin finite element method for the non-classical, linear thermoelastic model. The coupled problem is split into two contractive sub-problems, namely, the *mechanical phase* and *thermal phase*, on the basis of an entropy controlling mechanism. In the mechanical phase temperature is allowed to vary so as to ensure the entropy remains constant, while the thermal phase is a purely non-classical heat conduction problem in a fixed configuration. Each sub-problem is discretized using the time–discontinuous Galerkin finite element method, resulting in stable time-stepping sub-algorithms. A global stable algorithm is obtained by combining the algorithms for the sub-problems by way of a product method. A number of numerical examples are presented to demonstrate the performance and capability of the method.

The second part of this work concerns the formulation of a thermodynamically consistent generalized model of nonlinear thermoelasticity, whose linearization about a natural reference configuration includes the theory of Green and Naghdi. The generalized

model is based on the fundamental laws of continuum mechanics and thermodynamics, and is realized through two basic assumptions: The first is the inclusion into the state space of a vector field, which is known as the *thermal displacement*, and is a time primitive of the absolute temperature. The second is that the heat flux vector is additively split into two parts, which are referred to as the *energetic* and *dissipative* components of the heat flux vector. The application of the Coleman-Noll procedure leads to find constitutive relations for the stress, entropy, and energetic component of the heat flux as derivatives of the free energy function. Furthermore, a Clausius-Duhem–type inequality is assumed on a constitutive relation for the dissipative component of the heat flux vector to ensure thermodynamic consistency. A Lyapunov function is obtained for the generalized problem with finite strains; this serves as the basis for the stability analysis of the numerical methods designed for generalized thermoelasticity at finite strains.

Due to the lack of convexity of the elastic potential in the finite strain case, a direct extension of the time-discontinuous formulation from the linear to the finite strain case does not guarantee stability. For this reason, various numerical formulations both in monolithic and staggered approaches with fully or partially time-discontinuity assumptions are presented in the framework of the space-time methods. The stability of each of the numerical algorithms is thoroughly analysed.

The capability of the newly formulated generalized model of thermoelasticity in predicting various expected features of non-Fourier response is illustrated by a number of numerical examples. These also serve to demonstrate the performance of the space-time Galerkin method in capturing fine solution features.

Dedicated to my lovely daughter

Hasset

Acknowledgements

Firstly, I would like to express my sincere gratitude and utmost respect to my supervisor Prof. B. Daya Reddy for his guidance, patience and immense knowledge. I am equally grateful for my co-supervisor Dr. Andrew T. McBride for his critical contributions, insightful comments and suggestions throughout my study.

I would like to thank my wife Woinshet Defar for her encouragement and patience with me. She has been assisting me in commenting and proof reading throughout the writing of this thesis.

Most importantly of all, I wish to thank the African Institute of Mathematical Sciences (AIMS), where my academic ambition has started to realize. I am especially thankful to the director of AIMS Prof. Barry Green for encouraging and recommending me to work with Prof. B. Daya Reddy in this exciting field of research. It has been a privilege for me to work with him.

Last but most certainly not least, I wish to thank my mother W/ro Yenealem Alemu, my siblings Atsede Fenta, Lemlem Fenta, Yirga Alemu and Sinke Alemu for their love, encouragement and prayer throughout my life. They have been incredibly supportive in taking care of my lovely daughter Hasset with love and affection to help me concentrate on my thesis write up.

Contents

1

Introduction

A complete description of a given physical system requires a unified treatment. This often leads to a coupled problem consisting of dynamically interacting components which are physically and computationally heterogeneous. The different physical phenomena associated with the components that govern the system's response can be nonlinear, coupled and exhibit different time and length scales. An efficient algorithm for such problems is one which can take advantage of the different features of the components involved, and provide accurate numerical solutions in a reasonable computing time. Due to the increasing power of modern computers in combination with sophisticated numerical methods exploiting new hardware features, the demand for efficient solution algorithms for coupled problems is ever greater.

From a theoretical and computational standpoint, the individual physical processes that comprise many coupled problems are fairly well understood and elaborate models exist for their mathematical description. However, there are some instances in which a new model is required because the current standard model for describing certain physical phenomena is proven to be inadequate or even sometimes leads to contradictions of some well-established physical laws.

This thesis is concerned with the theoretical and computational analysis of coupled problems in thermoelasticity. The mathematical structure of the thermoelastic model considered includes non-classical models of dominantly hyperbolic type, which are characterized by the non-Fourier mechanism of thermal energy transport with finite speed. It is known that these problems support the propagation of high gradients, and in the nonlinear case, shocks can appear in a finite time, even if the initial and boundary conditions are smooth.

1.1 Thermoelastic models

The traditional heat conduction model based on Fourier's law [34] has been highly successful in a broad range of engineering applications. The model, being parabolic, is generally characterized by the propagation of thermal disturbances with infinite speed, a paradoxical phenomenon from the cause-and-effect relationship point of view. This side effect of Fourier's law becomes more apparent in applications involving small length scales at temperatures near absolute zero. As a consequence of this, approximation by the classical Fourier theory loses validity [36].

The earliest known conjecture on the existence of thermal propagation as waves with finite speed, also referred to as the *second sound* phenomenon, was given by Nernst [72] in 1917. Later, Tisze [94] in 1938 and Landau [60] in 1941 independently suggested the possibility of thermal waves in superfluid liquid helium, at temperatures below the so-called lambda transition near 2.2 K [29]. Peshkov [80] reported the first experimental evidence for the existence of second sound in 2He. Peshkov suggests that second sound might also be observed in pure crystalline materials on the basis of similarities between crystal materials and liquid helium. Laser pulsing experiments have shown that second sound can propagate in high-purity crystals of 4He [1], 3He [2], NaF [53], and Bi [71].

A closely-related anomalous phenomenon involving the diffusion of a solvent within a polymer is termed case II diffusion. It refers to the diffusion behaviour observed when a low-molecular weight solvent diffuses into a polymeric glass causing the polymeric network to rearrange in a finite time and manifests itself as a rubber-glass phase transition within the polymeric solid. The standard model for diffusion (termed Fick's law), with its assumption that the diffusive flux is proportional to the gradient of the concentration of the solvent species, is characterized by the non-physical phenomenon of instantaneous diffusion. A review of key literature on modelling of non-Fickian case II diffusion can be found in the articles [10, 39].

Arguably, one of the more complete macroscopic continuum formulations for case II diffusion has been proposed in the work of Govindjee and Simo [39]. Furthermore, a numerical implementation based on a combination of monolithic and fractional-step approaches in the context of finite element methods is extensively detailed in [96–98].

Cattaneo [18] was the first to introduce a non-Fourier theory of heat conduction in order to overcome the paradoxical prediction of the classical Fourier theory. His work is based on the concept of relaxing the heat flux from the classical Fourier law to obtain a constitutive relation with a non-Fourier effect. There have been several other attempts to develop continuum theories capable of predicting thermal waves propagating at finite speeds for various types of media. Among these, the works in [35, 40, 46, 63, 70] are notable. The constitutive equation for the heat flux according to Cattaneo is examined in terms of thermodynamics in [25, 26]. Later this result was extended in [73] to the case of deformable bodies.

A relatively more recent theory of non-classical heat conduction with and without deformation was proposed by Green and Naghdi [41–44]. Their work is based on the introduction of three types of constitutive relations for the heat flux, thereby resulting in three different models, namely type I, which is the classical theory, type II, a purely hyperbolic model which allows for the propagation of a heat pulse without damping, and type III, which is a combination I and II.

In recent years there has been a considerable amount of interest in the theory of Green and Naghdi. An extensive overview of the theory can be found in [19, 20, 49]. Theoretical results addressing existence and uniqueness [82, 83] and exponential stability [84] have also been investigated for some classes of the theory. The design of appropriate numerical methods has also been addressed in [11].

While the theory of Green and Naghdi is successful in removing the paradoxical nature of Fourier's law, its analysis is mainly limited to the linear case. One of the key contributions in the work presented here is a thermodynamically consistent formulation of generalized thermoelasticity at finite strains, whose linearization about a natural reference configuration is equivalent to that of Green and Naghdi. The new model is fully nonlinear and supports propagation of thermal energy as a nonlinear wave.

The generalized thermoelastic formulation is based on fundamental continuum and thermodynamic laws, in combination with two important assumptions:

1) The introduction of a time primitive of the absolute temperature, the so called thermal displacement, which enters into the thermoelastic state space through its gradient.

2) The heat flux vector is split into two components: one dissipative and the other energetic.

The first assumption is not unique to the generalized formulation. In fact, the theory of Green and Naghdi is based on this assumption. The role and interpretation of the thermal displacement have generated substantial discussion in the literature. Podio-Guidugli [81] sets out some of the history, the interpretation of this variable, as well as its use beyond thermomechanics, in models for dissipative materials and relativistic perfect fluids. Moreover, Dascalu and Kalpakides [28], emphasise the importance of the thermal displacement in arriving at a consistent theory of thermoelastic crack propagation.

In the context of generalized thermoelasticity the introduction of the thermal displacement allows the formulation of a thermodynamically consistent theory leading to a stable initial-value problem. That is, the solution to the problem provides a complete description of the solution in the form of the displacement, velocity, and temperature. It yields also the thermal displacement, which is a vehicle towards constructing a consistent theory, rather than being a variable of primarily physical interest.

For the second assumption, it has been suggested (see for example [36] and the references therein) that heat in solids is caused by quantized vibrations known as phonons [56, 91]. Moreover, two kinds of phonon interaction has been suggested [30], namely *normal* and *resistive processes*, where the first refers to conservation of momentum accounting for the wave mechanism of thermal energy transport, and the latter for processes that do not conserve phonon momentum, reflecting dissipation or diffusion mechanism. Motivated largely by these microscopic points of view, the second assumption addresses two fundamental modes of heat flow in the continuum case.

The aim of the present generalized formulation is to extend to finite deformations, in a thermodynamically consistent manner, the small-strain theory of Green and Naghdi. The resulting formulation allows for a full and physically meaningful description of thermomechanical behaviour to be obtained by computational means.

Yang *et al.* [106], have developed a consistent variational formulation of the coupled thermomechanical boundary–value problem for general dissipative Solids. The experimental validation of this model has been investigated in [92]. In this formulation, it

is shown that the conservation of energy and the balance of linear momentum can be derived from a common potential as Euler–Lagrange equations. In this sense the current generalized formulation bears some similarity in that the constitutive equations for the stress, entropy and heat flux are derived from a common free energy.

Further contributions to the theoretical analysis of the fully-nonlinear initial–boundary value problem (IBVP) in this thesis include the construction of a Lyapunov function, a positive-definite function of the state variables which decreases along the flow, for the generalized model of thermoelasticity. A class of physically admissible initial and boundary conditions are also suggested.

1.2 Computational methods for coupled problems

Computational methods for transient coupled problems typically fall within the two major approaches [6, 64]:

1) *Direct or Monolithic approaches:* The full problem is treated in its entirety. All the primary unknowns are solved for simultaneously at discrete time points using a monolithic time-stepping algorithm. For stability reasons, implicit schemes are often used.

2) *Splitting methods:* Operator-splitting is used to partition the full problem into a finite number of decoupled sub-problems, each describing a system with homogeneous features in the sense that each component exhibits a single time and/or length scale. Time-stepping algorithms that take advantage of the specific features are applied to each sub-problem. Finally, a global time-stepping algorithm is obtained by using a suitable product formula to piece the algorithms for the sub-problems together.

One of the primary disadvantages of using a monolithic approach for coupled problems is the resulting large algebraic system, which needs to be solved at each time step or iteration. Moreover, the time step length used in a monolithic scheme is often dictated by the component in the coupling with the fastest dynamics. This is a limiting factor in view of computational efficiency as an unnecessarily small time step length is used for the other components with slower dynamics. It is also noted in [6] that a monolithic approach often leads to a non-symmetric formulation. However, in the case where the

dynamics of the various components exhibit very strong coupling and nonlinearity, a monolithic approach may be the only feasible method. It is also important to note that the formulation of stable schemes is natural within a monolithic approach.

Some commercial software packages are specialized to solve a single class of dynamical system, such as elasticity, heat conduction, fluid flow problems, etc. Motivated in large part by the lack of single analysis software which can handle various coupled problems, combined with the need for circumventing the drawbacks of monolithic schemes, staggered schemes came into play as an alternative for solving coupled problems. Such staggered approaches has been investigated for a wide range of coupled problems with some success; notable works in this regard include [5, 31–33, 74–77, 85, 86, 90, 95, 107]. However, staggered schemes often lack stability. Some numerical stabilization features have been proposed [74, 107] to increase the stability property of the staggered scheme with varying degrees of success.

The design of a stable staggered algorithm for coupled problems can be expedited by understanding the full operator defining the problem, and by the point of view that a staggered scheme is just a product formula algorithm in which each sub-algorithm corresponds to one of the sub-operators in a given operator-splitting of the coupled problem. In this sense, the stability of a staggered algorithm is primarily determined by the stability of the sub-operator in the splitting. The second factor determining the stability is the numerical scheme used to approximate each of the sub-problems.

The main contribution in this thesis is the extension of the operator-splitting approach for classical thermoelasticity in [6] to the non-classical theory of thermoelasticity, and the rigorous stability anaysis of the operator-split in both the linear and nonlinear cases. The operator-splitting proposed in this thesis is based on separating the mechanical and thermal part of the problem with an entropy controlling mechanism in the sprit of Armero and Simo [6]. The first sub-problem is a mechanical problem with varying temperature that ensures that the entropy is constant in this phase of the split. It is then followed by the full thermal problem at fixed configuration.

1.3 Space-time finite element methods

Designing a robust and efficient numerical solution strategy for strongly-coupled problems of hyperbolic–type is challenging. This is particularly the case for the non-classical theory of thermoelasticity where the hyperbolic (or nearly hyperbolic) heat conduction equation is coupled with the classical hyperbolic elasticity problem. A standard approach for solving such time-dependent problems is the Method of Lines (MoL) in which the governing partial differential equation is first discretized in space using the finite element method (FEM), leading to a system of ordinary differential equations which can then be solved using the finite difference method. Despite its popularity, MoL struggles to accurately solve problems involving propagation of sharp gradients or discontinuities [51, 52].

Recently, a great deal of attention has been invested in designing a spatially discontinuous Galerkin (DG) approach for convection-dominated problems; see for example [22–24]. However, these methods, like MoL, are based on decoupling space and time in the sense that space and time are treated differently. Hulbert and Hughes [52] and Hughes and Hulbert [51] introduced a powerful scheme based on a space-time DG finite element methodology for linear elastodynamics problems. In their approach, space and time are treated simultaneously and the unknown fields are allowed to be discontinuous in time while continuous in space. Recently, the spacetime DG method has been used in [55] for classical thermoelasticity, using a monolithic approach where all the unknown fields are solved for simultaneously.

In [11] a numerical solution approach based on MoL was proposed for non-classical thermoelasticity in which time integration was done in two ways: continuous Galerkin FEM for type II and III, and mixed-discontinuous Galerkin FEM for the classical problem based on the Fourier law of heat conduction. A streamline-upwind numerical stabilization was added to localize numerical oscillations due to the propagation of sharp thermal waves.

In this work a stable numerical algorithm is developed for non-classical thermoelasticity. It is based on an operator-splitting technique motivated by Armero and Simo [6] for classical thermoelasticity, coupled with a spacetime DG methodology that extends the work of Hulbert and Hughes [52] which was formulated for linear elastodynamics. Major contributions in this work include the development of a time-DG formulation in which

continuity of the unknown fields is enforced weakly by using an L^2-inner product, in contrast to the energy-norm used in [52].

It is known that the elastic potential energy is not convex for finite strains. In fact a convexity assumption on the elastic potential energy would imply the non-physical behaviour that it is incompatible to the property that as the Jacobian of the deformation tends to zero the elastic stored energy approaches to infinity. A mild form of convexity that is consistent with the physics of a continuum body undergoing large deformations is *polyconvexity*. However, even with the polyconvexity assumption it is not yet known how a discontinuity jump in the displacement is related to a jump in the elastic potential energy. Hence a direct extension of the time-discontinuous Galerkin formulation for the linear problem to the generalized one at finite strains does not guarantee stability. For this reason, various numerical formulations, both monolithic and staggered, are presented based on space-time Galerkin methods. The stability of each of the numerical algorithms is thoroughly analyzed.

Numerical results for two sets of problem are presented. The first is designed with the objective of demonstrating the capability of the generalized model in capturing thermal propagation as a nonlinear wave in a two-dimensional domain. The results show the good performance of the numerical method in capturing the fine features of the solution. The second is an application in skin biothermomechanics. Both the classical and generalized thermoelastic models are used to analyze the thermomechanical response of the skin under various external thermal and mechanical loading conditions. The result, corresponding to the classical model, shows good agreement with the literature. Furthermore, the response obtained using the generalized model predicts the unique thermal propagation in skin (for which the experimental evidence is the subject of much debate), such as thermal oscillation and finite speed thermal wave propagation.

1.4 Outline

The thesis is organized in two parts.

Part I is dedicated to the linear thermoelastic theory of Green and Naghdi. Chapter 2 summarizes the governing equations of linear thermoelasticity as proposed by Green and Naghdi. The theory of semi-groups is employed to analyze the well-posedness of the

problem. A class of physically meaningful initial and boundary conditions is presented. In chapter 3, operator-splitting for the system of partial differential equations defining linear thermoelasticity is introduced, and the stability of the split problems analyzed. Time-discontinuous Galerkin formulations are presented for each of the sub-problems, and an algorithm for the full problem is constructed by using a single pass product formula. In chapter 4, the stability of the staggered algorithm presented in chapter 3 is analyzed in terms of the results of the stability analysis of the sub-algorithms comprising it. In chapter 5, a number of example problems in thermoelasticity are presented and solved with the purpose of demonstrating various features and the performance of the staggered algorithm. Issues addressed include improved efficiency over the monolithic scheme when a low-order approximation is used, the ability of the splitting algorithm to accurately represent second sound phenomena as compared to the monolithic scheme.

Part II of the thesis concerns the formulation of a thermodynamically consistent generalized model in the finite strain regime, and various computational methods for solving it. In chapter 6, the generalized problem is formulated based on the basic principles of continuum thermodynamics in conjunction with other assumptions, and a Coleman–Noll procedure for constitutive relations. A class of physically permissible initial and boundary conditions are presented, leading to a complete nonlinear initial boundary value problem (IBVP). The stability of the nonlinear IBVP is analyzed by constructing a Lyapunov function for the dynamics. The IBVP is linearized about a given state (natural configuration), showing the result to be equivalent to the linear theory of Green and Naghdi. In Chapter 7, various space-time finite element schemes (monolithic and staggered approaches) are developed. In Chapter 8, the stability of the schemes discussed in Chapter 7 is analyzed rigorously. An algorithm based on a Newton–type iterative procedure which extends the time-discontinuous Galerkin formulations developed for the linear problem in Chapter 4 is also developed, and its stability is analyzed. In Chapter 9, two sets of numerical examples are presented to illustrate the capability of the newly developed model, thereby demonstrating the performance of the numerical methods.

A summary of the main results and some concluding remarks on this work are presented in Chapter 10. Suggested areas for future research are also presented.

Some of the results in this work have appeared in the following publications [99, 100]

- M.F. Wakeni, B.D. Reddy and A.T. McBride. An unconditionally stable algorithm for generalized thermoelasticity based on operator-splitting and time-discontinuous Galerkin finite element methods. *Computer Methods in Applied Mechanics and Engineering*, 306(1):427–451, 2016.
- M.F. Wakeni, B.D. Reddy and A.T. McBride. A thermodynamically consistent formulation for generalized thermoelasticity at finite strains. *International Journal of Engineering and Science* (in review)

Part I

Linear generalized thermoelasticity

Summary: Linear generalized thermoelasticity

In part I, a time-stepping algorithm for the coupled problem of thermoelastic model is discussed. The model is a coupling between the non-classical heat conduction equation, due to Green and Naghdi, and classical linear elastodynamics at infinitesimal strains.

In Chapter 2, the complete IBVP for type III thermoelasticity, is summarized and the theory of semi-groups employed to prove its well-posedness. Moreover, the contractivity property of the dynamics is also shown.

A staggered time-stepping algorithm based on a stable operator-split and the time-discontinuous Galerkin formulations is presented in Chapter 3 for the type III thermoelastic model.

The stability of the time-stepping algorithm formulated in Chapter 3 is analyzed in Chapter 4. A sufficient condition for the stability of a staggered algorithm based on an operator-split is proved.

Finally, in Chapter 5, numerical examples are presented to illustrate the performance of the proposed algorithm and the capability of the non-Fourier model of thermoelasticity.

2

The model problem formulation

The objectives of this chapter are to present and summarize the governing equations of linear generalized (type III) thermoelasticity, which was first proposed by Green and Naghdi [41–44]. The theory of semi-groups is employed to analyze the well-posedness of the problem, thereby extending the existence and uniqueness result for the type II problem [82]. Results obtained in this chapter serve as the basis for the design and analysis of the numerical algorithms that will be discussed in subsequent chapters.

The rest of this chapter is organized as follows. In Section 2.1 the governing equations for the model problem are summarized in a general framework which accommodates both the classical and non-classical theories of thermoelasticity. Constitutive relations are derived in Section 2.2. In Section 2.3 a class of physically meaningful initial and boundary conditions are presented and the initial-boundary value problem (IBVP) is summarized. Finally, in Section 2.4 well-posedness of the generalized problem is established by employing the theory of semi-groups.

2.1 Governing equations

Consider a continuum body $\mathcal{B}$ occupying a reference configuration $\Omega \subset \mathbb{R}^d$ $(1 \leq d \leq 3)$ at time $t = 0$ as shown in the Fig. 2.1. The region Ω is assumed to be bounded with a piecewise smooth boundary denoted by Γ. A time domain of interest is the interval $\mathbb{I} = [0,\ T]$, $T > 0$. The displacement field is denoted by $\boldsymbol{u} : \Omega \times \mathbb{I} \to \mathbb{R}^d$, and $\boldsymbol{v} \coloneqq \dot{\boldsymbol{u}}$ is the velocity field, where the superposed dot denotes a time derivative. The density of the continuum body $\mathcal{B}$ is denoted by $\rho > 0$. We assume that the body $\mathcal{B}$ undergoes

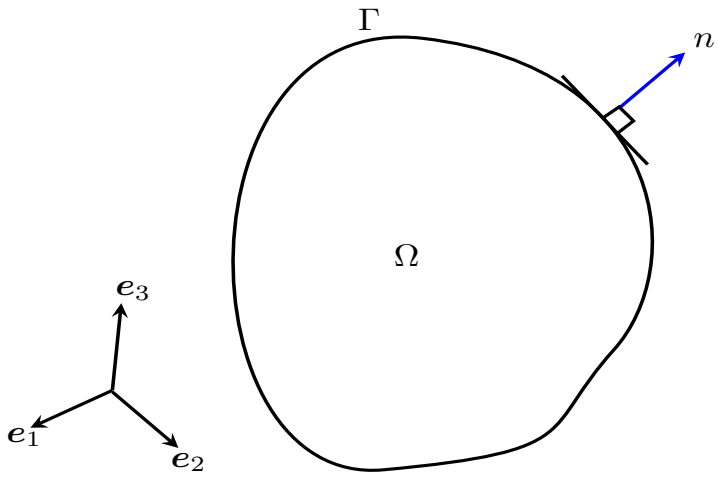

Fig. 2.1: Schematic of a continuum body in the reference configuration

infinitesimal deformations. The local form of the principle of linear momentum leads to the equation governing the motion of the body in the form

$$\rho \dot{\boldsymbol{v}} = \operatorname{div} \boldsymbol{\sigma} + \boldsymbol{b}. \tag{2.1}$$

Here $\boldsymbol{\sigma}$ denotes the stress tensor, $\boldsymbol{b}$ is the body force per unit volume, acting on $\mathcal{B}$. The consequence of the law of conservation of angular momentum is the classical result that the stress tensor $\boldsymbol{\sigma}$ is symmetric; that is

$$\boldsymbol{\sigma} = \boldsymbol{\sigma}^{\mathrm{T}} \quad \text{or} \quad \sigma_{ij} = \sigma_{ji}. \tag{2.2}$$

The scalar field $\vartheta : \Omega \times \mathbb{I} \to \mathbb{R}$ denotes the relative temperature with respect to a uniform reference value Θ_0 such that the absolute temperature Θ is given by $\Theta = \vartheta + \Theta_0$.

Following the theory of Green and Naghdi, we introduce an internal state variable known as the *thermal displacement* α, which is defined as a time primitive of an *empirical temperature* $\bar{\Theta}$, see, for example, [9, 11, 13]. The empirical temperature is an affine (monotonically increasing) function of the absolute temperature, and for simplicity it is assumed that the empirical temperature coincides with the absolute temperature. This then implies that the thermal displacement α is related to the absolute temperature by

$$\alpha = \alpha^0 + \int_0^t \Theta(\tau) d\tau, \tag{2.3}$$

where α^0 is an initial thermal displacement.

According to the theory of Green and Naghdi, the balance of energy is replaced by a balance law of entropy and the equation governing thermal conduction in the body is given by

$$\rho\Theta\dot{\eta} = \boldsymbol{h} \cdot \nabla\dot{\alpha} - \text{div } \boldsymbol{q} + \rho\Theta[s + \xi], \tag{2.4}$$

where η is the entropy density, $\boldsymbol{h}$ the entropy flux vector, $\boldsymbol{q}$ the heat flux vector, ξ the internal rate of entropy production, and the scalar field s is such that Θs represents the external heat source per unit mass. The entropy $(\boldsymbol{h}, s)$ and the heat $(\boldsymbol{q}, r)$ pairs are related using the classical thermodynamic assumption through the absolute temperature as

$$\boldsymbol{q} = \Theta\boldsymbol{h}, \quad \text{and} \quad r = \Theta s,$$

where the scalar r denotes the heat source per unit mass.

In summary, the local forms of the law of balance of linear momentum together with the entropy balance-based heat conduction equation are, for infinitesimal deformations, given by

$$\begin{aligned} \rho\dot{\boldsymbol{v}} &= \text{div } \boldsymbol{\sigma} + \boldsymbol{b}, \\ \rho\Theta\dot{\eta} &= \boldsymbol{h} \cdot \nabla\dot{\alpha} - \text{div } \boldsymbol{q} + \rho\Theta[s + \xi]. \end{aligned} \tag{2.5}$$

2.2 Constitutive relations

The mathematical descriptions (2.5) together with the thermal displacement-absolute temperature (2.3) and the displacement-velocity relations, and the symmetry (2.2) of the stress tensor $\boldsymbol{\sigma}$ are not adequate to completely specify the thermomechanics of the body. Additional information governing how the particular material behaves is required to complete the description. Such information is presented in material specific relations known as *constitutive relations*.

In the framework of the theory of Green and Naghdi, general constitutive equations for generalized thermoelasticity are derived from a free-energy (per unit mass) function $\Psi = \Psi(\boldsymbol{\varepsilon}, \Theta)$ using the relations

$$\boldsymbol{\sigma} = \frac{\partial \rho\Psi}{\partial \boldsymbol{\varepsilon}}, \quad \text{and} \quad \eta = -\frac{\partial \Psi}{\partial \Theta}, \tag{2.6}$$

where the symmetric infinitesimal strain tensor $\boldsymbol{\varepsilon}$ defined by

$$\boldsymbol{\varepsilon}(\boldsymbol{u}) \coloneqq \frac{1}{2}\big[\nabla \boldsymbol{u} + (\nabla \boldsymbol{u})^{\mathrm{T}}\big]. \tag{2.7}$$

Unless stated otherwise we sometimes write simply $\boldsymbol{\varepsilon}$, without an argument, to represent the infinitesimal strain tensor at a given displacement $\boldsymbol{u}$. The linear generalized problem of thermoelasticity is obtained from relation (2.6) by assuming a quadratic free energy function; that is,

$$\rho\Psi = \frac{1}{2}\boldsymbol{\varepsilon} : \mathbb{C}\boldsymbol{\varepsilon} - \vartheta \mathbf{m} : \boldsymbol{\varepsilon} - \frac{1}{2}\frac{\rho c}{\Theta_0}\vartheta^2 - \vartheta S_0, \tag{2.8}$$

where $\mathbb{C}$ is the fourth-order elasticity tensor. Within the framework of (type III) generalized thermoelasticity a constitutive equation for the heat flux is supplemented; that is,

$$\boldsymbol{q} = -[\mathbf{k}_1 \nabla\alpha + \mathbf{k}_2 \nabla\Theta], \tag{2.9}$$

where $\mathbf{k}_1$ is a symmetric and positive-definite tensor accounting for the non-classical thermal conduction, $\mathbf{k}_2$ a symmetric and positive-semidefinite classical heat conduction tensor, $c > 0$ is the linearized heat capacity, and S_0 is referred as the initial (reference entropy). The second-order tensor $\mathbf{m}$ is responsible for the thermoelastic coupling effect, known in the literature as the *Gough-Joule effect*. From (2.6) and (2.8), we obtain the linear constitutive equations for the stress and entropy density as

$$\boldsymbol{\sigma} = \mathbb{C}\boldsymbol{\varepsilon}(\boldsymbol{u}) - \mathbf{m}\vartheta, \quad \text{and} \quad \rho\eta = \frac{c\rho}{\Theta_0}\vartheta + \mathbf{m} : \boldsymbol{\varepsilon}(\boldsymbol{u}) + S_0, \tag{2.10}$$

It is assumed that the elasticity tensor $\mathbb{C}$ has the following symmetry properties:

$$\mathbb{C}_{ijkl} = \mathbb{C}_{jikl} = \mathbb{C}_{ijlk}, \tag{2.11}$$

$$\mathbb{C}_{ijkl} = \mathbb{C}_{klij}, \tag{2.12}$$

$$\mathbb{C}_{ijkl}\varepsilon_{ij}\varepsilon_{kl} > 0 \quad \text{for any non-zero symmetric second-order tensor } \boldsymbol{\varepsilon}. \tag{2.13}$$

Unless stated otherwise we use the notion that summation over repeated indices is implied. Equations (2.11) and (2.12) are minor and major symmetries of $\mathbb{C}$, respectively, while (2.13) is the positive-definiteness of $\mathbb{C}$. For an isotropic linear thermoelastic material the elasticity tensor $\mathbb{C}$, and the thermal conductivity tensors $\mathbf{k}_1$ and $\mathbf{k}_2$ are given by

$$\begin{aligned} \mathbb{C} &= \lambda \mathbf{1} \otimes \mathbf{1} + 2\mu \mathbf{I}, & \mathbf{k}_1 &= k_1 \mathbf{1}, & \mathbf{k}_2 &= k_2 \mathbf{1} \quad \text{or,} \\ \mathbb{C}_{ijkl} &= \lambda \delta_{ij}\delta_{jk} + \mu(\delta_{ik}\delta_{jl} + \delta_{il}\delta_{jk}), & [\mathbf{k}_1]_{ij} &= k_1 \delta_{ij}, & [\mathbf{k}_2]_{ij} &= k_3 \delta_{ij}, \end{aligned}$$

where $\mathbf{1}$ and $\mathbf{I}$ are the identity second- and fourth-order tensor respectively. The symbol δ_{ij} is the Kronecker delta, and the constants $k_1 > 0$ and $k_2 \geq 0$. The thermomechanical coupling tensor $\mathbf{m}$ takes the form

$$\mathbf{m} = 3\omega\kappa \mathbf{1}, \quad \text{or} \quad m_{ij} = 3\omega\kappa\delta_{ij},$$

where ω and $\kappa = \lambda + 2/3\mu$, denote, respectively, the thermal expansion coefficient and the bulk modulus, and μ and λ are the Lamé constants.

From the definition of the absolute temperature as the sum of relative and reference temperature, the left hand side of the thermal conduction equation (2.4) can also be written as

$$\rho\Theta\dot{\eta} = \rho\Theta_0\dot{\eta} + \rho\vartheta\dot{\eta}. \tag{2.14}$$

Note that the last term of (2.14) is nonlinear as well as the term $\boldsymbol{h} \cdot \nabla\dot{\alpha}$ in equation $(2.5)_2$. In the infinitesimal regime, we assume that the nonlinear terms are small enough

to be ignored. Consequently, by retaining the linear terms, (2.4) together with (2.1) and the relations between the thermal displacement and the absolute temperature, and the displacement and the velocity, and the constitutive equations (2.9) and (2.10), yield the first-order problem of evolution for (linear) generalized thermoelasticity as:

$$\left.\begin{aligned} \dot{\boldsymbol{u}} &= \boldsymbol{v}, \\ \rho\dot{\boldsymbol{v}} &= \operatorname{div}[\mathbb{C}\boldsymbol{\varepsilon} - \mathbf{m}\vartheta] + \boldsymbol{b}, \\ \dot{\alpha} &= \Theta, \\ \rho\Theta_0\dot{\eta} &= \operatorname{div}[\mathbf{k}_1\nabla\alpha + \mathbf{k}_2\nabla\Theta] + \rho r \end{aligned}\right\} \text{ in } \Omega \times [0,\ T]. \tag{2.15}$$

In this system, the primary unknown fields are the displacement $\boldsymbol{u}$, the velocity $\boldsymbol{v}$, the thermal displacement α, and the relative temperature ϑ. It is this form of the dynamical system (2.15) which is crucial in analysing the well-posedness and designing a staggered computational scheme based on operator-splitting in later chapters.

Remark:

- The linearized theory of generalized thermoelasticity (type III) (2.15) contains both type I and type II as a special cases. If $\mathbf{k}_1\nabla\alpha$ is omitted from (2.15), then one obtains type I (or classical thermoelastic model) where a parabolic heat conduction equation is coupled with the hyperbolic mechanical equation. If $\mathbf{k}_2$ is set to zero, one obtains the type II thermoelastcity where the part of the coupled system (2.15) which describes conduction of heat is now hyperbolic.

2.3 Initial boundary-value problem

Initially, a thermal configuration is assumed for which the thermal displacement α is homogeneous[1], that is $\alpha(t = 0) = 0$, while the rest of the unknown fields take some prescribed values. Consequently, the initial condition for the evolution equation (2.15), are

[1] It should be noted that the thermal displacement α, as an internal state variable whose precise interpretation in statistical mechanics is still sought, is not practically measurable.

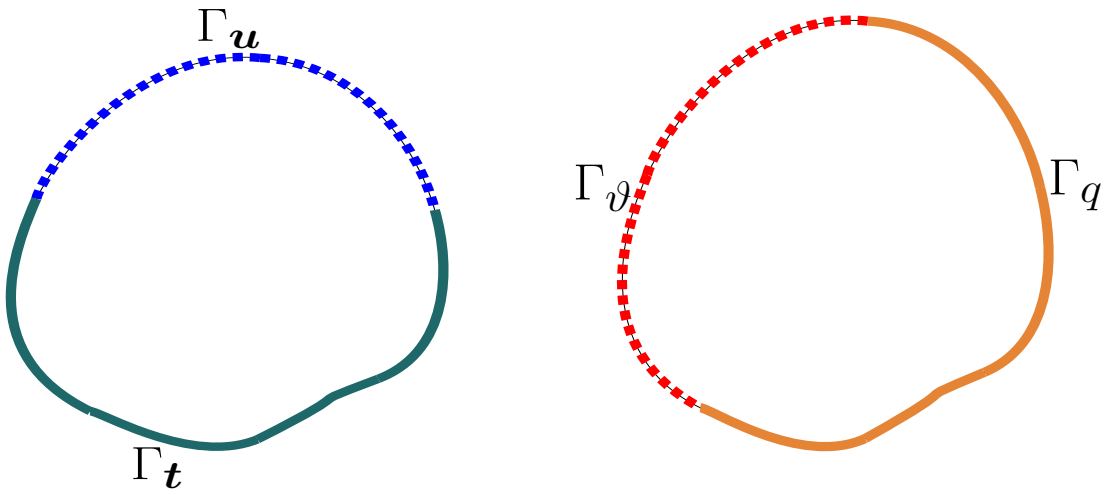

(a) (b)

Fig. 2.2: Schematic representation of the mechanical (a) and the thermal (b) boundary partitions of Γ

$$\left.\begin{aligned} &\boldsymbol{u} = \boldsymbol{u}^0, && \boldsymbol{v} = \boldsymbol{v}^0, \\ &\alpha = 0, && \vartheta = \vartheta^0, \end{aligned}\right\} \quad \text{on} \quad \Omega \times \{t = 0\} \tag{2.16}$$

where $\boldsymbol{u}^0$, $\boldsymbol{v}^0$, and ϑ^0, respectively are prescribed initial displacement, velocity, and relative temperature all defined on Ω.

Let $\{\Gamma_{\boldsymbol{u}}, \Gamma_{\boldsymbol{t}}\}$ and $\{\Gamma_{\vartheta}, \Gamma_q\}$ be two partitions of the boundary Γ containing mutually disjoint (non-overlapping) subsets of Γ as shown in the Fig. 2.2; that is,

$$\Gamma = \overline{\Gamma_{\boldsymbol{u}} \cup \Gamma_{\boldsymbol{t}}} = \overline{\Gamma_{\vartheta} \cup \Gamma_q}, \text{ with } \Gamma_{\boldsymbol{u}} \cap \Gamma_{\boldsymbol{t}} = \Gamma_{\vartheta} \cap \Gamma_q = \emptyset.$$

Let $\widehat{\boldsymbol{u}} : \Gamma_{\boldsymbol{u}} \times \mathbb{I} \to \mathbb{R}^d$, $\widehat{\boldsymbol{t}} : \Gamma_{\boldsymbol{t}} \times \mathbb{I} \to \mathbb{R}^d$, $\widehat{\vartheta} : \Gamma_{\vartheta} \times \mathbb{I} \to \mathbb{R}$, and $\widehat{q} : \Gamma_q \times \mathbb{I} \to \mathbb{R}$ be prescribed displacement, traction, relative temperature and flux fields. Thus the boundary conditions are given by

$$\begin{aligned} \boldsymbol{u} &= \widehat{\boldsymbol{u}} \quad \text{on} \quad \Gamma_{\boldsymbol{u}} \times \mathbb{I}, & \vartheta &= \widehat{\vartheta} \quad \text{on} \quad \Gamma_{\vartheta} \times \mathbb{I}, \\ \boldsymbol{\sigma}\mathbf{n} &= \widehat{\boldsymbol{t}} \quad \text{on} \quad \Gamma_{\boldsymbol{t}} \times \mathbb{I}, & \boldsymbol{q} \cdot \boldsymbol{n} &= \widehat{q} \quad \text{on} \quad \Gamma_q \times \mathbb{I}, \end{aligned} \tag{2.17}$$

where $\boldsymbol{n}$ denotes the outward unit normal field to Γ. Given that both the mechanical $(2.15)_{1,2}$ the non-classical thermal conduction $(2.15)_{3,4}$ sub-problems are hyperbolic, it

is important to note the analogy between the mechanical unknown fields $\boldsymbol{u}$, $\boldsymbol{v}$ and the thermal fields α, Θ, respectively.

Note that, here, the thermal Dirichlet boundary condition is given in terms of the temperature ϑ, not the thermal displacement α. It is also possible to substitute the displacement-velocity and thermal displacement-temperature relations into the evolution equation, thereby reducing the problem to a system of second-order in time coupled partial differential equations. In this case, the primary unknowns are only the displacement and thermal-displacement fields, $\boldsymbol{u}$ and α. As a result, specifying a thermal Dirichlet boundary equation would require prescribing the thermal displacement along the boundary, which is impractical since the precise physical interpretation of the thermal displacement field is still not known. An alternative is to prescribe the temperature along the Dirichlet boundary Γ_ϑ and a thermal boundary condition such that

$$\alpha(t)\Big|_{\Gamma_\vartheta} = \int_{t_0=0}^{t} \widehat{\Theta}(l)\Big|_{\Gamma_\vartheta} \,\mathrm{d}l, \qquad \text{for} \;\; t \in \mathbb{I},$$

where $\widehat{\Theta}$ is the temperature prescribed on the boundary Γ_ϑ. The evolution problem (2.15) along with the boundary and initial conditions (2.17) and (2.16) define the strong form of initial-boundary value problem (IBVP) of generalized (linear) thermoelasticity.

2.4 Well-posedness, dissipation and conservation

In this section we apply the theory of semigroups to analyze the well-posedness of the IBVP summarized in equation (2.15) along with the initial and boundary conditions (2.16) and (2.17) respectively. For this purpose, it is natural to consider the non-dimensionalized form of the IBVP.

Let L_c, T_c, M_c, and K_c be characteristic scalar quantities with the dimensions of length, time, mass, and temperature, respectively. Define the dimensionless variables

$$\tilde{\boldsymbol{u}} = \left[\frac{1}{L_c}\right]\mathbf{u}, \qquad \tilde{\boldsymbol{v}} = \left[\frac{T_c}{L_c}\right]\boldsymbol{v}, \qquad \tilde{\boldsymbol{x}} = \left[\frac{1}{L_c}\right]\boldsymbol{x}, \qquad \tilde{t} = \left[\frac{1}{T_c}\right]t,$$
$$\tilde{\Theta} = \left[\frac{1}{K_c}\right]\Theta, \qquad \tilde{\alpha} = \left[\frac{1}{T_c K_c}\right]\alpha, \qquad \tilde{\rho} = \left[\frac{L_c^3}{M_c}\right]\rho, \qquad \tilde{\Theta}_0 = \left[\frac{1}{K_c}\right]\Theta_0.$$

After substituting the constitutive equation $(2.10)_2$ and introducing the dimensionless variables, the non-dimensional form of (2.15) becomes

$$\begin{aligned}
\dot{\tilde{\boldsymbol{u}}} &= \tilde{\boldsymbol{v}},\\
\rho\dot{\tilde{\boldsymbol{v}}} &= \operatorname{div}[\tilde{\mathbb{C}}\boldsymbol{\varepsilon}(\tilde{\boldsymbol{u}}) - \tilde{\mathbf{m}}\tilde{\vartheta}] + \tilde{\rho}\,\tilde{\boldsymbol{b}},\\
\dot{\tilde{\alpha}} &= \tilde{\Theta},\\
\tilde{\rho}\tilde{c}\dot{\tilde{\Theta}} &= \operatorname{div}[\tilde{\mathbf{k}}_1\nabla\tilde{\alpha} + \tilde{\mathbf{k}}_2\nabla\tilde{\Theta}] - \tilde{\Theta}_0\tilde{\mathbf{m}} : \boldsymbol{\varepsilon}(\dot{\tilde{\boldsymbol{u}}}) + \tilde{\rho}\tilde{r},
\end{aligned} \tag{2.18}$$

where the spatial and time derivatives are with respect to the dimensionless space and time variables, and

$$\begin{aligned}
\tilde{\mathbb{C}} &= \left[\frac{L_c T_c^2}{M_c}\right]\mathbb{C}, \qquad & \tilde{\mathbf{m}} &= \left[\frac{L_c T_c^2 K_c}{M_c}\right]\mathbf{m}, \qquad & \tilde{\boldsymbol{b}} &= \left[\frac{T_c^2}{L_c}\right]\boldsymbol{b}, \qquad & \tilde{c} &= \left[\frac{K_c T_c^2}{L_c^2}\right]c,\\
\tilde{\mathbf{k}}_1 &= \left[\frac{T_c^4 K_c}{M_c L_c}\right]\mathbf{k}_1, \qquad & \tilde{\mathbf{k}}_2 &= \left[\frac{T_c^3 K_c}{M_c L_c}\right]\mathbf{k}_2, \qquad & \tilde{s} &= \left[\frac{T_c^3}{L_c^2}\right]s.
\end{aligned}$$

If we drop the tildes in equation (2.18), similar expressions to (2.15) are obtained. For the remainder of this section, whenever the system (2.15) is mentioned, unless stated otherwise, it refers to its non-dimensional form, and the initial and boundary conditions should also be understood accordingly.

The positive-definiteness property of $\mathbb{C}$ and $\mathbf{k}_1$, and the positive-semidefiniteness of $\mathbf{k}_2$ imply that the system (2.15) together with the initial and boundary conditions (2.17) and (2.16) define an evolution equation of a general form

$$\left.\begin{aligned}
\dot{\boldsymbol{\mathcal{X}}}(t) &= \mathbf{A}\boldsymbol{\mathcal{X}}(t) + \mathbf{f}\\
\boldsymbol{\mathcal{X}}(0) &= \boldsymbol{\mathcal{X}}^0
\end{aligned}\right\} \quad \text{in } \mathcal{V}, \tag{2.19}$$

where $\mathbf{A}$ is a closed linear operator with dense domain $\mathcal{D}(\mathbf{A}) \subset \mathcal{V}$ defined in some suitable Banach space $\mathcal{V}$. For the sake of convenience, we consider the case in which $\Gamma_{\boldsymbol{u}} = \Gamma_{\vartheta} = \Gamma$ and homogeneous thermal and mechanical Dirichlet boundary condition, and define the space $\mathcal{V}$ by

$$\mathcal{V} := \left\{(\boldsymbol{u}, \boldsymbol{v}, \alpha, \Theta)^T \in [H^1(\Omega)]^d \times [L^2(\Omega)]^d \times H^1(\Omega) \times L^2(\Omega) : \boldsymbol{u} = \mathbf{0}, \alpha = 0 \text{ on } \Gamma\right\}.$$

Clearly the space $\mathcal{V}$ is a Hilbert space.

The abstract solution vector is defined by $\boldsymbol{\mathcal{X}} = (\boldsymbol{u}, \boldsymbol{v}, \alpha, \vartheta)^T \in \mathcal{V}$, and the linear operator $\mathbf{A}$ and the source term $\mathbf{f}$ for generalized thermoelasticity, are defined by

$$\mathbf{A}\boldsymbol{\mathcal{X}} \coloneqq \begin{bmatrix} \boldsymbol{v} \\ \frac{1}{\rho}\mathrm{div}[\mathbb{C}\boldsymbol{\varepsilon}(\boldsymbol{u}) - \mathbf{m}\vartheta] \\ \vartheta + \Theta_0 \\ \frac{1}{\rho c}\mathrm{div}[\mathbf{k}_1\nabla\alpha + \mathbf{k}_2\nabla\Theta] - \frac{\Theta_0}{\rho c}\mathbf{m} : \boldsymbol{\varepsilon}(\boldsymbol{v}) \end{bmatrix}, \quad \mathbf{f} \coloneqq \begin{bmatrix} \mathbf{0} \\ \boldsymbol{b} \\ 0 \\ \frac{r}{c} \end{bmatrix}. \tag{2.20}$$

It is also assumed that both the body force $\boldsymbol{b}$ and the heat source r are homogeneous, which implies that $\mathbf{f} = \mathbf{0}$. We consider an inner product, $\langle \cdot,\ \cdot \rangle_{\mathcal{V}}$ on $\mathcal{V}$ defined by

$$\left\langle \boldsymbol{\mathcal{X}},\ \tilde{\boldsymbol{\mathcal{X}}} \right\rangle_{\mathcal{V}} = \langle \boldsymbol{\varepsilon}(\boldsymbol{u}),\ \mathbb{C}\boldsymbol{\varepsilon}(\tilde{\boldsymbol{u}}) \rangle + \langle \rho\boldsymbol{v},\ \tilde{\boldsymbol{v}} \rangle + \langle \mathbf{k}_1^*\nabla\alpha,\ \nabla\tilde{\alpha} \rangle + \langle c^*\vartheta,\ \tilde{\vartheta} \rangle,$$

where $\langle \cdot,\ \cdot \rangle$ denotes the standard L^2-inner product pairing of tensor, vector, or scalar fields, which should be understood in context, and $\mathbf{k}_1^* = \mathbf{k}_1(1/\rho\Theta_0)$ and $c^* = c/\Theta_0$. The norm on $\mathcal{V}$ induced by the inner product $\langle \cdot,\ \cdot \rangle_{\mathcal{V}}$ is denoted by $\| \cdot \|_{\mathcal{V}}$.

Note that the linear differential operator $\mathbf{A} : \mathcal{D}(\mathbf{A}) \subset \mathcal{V} \to \mathcal{V}$ is closed and the space

$$[\mathbf{H}_0^1(\Omega) \cap \mathbf{H}_0^2(\Omega)]^d \times [\mathbf{H}_0^1(\Omega)]^d \times (H_0^1(\Omega) \cap H_0^2(\Omega)) \times H_0^1(\Omega) \subset \mathcal{D}(\mathbf{A}),$$

is dense in $\mathcal{V}$. Hence $\mathcal{D}(\mathbf{A})$ is dense in $\mathcal{V}$.

An important inequality concerning the evolution equation of (2.19) is the *dissipativity property* of the operator $\mathbf{A}$. An operator $\mathbf{A}$ on a closed subspace $\mathcal{D}(\mathbf{A})$ of a Hilbert space $\mathcal{V}$ endowed with an inner product $\langle \cdot, \cdot \rangle_{\mathcal{V}}$ is said to be dissipative if it satisfies the inequality $\langle \mathbf{A}\boldsymbol{\mathcal{X}},\ \boldsymbol{\mathcal{X}} \rangle_{\mathcal{V}} \leq 0$ for each $\boldsymbol{\mathcal{X}} \in \mathcal{D}(\mathbf{A})$ [6]. If the operator $\mathbf{A}$ is dissipative, the norm of the solution of the corresponding evolution equation is monotonically decreasing in time, which is referred to as *contractivity* of the solution. That is, for a solution $\boldsymbol{\mathcal{X}}$ of the evolution problem (2.19), assuming dissipativity of $\mathbf{A}$, we obtain

$$\frac{d}{dt}\|\boldsymbol{\mathcal{X}}\|_{\mathcal{V}} = \frac{d}{dt}\langle \boldsymbol{\mathcal{X}}, \boldsymbol{\mathcal{X}} \rangle_{\mathcal{V}} = 2\left\langle \dot{\boldsymbol{\mathcal{X}}}, \boldsymbol{\mathcal{X}} \right\rangle_{\mathcal{V}} = 2\langle \mathbf{A}\boldsymbol{\mathcal{X}},\ \boldsymbol{\mathcal{X}} \rangle \leq 0.$$

Now, we shall show that the operator $\mathbf{A}$ defined in (2.20) is dissipative. Let $\boldsymbol{\mathcal{X}} = (\boldsymbol{u}, \boldsymbol{v}, \alpha, \vartheta)^T$ be in the domain of $\mathbf{A}$, $\mathcal{D}(\mathbf{A})$, satisfying the homogeneous boundary con-

ditions. Then

$$\begin{aligned}\langle \boldsymbol{\mathcal{X}},\ \mathbf{A}\boldsymbol{\mathcal{X}}\rangle_{\mathcal{V}} &= \langle \boldsymbol{\varepsilon}(\boldsymbol{u}),\ \mathbb{C}\boldsymbol{\varepsilon}(\boldsymbol{v})\rangle + \langle \rho\boldsymbol{v},\ \frac{1}{\rho}\mathrm{div}[\mathbb{C}\boldsymbol{\varepsilon}(\boldsymbol{u}) - \mathbf{m}\vartheta]\rangle \\ &\quad + \langle \mathbf{k}_1^*\nabla\alpha,\ \nabla\vartheta\rangle + \langle c^*\vartheta,\ \frac{1}{\rho c}\mathrm{div}[\mathbf{k}_1\nabla\alpha + \mathbf{k}_2\nabla\Theta] - \frac{\Theta_0}{c}\mathbf{m} : \boldsymbol{\varepsilon}(\boldsymbol{v})\rangle \\ &= \langle \boldsymbol{\varepsilon}(\boldsymbol{u}),\ \mathbb{C}\boldsymbol{\varepsilon}(\boldsymbol{v})\rangle - \langle \boldsymbol{\varepsilon}(\boldsymbol{v}),\ \mathbb{C}\boldsymbol{\varepsilon}(\boldsymbol{u})\rangle + \langle \boldsymbol{\varepsilon}(\boldsymbol{v}),\ \mathbf{m}\vartheta\rangle + \langle \frac{1}{\rho\Theta_0}\mathbf{k}_1\nabla\alpha,\ \nabla\Theta\rangle \\ &\quad - \langle \frac{1}{\rho\Theta_0}\mathbf{k}_1\nabla\Theta,\ \nabla\alpha\rangle - \langle \frac{1}{\rho\Theta_0}\mathbf{k}_2\nabla\Theta,\ \nabla\Theta\rangle - \langle \vartheta,\ \mathbf{m} : \boldsymbol{\varepsilon}(\boldsymbol{v})\rangle \\ &= -\langle \frac{1}{\rho\Theta_0}\mathbf{k}_2\nabla\Theta,\ \nabla\Theta\rangle \leq 0. \end{aligned} \tag{2.21}$$

Generally, since $\mathbf{k}_2$ is positive-semidefinite equation (2.21) leads to dissipation. In the limiting case where $\mathbf{k}_2$ vanishes, that is type II, the above argument implies conservation in the energy-norm defined by

$$\mathscr{E}(t) := \|\boldsymbol{\mathcal{X}}\|_{\boldsymbol{V}}^2 = \frac{1}{2}\int_\Omega [\boldsymbol{\varepsilon}(\boldsymbol{u}) : \mathbb{C}\boldsymbol{\varepsilon}(\boldsymbol{u}) + \rho\boldsymbol{v}\cdot\boldsymbol{v} + \mathbf{k}_1^*\nabla\alpha\cdot\nabla\alpha + c^*\vartheta^2]\mathrm{d}\Omega. \tag{2.22}$$

This is the reason why type II is also referred to as the theory of thermoelasticity *without energy dissipation*; see, for example, [41, 43, 82].

Another important relation concerning the operator $\mathbf{A}$ is that it should satisfy the following: for all $\boldsymbol{\mathcal{X}}^* \in \mathcal{V}$, there exists $\boldsymbol{\mathcal{X}}$ in $\mathcal{D}(\mathbf{A})$ such that

$$\boldsymbol{\mathcal{X}} - \mathbf{A}\boldsymbol{\mathcal{X}} = \boldsymbol{\mathcal{X}}^*; \tag{2.23}$$

in other words, the operator $(\mathbf{1} - \mathbf{A}) : \mathcal{D}(\mathbf{A}) \to \mathcal{V}$ is onto.

To show that $\mathbf{A}$ satisfies the relation (2.23), we proceed as follows. Let $\boldsymbol{\mathcal{X}} = (\boldsymbol{u}, \boldsymbol{v}, \alpha, \vartheta)^T$ and $\boldsymbol{\mathcal{X}}^* = (\boldsymbol{u}^*, \boldsymbol{v}^*, \alpha^*, \vartheta^*)^T$; then the definition of $\mathbf{A}$ (2.23) implies that

$$\begin{aligned} \boldsymbol{u} - \boldsymbol{v} &= \boldsymbol{u}^*, \\ \boldsymbol{v} - \frac{1}{\rho}\mathrm{div}[\mathbb{C}\boldsymbol{\varepsilon}(\boldsymbol{u}) - \mathbf{m}\vartheta] &= \boldsymbol{v}^*, \\ \alpha - \vartheta &= \alpha^*, \\ \vartheta - \frac{1}{\rho c}\mathrm{div}[\mathbf{k}_2\nabla\alpha + \mathbf{k}_3\nabla\Theta] + \frac{\Theta_0}{c}\mathbf{m} : \boldsymbol{\varepsilon}(\boldsymbol{v}) &= \vartheta^*. \end{aligned} \tag{2.24}$$

Substitution of equations $(2.24)_1$ and $(2.24)_3$ into the remaining equations of (2.24) leads to the (equilibrium) problem: find $\boldsymbol{\mathcal{X}} = (\boldsymbol{u}, \boldsymbol{v}, \alpha, \vartheta)^T \in \mathcal{D}(\mathbf{A})$ such that $\boldsymbol{v} = \boldsymbol{u} - \boldsymbol{u}^*$, $\vartheta = \alpha - \alpha^*$ and satisfying

$$\begin{aligned} \rho^2\Theta_0\boldsymbol{u} - \rho\Theta_0\mathrm{div}[\mathbb{C}\boldsymbol{\varepsilon}(\boldsymbol{u}) - \mathbf{m}\alpha] &= \mathring{\boldsymbol{u}}, \\ \rho c\alpha - \mathrm{div}[\mathbf{k}\nabla\alpha] + \rho\Theta_0\mathbf{m} : \boldsymbol{\varepsilon}(\boldsymbol{u}) &= \mathring{\alpha}, \end{aligned} \tag{2.25}$$

where $\mathring{\boldsymbol{u}} = \rho^2\Theta_0\boldsymbol{u}^* + \rho^2\Theta_0\boldsymbol{v}^* + \rho\Theta_0\mathrm{div}[\mathbf{m}\alpha^*]$, $\mathring{\alpha} = \rho c\alpha^* + \rho c\vartheta^* - \mathrm{div}[\mathbf{k}_3\nabla\alpha^*] + \rho\Theta_0\mathbf{m} : \boldsymbol{\varepsilon}(\boldsymbol{u}^*)$, and $\mathbf{k} = \mathbf{k}_2 + \mathbf{k}_3$.

The weak form of equation (2.25) reads: find $\boldsymbol{\mathcal{X}} = (\boldsymbol{u}, \boldsymbol{v}, \alpha, \vartheta)^T \in \mathcal{V}$ such that $\boldsymbol{v} = \boldsymbol{u} - \boldsymbol{u}^*$, $\vartheta = \alpha - \alpha^*$ and satisfying

$$B(\boldsymbol{\mathcal{X}}, \boldsymbol{\xi}) = l(\boldsymbol{\xi}) \tag{2.26}$$

for all $\boldsymbol{\xi} := (\boldsymbol{w}, \boldsymbol{\nu}, \beta, \varpi) \in \mathcal{V}$. The bilinear form $B(\cdot,\ \cdot)$ and the right hand side functional $l(\cdot)$ are given by

$$\begin{aligned} B(\boldsymbol{\mathcal{X}}, \boldsymbol{\xi}) = {} & \langle \rho^2\Theta_0\boldsymbol{u}, \boldsymbol{w}\rangle + \langle \rho\Theta_0\mathbb{C}\boldsymbol{\varepsilon}(\boldsymbol{u}), \boldsymbol{\varepsilon}(\boldsymbol{w})\rangle - \langle \rho\Theta_0\mathbf{m}\alpha, \boldsymbol{\varepsilon}(\boldsymbol{w})\rangle \\ & + \langle \rho c\alpha, \beta\rangle + \langle \mathbf{k}\nabla\alpha, \nabla\beta\rangle + \langle \rho\Theta_0\mathbf{m} : \boldsymbol{\varepsilon}(\boldsymbol{u}), \beta\rangle, \end{aligned} \tag{2.27}$$

$$l(\boldsymbol{\xi}) = \langle \mathring{\boldsymbol{u}}, \boldsymbol{w}\rangle + \langle \mathring{\alpha}, \beta\rangle. \tag{2.28}$$

Note that $\mathring{\boldsymbol{u}} \in [\mathbf{H}^{-1}(\Omega)]^d$ and $\mathring{\alpha} \in \mathbf{H}^{-1}(\Omega)$ and the symbol $\langle\cdot,\cdot\rangle$ in equation (2.28) represents duality pairing in their respective spaces.

From the definition of $B(\cdot,\cdot)$, we can easily see that it is a bounded bilinear form. Since

$$B(\boldsymbol{\mathcal{X}}, \boldsymbol{\mathcal{X}}) = \langle \rho^2\Theta_0\boldsymbol{u}, \boldsymbol{u}\rangle + \langle \rho\Theta_0\mathbb{C}\boldsymbol{\varepsilon}(\boldsymbol{u}), \boldsymbol{\varepsilon}(\boldsymbol{u})\rangle + \langle \rho c\alpha, \alpha\rangle + \langle \mathbf{k}\nabla\alpha, \nabla\alpha\rangle,$$

$B(\cdot,\cdot)$ is $([\mathbf{H}_0^1(\Omega)]^d \times \mathbf{H}_0^1(\Omega))$-elliptic. By applying the Lax-Milgram theorem we conclude that there exists $\boldsymbol{\mathcal{X}} \in \mathcal{V}$ which solves the weak problem (2.26), and hence solves equation (2.24). Therefore, this proves the surjectivity of the resolvent operator $(\mathbf{1} - \mathbf{A})$.

In conclusion, we have seen that the operator $\mathbf{A}$ defining the non-classical linear thermoelasticity (type III)

i) is closed,

ii) has a dense domain $\mathcal{D}(\mathbf{A})$ in $\mathcal{V}$,

iii)is dissipative, and

iv)is such that $(\mathbf{1} - \mathbf{A}) : \mathcal{D}(\mathbf{A}) \subset \mathcal{V} \to \mathcal{V}$ is onto.

Therefore, by the Lumer-Phillips theorem, $\mathbf{A}$ generates a strongly continuous semi-group of contractions in $\mathcal{V}$, (see for example [82] and the references therein.) In other words, the problem (2.19) is well-defined and contractive. This also means that the dynamical system represented by the equation of non-classical thermoelasticity of type III is, in general, stable in the sense of Lyapunov.

3

A stable staggered algorithm based on operator-splitting and the time-discontinuous Galerkin method

In this chapter, we develop a new numerical scheme based on operator-splitting and time-discontinuous Galerkin methods for the generalized linear thermoelasticity problem discussed in Chapter 2. The full problem is first split into two sub-problems, namely the mechanical and thermal phases. The mechanical phase is hyperbolic and equivalent to the classical linear elasticity problem, while the problem in the thermal phase describes the mechanism of heat conduction as a wave and diffusion. Mathematically, each sub-problem is well-posed. Later a time-stepping numerical algorithm is developed using the time-discontinuous Galerkin finite element method. The sub-problems are then merged to give an algorithm for the global problem.

This chapter is organised as follows. In Section 3.1 concepts concerning time-stepping algorithms are discussed. Operator-splitting and algorithms based on operator-splitting are reviewed. Sufficient conditions for an algorithm based on operator-splitting to be consistent and stable are discussed. In Section 3.2 an operator split for generalized thermoelasticity into two sub-problems, namely the mechanical and thermal phase, is presented. The sub-problems are analyzed and shown to be contractive, implying that each is well-posed. Finally, in Section 3.3, the time-discontinuous weak formulations for each sub-problem are presented.

3.1 Algorithms based on operator-splitting

Consider an abstract evolution problem of the form (2.19). A one-parameter family of maps $\mathbb{A}^{\Delta t} : \mathcal{V} \to \mathcal{V}$, where $\Delta t \geq 0$, is said to be a *time-stepping algorithm* for

the evolution problem (2.19) defined by the operator $\mathbf{A}$ on the (Banach space) $\mathcal{V}$ if it satisfies the following conditions:

i) $\mathbb{A}^{\Delta t} = \mathbf{I}$ (identity map on $\mathcal{V}$) if $\Delta t = 0$;

ii) for each $\Delta t \geq 0$, the map

$$\Delta t \mapsto \mathbb{A}^{\Delta t}\boldsymbol{\mathcal{X}}, \quad \forall \boldsymbol{\mathcal{X}} \in \mathcal{V},$$

is continuous. In this case we also say that $\mathbb{A}^{\Delta t}$ depends continuously on Δt.

Consider a non-overlapping subdivision (not necessarily uniform) of the time interval of interest $\mathbb{I} = [0,\ T]$ into N subintervals of the form $I_n = [t_n,\ t_{n+1}]$ with step length $\Delta t_n = t_{n+1} - t_n$. Denote by $\boldsymbol{\mathcal{X}}^n$ a given (approximate) solution at time t_n; then $\boldsymbol{\mathcal{X}}^{n+1} := \mathbb{A}^{\Delta t_n}\boldsymbol{\mathcal{X}}^n$ defines the solution at time t_{n+1}. A given algorithm $\mathbb{A}^{\Delta t}$ is said to be *consistent* with the evolutionary problem (2.19) if for all $\boldsymbol{\mathcal{X}} \in \mathcal{V}$,

$$\frac{\mathrm{d}}{\mathrm{d}\epsilon}\left[\mathbb{A}^{\epsilon}\boldsymbol{\mathcal{X}}\right]_{\epsilon=0} := \lim_{\Delta t \to 0^+} \frac{\mathbb{A}^{\Delta t}\boldsymbol{\mathcal{X}} - \boldsymbol{\mathcal{X}}}{\Delta t} = \mathbf{A}\boldsymbol{\mathcal{X}}, \qquad \forall \boldsymbol{\mathcal{X}} \in \mathcal{D}(\mathbb{A}). \tag{3.1}$$

Remark: Consistency is a concept which is primarily concerned with the extent to which the discrete and exact solutions agree with each other. In the finite element context, consistency can be determined by showing, under some suitable regularity assumptions, that a solution of the strong form of the problem satisfies its discrete version, and vice versa.

Now, assume that the operator $\mathbf{A}$ can be split additively into two operators $\mathbf{A}_1$ and $\mathbf{A}_2$; that is

$$\mathbf{A} = \mathbf{A}_1 + \mathbf{A}_2.$$

Consider the sub-problems corresponding to the operators $\mathbf{A}_i$, $i = 1, 2$ which are defined by

$$\dot{\boldsymbol{\mathcal{X}}}_i = \mathbf{A}_i\boldsymbol{\mathcal{X}}_i\,; \quad \boldsymbol{\mathcal{X}}_i(0) = \boldsymbol{\mathcal{X}}_i^0, \quad i = 1, 2, \tag{3.2}$$

where $\boldsymbol{\mathcal{X}}_i^0$'s are some initial values in the domain of $\mathbf{A}$. Let $\mathbb{A}_i^{\Delta t}$ be time-stepping algorithms corresponding to the sub-problems (3.2). A time-stepping algorithm $\mathbb{A}^{\Delta t}$ for the global problem is formally obtained by taking products of the algorithms as

$$\mathbb{A}^{\Delta t} = \mathbb{A}_2^{\Delta t} \circ \mathbb{A}_1^{\Delta t} \quad \text{or equivalently } \mathbb{A}^{\Delta t} = \mathbb{A}_2^{\Delta t}\mathbb{A}_1^{\Delta t}. \tag{3.3}$$

The algorithm $\mathbb{A}^{\Delta t}$ is referred to as a *single-pass algorithm*, as information is allowed to pass between the individual algorithms only once during the process of approximating the solution for the global problem. The convergence of the single-pass algorithm has been shown by applying the *Lie-Trotter-Kato product formula* [21]. Note that the single-pass algorithm depends on the order of the algorithms of the sub-problem, in the sense that the algorithm with $\mathbb{A}_2^{\Delta t}$ which is applied first then information (intermediate solution) passed to $\mathbb{A}_1^{\Delta t}$, is essentially different from the one with the reverse order. Such product algorithms are also referred to as a *sequential split algorithms*.

The following lemma relates to stability and consistency of the individual algorithm with the single-pass global algorithm.

Lemma 3.1. *In the linear case, if each algorithm $\mathbb{A}_i^{\Delta t}$ $(i = 1, 2)$ is consistent, then the single-pass algorithm* (3.3) *is also consistent.*

Proof. The proof of consistency employs the product formula for differentiation together with the definition of consistency (3.1). From the formula (3.3) and consistency assumptions on $\mathbb{A}_i^{\Delta t}$, for any $\boldsymbol{\mathcal{X}} \in \mathcal{V}$ we have

$$\begin{aligned}
\frac{\mathrm{d}}{\mathrm{d}\epsilon}\mathbb{A}^{\epsilon}\boldsymbol{\mathcal{X}}\bigg|_{\epsilon=0} &= \frac{\mathrm{d}}{\mathrm{d}\epsilon}\left[\mathbb{A}_1^{\epsilon}\mathbb{A}_2^{\epsilon}\boldsymbol{\mathcal{X}}\right]\bigg|_{\epsilon=0} \\
&= \left[\left(\frac{\mathrm{d}}{\mathrm{d}\epsilon}\mathbb{A}_1^{\epsilon}\right)\mathbb{A}_2^{\epsilon}\boldsymbol{\mathcal{X}} + \mathbb{A}_1^{\epsilon}\left(\frac{\mathrm{d}}{\mathrm{d}\epsilon}\mathbb{A}_2^{\epsilon}\right)\boldsymbol{\mathcal{X}}\right]_{\epsilon=0} \\
&= \mathbf{A}_1\mathbf{I}\boldsymbol{\mathcal{X}} + \mathbf{I}\mathbf{A}_2\boldsymbol{\mathcal{X}} \\
&= [\mathbf{A}_1 + \mathbf{A}_2]\boldsymbol{\mathcal{X}} \\
&= \mathbf{A}\boldsymbol{\mathcal{X}}.
\end{aligned}$$

Any numerical algorithm based on discretizing an operator on an infinite dimensional spaces generates a *truncation error*. In addition to such errors from the individual algorithms $\mathbb{A}_i^{\Delta t}$, the merging of these algorithms to obtain a global algorithm introduces another mechanism of error which referred to as a *splitting error*. For example, a single-pass algorithm is only first-order accurate in time independent of the order of accuracy of the individual operators (see for example [50]). There are, however, higher-order

algorithms based on the operator-splitting strategy, for example,

$$\begin{aligned} &\text{Marchuk-Strang split:} && \mathbb{A}^{\Delta t} = \mathbb{A}_1^{\Delta t/2}\mathbb{A}_2^{\Delta t}\mathbb{A}_1^{\Delta t/2}; \\ &\text{Double-pass split:} && \mathbb{A}^{\Delta t} = \frac{1}{2}(\mathbb{A}_2^{\Delta t}\mathbb{A}_1^{\Delta t} + \mathbb{A}_1^{\Delta t}\mathbb{A}_2^{\Delta t}). \end{aligned} \tag{3.4}$$

The Marchuk–Strang split is second-order accurate, while the double-pass split is only first-order. Note that, in the Marchuk–Strang splitting algorithm, the sub-algorithm $\mathbb{A}_1$ is applied twice with half $\Delta t/2$ of the full step size and $\mathbb{A}_2$ is applied only once with full step size Δt. While, in the double-pass split algorithm, information is passed in both ways with each algorithm involved twice with the full time step length, which doubles the complexity of the single-pass split algorithm (3.3).

Remarks:

1. One situation in which operator-splitting schemes might be advantageous over a monolithic approach is for coupled problems involving different classes of sub-problems. Such multi-physics problems can be handled in a quite natural way which allows the use of different classes of methods to efficiently solve each sub-problems so that they can be joined together in a suitable way to form the global algorithms. Such splitting schemes can be very important, for example, in problems involving interaction of fluid and structure.
2. Splitting schemes can be constructed for coupled problems exhibiting multiple time scales. In such cases, the step size for each component is chosen according to the activity level. The schemes for each component should be sufficiently accurate for the global algorithm to be useful. In fact, the mechanism of capturing different time scales is natural in splitting schemes, whereas, a standard monolithic scheme only admits a single time-step which depends on scale of the fastest component.
3. One of the limiting factors of splitting schemes is that it is difficult to construct schemes which are higher than second-order accurate. However, the design of higher order p- and hp-adaptive schemes are effective with monolithic schemes. The reason for this is that the accuracy of the staggered scheme is restricted by the order of splitting in the product formula.

4. Operator-splitting is not always an effective strategy, especially when the coupling between the physical phenomena represented in two or more systems is too strong. In this case, for efficiency and accuracy reasons, an adaptive hybrid method which involves, within one scheme, switching between a monolithic and a splitting technique may be used [97].

3.2 An operator split for generalized thermoelasticity

In this section we present an operator split for generalized thermoelasticity into two operators in which each of the corresponding sub-problems replicates the contractivity property of the coupled system. The operator split disscussed here is inspired by the work of Armero and Simo [6] for classical thermoelasticity. The resulting operators in the split account for the decoupled problems of linear elasticity at constant entropy (also referred to as *isentropic elasticity* or *the mechanical phase*), and non-classical heat conduction (*thermal phase*) in a rigid body. It was shown that this split, for the classical thermoelastictiy, inherits the same contractivity of the full problem, thus leading to unconditionally stable product formula algorithm [6]. In stark contrast to this stability property, Armero and Simo showed that the classical staggered algorithms based on an isothermal mechanical phase followed by a heat conduction are, at best, conditionally stable.

For convenience, we replace the temperature ϑ by the entropy η in the list of unknowns in the generalized thermoelasticity problem, and we then represent the vector of unknowns by $\boldsymbol{\Sigma} = (\boldsymbol{u}, \boldsymbol{v}, \alpha, \eta)^{\mathsf{T}} \in \mathcal{D}(\mathbf{A})$, where

$$\mathbf{A}\boldsymbol{\Sigma} = \begin{bmatrix} \boldsymbol{v} \\ \dfrac{1}{\rho}\mathrm{div}[\mathbb{C}\boldsymbol{\varepsilon}(\boldsymbol{u}) - \mathbf{m}\vartheta] \\ \vartheta + \Theta_0 \\ \dfrac{1}{\rho\Theta_0}\mathrm{div}[\mathbf{k}_1\nabla\alpha + \mathbf{k}_2\nabla\Theta] \end{bmatrix}. \tag{3.5}$$

The source term is $\mathbf{f} = [\mathbf{0},\ \boldsymbol{b},\ 0,\ r/\Theta_0]^{\mathsf{T}}$ and the evolution equation (2.15) may be written in the form

$$\dot{\boldsymbol{\Sigma}} = \mathbf{A}\boldsymbol{\Sigma} + \boldsymbol{f}. \tag{3.6}$$

Next, we consider an additive split of the operator $\mathbf{A}$ in (3.5) such that $\mathbf{A} = \mathbf{A}_1 + \mathbf{A}_2$, where

$$\mathbf{A}_1\boldsymbol{\Sigma} = \begin{bmatrix} \boldsymbol{v} \\ \frac{1}{\rho}\mathrm{div}[\mathbb{C}\boldsymbol{\varepsilon}(\boldsymbol{u}) - \mathbf{m}\vartheta] \\ 0 \\ 0 \end{bmatrix}, \qquad \mathbf{A}_2\boldsymbol{\Sigma} = \begin{bmatrix} \mathbf{0} \\ \mathbf{0} \\ \vartheta + \Theta_0 \\ \frac{1}{\rho c}\mathrm{div}[\mathbf{k}_1\nabla\alpha + \mathbf{k}_2\nabla\Theta] \end{bmatrix}. \tag{3.7}$$

We refer to (3.7) as an *adiabatic split* following the terminology used in [6] for the classical problem.

The key aspect of the split (3.7) is the inclusion of the entropy η as part of the vector $\boldsymbol{\Sigma}$ of unknowns. The structural elastic heating term $(\Theta_0/\rho c)\mathbf{m} : \boldsymbol{\varepsilon}(\boldsymbol{v})$ drives a time-varying temperature (computed explicitly in a closed form) which corresponds to a vanishing rate of entropy, that is, $\dot{\eta} = 0$. The temperature dependence of the stress constitutive equation $(2.10)_1$ will be updated by the time-varying temperature in the mechanical phase. Ultimately, the problem in the mechanical phase is reduced to the classical elastodynamics corresponding to the entropy constraint $\dot{\eta} = 0$. The thermal phase is essentially a non-classical heat conduction problem at fixed configuration.

It is also essential to note that, in the mechanical phase, α is not coupled with the other equations (it only appears in the equation $\dot{\alpha} = 0$). Hence it should be treated as an extra variable which is constant in time during the mechanical phase while the temperature is varied.

The adiabatic split is particularly important because the sub-problems replicate the contractivity property of the global problem discussed in Section 2.4. This can be shown by employing the same line of argument leading to the dissipation (2.21) of the global operator. Thus, we obtain the estimates

$$\left.\begin{aligned} &\langle \mathbf{A}_1\boldsymbol{\Sigma}, \boldsymbol{\Sigma}\rangle_{\mathcal{V}} = 0, \\ &\langle \mathbf{A}_2\boldsymbol{\Sigma}, \boldsymbol{\Sigma}\rangle_{\mathcal{V}} = -\langle \frac{\rho c}{\Theta_0}\mathbf{k}_3\nabla\Theta, \nabla\Theta\rangle \leq 0 \end{aligned}\right\}, \quad \text{for all } \boldsymbol{\Sigma} \in \mathcal{D}(\mathbf{A}_1) \cap \mathcal{D}(\mathbf{A}_2).$$

In general, since $\mathbf{k}_2$ is positive-semidefinite, both operators $\mathbf{A}_1$ and $\mathbf{A}_2$ are dissipative. In particular, if $\mathbf{k}_2 = 0$, the sub-systems corresponding to $\mathbf{A}_2$, the non-classical heat conduction problem at fixed configuration, is energy conserving. That is, it represents

heat conduction without energy loss (type II) in a rigid body. Moreover, it can be shown that both of the sub-operators satisfy all the conditions, ensuring that each generates a strongly continuous semigroup of contraction following the same line of argument as for the well-posedness of the global problem in Section 2.4.

In this thesis, we restrict our attention to a single-pass global algorithm which merges the thermal and mechanical time-stepping algorithms. The numerical scheme formulated in the subsequent section is based on the operator-splitting approach discussed in Section 3.2. At each time subdivision $I_n = [t_n,\ t_{n+1}]$, both the mechanical phase and thermal phase are discretized using the time-discontinuous Galerkin finite element methodology, in which both space and time are treated in the finite element frame work with a discontinuous Galerkin formulation in time.

3.3 Time-discontinuous weak formulation

We now formulate time-discontinuous weak formulations for the thermal and mechanical problems separately. The consistency of the weak statements are also presented.

Useful notation

Recall from Section 3.1 the time subdivision $I_n = [t_n, t_{n+1}]$. Consequently, consider the space-time domain $\mathbb{\Omega} = \Omega \times [0,\ T]$ as space-time slabs as shown in Fig 3.1 and denote the space-time slab of level n by $\mathbb{\Omega}_n$, where

$$\mathbb{\Omega}_n = \Omega \times I_n.$$

The corresponding space-time boundaries for the partition of the spatial boundary have the form $\mathbb{\Gamma}^n_{\square} = \Gamma_{\square} \times I_n$, where the subscript symbol $\square$ represents the subscripts of the boundary identifiers $\boldsymbol{u}$, $\boldsymbol{t}$, ϑ or q. Next, we define (smooth) manifolds for admissible functions $\boldsymbol{u}$, $\boldsymbol{v}$, α, and ϑ by

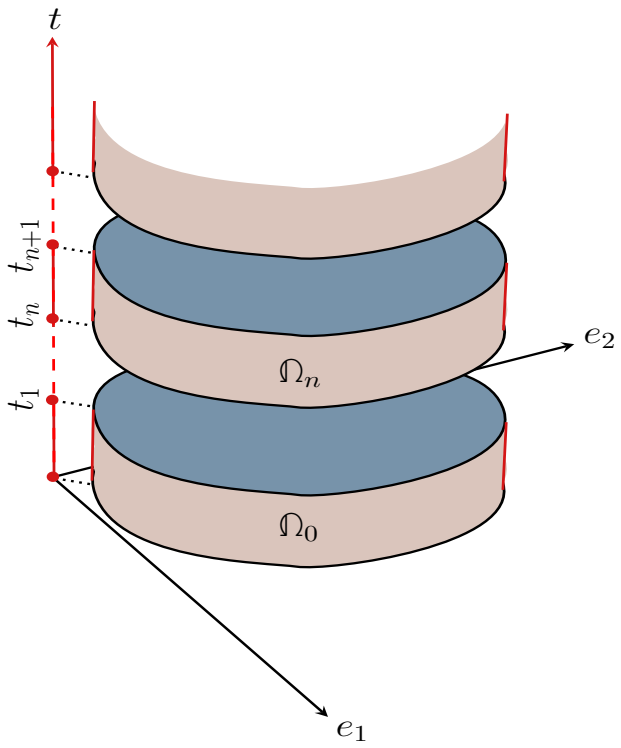

Fig. 3.1: Schematic of space-time slabs

$$
\begin{aligned}
\mathbb{V}_{\boldsymbol{u}} &:= \left\{ \boldsymbol{u} : \mathbb{\Omega}_n \mapsto \mathbb{R}^d \middle| \quad \boldsymbol{u}|_{\mathbb{\Gamma}^n_{\boldsymbol{u}}} = \bar{\boldsymbol{u}} \right\}, \\
\mathbb{V}_{\boldsymbol{v}} &:= \left\{ \boldsymbol{v} : \mathbb{\Omega}_n \mapsto \mathbb{R}^d \middle| \quad \boldsymbol{v}|_{\mathbb{\Gamma}^n_{\boldsymbol{v}}} = \dot{\bar{\boldsymbol{u}}} \right\}, \\
\mathbb{V}_{\alpha} &:= \left\{ \alpha : \mathbb{\Omega}_n \mapsto \mathbb{R} \middle| \quad \dot{\alpha}|_{\mathbb{\Gamma}^n_{\alpha}} = \bar{\vartheta} + \Theta_0 \right\}, \\
\mathbb{V}_{\vartheta} &:= \left\{ \vartheta : \mathbb{\Omega}_n \to \mathbb{R} \middle| \quad \vartheta|_{\mathbb{\Gamma}^n_{\vartheta}} = \bar{\vartheta} \right\}.
\end{aligned}
\tag{3.8}
$$

Note that in the definition of $\mathbb{V}_{\alpha}$ the thermal boundary condition is enforced as a time derivative of the thermal displacement field along the thermal Dirchlet boundary in the time interval I_n. Such boundary conditions require special treatment in the implementation of the numerical scheme as described in the subsequent sections.

3.3.1 Space-time Galerkin FEM spaces

In this section we briefly present the construction of the finite dimensional trial and weighting spaces of functions for the state variables in question in the space-time slab $\mathbb{\Omega}_n$.

First, the space-time slab $\mathbb{\Omega}_n$ is triangulated into non-overlapping elements, as shown in the Fig 3.2, on which conforming (piecewise continuous) scalar valued shape functions

$$N^A : \mathbb{\Omega}_n \to \mathbb{R}, \quad \text{with} \quad N^A((\boldsymbol{X}, t)_B) = \delta^A_B,$$

are defined. Here the superscript A denotes a space-time node number, $(\boldsymbol{X}, t)_B$ is a space-time node with number B, and δ^A_B is the Kronecker delta function. The set $\{N^A : A = 1, \cdots, n_{\text{node}}\}$ of all shape functions forms a basis of a finite dimensional space of scalar valued functions from which finite-dimensional version of the trial state spaces of displacement functions $\mathbb{V}^h_{\boldsymbol{u}} \subset \mathbb{V}_{\boldsymbol{u}}$, velocity functions $\mathbb{V}^h_{\boldsymbol{v}} \subset \mathbb{V}_{\boldsymbol{v}}$, thermal displacement functions $\mathbb{V}^h_\alpha \subset \mathbb{V}_\alpha$, and relative temperature functions $\mathbb{V}^h_\vartheta \subset \mathbb{V}_\vartheta$ are defined via the formulae

$$u^h_j(\boldsymbol{X}, t) = \sum_A U^A_j N^A(\boldsymbol{X}, t), \tag{3.9}$$

$$v^h_j(\boldsymbol{X}, t) = \sum_A V^A_j N^A(\boldsymbol{X}, t), \tag{3.10}$$

$$\alpha^h(\boldsymbol{X}, t) = \sum_A \beta^A N^A(\boldsymbol{X}, t) \in \mathbb{V}^h_\alpha, \tag{3.11}$$

$$\vartheta^h(\boldsymbol{X}, t) = \sum_A \pi^A N^A(\boldsymbol{X}, t) \in \mathbb{V}^h_\vartheta, \tag{3.12}$$

with $\boldsymbol{u}^h = \{u^h_j\}^d_{j=1} \in \mathbb{V}^h_{\boldsymbol{u}}$, $\boldsymbol{v}^h = \{v^h_j\}^d_{j=1} \in \mathbb{V}^h_{\boldsymbol{v}}$, and β^A and π^A are the nodal values of $\alpha^h \in \mathbb{V}^h_\alpha$ and $\vartheta^h \in \mathbb{V}^h_\vartheta$ respectively. Similarly, from the functions defined in (3.9)–(3.12) we construct finite dimensional weighting function spaces $\mathbb{S}^h_{\boldsymbol{u}} \subset \mathbb{S}_{\boldsymbol{u}}$, $\mathbb{S}^h_{\boldsymbol{V}} \subset \mathbb{S}_{\boldsymbol{V}}$, $\mathbb{S}^h_\alpha \subset \mathbb{S}_\alpha$, and $\mathbb{S}^h_\vartheta \subset \mathbb{S}_\vartheta$.

Depending on the context we denote by $\langle \cdot,\ \cdot \rangle$, and $(\cdot,\ \cdot)_n$, respectively, the space and space-time L_2-inner product on Ω and $\mathbb{\Omega}_n$ of scalars, vectors or tensors; that is

$$\langle f,\ g \rangle = \int_\Omega f\, g \ \mathrm{d}\Omega, \tag{3.13}$$

$$(f,\ g)_n = \int_{t_n}^{t_{n+1}} \langle f,\ g \rangle \ \mathrm{d}t, \tag{3.14}$$

for any function f and g defined on $\mathbb{\Omega}_n$.

The boundary version of the space-time integral will have the form

$$(f,\ g)_{\mathbb{I}_n^\square} = \int_{t_n}^{t_{n+1}} \int_{\Gamma_\square} f\, g\ \mathrm{d}\Omega \mathrm{d}t.$$

The jump in a time-discontinuous function f at time τ is defined by

$$[\![f(\tau)]\!] = f(\tau^+) - f(\tau^-),$$

where the left and right values of f are

$$f(\tau^\pm) = \lim_{t \to \tau^\pm}\ f(t).$$

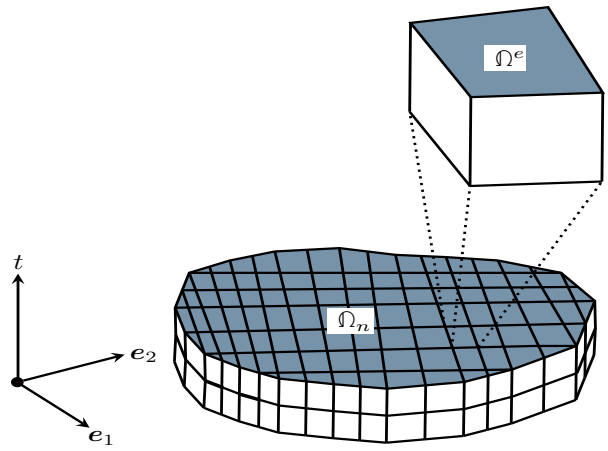

Fig. 3.2: Typical space-time slab mesh

3.3.2 Mechanical problem/phase

Recall that the problem in the mechanical phase is given by

$$\begin{aligned} \dot{\boldsymbol{u}} &= \boldsymbol{v}, \\ \rho\dot{\boldsymbol{v}} &= \mathrm{div}[\mathbb{C}\boldsymbol{\varepsilon} - \mathbf{m}\vartheta] + \boldsymbol{b}, \\ \dot{\alpha} &= 0, \\ \rho\Theta_0\dot{\eta} &= 0, \end{aligned} \tag{3.15}$$

subject to some initial and boundary conditions which will be discussed below. Here the domain of the problem is the space-time slab Ω_n, with boundaries as shown in Fig. 3.3.

Given (approximate) solutions $\boldsymbol{u}(\tau)$,$\boldsymbol{v}(\tau)$, $\alpha(\tau)$, and $\vartheta(\tau)$ at the end of the previous slab Ω_{n-1}; that is, on $\tau = t_n^-$, the objective in the mechanical phase is to find (predictor) solutions $\boldsymbol{u}(t)$, $\boldsymbol{v}(t)$, $\alpha(t)$, and an *intermediate temperature*[1] $\vartheta^I(t)$ with $t \in I_n$ that will be passed to the thermal phase. Since $\dot{\alpha} = 0$ during the mechanics, its value in the current slab equals that of at the end of the previous slab Ω_{n-1}, that is $\alpha(t) = \alpha(t_n^-)$.

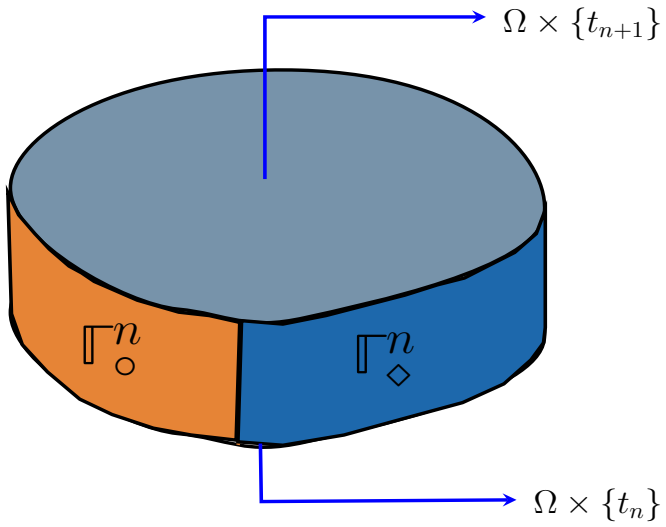

Fig. 3.3: The n^{th} space-time slab and its boundaries

Applying the constitutive relation $(2.10)_2$ to $(3.15)_4$ leads to

$$\rho\Theta_0\dot{\eta} = \frac{\mathrm{d}}{\mathrm{d}t}\left[\rho c\vartheta + \rho\Theta_0\mathbf{m} : \boldsymbol{\varepsilon}(\boldsymbol{u})\right] = 0 \quad \text{on} \quad \Omega_n. \tag{3.16}$$

Equation (3.16) is then solved in closed form to obtain ϑ^I on the n^{th} space-time slab Ω_n. As a consequence the explicit formula for ϑ^I in terms of the rest of the state variables in the current space-time slab Ω_n and at the end of Ω_{n-1}, ϑ^I is given by

[1] The phrase 'intermediate temperature' is used to emphasize that the solution is determined before the problem is completely solved; and it is then used as an input to redefine the problem in the mechanical phase.

$$\vartheta^I(t) = \vartheta(t_n^-) - \frac{\Theta_0}{c}\mathbf{m} : [\boldsymbol{\varepsilon}(t) - \boldsymbol{\varepsilon}(t_n^-)], \qquad \text{for } \; t \in (t_n, t_{n+1}), \tag{3.17}$$

where $\boldsymbol{\varepsilon}(t)$, $\boldsymbol{\varepsilon}(t_n^-)$ represent the infinitesimal strain tensors for the displacement at t and t_n^-, respectively. Substitution of the explicit formula (3.17) for ϑ^I into the constitutive relation for the stress $(2.10)_1$ (which depends on the temperature) leads to the problem in the mechanical phase in the form

$$\begin{aligned} \dot{\boldsymbol{u}} &= \boldsymbol{v}, \\ \rho\dot{\boldsymbol{v}} &= \operatorname{div}[\mathbb{C}_{\mathrm{ad}}\boldsymbol{\varepsilon}(\boldsymbol{u})] + \boldsymbol{f}, \end{aligned}$$

where the so called *adiabatic elasticity tensor* $\mathbb{C}_{\mathrm{ad}}$, and the modified loading $\boldsymbol{f}$ are given by

$$\mathbb{C}_{\mathrm{ad}} = \mathbb{C} + (\Theta_0/c)\mathbf{m} \otimes \mathbf{m}, \quad \text{and} \quad \boldsymbol{f} = \boldsymbol{b} + \operatorname{div} \check{\boldsymbol{\sigma}}.$$

Here $\check{\boldsymbol{\sigma}} = -\mathbf{m}[\vartheta(t_n^-) + (\Theta_0/c)\mathbf{m} : \boldsymbol{\varepsilon}(t_n^-)]$ denotes the component of the stress tensor such that $\boldsymbol{\sigma} = \mathbb{C}_{\mathrm{ad}}\boldsymbol{\varepsilon} + \check{\boldsymbol{\sigma}}$. Consequently, the space-time boundary condition which arises from the Neumann boundary condition reads

$$[\mathbb{C}_{\mathrm{ad}}\boldsymbol{\varepsilon}]\boldsymbol{n} + \check{\boldsymbol{\sigma}}\boldsymbol{n} = \boldsymbol{\sigma}\boldsymbol{n} = \widehat{\boldsymbol{t}} \qquad \text{on } \; \mathbb{\Gamma}_{\boldsymbol{t}}^n.$$

Note that, since the thermomechanical coupling tensor $\mathbf{m}$ is positve-semidefinite the adiabatic elasticity tensor $\mathbb{C}_{\mathrm{ad}}$ retains the positive-definiteness and symmetry properties of the classical elasticity tensor $\mathbb{C}$. The modified loading $\boldsymbol{f}$ contains information about the states of the displacement and the temperature at the end of the previous space time slab $\mathbb{\Omega}_{n-1}$. Mathematically, the problem (3.3.2) is essentially equivalent to classical linear elasticity.

At this stage, what remains is essentially to find the solutions $\boldsymbol{u}$ and $\boldsymbol{v}$ on the current slab $\mathbb{\Omega}_n$. Approximation of these solutions will be done in the space-time finite element framework based on a time-discontinuous weak formulation of the strong form (3.3.2) subject to the corresponding boundary conditions and $\boldsymbol{u}(t_n^-)$ and $\boldsymbol{v}(t_n^-)$ as initial conditions[2] with respect to the current space-time slab.

[2] Locally, in space-time finite elements context, space and time in the slab $\mathbb{\Omega}_n$ are basically indistinguishable, as a result the current initial conditions $\boldsymbol{u}(t_n^-)$ and $\boldsymbol{v}(t_n^-)$ can be viewed as Dirichlet boundary conditions prescribed on the space-time boundary $\Omega \times \{t_n\}$, as shown in Fig. 3.3.

To give a complete definition of the time-discontinuous weak problem of the mechanical phase (3.3.2), we first define the weight function spaces for displacement $\boldsymbol{u}$ and velocity $\boldsymbol{v}$ vector fields by

$$\begin{aligned}\mathbb{S}_{\boldsymbol{u}} &\coloneqq \big\{\bar{\boldsymbol{u}}\colon \Omega_n \mapsto \mathbb{R}^d \big|\ \bar{\boldsymbol{u}}\big|_{\Gamma^n_{\boldsymbol{u}}} = \boldsymbol{0}\},\\ \mathbb{S}_{\boldsymbol{v}} &\coloneqq \big\{\bar{\boldsymbol{v}}\colon \Omega_n \mapsto \mathbb{R}^d \big|\ \bar{\boldsymbol{v}}\big|_{\Gamma^n_{\boldsymbol{v}}} = \boldsymbol{0}\}.\end{aligned} \tag{3.18}$$

Recall the definition of the trial function spaces $\mathbb{V}_{\boldsymbol{u}}$ and $\mathbb{V}_{\boldsymbol{v}}$, for classical linear elastodynamics where one typically chooses

$$\mathbb{V}_{\boldsymbol{u}},\ \mathbb{S}_{\boldsymbol{u}} \in [H^1(\Omega;\ I_n)]^d, \qquad \text{and } \mathbb{V}_{\boldsymbol{v}},\ \mathbb{S}_{\boldsymbol{v}} \in [L^2(\Omega;\ I_n)]^d,$$

where $[H^1(\Omega;\ I_n)]^d$ and $[L^2(\Omega;\ I_n)]^d$ are spaces of sufficiently smooth mappings from I_n into $H^1(\Omega)$ and $[L^2(\Omega)$, respectively.

The time-discontinuous weak statement for the problem (3.15) in the mechanical phase reads as follows: find $(\boldsymbol{u}, \boldsymbol{v}) \in \mathbb{V}_{\boldsymbol{u}} \times \mathbb{V}_{\boldsymbol{v}}$ such that for all $(\bar{\boldsymbol{u}}, \bar{\boldsymbol{v}}) \in \mathbb{S}_{\boldsymbol{u}} \times \mathbb{S}_{\boldsymbol{v}}$

$$A_n^M\big((\boldsymbol{u}, \boldsymbol{v}), (\bar{\boldsymbol{u}}, \bar{\boldsymbol{v}})\big) = b_n^M\big((\bar{\boldsymbol{u}}, \bar{\boldsymbol{v}})\big), \tag{3.19}$$

where

$$\begin{aligned}A_n^M\big((\boldsymbol{u}, \boldsymbol{v}), (\bar{\boldsymbol{u}}, \bar{\boldsymbol{v}})\big) &= (\dot{\boldsymbol{u}},\ \bar{\boldsymbol{u}})_{\Omega_n} - (\boldsymbol{v},\ \bar{\boldsymbol{u}})_{\Omega_n} + (\rho\dot{\boldsymbol{v}},\ \bar{\boldsymbol{v}})_{\Omega_n} + (\mathbb{C}_{\text{ad}}\boldsymbol{\varepsilon}(\boldsymbol{u}),\ \boldsymbol{\varepsilon}(\bar{\boldsymbol{v}}))_{\Omega_n}\\ &\qquad + \langle \boldsymbol{u}(t_n^+),\ \bar{\boldsymbol{u}}(t_n^+)\rangle + \langle \rho\boldsymbol{v}(t_n^+),\ \bar{\boldsymbol{v}}(t_n^+)\rangle,\\ b_n^M\big((\bar{\boldsymbol{u}}, \bar{\boldsymbol{v}})\big) &= (\widehat{\boldsymbol{t}},\ \bar{\boldsymbol{v}})_{\Gamma^n_{\boldsymbol{t}}} + (\boldsymbol{b},\ \bar{\boldsymbol{v}})_{\Omega_n} - (\check{\boldsymbol{\sigma}},\ \boldsymbol{\varepsilon}(\bar{\boldsymbol{v}}))_{\Omega_n} + \langle \boldsymbol{u}(t_n^-),\ \bar{\boldsymbol{u}}(t_n^+)\rangle\\ &\qquad + \langle \rho\boldsymbol{v}(t_n^-),\ \bar{\boldsymbol{v}}(t_n^+)\rangle.\end{aligned}$$

Following the standard Galerkin finite element approach, the space-time slab Ω_n is further triangulated into space-time simplexes on which conforming scalar valued shape functions are defined resulting in a finite number of piecewise continuous functions, which are taken to be basis functions for a finite element space. From such a space of functions we then construct the finite dimensional counterpart of the trial (3.8) and weighted (3.18) spaces. Later, the finite dimensional trial and weighted functions are used in the time-discontinuous weak formulation leading to a system of linear algebraic equations. Finally, the system will be solved to obtain approximate solutions $\boldsymbol{u}$ and $\boldsymbol{v}$

in the current slab $\mathbb{\Omega}_n$. In summary, the solutions of the mechanical phase at the end of the current space-time slab are $\boldsymbol{u}(t_{n+1}^-)$, $\boldsymbol{v}(t_{n+1}^-)$, $\alpha(t_n^-)$, and $\vartheta^I(t_{n+1}^-)$.

Remarks

1) The main difference between the DG formulation presented here in (3.19) and that of in [52] is the inner product used to weakly enforce the problem (3.15). The current formulation employs the space-time L^2-inner product as defined in (3.13), while in [52] an energy-inner product is used to weakly enforce the mechanical problem.

2) The formulation (3.19) is consistent with the local form (3.15). This can be seen from the Euler-Lagrange form of (3.19) given by

$$
\begin{aligned}
0 &= A_n^M\big((\boldsymbol{u},\boldsymbol{v}),(\bar{\boldsymbol{u}},\bar{\boldsymbol{v}})\big) - b_n^M\big((\bar{\boldsymbol{u}},\bar{\boldsymbol{v}})\big),\\
&= (\dot{\boldsymbol{u}}-\boldsymbol{v},\ \bar{\boldsymbol{u}})_{\mathbb{\Omega}_n} + (\rho\dot{\boldsymbol{v}} - \mathrm{div}[\mathbb{C}_{\mathrm{ad}}\boldsymbol{\varepsilon}(\boldsymbol{u})] - \boldsymbol{f},\ \bar{\boldsymbol{v}}) \qquad \text{(equation of motion)}\\
&\quad + \langle [\![\boldsymbol{u}]\!]_n,\ \bar{\boldsymbol{u}}(t_n^+)\rangle \qquad \text{(displacement continuity)}\\
&\quad + \langle [\![\rho\boldsymbol{v}]\!]_n,\ \bar{\boldsymbol{v}}(t_n^+)\rangle, \qquad \text{(velocity continuity)} \qquad (3.20)
\end{aligned}
$$

that upon substitution of a sufficiently smooth solution pair $(\boldsymbol{u},\boldsymbol{v})$ of the strong form (3.15) into (3.20), the weak forms of the jumps and the equation of motion vanish.

3) The jump terms provide the stability of the scheme without degrading the accuracy. The fact that the weak formulation used the space-time L^2-inner product to enforce the displacement-velocity relation $(3.3.2)_1$ produces a formalism can be readily extended to the nonlinear case without eliminating the jump term from the displacement-velocity relation.

4) Another consequence of using the L^2-inner product is that a Dirichlet-type boundary condition may not be necessary to define the velocity trial and weight function spaces, as it will be taken care of using the weak form of the displacement-velocity relation and the enforcement of the displacement Dirichlet boundary condition. In this case, we may replace both the velocity trial $\mathbb{V}_{\boldsymbol{v}}$ and test $\mathbb{S}_{\boldsymbol{v}}$ spaces by $[L^2(\mathbb{\Omega}_n; I_n)]^d$, which basically avoids the complication in incorporating the boundary condition into the discrete problem.

3.3.3 Thermal problem

The thermal phase represents, in the general context, the propagation of thermal energy at fixed configuration and velocity (i.e. in a rigid body). Hence the strong form of the problem in the thermal phase reads

$$\begin{aligned} \dot{\boldsymbol{u}} &= \mathbf{0}, \\ \rho\dot{\boldsymbol{v}} &= \mathbf{0}, \\ \dot{\alpha} &= \Theta, \\ \rho\Theta_0\dot{\eta} &= \operatorname{div}[\mathbf{k}_1\nabla\alpha + \mathbf{k}_2\nabla\Theta] + \rho r, \end{aligned}$$

subject to appropriate initial and boundary conditions which will be discussed later. Once again the domain of definition is the n^{th} space-time slab Ω_n with its boundaries, as shown in Fig. 3.3.

At this stage, it is important to note that for single-pass algorithms, in each space-time slab the problem in mechanical phase is first solved and then its solution at the end of the slab is passed to the problem in the thermal phase. The solution of the problem in the thermal phase is, therefore, taken as an approximate solution to the global coupled problem in that particular slab. To this end, the solutions $\boldsymbol{u}(t_{n+1}^-)$, $\boldsymbol{v}(t_{n+1}^-)$, $\alpha(t_n^-)$, and $\vartheta^I(t_{n+1}^-)$ from the mechanical phase are used as initial conditions for the problem in the thermal phase.

Note that the displacement and velocity fields are fixed during the thermal phase, which implies that their values from the mechanical phase at the end of the previous slab are also the solutions in the thermal phase. In other words, during the thermal phase the displacement and velocity are fixed at the values $\boldsymbol{u}(t_{n+1}^-)$ and $\boldsymbol{v}(t_{n+1}^-)$.

Consequently, the thermal phase is reduced to the problem of finding (approximate) solutions $\alpha(t_{n+1}^-)$, and $\vartheta(t_{n+1}^-)$ which, in some weak sense, satisfy

$$\begin{aligned} \dot{\alpha} &= \Theta, \\ \rho\Theta_0\dot{\eta} &= \operatorname{div}[\mathbf{k}_1\nabla\alpha + \mathbf{k}_2\nabla\Theta] + \rho r, \end{aligned} \tag{3.21}$$

on the space-time domain $\mathbb{\Omega}_n$ subject to appropriate initial and boundary conditions. The role played by enforcing the heat conduction equation (3.21) allows us to express the initial conditions in terms of the entropy and thermal displacement.

Let us, for now, denote the entropy corresponding to the mechanical and thermal phases by η^M and η^T respectively. Then as the entropy is fixed at $\eta(t_n^-)$ during the mechanical phase, we obtain

$$\eta^T(t_n^-) = \eta^M(t_{n+1}^-) = \eta(t_n^-). \tag{3.22}$$

The jump $[\![\Theta_0\rho\eta^T(t_n)]\!]$ with respect to the thermal phase at the interface of the previous and the current space-time slabs $\mathbb{\Omega}_{n-1}$ and $\mathbb{\Omega}_n$ becomes

$$\begin{aligned}
[\![\Theta_0\rho\eta^T(t_n)]\!] &= \Theta_0\rho\eta^T(t_n^+) - \Theta\rho\eta^T(t_n^-),\\
&= \Theta_0\rho\eta(t_n^+) - \Theta_0\rho\eta^M(t_{n+1}^-),\\
&= \Theta_0\rho\eta(t_n^+) - \Theta_0\rho\eta(t_n^-), \qquad \text{(by (3.22))}\\
&= [\![\Theta_0\rho\eta(t_n)]\!].
\end{aligned} \tag{3.23}$$

The solution of the thermal phase is the solution of the global problem: this is the reason why we omit the superscript T in second step of (3.23). From the time derivative of the entropy and constitutive relation $(2.10)_2$, in the thermal phase we obtain

$$\Theta_0\rho\dot{\eta} = \rho c\dot{\vartheta} + \Theta_0\mathbf{m} : \boldsymbol{\varepsilon}(\boldsymbol{v}(t_{n+1}^-)).$$

In addition to the jump of the entropy (3.23) we also have the jump in the thermal displacement given by

$$[\![\alpha^T(t_n)]\!] = \alpha^T(t_n^+) - \alpha^T(t_n^-) = \alpha(t_n^+) - \alpha(t_n^-).$$

To define the time-discontinuous weak formulation for the thermal phase we first define the spaces of test functions for thermal displacement α and temperature ϑ by:

$$\begin{aligned}
\mathbb{S}_\alpha &\coloneqq \big\{\bar{\alpha}\colon \mathbb{\Omega}_n \mapsto \mathbb{R}\big|\ \bar{\alpha}\big|_{\mathbb{\Gamma}_\vartheta^n} = 0\big\},\\
\mathbb{S}_\vartheta &\coloneqq \big\{\bar{\vartheta}\colon \mathbb{\Omega}_n \mapsto \mathbb{R}\big|\ \bar{\vartheta}\big|_{\mathbb{\Gamma}_\vartheta^n} = 0\big\}.
\end{aligned} \tag{3.24}$$

Formally, the time-discontinuous Galerkin weak formulation of the problem (3.21) in the thermal phase reads as: find $(\alpha, \vartheta) \in \mathbb{V}_\alpha \times \mathbb{V}_\vartheta$ such that for each $(\bar{\alpha}, \bar{\vartheta}) \in \mathbb{S}_\alpha \times \mathbb{S}_\vartheta$

$$A_n^T\big((\alpha, \vartheta), (\bar{\alpha}, \bar{\vartheta})\big) = b_n^T\big((\bar{\alpha}, \bar{\vartheta})\big), \tag{3.25}$$

where

$$\begin{aligned} A_n^T\big((\alpha, \vartheta), (\bar{\alpha}, \bar{\vartheta})\big) &= (\dot{\alpha},\ \bar{\alpha})_{\mathfrak{Q}_n} - (\Theta,\ \bar{\alpha})_{\mathfrak{Q}_n} + (\rho c\dot{\vartheta},\ \bar{\vartheta})_{\mathfrak{Q}_n} + (\boldsymbol{q},\ \nabla\bar{\vartheta})_{\mathfrak{Q}_n} \\ &\quad + \langle \alpha(t_n^+),\ \bar{\alpha}(t_n^+)\rangle + \langle \Theta_0\rho\eta(t_n^+),\ \bar{\vartheta}(t_n^+)\rangle, \end{aligned}$$

$$\begin{aligned} b_n^T\big((\bar{\alpha}, \bar{\vartheta})\big) &= \langle \alpha(t_n^-),\ \bar{\alpha}(t_n^+)\rangle - (\Theta_0\mathbf{m} : \boldsymbol{\varepsilon}(\boldsymbol{v}(t_{n+1}^-)),\ \bar{\vartheta})_{\mathfrak{Q}_n} \\ &\quad + \langle \Theta_0\rho\eta(t_n^-),\ \bar{\vartheta}(t_n^+)\rangle + (\widehat{h}, \bar{\vartheta})_{\mathbb{\Gamma}_\vartheta^n} + (\rho r, \bar{\vartheta})_{\mathfrak{Q}_n}. \end{aligned}$$

By applying the standard finite element procedure on space-time slab, we solve the algebraic version of (3.25) to obtain the final solution $\boldsymbol{u}(t_{n+1}^-)$, $\boldsymbol{v}(t_{n+1}^-)$, $\alpha(t_{n+1}^-)$, and $\vartheta(t_{n+1}^-)$ for the global coupled problem at the end of the current space-time slab $\mathfrak{Q}_n$.

The consistency of weak formulation (3.25) with the point-wise form (3.21) is apparent from the Euler-Lagrange form

$$\begin{aligned} 0 &= A_n^T\big((\alpha, \vartheta), (\bar{\alpha},\ \bar{\vartheta})\big) - b_n^T\big((\bar{\alpha}, \bar{\vartheta})\big) \\ &= (\dot{\alpha} - \Theta, \bar{\alpha})_{\mathfrak{Q}_n} \\ &\quad + (\rho\Theta_0\dot{\eta} + \operatorname{div}\boldsymbol{q} + \rho r,\ \bar{\vartheta})_{\mathfrak{Q}_n} && \text{(Energy balance)} \\ &\quad + \langle [\![\alpha(t_n)]\!],\ \bar{\alpha}(t_n^+)\rangle && (\alpha\text{-continuity}) \\ &\quad + \langle [\![\Theta_0\rho\eta(t_n)]\!],\ \bar{\vartheta}(t_n^+)\rangle, && (\vartheta\text{-continuity}) \end{aligned}$$

which reveals that a sufficiently smooth solution of the strong problem (3.21) also satisfies (3.25), in which case, the jump terms vanish for the smooth solution.

Remark: The use of the L^2-inner product to enforce the thermal problem allows one to omit the boundary restriction when we define the thermal displacement trial and weight function space. i.e.

$$\mathbb{V}_\alpha = \mathbb{S}_\alpha \coloneqq L^2(\Omega;\ I_n).$$

This is a very important observation in terms of the practical implementation as no boundary condition is needed with respect to α. However, the energy-inner product

based formulation of Hughes and Hulbert [51] requires the implementation of consistent (which, in a way, is repetitive) boundary conditions for both α and ϑ. This implementation simplicity persists to the nonlinear case as well.

4

Numerical stability

In this chapter we address the issue of numerical stability of the scheme for linear generalized thermoelasticity based on operator-splitting and the time-discontinuous Galerkin formulation.

The notion of stability in a time-stepping algorithmic sense is briefly reviewed in Section 4.1. Stability results for both the mechanical and thermal phase numerical schemes are then presented and proven.

4.1 Algorithmic stability

Let $\boldsymbol{\mathcal{X}}^0$ and $\tilde{\boldsymbol{\mathcal{X}}}^0$ be two initial conditions for which an algorithm $\mathbb{A}^{\Delta t_n}$, which corresponds to the time domain decomposition into subintervals I_n with step length Δt_n as presented in Section 3.1, generates the sequence of (approximate) solutions $\{\boldsymbol{\mathcal{X}}^n\}_{n=0}^N$ and $\{\tilde{\boldsymbol{\mathcal{X}}}^n\}_{n=0}^N$; that is

$$\boldsymbol{\mathcal{X}}^{n+1} = \mathbb{A}^{\Delta t_n}\boldsymbol{\mathcal{X}}^n, \quad \text{and} \quad \tilde{\boldsymbol{\mathcal{X}}}^{n+1} = \mathbb{A}^{\Delta t_n}\tilde{\boldsymbol{\mathcal{X}}}^n \quad n = 0, 1, \ldots, N-1.$$

We say that the algorithm $\mathbb{A}^{\Delta t_n}$ is *stable* if there exists $\beta \geq 0$ such that

$$\|\mathbb{A}^{\Delta t_n}\boldsymbol{\mathcal{X}}^n - \mathbb{A}^{\Delta t_n}\tilde{\boldsymbol{\mathcal{X}}}^n\|_{\mathcal{V}} \leq \|\boldsymbol{\mathcal{X}}^n - \tilde{\boldsymbol{\mathcal{X}}}^n\|_{\mathcal{V}}, \tag{4.1}$$

for all $0 \leq \Delta t_n \leq \beta$ and $n = 0, 1, \ldots, N$. In the nonlinear context, the estimate (4.1) is also referred to as *B-stability*. If $\beta = \infty$, we say that the algorithm is unconditionally (B-)stable.

Observe that, in the linear case, the difference $\boldsymbol{e}^n = \boldsymbol{\mathcal{X}}^n - \tilde{\boldsymbol{\mathcal{X}}}^n$ is also a solution corresponding to the initial data $\boldsymbol{e}^0 = \boldsymbol{\mathcal{X}}^0 - \tilde{\boldsymbol{\mathcal{X}}}^0$. Thus, the stability estimate (4.1) is equivalent to

$$\|\boldsymbol{\mathcal{X}}^{n+1}\|_{\mathcal{V}} \leq \|\boldsymbol{\mathcal{X}}^n\|_{\mathcal{V}}, \quad \text{or} \quad \mathscr{E}(\boldsymbol{\mathcal{X}}^{n+1}) \leq \mathscr{E}(\boldsymbol{\mathcal{X}}^n) \qquad \text{for all } n = 0, 1, \ldots, N-1, \quad (4.2)$$

for each sequence of approximate solutions $\{\boldsymbol{\mathcal{X}}^n\}_{n=0}^N$ generated by the algorithm $\mathbb{A}^{\Delta t_n}$. Here $\mathscr{E}(\cdot)$ denotes the so-called *canonical free energy functional* for the linear generalized thermoelasticity as defined in (2.22).

The following Lemma relates the stability of a time-stepping algorithm based on operator-splitting to that of the individual algorithm comprising it. Consequently, for such time-stepping algorithm to be stable, it suffices to show that individual algorithms are stable.

Lemma 4.1. *In the linear case, if each algorithm $\mathbb{A}_i^{\Delta t}$ with $i = 1, 2$ is stable, then the single-pass algorithm* (3.3) *is also stable.*

Proof. Let $\{\boldsymbol{\mathcal{X}}^n\}_{n=0}^N$ and $\{\tilde{\boldsymbol{\mathcal{X}}}^n\}_{n=0}^N$ be two sequences of approximate solutions generated by $\mathbb{A}^{\Delta t}$, then we have

$$\begin{aligned}
\|\mathbb{A}^{\Delta t_n}\boldsymbol{\mathcal{X}}^n - \mathbb{A}^{\Delta t_n}\tilde{\boldsymbol{\mathcal{X}}}^n\| &= \|\mathbb{A}_1^{\Delta t_n}\mathbb{A}_2^{\Delta t_n}\boldsymbol{\mathcal{X}}^n - \mathbb{A}_1^{\Delta t_n}\mathbb{A}_2^{\Delta t_n}\tilde{\boldsymbol{\mathcal{X}}}^n\| \\
&\leq \|\mathbb{A}_2^{\Delta t_n}\boldsymbol{\mathcal{X}}^n - \mathbb{A}_2^{\Delta t_n}\tilde{\boldsymbol{\mathcal{X}}}^n\| \quad \text{(by stability of } \mathbb{A}_1^{\Delta t}\text{)} \\
&\leq \|\boldsymbol{\mathcal{X}}^n - \tilde{\boldsymbol{\mathcal{X}}}^n\| \qquad \text{(by stability of } \mathbb{A}_2^{\Delta t}\text{)}.
\end{aligned}$$

□

For the sake of simplicity it is assumed that the heat source $r = 0$, there is no external loading ($\boldsymbol{b} = \boldsymbol{0}$), and thermal and mechanical boundary conditions are homogeneous. This is equivalent to the case in which the coupled system (2.15) is purely driven by the initial conditions. The reason for this assumption is that the question of interest is how the norm (energy) of the initial condition changes in time.

4.1.1 Mechanical phase

The mechanical version of the energy (2.22) denoted $\mathscr{E}^M(\cdot)$ is given by

$$\mathscr{E}^M\big((\boldsymbol{u},\boldsymbol{v})\big) = \frac{1}{2}\int_\Omega \big[\boldsymbol{\varepsilon}(\boldsymbol{u}) : \mathbb{C}_{\rm ad}\boldsymbol{\varepsilon}(\boldsymbol{u}) + \rho\boldsymbol{v}\cdot\boldsymbol{v}\big]\ \mathrm{d}\Omega,$$
$$= \frac{1}{2}\langle \mathbb{C}_{\rm ad}\boldsymbol{\varepsilon}(\boldsymbol{u}),\ \boldsymbol{\varepsilon}(\boldsymbol{u})\rangle + \frac{1}{2}\langle \rho\boldsymbol{v},\ \boldsymbol{v}\rangle \tag{4.3}$$

which is of course the total mechanical energy of the mechanical phase. The stability of the time-discontinuous scheme (3.19) corresponding to the mechanical phase is given in the following proposition.

Proposition 4.1. *The time-discontinous Galerkin scheme* (3.19) *for the mechanical phase is (unconditonally) stable. That is, the energy estimate*

$$\mathscr{E}^M\big((\boldsymbol{u}(t_{n+1}^-),\boldsymbol{v}(t_{n+1}^-))\big) \le \mathscr{E}^M\big((\boldsymbol{u}(t_n^-),\boldsymbol{v}(t_n^-))\big) \qquad \forall n = 0,\ 1,\ldots,N-1, \tag{4.4}$$

holds for any discrete[1] *solution* $\{(\boldsymbol{u}(t_n^-),\boldsymbol{v}(t_n^-))\}_{n=0}^N$.

Proof. We use the elliptic- and L^2-projection operators $\boldsymbol{\pi} : [H^1_{\Gamma_u}(\Omega)]^d \to \mathbb{S}_{\boldsymbol{u}}(t)$ and $\widehat{\boldsymbol{\pi}} : [L^2(\Omega)]^d \to \mathbb{S}_{\boldsymbol{v}}(t)$ respectively defined as: for $\boldsymbol{u} \in [H^1_{\Gamma_u}(\Omega)]^d$ and $\boldsymbol{w} \in [L^2(\Omega)]^d$ by

$$\begin{aligned} \langle \mathbb{C}_{\rm ad}\boldsymbol{\varepsilon}(\boldsymbol{\pi}\boldsymbol{u}),\ \boldsymbol{\varepsilon}(\boldsymbol{\varphi})\rangle &= \langle \mathbb{C}_{\rm ad}\boldsymbol{\varepsilon}(\boldsymbol{u}),\ \boldsymbol{\varepsilon}(\boldsymbol{\varphi})\rangle, \qquad && \forall \boldsymbol{\varphi} \in \mathbb{S}_{\boldsymbol{u}}(t), \\ \langle \widehat{\boldsymbol{\pi}}\boldsymbol{w},\ \boldsymbol{\psi}\rangle &= \langle \boldsymbol{w},\ \boldsymbol{\psi}\rangle, && \forall \boldsymbol{\psi} \in \mathcal{S}_{\boldsymbol{u}}(t), \end{aligned} \tag{4.5}$$

where $\mathbb{S}_\square(t)$ refers to the space of functions in $\mathcal{S}_\square$ at a fixed but arbitrary $t \in I_n$, and $H^1_{\Gamma_{\boldsymbol{u}}}$ denotes the space of functions in $H^1(\Omega)$ which vanish along the boundary $\Gamma_{\boldsymbol{u}}$. We also use the relation given in [54] that

$$\mathrm{div}\ [\mathbb{C}_{\rm ad}\boldsymbol{\varepsilon}(\boldsymbol{\pi}\boldsymbol{u})] = \widehat{\boldsymbol{\pi}}\mathrm{div}\ [\mathbb{C}_{\rm ad}\boldsymbol{\varepsilon}(\boldsymbol{u})]. \tag{4.6}$$

Given the solution $(\boldsymbol{u}(t_n^-),\boldsymbol{v}(t_n^-))$ of (3.19) at the end of the previous space-time slab $\mathbb{\Omega}_{n-1}$, let $(\boldsymbol{u},\boldsymbol{v})$ be the solution of (3.19) in the current space-time slab $\mathbb{\Omega}_n$.

Choosing the test function vector $(\bar{\boldsymbol{u}},\bar{\boldsymbol{v}}) = (\widehat{\boldsymbol{\pi}}\mathrm{div}[\mathbb{C}_{\rm ad}\boldsymbol{\varepsilon}(\boldsymbol{u})],\boldsymbol{0})$ in (3.19) we obtain

$$0 = \big(\dot{\boldsymbol{u}},\ \widehat{\boldsymbol{\pi}}\mathrm{div}[\mathbb{C}_{\rm ad}\boldsymbol{\varepsilon}(\boldsymbol{u})]\big)_{\mathbb{\Omega}_n} - \big(\boldsymbol{v},\ \widehat{\boldsymbol{\pi}}\mathrm{div}[\mathbb{C}_{\rm ad}\boldsymbol{\varepsilon}(\boldsymbol{u})]\big)_{\mathbb{\Omega}_n} + \langle [\![\boldsymbol{u}(t_n)]\!],\ \widehat{\boldsymbol{\pi}}\mathrm{div}[\mathbb{C}_{\rm ad}\boldsymbol{\varepsilon}(\boldsymbol{u}(t_n^+))]\rangle. \tag{4.7}$$

[1] Note that, in the time-discontinuous context, at each time step t_n we have two values, one from the left and the other from the right of t_n. For the sake of stability analysis of the semi-discrete scheme (3.19), we choose the sequence of solutions from the left of each time step.

The use of (4.6) in (4.7), the definition of the projection operator $\boldsymbol{\pi}$, and integration by parts (note the homogeneous boundary conditions) lead to

$$\big(\boldsymbol{\varepsilon}(\dot{\boldsymbol{u}}),\ \mathbb{C}_{\mathrm{ad}}\boldsymbol{\varepsilon}(\boldsymbol{u})\big)_{\Omega_n} - \big(\boldsymbol{\varepsilon}(\boldsymbol{v}),\ \mathbb{C}_{\mathrm{ad}}\boldsymbol{\varepsilon}(\boldsymbol{u})\big)_{\Omega_n} + \langle[\![\boldsymbol{\varepsilon}(t_n)]\!],\ \mathbb{C}_{\mathrm{ad}}\boldsymbol{\varepsilon}(\boldsymbol{u}(t_n^+))\rangle = 0. \tag{4.8}$$

Again if we choose $(\bar{\boldsymbol{u}}, \bar{\boldsymbol{v}}) = (\boldsymbol{0}, \boldsymbol{v})$ corresponding to (3.19), we obtain

$$\big(\rho\dot{\boldsymbol{v}},\ \boldsymbol{v}\big)_{\Omega_n} + \big(\mathbb{C}_{\mathrm{ad}}\boldsymbol{\varepsilon}(\boldsymbol{u}),\ \boldsymbol{\varepsilon}(v)\big)_{\Omega_n} + \langle[\![\rho\boldsymbol{v}(t_n)]\!],\ \boldsymbol{v}(t_n^+)\rangle = 0. \tag{4.9}$$

Summing the equations (4.8) and (4.9),

$$(\boldsymbol{\varepsilon}(\dot{\boldsymbol{u}}^h), \mathbb{C}_{ad}\boldsymbol{\varepsilon}(\boldsymbol{u}^h))_{Q_n} + (\rho\dot{\boldsymbol{v}}^h, \boldsymbol{v}^h)_{Q_n} + \langle[\![\boldsymbol{\varepsilon}(\boldsymbol{u}^h)]\!]_n, \mathbb{C}_{ad}\boldsymbol{\varepsilon}(\boldsymbol{u}^h(t_n^+))\rangle + \langle[\![\rho\boldsymbol{v}^h]\!]_n, \boldsymbol{v}^h(t_n^+)\rangle = 0. \tag{4.10}$$

Taking the time derivative out of the integral over the spatial domain, (4.10) becomes

$$\begin{aligned} &\frac{1}{2}\langle\boldsymbol{\varepsilon}(t_{n+1}^-),\ \mathbb{C}_{\mathrm{ad}}\boldsymbol{\varepsilon}(t_{n+1}^-)\rangle + \frac{1}{2}\langle\rho\boldsymbol{v}(t_{n+1}^-),\ \boldsymbol{v}(t_{n+1}^-)\rangle \\ &- \frac{1}{2}\langle\boldsymbol{\varepsilon}(t_n^+),\ \mathbb{C}_{\mathrm{ad}}\boldsymbol{\varepsilon}((t_n^+))\rangle - \frac{1}{2}\langle\rho\boldsymbol{v}(t_n^+),\ \boldsymbol{v}(t_n^+)\rangle \\ &+ \langle[\![\boldsymbol{\varepsilon}(t_n)]\!],\ \mathbb{C}_{\mathrm{ad}}\boldsymbol{\varepsilon}(\boldsymbol{u}(t_n^+))\rangle + \langle[\![\rho\boldsymbol{v}(t_n)]\!], \boldsymbol{v}(t_n^+)\rangle = 0. \end{aligned} \tag{4.11}$$

From (4.3) and (4.11), after some algebraic manipulations, we obtain the relation between energies of the solution at the end of the previous and current slabs which is given by

$$\mathscr{E}^M\big((\boldsymbol{u}(t_{n+1}^-), \boldsymbol{v}(t_{n+1}^-))\big) + \mathscr{E}^M\big((\![\boldsymbol{u}(t_n)]\!], [\![\boldsymbol{v}(t_n)]\!])\big) = \mathscr{E}^M\big((\boldsymbol{u}(t_n^-), \boldsymbol{v}(t_n^-))\big). \tag{4.12}$$

The adiabatic elasticity tensor $\mathbb{C}_{\mathrm{ad}}$ is positive definite and the density ρ is a positive constant the energy of the jumps $\mathscr{E}^M\big((\![\boldsymbol{u}(t_n)]\!], [\![\boldsymbol{v}(t_n)]\!])\big)$ is non-negative. Hence the relation (4.11) leads to the required stability estimate (4.4). In fact, the total numerical dissipation added is precisely equal to

$$\sum_{n=0}^{N-1} \mathscr{E}^M\big((\![\boldsymbol{u}(t_n)]\!], [\![\boldsymbol{v}(t_n)]\!])\big). \tag{4.13}$$

The consistency of the time-discontinuous weak formulation (3.19) implies that the jump (4.13) error should approach to zero as the space-time mesh refinement h ap-

proaches zero. Thus, the point-wise jump across the interfaces of the space-time slabs can serve as an error indicator in an h-adaptive scheme. $\square$

4.1.2 Thermal phase

It is important to note that, in the thermal phase, the thermomechanical coupling term is constant in time and independent of the current unknown state variables, the thermal displacement α and relative temperature ϑ. In other words, viewing the thermal phase as a separate problem, the coupling term only serves as an externally prescribed agent such as the heat source. It is clear that those external agents, once fixed, do not affect the stability of the system as it is always possible to redefine the state variables so that the problem can be converted into one without external sources. This in turn leads to a situation in which the problem is driven by the initial conditions alone. As a consequence of this, for the sake of simplicity in the analysis of algorithmic stability of the time-discontinuous scheme (3.25), we assume that the thermomechanical coupling term is zero during the thermal phase; that is,

$$\mathbf{m} : \boldsymbol{\varepsilon}(\boldsymbol{v}(t_{n+1}^-)) = 0.$$

For the problem in the thermal phase we use the energy norm in the form

$$\begin{aligned} \mathscr{E}^T\big((\alpha,\vartheta)\big) &= \int_\Omega [\nabla\alpha \cdot \mathbf{k}_1 \nabla\alpha + c\vartheta^2] \, \mathrm{d}\Omega \\ &= \langle \nabla\alpha,\ \mathbf{k}_1\nabla\alpha\rangle + \langle c\vartheta,\ \vartheta\rangle. \end{aligned} \tag{4.14}$$

In the following a result stating the stability of the time-discontinuous semi-discrete scheme (3.25) is given.

Proposition 4.2. *The time-discontinuous scheme* (3.25) *associated to the thermal phase is (unconditionally) stable. That is, the energy estimate*

$$\mathscr{E}^T\big((\alpha(t_{n+1}^-),\vartheta(t_{n+1}^-))\big) \leq \mathscr{E}^T\big((\alpha(t_n^-),\vartheta(t_n^-))\big) \qquad \forall n = 1,\ 2,\ ,\ \cdots,\ N-1, \tag{4.15}$$

holds for any discrete solution $\{(\alpha(t_n^-),\vartheta(t_n^-))\}_{n=0}^N$.

Proof. Following the same line of argument leading to (4.11) we obtain

$$
\begin{aligned}
&\frac{1}{2}\langle \nabla\alpha(t_{n+1}^-),\ \mathbf{k}_1\nabla\alpha(t_{n+1}^-)\rangle + \frac{1}{2}\langle c\vartheta(t_{n+1}^-),\ \vartheta(t_{n+1}^-)\rangle \\
&-\frac{1}{2}\langle \nabla\alpha(t_n^-),\ \mathbf{k}_1\nabla\alpha(t_n^-)\rangle - \frac{1}{2}\langle c\vartheta(t_{n+1}^-),\ \vartheta(t_{n+1}^-)\rangle \qquad . \qquad (4.16)\\
&+\big(\nabla\Theta,\ \mathbf{k}_2\nabla\Theta\big)_{\Omega_n} + \langle [\![\nabla\alpha(t_n^-)]\!],\ \mathbf{k}_1\nabla\alpha(t_n^+)\rangle + \langle [\![c\vartheta(t_n)]\!],\ \vartheta(t_n^+)\rangle = 0
\end{aligned}
$$

From (4.16) and (4.14), and after some algebraic manipulations, we obtain

$$
\mathscr{E}^T\big((\alpha(t_{n+1}^-),\vartheta(t_{n+1}^-))\big)+\big(\nabla\Theta,\ \mathbf{k}_2\nabla\Theta\big)_{\Omega_n}+\mathscr{E}^T\big(([\![\alpha(t_n)]\!],[\![\vartheta(t_n)]\!])\big) = \mathscr{E}^T\big((\alpha(t_n^-),\vartheta(t_n^-))\big).
$$

□

Using the fact that the energy of the jump terms is non-negative and the heat conduction $\mathbf{k}_2$ is positive semi-definite, the energy stability estimate (4.15) holds.

The following result states the stability of the single-pass algorithm, which is constructed in such a way that the mechanical algorithm is followed by that of the thermal algorithm, for the coupled problem of linear generalized thermoelasticity.

Proposition 4.3. *The single-pass algorithm in which the mechanical phase is solved first, followed by the thermal phase, is unconditionally stable.*

Proof. The result immediately follows from Lemma 4.1 and the Propositions 4.1 and 4.2. □

Remarks

1) As indicated in the previous chapter, the time-discontinuous weak formulation introduced in [52] uses the energy inner product to weakly enforce continuity of the displacement and velocity vectors along the interfaces of space-time slabs, while the present formulation uses the L^2-inner product. However, the use of the projection operators, defined in (4.5), reveals that the two formulations are equivalent to each other in the linear regime.

2) The energy of the jumps terms $\mathscr{E}^M\big(([\![\boldsymbol{u}(t_n)]\!],[\![\boldsymbol{v}(t_n)]\!])\big)$ and $\mathscr{E}^T\big(([\![\alpha(t_n)]\!],[\![\vartheta(t_n)]\!])\big)$ associated with the mechanical and thermal phase, respectively, accounts for the numerical dissipation that is responsible for the excellent stability behaviour of the global scheme.

3) The stability analyses carried out in this chapter are for the semi-discrete formulations in which only the time domain is discretized, leading to a series of problems on a hierarchy of space-time slabs. However, the arguments leading to the stability results of both of the schemes in the mechanical and thermal phases are independent of the discretization of the space-time slabs as long as conforming space-time finite element procedures are employed. Therefore, the stability results in this chapter are equally applicable to the fully discrete scheme.

5

Numerical investigation

In this chapter, we present a range of numerical results for type II and III problems of non-classical thermoelasticity. We start by comparing convergence of the proposed splitting scheme against a monolithic approach in which all the governing equations are solved simultaneously using the time-DG finite element method. For this, a 1-D problem of non-dimensional form is considered. The result show excellent agreement between the monolithic and the splitting schemes. Then we present various results in 1-D and 2-D. The examples in this case are designed to illustrate two key features of the time-DG scheme: (i) its performance in solving problems that involve the propagation of sharp gradients without creating spurious oscillations; and (ii) its ability to capturing the unique aspects of the non-classical theory, for example, the propagation of thermal waves and the complex response due to the coupling with the elasticity problem.

The family of problems considered in this section are organized as follows. To analyze the rate of convergence and capability of the proposed scheme, a non-dimensional form of a 1-D non-classical thermoelastic problem is presented in Section 5.1. The performance of the splitting algorithm is examined in Section 5.2.1 for an initial temperature pulse propagation in a two dimensional square plate under plane strain condition. Finally, in Section 5.2.2, a quasi-static expansion of a thick walled, infinitely long cylinder under plane strain conditions is presented, which is modelled using type I and type III theories thermoelasticity. The remarkable difference in thermal responses between the two models is also analyzed.

All simulations were performed on an Intel Core i7-4700MQ 2.4 GHz processor with 8 cores and memory capacity of 8 GB. The efficiency of the monolithic and splitting algorithms was compared using a serial computation on a single core.

The 1-D problems were solved using time-discontinuous finite element program written in the high-level language Matlab [66] for the purpose of this investigation for both monolithic and splitting approaches. Routines for computing the element contributions on rectangular space-time elements were constructed analytically in Mathematica [65] and then exported to Matlab. All computations were performed on uniform space-time meshes. As a result, element contributions were computed automatically from a typical space-time cell. Matlab direct solver is used for all computations in the 1-D case.

The 2-D problems were solved using a Mathematica-based time-discontinuous Galerkin finite element code developed by the author which utilizes AceGEN/FEM library [58]. AceGEN/FEM is a general finite element library for Mathematica which combines symbolic and numeric approaches. AceFEM uses the parallelized direct solver PARDISO [59, 87].

5.1 Non-dimensional 1-D generalized thermoelastcity

The non-dimensional form of 1-D generalized thermoelastic problem given in (2.15) is

$$\begin{aligned}
&\partial_\tau \bar{u} = \bar{v},\\
&\partial_\tau \bar{v} = \partial_\xi[\varepsilon_1 \partial_\xi \bar{u} - \bar{\vartheta}] + \bar{b},\\
&\partial_\tau \bar{\alpha} = \bar{\vartheta},\\
&\partial_\tau \bar{\vartheta} = \partial_\xi[\partial_\xi \alpha + k\partial_\xi \bar{\vartheta}] - \varepsilon_2 \partial_\xi \bar{v} + \bar{s},
\end{aligned} \tag{5.1}$$

with the dimensionless parameters

$$\varepsilon_1 = \left(\frac{v_f}{v_s}\right)^2, \qquad \varepsilon_2 = \frac{\Theta_0 m^2 E}{\rho c}, \quad \text{and} \quad k = \frac{k_2}{\sqrt{\rho c}},$$

where ε_1 denotes the square of the ratio of uncoupled velocities of the mechanical wave (or first sound) and thermal wave (or second sound), ε_2 denotes the strength of the thermomechanical coupling, and k represents the non-dimensional classical thermal diffusivity. The speed of first sound v_f is the speed of sound in the medium, that is,

$$v_f = \sqrt{\frac{E}{\rho}},$$

where E denotes the Young's modulus of the medium, while that of the second sound v_s is a characteristic feature of the theory of non-classical heat conduction by Green and Naghdi that represents the speed in which a thermal disturbance travels through the medium:

$$v_s = \sqrt{\frac{k_1}{\rho c}},$$

where k_1 is the non-classical thermal conductivity coefficient. The non-dimensional variables are given by

$$\xi = x_{_c}^{-1}x, \quad \tau = t_{_c}^{-1}t, \quad \bar{u} = u_{_c}^{-1}u, \quad \bar{v} = \frac{t_{_c}}{u_{_c}}v, \quad \bar{\alpha} = \alpha_{_c}^{-1}\alpha, \quad \bar{\vartheta} = \frac{t_{_c}}{\alpha_{_c}}\vartheta,$$

where $x_{_c}$, $t_{_c}$, $u_{_c}$, $\alpha_{_c}$ are characteristic quantities having the same dimension as x, t, u, α respectively that can be chosen according to the relations

$$\frac{x_{_c}}{t_c} = v_{_s}, \quad \frac{u_{_c}}{\alpha_{_c}} = \frac{mv_{_f}}{\rho}.$$

The nondimensional energy counterpart of (2.22) is given by

$$[\mathcal{E}(\bar{\boldsymbol{\chi}})]^2 = \int_0^{\bar{L}} \left[\varepsilon_{_1}[\partial_{_\xi}\bar{u}]^2 + \bar{v}^2 + \frac{1}{\varepsilon_{_2}}[\partial_{_\xi}\bar{\alpha}]^2 + \frac{1}{\varepsilon_{_2}}\bar{\vartheta}^2\right]\mathrm{d}\xi, \tag{5.2}$$

and the L^2-norm is

$$\|\bar{\boldsymbol{\chi}}\|^2 = \int_0^{\bar{L}} \left[\bar{u}^2 + \bar{v}^2 + \bar{\alpha}^2 + \bar{\vartheta}^2\right]\mathrm{d}\xi, \tag{5.3}$$

where $\bar{\boldsymbol{\chi}} = (\bar{u}, \bar{v}, \bar{\alpha}, \bar{\vartheta})^T$ is the state vector at a given time.

Convergence

For the purpose of the convergence analysis an exact solution to problem (5.1) is obtained in such a way that source terms $\bar{b}$ and $\bar{s}$ are suitably prescribed for a given state vector $\bar{\boldsymbol{\chi}} = (\bar{u}, \bar{\alpha}, \bar{\alpha}, \bar{\vartheta})^T$ to be an exact solution [55]. To this end let the source terms be

$$\begin{aligned} \bar{b} &= \frac{\pi^2}{4}\left[(\varepsilon_{_1} - 1)\sin(\pi\xi)\sin(\pi\tau) + \cos(\pi\xi)\cos(\pi\tau)\right], \\ \bar{s} &= \frac{\pi^2}{4}\left[k\pi\sin(\pi\xi)\cos(\pi t) + \varepsilon_{_2}\cos(\pi\xi)\cos(\pi\tau)\right], \end{aligned} \tag{5.4}$$

so that the exact solutions are

$$\begin{aligned} \bar{u}(\xi,\tau) &= \bar{\alpha} = \frac{1}{4}\sin(\pi\xi)\sin(\pi\tau), \\ \bar{v}(\xi,\tau) &= \bar{\vartheta} = \frac{\pi}{4}\sin(\pi\xi)\cos(\pi\tau), \end{aligned} \tag{5.5}$$

defined on the space-time domain $(\xi,\tau) \in [0,\bar{L}] \times [0,\bar{T}]$. Note that Dirichlet boundary conditions are derived from the analytic solutions (5.5) for all the primary fields. For the convergence analysis the values of the non-dimensional parameters are taken as $\varepsilon_{_1} = 4$, $\varepsilon_{_2} = 0.2$, $k = 0$. These values represents a strongly-coupled problem of two purely hyperbolic systems (type II thermoelasticity). The space-time domain corresponds to $\bar{L} = 1$ and $\bar{T} = 0.25$. Simulations were performed using both bilinear Q1 and biquadratic Q2 finite elements in each space-time slab with each element having an aspect ratio of one (i.e. $h = \Delta\xi = \Delta\tau$).

To compare the convergence rates of the monolithic and splitting schemes, we evaluate the L^2 and H^1 norms (spatial integrals over $[0,\ \bar{L}]$), as given in equations (5.2) and (5.3), respectively, of the error $\boldsymbol{e} = \boldsymbol{\chi}_{\text{ex}}(\bar{T}) - \boldsymbol{\chi}^h(\bar{T})$, where $\boldsymbol{\chi}_{\text{ex}}$ denotes the exact solution (5.5) and $\boldsymbol{\chi}^h$ the numerical solution corresponding to the source terms (5.4). Fig. 5.1 (a) & (b) report the *spatial convergence* results of the monolithic and operator-splitting approaches with Q1 and Q2 space-time finite element interpolations, respectively. Fig. 5.1 (a) shows a superlinear order of convergence of the Q1 splitting scheme, whereas the monolithic scheme is shown to have convergence of second-order. In contrast, Fig. 5.1 (b) shows that the convergence of the splitting scheme is degraded to just first-order with Q2, while the monolithic scheme shows more than cubic order of convergence.

Fig. 5.1 (c) & (d) present the *temporal convergence* results of the two approaches with errors of the approximate solutions computed at the mid-point, $\xi = \bar{L}/2$, and $\tau = \bar{T}$ using the ℓ_2 4-vector norm; the Euclidean metric in $\mathbb{R}^4$. Almost the same convergence behaviour is also observed temporally as was shown spatially. In this case, it is shown that splitting scheme performs better in Q1 than in Q2. Remarkably, the temporal convergence of the monolithic scheme is increased by more than 100 % from Q1 and Q2. As is expected, the first-order operator-splitting scheme performs poorly in Q2.

To compare the efficiency of the two algorithms, the respective codes are organized in such a way that computations of the element stiffness matrices and right hand-side vectors are based on essentially the same optimized routines. Matlab direct solver were used in both schemes. The only major factor that determines the efficiency of the codes of the two schemes is the time spent in solving the linear systems at each step. For this, Fig. 5.2 (a) & (b) summarize the time spent by each of the approaches as the space-time domain is uniformly refined. The horizontal axes show the total number of degree-of-freedoms per slab while the vertical axis represents the corresponding CPU times spent running each algorithm. As is shown from the figures, the times in Q1 and Q2 grow in the same fashion. Considering the difference in convergence rates between the monolithic and splitting schemes in low-order approximations such as Q1, the latter approach might be advantageous in terms of efficiency. However, this is not the case for the Q2 approximation as is evident from the gain in the case of the monolithic approach and the loss in the case of the splitting scheme as we move from lower- to higher-order schemes. However, as was discussed in Chapter 3 a second-order double–pass, staggered, time-stepping algorithm $(3.4)_1$ can be constructed. The construction and analysis of such higher-order operator-splitting algorithms will not be dealt in this thesis.

Laser pulse propagation

Consider a one-dimensional bar occupying the interval $\xi \in [0, 1]$, heated by a pulsing laser applied at the left end having the form similar to that considered in [68] for non-Fourier heat conduction problem:

$$\bar{s}(\xi, \tau) = \frac{1}{D\tau_{_p}} \exp\left[\left(\frac{\xi}{D}\right)^2 - \left(\frac{\tau}{\tau_{_p}}\right)^2\right].$$

Here D is the depth and $\tau_{_p}$ the characteristic duration of the pulse. The bar is clamped at both ends at all times and has homogeneous initial conditions. We consider a situation in which a highly localized thermal pulse both in space and time described by the constants $\tau_{_p} = 0.01$ and $D = 0.02$ is applied at the left end of the bar. The parameters considered here are $\varepsilon_1 = 9$, which represents a $3:1$ ratio of *uncoupled* speeds of first

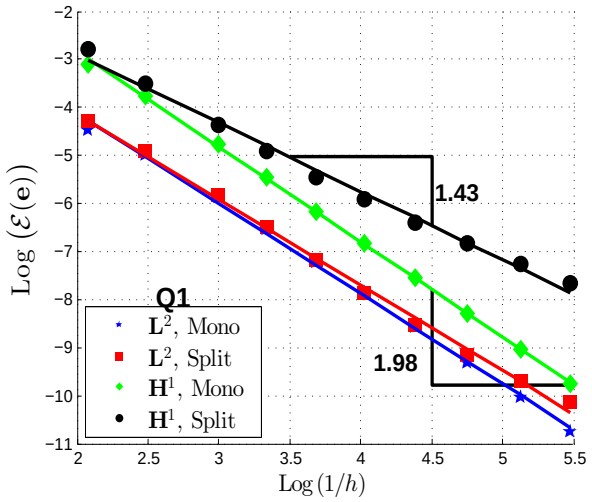

(a) Q1: Spatial convergence

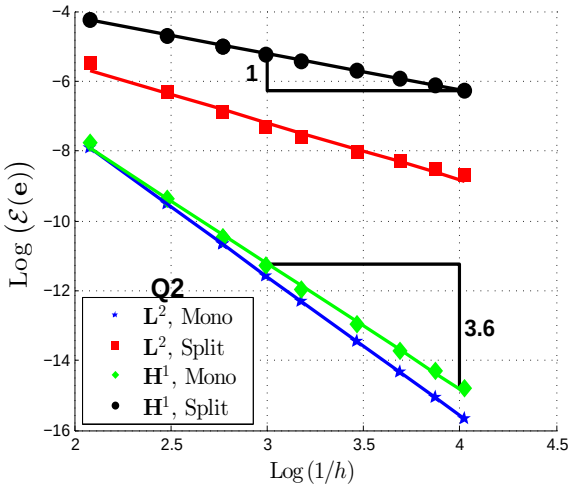

(b) Q2: Spatial convergence

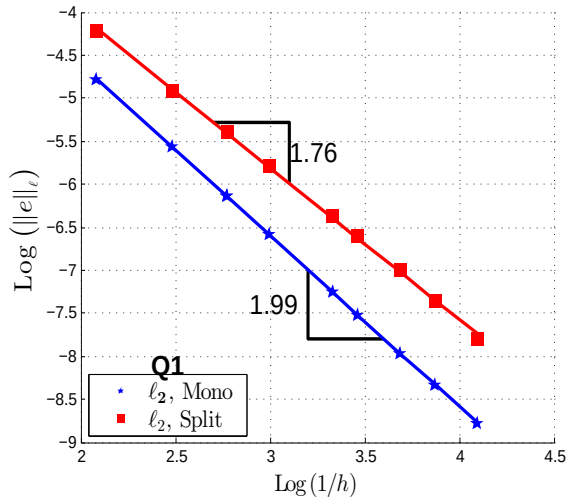

(c) Q1: Temporal convergence

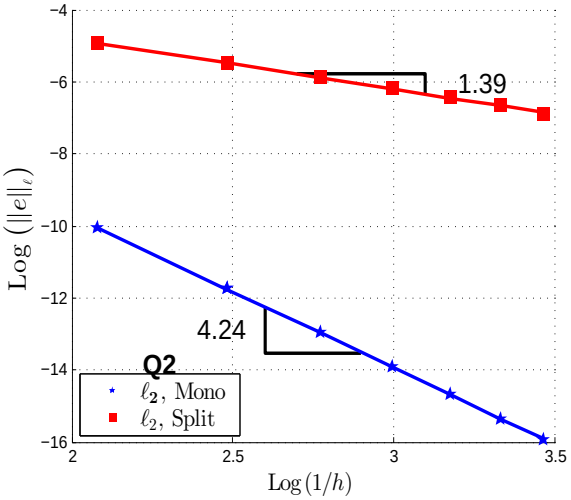

(d) Q2: Temporal convergence

Fig. 5.1: Type II thermo-mechanical problem: Rate of convergence using monolithic and splitting approaches where the error norms in (a) and (b) are computed at $\tau = 0.25$ over the whole spatial domain, while the ℓ_2-errors are evaluated at $\tau = \bar{T}/4$ and $\xi = \bar{L}/2$.

sound to second sound, and $\varepsilon_2 = 1$ accounts for a strongly-coupled system. Both ends of the bar are thermally insulated. Bilinear elements (Q1) are used in each space-time slab with mesh dimension $\Delta\xi = \Delta\tau = h$. The simulations are carried out over the period of $\bar{T} = 1$ unit of non-dimensional time. The mesh parameter $h = 0.001$ is chosen such that the width of the pulse is greater than the mesh size. In other words, the

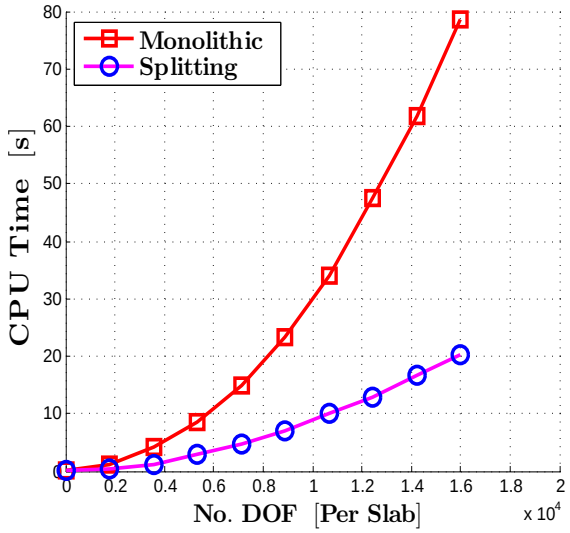

(a) Q1

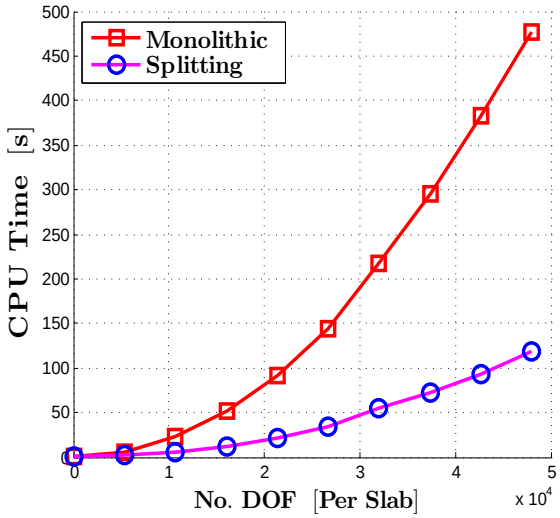

(b) Q2

Fig. 5.2: Comparison of efficiency of the monolithic and splitting algorithms in Q1 and Q2 cases. CPU time is measured using a serial computation on a single core.

mesh is chosen so that the laser pulse can be described accurately by the bilinear finite elements.

Fig. 5.3 (a) & (b) show the propagation, in space and time, of the thermal disturbance caused by the pulsing laser heat source applied at the left end of the bar, computed using the monolithic and the splitting schemes, respectively. As can be seen from the figures, immediately after the pulse is applied, two thermal waves with different amplitude and speed emerge. The larger and the slower wave is the one which is driven by the thermal equations, while the smaller and the faster one is induced by the mechanical equations through the coupling. The larger thermal wave travels with a speed slightly less than that of second sound, whereas the smaller thermal wave is travelling with a speed slightly greater than that of first sound. For this reason, it appears that the larger wave traverses the bar once, while the smaller traverses it just more than three times. Note that the ratio of uncoupled speed of first to second sound is exactly $3:1$.

There are two features which show the strength of the thermomechanical coupling: the first is that the ratio of the speeds of the two thermal waves is noticeably different from what is expected in the uncoupled case, and the other is that the coupling is strong enough to induce a stress wave which in turn induces the faster thermal wave.

Furthermore, this problem represents a strongly coupled system of two second-order hyperbolic sub-systems involving propagation of sharp gradients. Such a problem is typically very difficult to approximate using the standard semi-discrete approach Method–of–Lines (MoL) unless some kind of stabilization term (or an artificial viscosity) is added. This is equivalent to changing the system from non-dissipative to dissipative, or a very fine mesh is used together with a very small time-step, which is undesirable from a computational cost point of view.

What is remarkable about the current scheme is that it resolves the propagation of high gradients accurately while the amplitudes of the thermal waves appear to be constant, showing that the very small numerical dissipation is enough to damp out any numerical oscillation. The two approximate solution profiles in Fig. 5.3 (a) and (b) are nearly identical. The agreement demonstrates that the splitting scheme maintains the accuracy of the monolithic scheme while the efficiency is considerably improved (about 4 times faster) by the splitting scheme since two smaller systems are solved at each space-time slab. The result obtained here can be qualitatively compared to those in [13].

As shown from Fig. 5.4, other than some small numerical instabilities when the waves interact either with the boundary or each other, the energy computed using the H^1-norm remains essentially constant after the pulse is applied. This phenomenon is a characteristic feature of type II thermoelasticity which is shown in Section 2.4. The L^2-norm shows a more profound variation than the energy-norm immediately after the pulse is applied and when the two waves interact with each other, but it shows no change when the waves interact with the boundary. These observations suggest that the numerical instability arising from the the interaction of waves with the boundaries may come from errors in the gradient of the approximate solution states.

Fig. 5.5 (a) and (b) show the temperature profiles for $k = 0.1$, which correspond to Type III thermoelasticity, approximated using the monolithic and splitting schemes, respectively. This case is characterized by dissipation of energy while a wave scenario is still evident. The thermal wave driven by the temperature equations is damped out

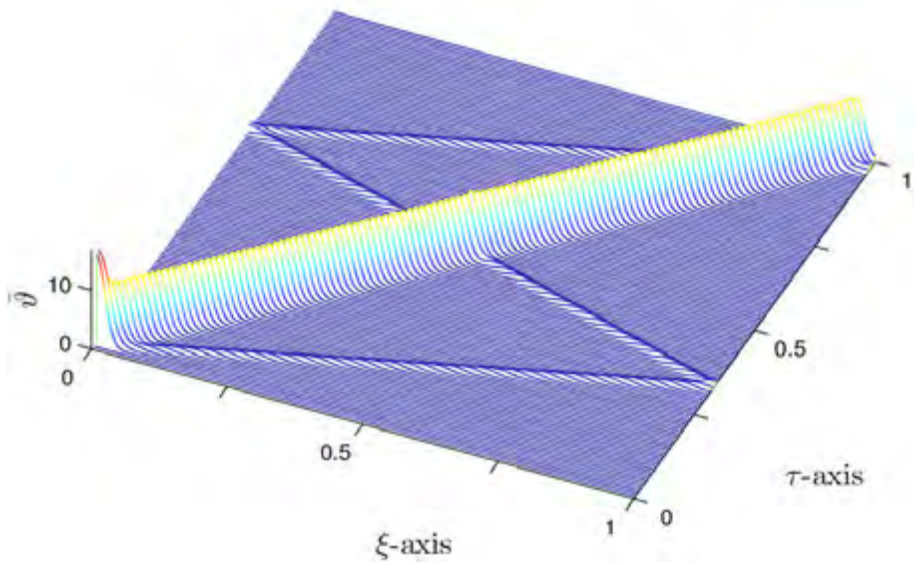

(a) Monolithic

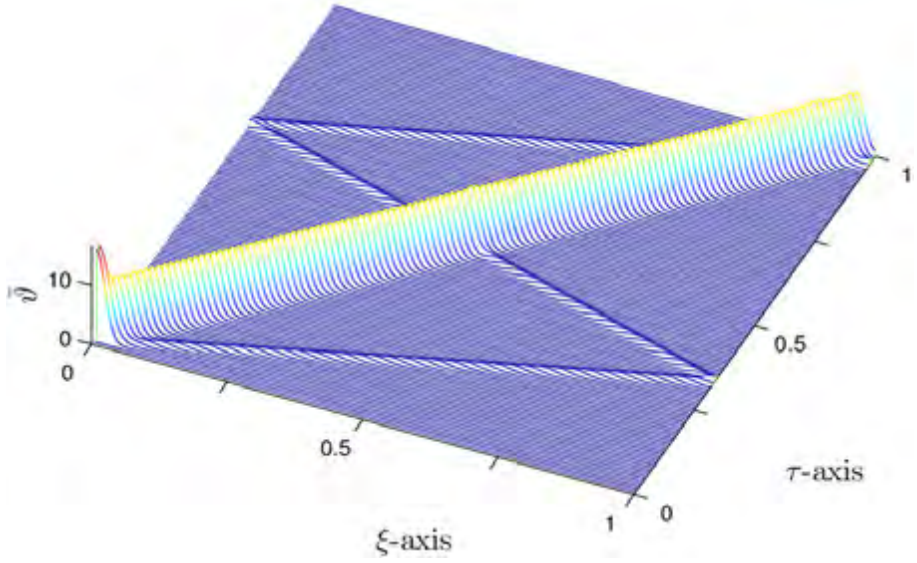

(b) Splitting

Fig. 5.3: Propagation of a laser pulse in type II thermoelasticity: temperature profile of the rod over the time period with $\varepsilon_1 = 9$, $\varepsilon_2 = 0.5$, $k = 0$ and $\Delta\xi = \Delta\tau = 0.001$.

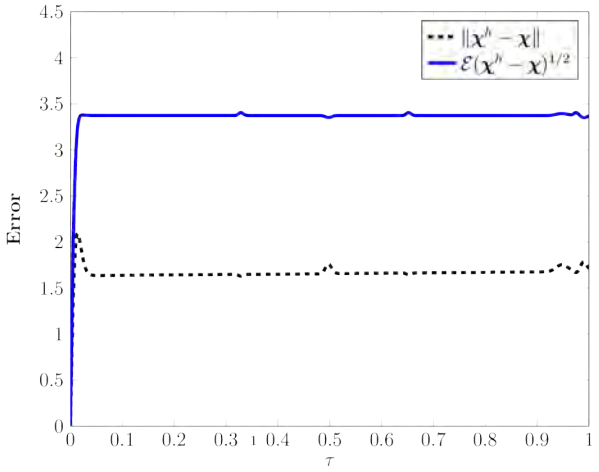

(a) Monolithic

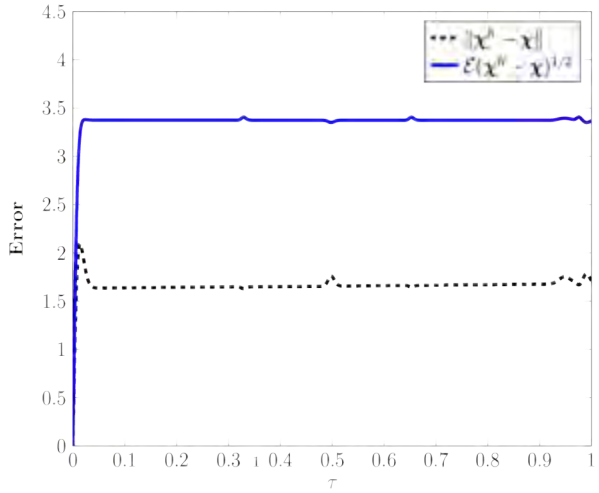

(b) Splitting

Fig. 5.4: Propagation of laser pulse in type II thermoelasticity: the H^1-Energies and L^2-norms corresponding to monolithic and splitting approaches

quickly. The mechanically induced thermal wave remains localized for almost the entire duration and is travelling with a speed nearly equal to the speed of the first sound.

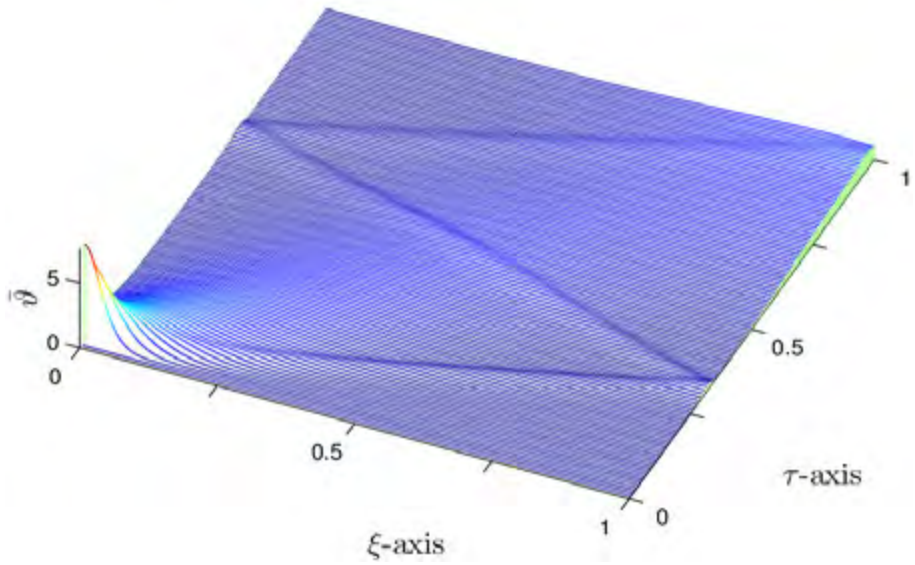

(a) Monolithic

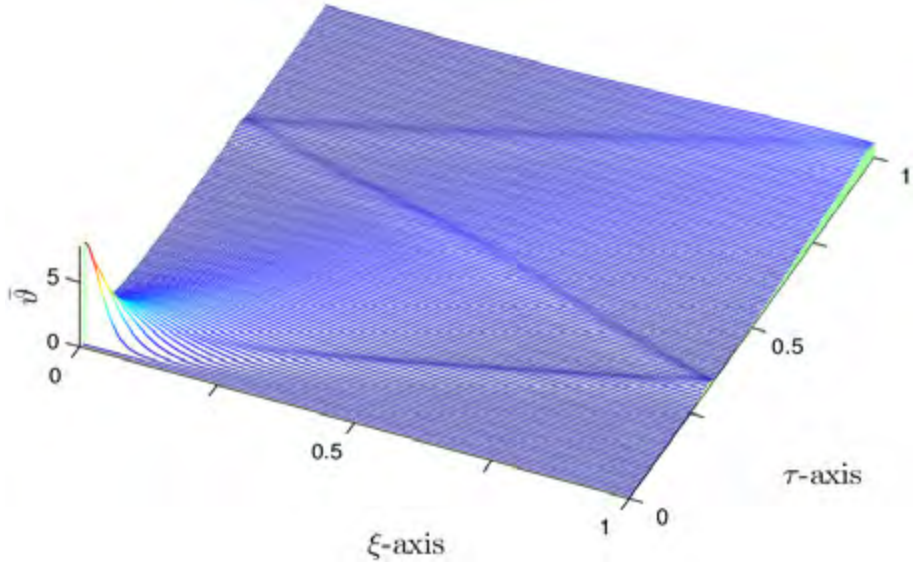

(b) Splitting

Fig. 5.5: Propagation of a laser pulse in type III thermoelasticity: temperature profile of the rod over the time period with $k = 0.1$, $\varepsilon_1 = 9$, $\varepsilon_2 = 0.5$, and $\Delta\xi = \Delta\tau = 0.001$

5.2 Two dimensional problems

5.2.1 Initial heat pulse propagation

In this problem, we consider a non-dimensional form of the type III problem of initial thermal pulse propagation in a square plate occupying the region $\Omega = [-1, 1] \times [-1, 1]$ under the plane strain assumption. A similar problem with the dimensions is addressed in [13]. The boundary of the specimen is mechanically clamped and fixed at the reference temperature $\Theta_0 = 1$ (i.e. the temperature of the ambient space). Homogenous thermal boundary condition is used over the entire boundary, i.e, $\widehat{q} = 0$ on $\Gamma_q = \Gamma$. Initially, it is at rest but a temperature pulse is initialized at the center of the plate. The initial condition for the relative temperature ϑ is given by

$$\vartheta(\boldsymbol{x}, 0) = A \exp\left[\frac{\boldsymbol{x} \cdot \boldsymbol{x}}{D}\right],$$

where D, as in the previous example in Section 5.1, is a constant characterizing the width of the initial temperature pulse and A is the amplitude. The material parameters used in the simulation are scaled according to the specifications summarized in Table 5.1. The time-DG finite element mesh consists of 8 node isoparametric cubes with an element thickness of $\Delta t = 0.01$ in the time direction and 100×100 spatial elements per slab are used to describe the initial thermal pulse propagation.

Fig. 5.6 shows snapshots of propagation of an initial temperature pulse with $D = 100$ and $A = 4$ at times $t = 0$, $t = 0.2$, $t = 0.3$, and $t = 0.4$. The initial pulse may be thought of as a thermal configuration just after an intense and highly localized laser heat source is applied at the centre. The temperature profile gradually widens and a smaller but faster mechanically driven wave emerges, while the the second sound wave is driven by the temperature equations and moves with a slower speed. In this case, the classical conductivity parameter κ_2 gives additional stability but it is not so high as to smear out the two wave phenomena.

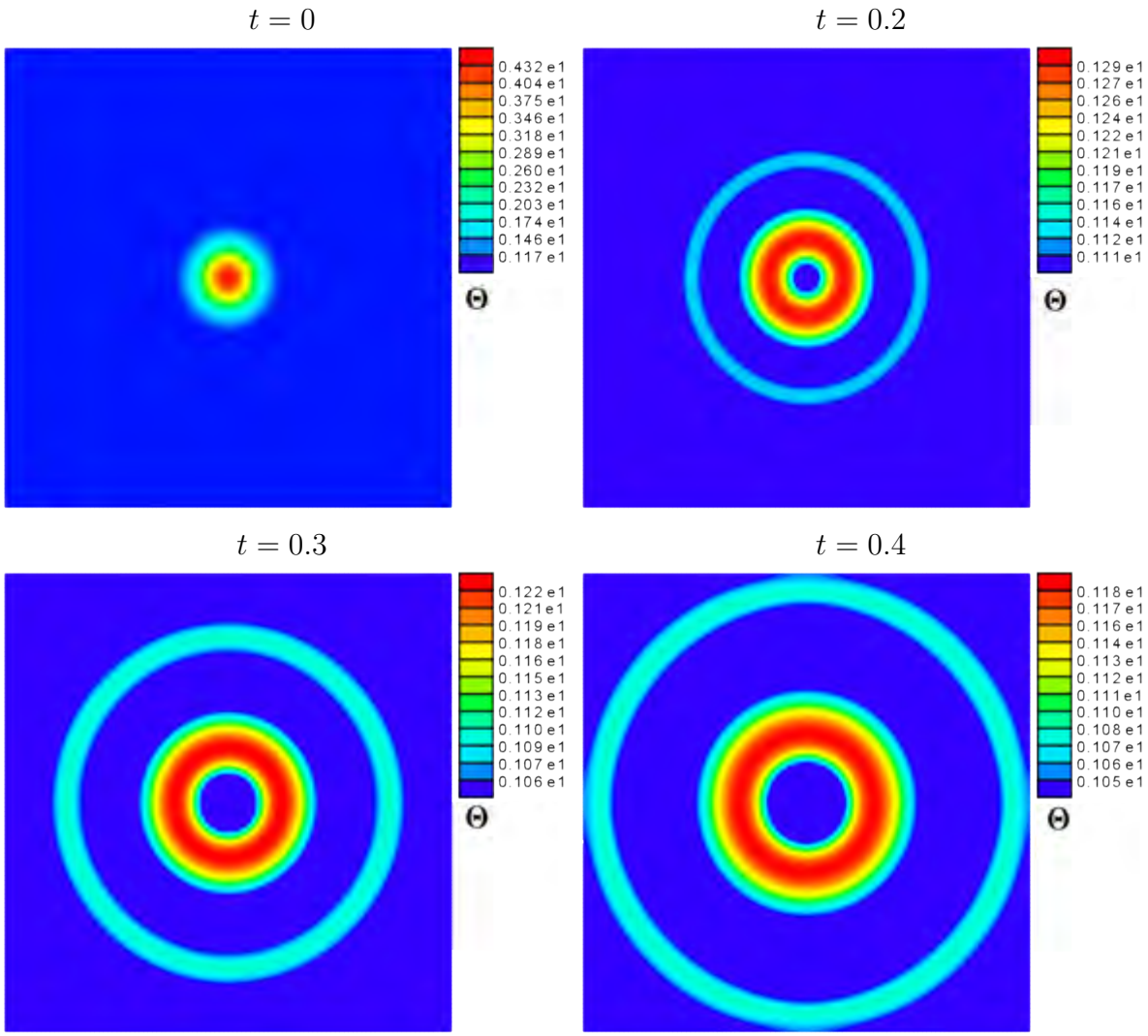

Fig. 5.6: Temperature distribution in a square plate according to type III thermoelasticity where an initial pulse localized in space is initiated at the centre.

Table 5.1: Pulse propagation: non-dimensional material properties

Speed of first sound	$\sqrt{E/\rho}$	1.96
Speed of second sound	$\sqrt{\kappa_2/\rho c}$	0.65
Conductivity ratio	κ_2/κ_3	100

5.2.2 Quasi-static case: Expansion of a thick walled cylinder

This problem deals with the quasi-static, small strain, thermo-mechanical interaction in a thick walled cylinder as it expands as a result of an inner wall Dirichlet-type boundary condition, in plane strain case. The material considered is isotropic both thermally and mechanically. The thermal variation is purely the result of mechanical changes (the expansion of the cylinder) unlike in the previous examples (Sections 5.1 and 5.2.1) in which thermal variations cause mechanical effects.

The cylinder cross-section occupies the region $\Omega = \{(x, y) : r_0^2 \leq x^2 + y^2 \leq R^2\}$ with inner and outer radii $r_0 = 10$ mm and $R = 20$ mm, respectively. A zero heat flux boundary condition is maintained on the inner wall, while the outer wall is kept at the reference temperature Θ_0. The inner wall has a prescribed radial displacement of 1 mm per second, while the outer wall is mechanically free.

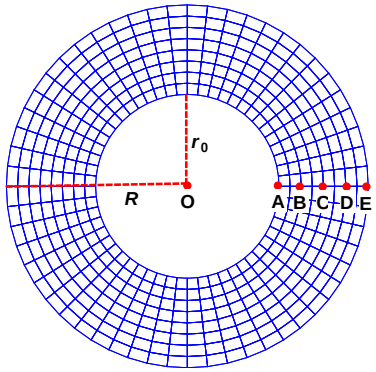

Fig. 5.7: Finite element mesh for the problem of expansion of a thick-walled cylinder.

The problem is analyzed for 20 seconds until the inner wall reaches a radius of $r = 3r_0$. The problem is simulated using a staggered scheme based on the time-discontinuous Galerkin formulation in which only the thermal fields (i.e. α and ϑ) are allowed to be discontinuous across space-time interfaces. The time-DG finite element mesh consists of trilinear shape functions of 56 elements around the circumference of the cylinder with 8 elements radially and one-element thickness in the temporal direction with step length $\Delta t = 0.1$ s for each space-time slab. In this quasi-static case, since only the thermal equations contain temporal derivatives then the thermal fields are allowed to

be discontinuous while displacement continuity across the interfaces of each space-time slab is enforced in a strong sense. This implies that the numerical dissipation comes from the weak enforcement of the continuity of the thermal fields only.

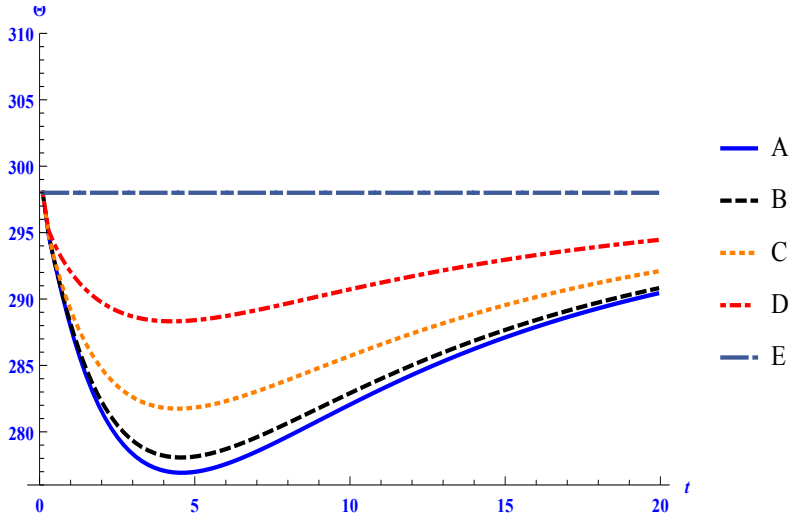

(a) **Type I**

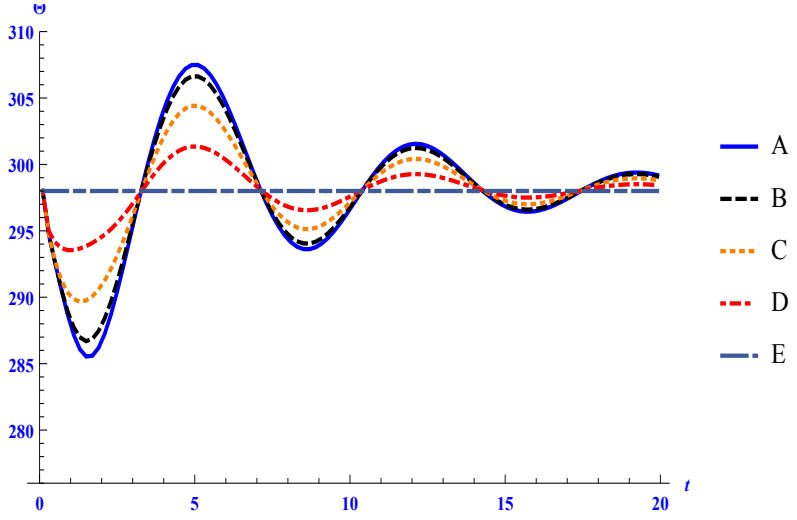

(b) **Type III**

Fig. 5.8: Temperature profile of five points in the cylinder which are 0 mm, 2.5 mm, 5 mm, 7.5 mm, and 10 mm away from the inner wall and shown with the labels A, B, C, D, and E

We consider two cases: the first is classical or type I thermoelasticity with $k_2 = 45$ N/sK and the other is type III thermoelasticity with $k_1 = 90$ N/K and $k_2 = 30$ N/sK.

Fig. 5.8 shows temperature variations over time for each case (type I and III) sampled at the equally spaced points along the radial direction labeled A-E as shown in the Fig. 5.7. The Gough-Joule effect is exhibited in Fig 5.8 (a) as the temperature drop in the cylinder is accompanied by stretching. The temperature of the cylinder starts to pick up after a minimum (below the reference temperature Θ_0) is reached, and eventually tends to equilibrium. As expected, in both cases, the temperature of the entire cylinder converges to the reference temperature as time increases. The sinusoidal thermal response of type III, as shown in Fig. 5.8 (b), is due to a temperature wave moving back and forth indicating the second sound phenomenon. The wave length of the sinusoidal wave pattern is proportional to the characteristic time that the second sound thermal wave takes to propagate across the thickness of the cylinder. The decay in the amplitude of the temperature profile indicates the dissipative nature of the type III model. However, this is not the case for type II response (not shown here), in which case, the thermal propagation is expected to be sinusoidal as in the type III but without decaying in amplitude.

Part II

Nonlinear generalized thermoelasticity

Summary: Nonlinear generalized thermoelasticity

Part II deals with the formulation of a thermodynamically consistent extension of the linear model discussed in Part I to finite strains, and the numerical approximation thereof. The linear model arises as a linearization of the new generalized model about a natural configuration.

In Chapter 6, a generalized theory of thermoelasticity is formulated in a thermodynamically consistent manner. A class of physically meaningful initial and boundary conditions are presented, thereby the nonlinear IBVP is summarized. A Lyanpunov function is presented for the dynamical system defined by the IBVP.

In Chapter 7, various time-stepping algorithms for the nonlinear IBVP based on space-time Galerkin formulation in both monolithic and staggered approaches are presented.

The stability of each of the time-stepping algorithms presented in Chapter 7 is discussed in Chapter 8. The stability analysis is based on the energy method for the discrete problems.

In Chapter 9, numerical examples are presented which serve to illustrate the performance of the time-discontinuous formulation, and the capability of the new nonlinear model in explaining those non-Fourier thermal propagation phenomena reported experimentally.

6

A thermodynamically consistent formulation of generalized thermoelasticity at finite strains

This chapter is concerned with a thermodynamically consistent formulation of a fully nonlinear coupled problem of generalized thermoelasticity inspired by the work of Green and Naghdi. The formulation is based on the basic laws of continuum thermodynamics, the balance laws of momentum, the balance of energy, and the entropy imbalance. However, the point of departure from the classical theory comes from two assumptions: the first is the heat flux is additively composed of two parts, namely the dissipative and energetic components; and the other is the inclusion of a time primitive of the absolute temperature, the so-called thermal displacement, in the state variables.

Thermodynamic restrictions on the constitutive relations are derived using the procedure of Coleman and Noll [27]. Stability of the system of partial differential equations governing the thermomechanical coupling in the non-classical regime is proved in the sense of Lyapunov. The other notable aspect of the model is that the linearized theory is similar to that of Green and Naghdi except for some differences in the interpretation of the material parameters.

The rest of the chapter is organised as follows. In Section 6.1, geometric and kinematical descriptions of the continuum body are presented. In Section 6.2 the fundamental laws of continuum thermodynamics are summarized. Constitutive relations for the stress, the entropy and the energetic component of the heat flux are derived from a free energy via the Coleman-Noll procedure in Section 6.3. Next, in Section 6.4 the initial boundary value problem (IBVP) of non-classical thermoelasticity is summarized. A class of physically meaningful initial and boundary conditions are also proposed. Finally, in Section 6.5 a Lyapunov function for the dynamics generated by the IBVP

rendering the system nonlinearly stable is obtained, and the the linearized form of the IBVP is summarized.

6.1 Kinematic relation

Consider a continuum body $\mathcal{B}$ occupying an open subset Ω of $\mathbb{R}^d$ equipped with an arbitrary but fixed Cartesian coordinate system with orthonormal basis $\{\boldsymbol{E}^A : A = 1, \cdots, d\}$, at some reference time $t = 0$ (see Fig. 6.1). The initial placement (configuration) Ω of the body $\mathcal{B}$ is referred to as the *reference configuration*. The position of a material point $P \in \mathcal{B}$ in the reference configuration is represented by its position vector $\boldsymbol{X}$.

Let the time domain of interest be $\mathbb{I} = [0,\ T]$. As the body deforms, its motion is described by a smooth and invertible map

$$\boldsymbol{\varphi} : \Omega \times \mathbb{I} \to \mathbb{R}^d. \tag{6.1}$$

We call the map $\boldsymbol{\varphi}$ the *motion* of the body $\mathcal{B}$. The motion $\boldsymbol{\varphi}(\Omega, t)$ of the reference configuration Ω, denoted Ω_t, is referred to as the current (spatial) configuration of the body $\mathcal{B}$ at the current time t. The position vector $\boldsymbol{x}$ of a point in the current configuration Ω_t is referred to as *spatial point*. A material point $\boldsymbol{X}$ is related to its spacial counterpart $\boldsymbol{x}$ via the motion as:

$$\boldsymbol{\varphi}(\boldsymbol{X}, t) = \boldsymbol{x}.$$

The displacement and velocity vector fields, respectively, parametrized in terms of the reference placement at the time t are defined by

$$\boldsymbol{u}(\boldsymbol{X}, t) \coloneqq \boldsymbol{\varphi}(\boldsymbol{X}, t) - \boldsymbol{X}, \qquad \text{and} \quad \boldsymbol{V}(\boldsymbol{X}, t) \coloneqq \dot{\boldsymbol{u}}(\boldsymbol{X}, t) = \frac{\partial}{\partial t}\boldsymbol{\varphi}(\boldsymbol{X}, t).$$

We denote the gradient and divergence operators, respectively, in the reference configuration by $\nabla(\,\cdot\,)$ and $\mathrm{Div}\,(\,\cdot\,)$, and, for example, for a material vector field $\boldsymbol{f}$ write

$$(\nabla \boldsymbol{f})_{AB} = \frac{\partial f_A}{\partial X_B}, \qquad \text{and} \quad \mathrm{Div}\, \boldsymbol{f} = \frac{\partial f_A}{\partial X_A}.$$

We define the tensor quantity $\boldsymbol{F}$ at the material point $\boldsymbol{X}$ at the current time t by

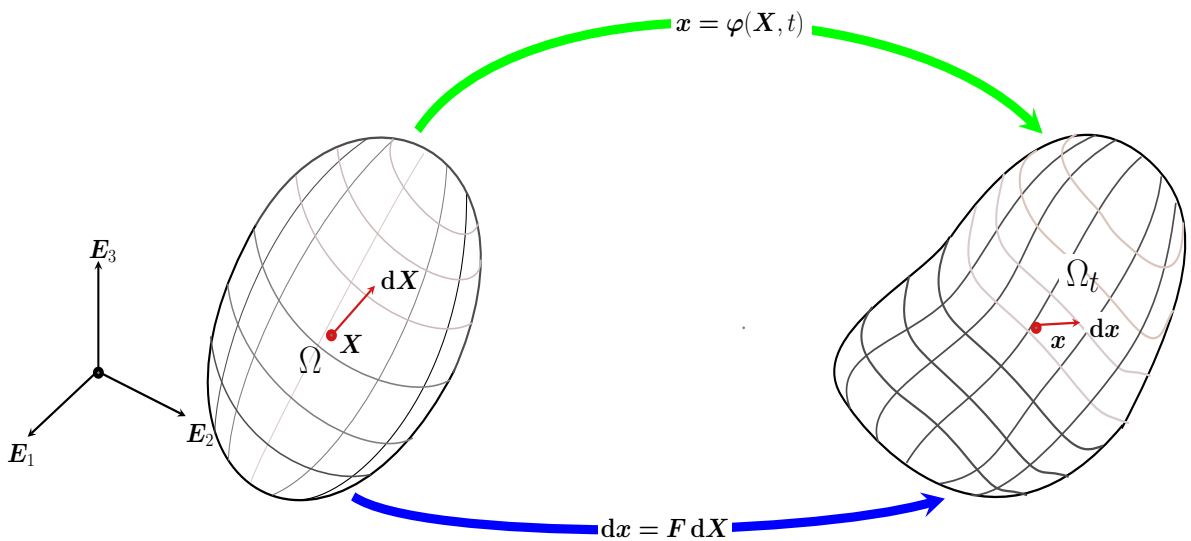

Fig. 6.1: Deformation (motion) of a continuum body from reference (left) to spatial (right) configuration

$$\boldsymbol{F}(\boldsymbol{X}, t) \coloneqq \nabla \boldsymbol{\varphi}(\boldsymbol{X}, t), \quad \text{or} \quad F_{aB} \coloneqq \frac{\partial \varphi_a}{\partial X_B}.$$

The tensor $\boldsymbol{F}$ is a primary measure of deformation in the continuum body, and is called the *deformation gradient tensor*. The deformation gradient $\boldsymbol{F}$ may be written in terms of the displacement vector field $\boldsymbol{u}$ as $\boldsymbol{F} = \nabla \boldsymbol{u} + \boldsymbol{1}$, where $\boldsymbol{1}$ denotes the identity material tensor.

As a transformation tensor $\boldsymbol{F}$ sends material vectors (those vectors that live in the reference coordinate system) to spatial vectors (those vectors that live in the spatial coordinate system). For an arbitrary material point $\boldsymbol{X}$ and time t, an infinitesimal reference volume element $\mathrm{d}\Omega$ associated with the material point is mapped into a volume element $\mathrm{d}\omega$ in the current configuration by the Jacobian $J(\boldsymbol{X}, t) = \det \boldsymbol{F}(\boldsymbol{X}, t)$ via the relation

$$\mathrm{d}\omega = J(\boldsymbol{X}, t)\mathrm{d}\Omega.$$

Thus, an admissible configuration is one in which the Jacobian J is positive.

Strain measures

Two commonly used measures of stretch and strain in continuum mechanics are the *right Cauchy-Green tensor* $\boldsymbol{C}$ and the *Green-Lagrange strain tensor* $\boldsymbol{E}$. They are defined by

$$\boldsymbol{C} \coloneqq \boldsymbol{F}^{\mathrm{T}}\boldsymbol{F}, \qquad \text{and} \qquad \boldsymbol{E} \coloneqq \frac{1}{2}(\boldsymbol{C} - \boldsymbol{1}),$$

or in index notation

$$C_{AB} \coloneqq F_{aA}F_{aB}, \qquad \text{and} \qquad E_{AB} \coloneqq \frac{1}{2}(C_{AB} - \delta_{AB}).$$

Note that $\boldsymbol{C}$ is positive-definite and symmetric; that is

$$\boldsymbol{C}^{\mathrm{T}} = \boldsymbol{C} \quad \text{and} \quad \boldsymbol{\xi} \cdot \boldsymbol{C}\boldsymbol{\xi} > 0,$$

for any nonzero material vector $\boldsymbol{\xi}$. Consequently, the tensor $\boldsymbol{E}$ is also symmetric; that is, $\boldsymbol{E}^{\mathrm{T}} = \boldsymbol{E}$. Note also that both $\boldsymbol{C}$ and $\boldsymbol{E}$ map material vectors to material vectors.

In terms of the gradient of the displacement vector field $\boldsymbol{u}$, in the reference configuration the Green-Lagrange strain tensor $\boldsymbol{E}$ may also be written as

$$\boldsymbol{E} = \frac{1}{2}\big[\nabla\boldsymbol{u} + (\nabla\boldsymbol{u})^{\mathrm{T}} + (\nabla\boldsymbol{u})^{\mathrm{T}}\nabla\boldsymbol{u}\big]. \tag{6.2}$$

Under the assumption of infinitesimal-deformation, the second-order quantity $(\nabla\boldsymbol{u})^{\mathrm{T}}\nabla\boldsymbol{u}$ is negligible compared to the rest of the terms in the right hand side of (6.2). Ignoring this second-order terms leads to the infinitesimal counterpart of the strain tensor $\boldsymbol{E}$ given in (2.7).

Stress

Consider an arbitrary, oriented surface $\mathcal{S}$ with unit normal $\boldsymbol{N}$ in the interior of the reference placement Ω, as shown in Fig 6.2. Let the image of $\mathcal{S}$ under the motion $\boldsymbol{\varphi}(\cdot, t)$ in the interior of the current placement Ω_t be $\mathcal{S}_t$ with normal $\boldsymbol{n}$. The surface $\mathcal{S}_t$ divides the region Ω_t into two subregions, such that Ω_t^+ denotes the part of Ω_t that the normal

vector $\boldsymbol{n}$ points to, while Ω_t^- represents the remaining part. By *Cauchy's hypothesis* there exists a *surface-traction field* $\boldsymbol{t}(\boldsymbol{n}, \boldsymbol{x}, t)$ defined at a point $\boldsymbol{x}$ on the surface $\mathcal{S}_t$ with unit normal $\boldsymbol{n}$. The field $\boldsymbol{t}(\boldsymbol{n}, \boldsymbol{x}, t)$ represents the force at $\boldsymbol{x}$ that Ω_t^- exerts on Ω_t^+ associated to the unit normal $\boldsymbol{n}$.

One of the most crucial results in continuum mechanics is *Cauchy's theorem*. It states that for each pair $(\boldsymbol{n}, \boldsymbol{x})$ relative to the current placement Ω_t there exists a spatial tensor $\boldsymbol{\sigma}$, called the *Cauchy stress*, such that

$$\boldsymbol{t} = \boldsymbol{\sigma}\boldsymbol{n}.$$

The reference configuration counterpart of the Cauchy stress $\boldsymbol{\sigma}$ is known as the

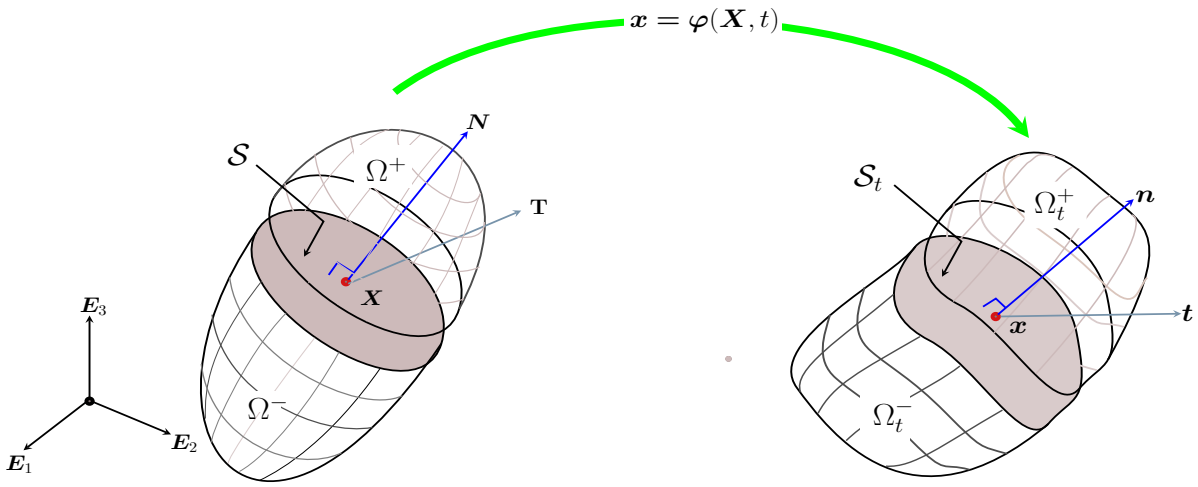

Fig. 6.2: Surface-traction filed in the reference (left) and spatial (right) configurations

first Piola-Kirchhoff stress tensor[1], denoted $\boldsymbol{P}$, with surface-traction vector field $\mathbf{T}(\boldsymbol{N}, \boldsymbol{X}, t)$. The pairs $(\boldsymbol{P}, \mathbf{T})$ and $(\boldsymbol{\sigma}, \boldsymbol{t})$ in the reference and current configuration, respectively, are related through

[1] As a consequence of the conservation of angular momentum, it is shown that the Cauchy stress tensor $\boldsymbol{\sigma}$ is symmetric; on the other hand, the first Piola-Kirchhoff stress tensor $\boldsymbol{P}$ is not symmetric.

$$\mathbf{T}\mathrm{d}A = \boldsymbol{t}\mathrm{d}a = \boldsymbol{\sigma}\boldsymbol{n}\mathrm{d}a = \boldsymbol{P}\boldsymbol{N}\mathrm{d}A, \tag{6.3}$$

where $\mathrm{d}A$ and $\mathrm{d}a$ are area elements in the reference and current configuration, associated with the normals $\boldsymbol{N}$ and $\boldsymbol{n}$, respectively.

The relation (6.3) leads to an explicit relation between the first Piola-Kirchhoff stress tensor $\boldsymbol{P}$ and the Cauchy stress tensor $\boldsymbol{\sigma}$ by

$$\boldsymbol{P} = J\boldsymbol{\sigma}\boldsymbol{F}^{-\mathrm{T}} \qquad \text{or} \qquad P_{aA} = J\sigma_{ab}F^{-1}_{Ab}. \tag{6.4}$$

Note that $\boldsymbol{P}$ maps material vectors to spatial vectors.

6.2 Balance laws

In this section we review the balance laws describing the thermomechanics of a continuum body without regard to the particular material behaviour constituting the body. These laws alone are not sufficient to fully specify how a particular body behaves in a thermomechanical framework. In the subsequent sections, constitutive laws that account for material behaviour will be presented in a non-classical and thermodynamically consistent way. The phrase 'thermodynamically consistent' is used to emphasize that the constitutive relations to be discussed are compatible with the laws of thermodynamics while, in addition to the familiar mechanism of conduction of thermal energy by conduction, they also allow a non-Fourier mechanism of transfer of heat as a wave.

Balance laws of linear momentum.

In any physical system the total linear momentum must be conserved. Mathematically, this law states that, for an arbitrary volume element, the time-rate-of-change of linear momentum in the element is balanced by the total forces acting on the element. Forces acting on the element are comprised of the *traction force* and the *body forces*. Traction forces are forces that the element exchanges with the surrounding environment through its boundary, while body forces are forces fields that are distributed over the material element by an external agent.

Let $\rho_0 > 0$ be the density of the continuum body in the reference configuration, $\boldsymbol{b} : \Omega \times \mathbb{I} \to \mathbb{R}^d$ the external body force density acting on the body. Applying the standard argument in continuum mechanics that is used to translate such averaging law on an arbitrary mass element to a pointwise statement, the local form of the balance law of linear momentum, written in terms of the reference configuration, reads

$$\rho_0 \dot{\boldsymbol{V}} = \operatorname{Div} \boldsymbol{P} + \rho_0 \boldsymbol{b}. \tag{6.5}$$

Balance laws of angular momentum

For an arbitrary volume element, the time-rate-of-change of angular momentum of the element is balanced by total moment resulted by the body and surface-traction forces. An important consequence of this balance law is the that the Cauchy stress tensor $\boldsymbol{\sigma}$ is symmetric, which in turn, by (6.4) and positivity of the Jacobian J, leads to

$$\boldsymbol{P}\boldsymbol{F}^{\mathrm{T}} = \boldsymbol{F}\boldsymbol{P}^{\mathrm{T}}. \tag{6.6}$$

Balance of energy (First law of thermodynamics)

The theory of Green and Naghdi relies on an entropy equality obtained by adding an expression for entropy production to the entropy inequality (see Chapter 2), whereas the current formulation is based on the balance of energy and entropy inequality as is the case in the classical formulation of thermoelasticity.

The balance of energy is a statement about conservation of total energy in a given closed physical system. It states that the time-rate-of-change of total internal energy of the system is equal to the sum of the internal stress power, the heat energy exchanged with the environment through the boundary, and the heat source. The balance of energy in terms of the reference equation, in its local form, reads

$$\dot{\mathcal{E}} = \boldsymbol{P} : \dot{\boldsymbol{F}} - \operatorname{Div} \boldsymbol{Q} + R, \tag{6.7}$$

where $\mathcal{E}$, $\boldsymbol{Q}$, and R are the internal energy, Piola heat flux vector, and heat source per unit volume.

Entropy imbalance (second law of thermodynamics)

The second law of thermodynamics places restrictions on how a given thermodynamic process evolves. It states that any closed system is associated with an increasing (or at least constant) entropy. It specifies the direction of any thermodynamic process. Precisely, the entropy imbalance, with respect to the reference configuration, is given by the inequality

$$\dot{\eta} \geq -\mathrm{Div}\, \boldsymbol{H} + S, \tag{6.8}$$

where η, $\boldsymbol{H}$, and S are the entropy, Piola entropy flux vector, and entropy source, respectively.

In the framework of the classical theory of thermoelasticity, see, for example [45] pp. 187, the absolute temperature Θ is used to relate heat flux (resp. heat source) with entropy flux (resp. entropy source). In the current formulation, motivated by the theory of Green and Naghdi discussed in Chapter 2, we further assume the existence of a scalar field α, referred to as the *thermal displacement*, such that

$$\dot{\alpha} > 0,$$

and that

$$\mathbf{H} = \frac{\boldsymbol{Q}}{\dot{\alpha}}, \quad \text{and} \quad S = \frac{R}{\dot{\alpha}}. \tag{6.9}$$

See also [12] for a discussion of this assumption in a general context. We then proceed to define the absolute temperature by

$$\Theta = \dot{\alpha}.$$

Next, substitution of (6.9) into (6.8) leads to

$$\dot{\eta} \geq -\mathrm{Div}\left[\frac{\boldsymbol{Q}}{\Theta}\right] + \frac{R}{\Theta} \quad \text{or} \quad \Theta\dot{\eta} \geq -\mathrm{Div}\mathbf{Q} + \frac{1}{\Theta}\boldsymbol{Q}\cdot\nabla\Theta + R. \tag{6.10}$$

By subtracting the inequality (6.10) from the energy balance equation (6.7) and subtracting $\dot{\Theta}\eta$ from both sides of the resulting inequality, we obtain

$$\frac{\partial}{\partial t}\big[\mathcal{E} - \Theta\eta\big] \leq \boldsymbol{P} : \dot{\boldsymbol{F}} - \dot{\Theta}\eta - \frac{1}{\Theta}\boldsymbol{Q}\cdot\nabla\Theta. \tag{6.11}$$

On defining the Helmholtz free-energy through the Legendre transformation

$$\Psi = \mathcal{E} - \Theta\eta, \tag{6.12}$$

(6.11) yields the local form of the free-energy imbalance

$$\dot{\Psi} - \boldsymbol{P} : \dot{\boldsymbol{F}} + \dot{\Theta}\eta + \frac{1}{\Theta}\boldsymbol{Q} \cdot \nabla\Theta = -\Theta\Xi \leq 0. \tag{6.13}$$

Here Ξ denotes the rate of entropy production (while $\Theta\Xi$ is the rate of energy dissipation).

6.3 Thermodynamics and constitutive relations

In this section, we present a thermodynamically consistent formulation of the constitutive equations in the generalized thermoelastic framework. In the current formulation we first assume that the heat flux $\boldsymbol{Q}$ is split additively as

$$\boldsymbol{Q} = \boldsymbol{Q}_E + \boldsymbol{Q}_D, \tag{6.14}$$

where $\boldsymbol{Q}_D$ does not depend on α or its gradient $\nabla\alpha$, while the dependence of $\boldsymbol{Q}_D$ on state variables is not restricted a priori. For reasons that will become clear, we refer to $\boldsymbol{Q}_E$ as the *energetic* and $\boldsymbol{Q}_D$ as the *dissipative* components of the heat flux $\boldsymbol{Q}$. As a consequence of the split (6.14), the free-energy imbalance (6.13) becomes

$$\dot{\Psi} - \boldsymbol{P} : \dot{\boldsymbol{F}} + \dot{\Theta}\eta + \frac{1}{\Theta}\boldsymbol{Q}_E \cdot \nabla\Theta + \frac{1}{\Theta}\boldsymbol{Q}_D \cdot \nabla\Theta = -\Theta\Xi \leq 0. \tag{6.15}$$

Looking at the variables involved in the free-energy imbalance (6.15), we assume that the state of the system under consideration depends on the set of state variables

$$\mathscr{A} = \{\boldsymbol{F}, \Theta, \nabla\alpha, \nabla\Theta\}. \tag{6.16}$$

Note that the inclusion of α in the state variables through its gradient. Thus the free energy Ψ, the the first Piola-Kirchhoff stress $\boldsymbol{P}$, the entropy η, and the heat flux components $\boldsymbol{Q}_E$ and $\boldsymbol{Q}_D$ are determined by constitutive equations of the form

$$\Psi = \Psi(\mathscr{A}), \qquad \boldsymbol{P} = \boldsymbol{P}(\mathscr{A}), \qquad \eta = \eta(\mathscr{A}),$$
$$\boldsymbol{Q}_E = \boldsymbol{Q}_E(\mathscr{A}), \tag{6.17}$$

We now apply the Coleman–Noll procedure to ensure that the constitutive equations (6.17) satisfy the laws of thermodynamics. If the constitutive equation for the free energy is differentiated with respect to time, one obtains

$$\dot{\Psi} = \frac{\partial \Psi}{\partial \boldsymbol{F}} : \dot{\boldsymbol{F}} + \frac{\partial \Psi}{\partial \Theta}\, \dot{\Theta} + \frac{\partial \Psi}{\partial \boldsymbol{\Lambda}} \cdot \dot{\boldsymbol{\Lambda}} + \frac{\partial \Psi}{\partial \mathbf{G}} \cdot \dot{\mathbf{G}}, \tag{6.18}$$

where $\boldsymbol{\Lambda} = \nabla \alpha$ and $\mathbf{G} = \nabla \Theta$.

Substitution of the time derivative of the free energy (6.18) into the free imbalance (6.15) yields

$$\left(\frac{\partial \Psi}{\partial \boldsymbol{F}} - \boldsymbol{P}\right) : \dot{\boldsymbol{F}} + \left(\frac{\partial \Psi}{\partial \Theta} + \eta\right) \dot{\Theta} + \left(\frac{\partial \Psi}{\partial \boldsymbol{\Lambda}} + \frac{1}{\Theta}\boldsymbol{Q}_E\right) \cdot \dot{\boldsymbol{\Lambda}} + \frac{\partial \Psi}{\partial \mathbf{G}} \cdot \dot{\mathbf{G}} + \frac{1}{\Theta}\boldsymbol{Q}_D \cdot \nabla \Theta \leq 0, \tag{6.19}$$

which must be satisfied for all states.

Since $\dot{\boldsymbol{F}}$, $\dot{\Theta}$, $\dot{\boldsymbol{\Lambda}}$, $\dot{\mathbf{G}}$, and their time primitives can be chosen arbitrarily in order to maintain the inequality (6.19) we may choose the constitutive equations and thermodynamic restrictions as

$$\boldsymbol{P} = \frac{\partial \Psi}{\partial \boldsymbol{F}}, \quad \eta = -\frac{\partial \Psi}{\partial \Theta}, \quad \frac{1}{\Theta}\boldsymbol{Q}_E = -\frac{\partial \Psi}{\partial \boldsymbol{\Lambda}}, \quad \frac{\partial \Psi}{\partial \mathbf{G}} = \mathbf{0}, \quad \text{and} \quad \boldsymbol{Q}_D \cdot \nabla \Theta \leq 0. \tag{6.20}$$

As a consequence, the rate of entropy production in any thermodynamically admissible process becomes

$$\Xi = -\frac{1}{\Theta^2}\boldsymbol{Q}_D \cdot \nabla \Theta.$$

Note that $\dot{\boldsymbol{\Lambda}} = \nabla \Theta$. Equation $(6.20)_4$ reveals that the free energy does not depend on $\nabla \Theta$.

For instance, a class of such free energy functions in the non-classical case has the form

$$\Psi = \Psi_{\mathrm{c}} + \frac{1}{2}\mathbf{K}_1 \nabla \alpha \cdot \nabla \alpha, \tag{6.21}$$

where Ψ_c denotes any classical free energy function for thermo-hyperelasticity and $\mathbf{K}_1$ a symmetric and positive-definite non-classical conductivity second-order tensor. Equation (6.21) and the constitutive equation $(6.20)_3$ imply that the energetic component of heat flux $\boldsymbol{Q}_E$ is linear in $\nabla\alpha$.

Field equation for thermal conduction

Consequently, by (6.18) and (6.20), the time derivative of the free energy becomes

$$\dot{\Psi} = \boldsymbol{P} : \dot{\boldsymbol{F}} - \eta\dot{\Theta} - \frac{1}{\Theta}\boldsymbol{Q}_E \cdot \dot{\boldsymbol{\Lambda}}. \tag{6.22}$$

Next, by the Legendre transformation (6.12), from (6.22) the time derivative of the internal energy is

$$\dot{\mathcal{E}} = \Theta\dot{\eta} + \boldsymbol{P} : \dot{\boldsymbol{F}} - \frac{1}{\Theta}\boldsymbol{Q}_E \cdot \dot{\boldsymbol{\Lambda}}. \tag{6.23}$$

By combining (6.7) and (6.23) we obtain the field equation of thermal conduction in the conservation form

$$\Theta\dot{\eta} = -\mathrm{Div}\boldsymbol{Q} + \frac{1}{\Theta}\boldsymbol{Q}_E \cdot \nabla\Theta + R. \tag{6.24}$$

From $(6.20)_{1,2}$ and assuming sufficiently smoothness on Ψ with respect to its arguments,

$$\frac{\partial\eta}{\partial\boldsymbol{F}} = -\frac{\partial^2\Psi}{\partial\boldsymbol{F}\partial\Theta} = -\frac{\partial^2\Psi}{\partial\Theta\partial\boldsymbol{F}} = -\frac{\partial\boldsymbol{P}}{\partial\Theta}. \tag{6.25}$$

Using equation (6.25) the conservation form (6.24) yields the field equation

$$\rho_0 c_{_F}\dot{\Theta} = -\mathrm{Div}\boldsymbol{Q} + \frac{1}{\Theta}\boldsymbol{Q}_E \cdot \nabla\Theta + \Theta\frac{\partial\boldsymbol{P}}{\partial\Theta} : \dot{\boldsymbol{F}} + \rho_0 R,$$

where $c_{_F}$ is the heat capacity and is defined by

$$\rho_0 c_{_F} = -\Theta\frac{\partial^2\Psi}{\partial\Theta^2}. \tag{6.26}$$

6.4 The initial-boundary value problem

In this section we summarize the initial boundary-value problem for coupled, generalized thermoelasticity in a general nonlinear framework that have been developed in the preceding sections.

Governing equations

The displacement–velocity relation ($\dot{\boldsymbol{u}} = \boldsymbol{V}$), the balance of linear momentum (6.5), the thermal displacement–temperature relation ($\dot{\alpha} = \Theta$) along with the thermal conduction equation in conservation form (6.24) lead to the first-order (in time) system of nonlinear partial differential equation governing the strong coupling of thermoelastic behaviour in the generalized setting, and is given by

$$\left.\begin{aligned} \dot{\boldsymbol{u}} &= \boldsymbol{V} \\ \rho_0 \dot{\boldsymbol{V}} &= \mathrm{Div}\boldsymbol{P} + \rho_0 \boldsymbol{b} \\ \dot{\alpha} &= \Theta \\ \Theta\dot{\eta} &= -\mathrm{Div}\boldsymbol{Q} + \frac{1}{\Theta}\boldsymbol{Q}_E \cdot \nabla\Theta + R \end{aligned}\right\} \quad \text{in} \quad \Omega \times \mathbb{I}. \tag{6.27}$$

The constitutive equations are derived from a potential Ψ denoting the classical Helmholtz free energy function, such that

$$\boldsymbol{P} = \frac{\partial \Psi}{\partial \boldsymbol{F}}, \qquad \eta = -\frac{\partial \Psi}{\partial \Theta}, \qquad \boldsymbol{Q} = \boldsymbol{Q}_E + \boldsymbol{Q}_D \quad \text{and} \quad \boldsymbol{Q}_E = -\Theta \frac{\partial \Psi}{\partial \boldsymbol{\Lambda}}. \tag{6.28}$$

Equation (6.28) together with a constitutive relation for the dissipative component $\boldsymbol{Q}_D$ of the heat flux satisfying an inequality of the form $\boldsymbol{Q}_D \cdot \nabla\Theta \leq 0$ complete the set of constitutive equations for system (6.27).

Initial and boundary conditions

Physically meaningful initial and boundary conditions in the non-classical theory are proposed in Chapter 2 for the linear problem. Basically the initial conditions in the nonlinear case follow in a similar fashion. To this end, initially the primary unknowns are prescribed, and have the form

$$\boldsymbol{u}|_{t=0} = \boldsymbol{u}^0, \quad \boldsymbol{V}|_{t=0} = \boldsymbol{V}^0, \quad \alpha|_{t=0} = 0, \quad \text{and} \quad \vartheta|_{t=0} = \vartheta^0, \tag{6.29}$$

where $(\,\cdot\,)^0$ are initially predefined functions on Ω and ϑ is the relative temperature with respect to the reference temperature Θ_0 such that $\Theta = \vartheta + \Theta_0$. The consistency condition on the motion, that is $\boldsymbol{\varphi}|_{t_0} = \boldsymbol{X}$, necessitates that the displacement field initially be zero, $\boldsymbol{u}|_{t_0} = \boldsymbol{0}$.

For the boundary conditions, as we did in the linear case in Chapter 2, we first consider the decomposition of the boundary Γ into two mutually disjoint partition sets $\{\Gamma_{\boldsymbol{u}},\ \Gamma_{\mathbf{T}}\}$, and $\{\Gamma_{\vartheta},\ \Gamma_{Q}\}$ such that

$$\Gamma_{\boldsymbol{u}} \cap\ \Gamma_{\mathbf{T}} = \Gamma_{\vartheta} \cap\ \Gamma_{Q} = \emptyset, \quad \text{and} \quad \Gamma = \overline{\Gamma_{\boldsymbol{u}} \cup\ \Gamma_{\mathbf{T}}} = \overline{\Gamma_{\vartheta} \cup\ \Gamma_{Q}}.$$

Hence physically meaningful boundary conditions have the form

$$\begin{aligned} \boldsymbol{u} &= \widehat{\boldsymbol{u}} \quad \text{on} \quad \Gamma_{\boldsymbol{u}} \times \mathbb{I}, \quad \text{and} \quad \boldsymbol{P}\boldsymbol{N} = \widehat{\mathbf{T}} \quad \text{on} \quad \Gamma_{\mathbf{T}} \times \mathbb{I}, \\ \vartheta &= \widehat{\vartheta} \quad \text{on} \quad \Gamma_{\vartheta} \times \mathbb{I}, \quad \text{and} \quad \boldsymbol{Q} \cdot \boldsymbol{N} = \widehat{Q} \quad \text{on} \quad \Gamma_{Q} \times \mathbb{I}, \end{aligned} \tag{6.30}$$

where $\widehat{(\,\cdot\,)}$ denote prescribed functions on the corresponding partitions of Γ.

Therefore, the system (6.27) together with the constitutive relations (6.28), the initial and boundary conditions (6.29) and (6.30) conclude the local description of the initial-boundary value problem (IBVP) for coupled, generalized thermoelasticity.

6.5 Stability

The notion of stability plays a central role in the study of dynamical systems. Stability of nonlinear dynamical systems such as the IBVP for generalized thermoelasticity (6.27) is suitably analyzed in the sense of Lyapunov. In this section, we are particularly interested in addressing the stability of natural (equilibrium) states of the dynamical system. Let $\boldsymbol{\mathcal{X}}^*$ be a natural (equilibrium) state state of the IBVP (6.27) in the absence of loading. We say the dynamical system is stable for the state $\boldsymbol{\mathcal{X}}$ if there exists a scalar valued function V defined on a subspace of the state space containing the natural state and satisfying the following:

1) $V(\boldsymbol{\mathcal{X}}^*) = 0$,

2) V is positive-definite; that is, $V(\boldsymbol{\mathcal{X}}) > 0$ for each $\boldsymbol{\mathcal{X}} \neq \boldsymbol{\mathcal{X}}^*$ and

3) $\dot{V}(\boldsymbol{\mathcal{X}}) \leq 0$ along the solution of the evolution equation (6.27).

Note that the existence of a Lyapunov function is only a sufficient condition for stability. A system can be shown to be stable, while existence of a Lyapunov function may not be guaranteed. The contractivity property (2.21) is a linear counterpart of nonlinear stability, in which case we use the norm of the solution as a Lyapunov function.

The rest of this section is devoted to the stability of the nonlinear, generalized thermoelasticity problem (6.27). Attention is restricted to the case of no heat sources, $R = 0$, no body force, $\boldsymbol{b} = \boldsymbol{0}$, and the boundary Γ is fixed at a constant reference temperature Θ_0 and the displacement is zero, $\widehat{\boldsymbol{u}}|_{\Gamma} = \boldsymbol{0}$.

For the sake of simplicity, we redefine[2] α so that $\dot{\alpha} = \vartheta$. Consequently, defining the state vectors by $\boldsymbol{\mathcal{X}} = (\boldsymbol{u}, \boldsymbol{V}, \alpha, \vartheta)^{\mathsf{T}}$ in some admissible[3] subset of a Banach space, for the setup just described, the homogeneous state $\boldsymbol{\mathcal{X}}^* = \boldsymbol{0}$ is an equilibrium state. The functional V defined by

$$V(\boldsymbol{\mathcal{X}}) = \int_{\Omega} \left[\Psi + \vartheta\eta + \frac{1}{2}\rho_0 \boldsymbol{V}\cdot\boldsymbol{V}\right] \mathrm{d}\Omega, \tag{6.31}$$

corresponding to the specific conditions described above defines a Lyapunov function for the IBVP (6.27). The first two conditions 1) and 2) are are satisfied if Ψ verifies similar condition which is the case in the finite strain regime. Condition 3) is shown by differentiating V with respect to time so that

[2] For example, if we replace the term $\alpha + t\Theta_0$ by α we get $\dot{\alpha} = \vartheta$

[3] A given state is said to be admissible if it corresponds to a positive Jacobian, that is, $\det\boldsymbol{F} = \det(\nabla\boldsymbol{u}+\boldsymbol{1}) > 0$.

$$
\begin{aligned}
\frac{\mathrm{d}}{\mathrm{d}t}V &= \int_\Omega \left[\boldsymbol{P} : \dot{\boldsymbol{F}} - \eta\dot{\Theta} - \frac{1}{\Theta}\boldsymbol{Q}_E \cdot \nabla\Theta + \dot{\Theta}\eta + \vartheta\dot{\eta} + \rho_0 \dot{\boldsymbol{V}} \cdot \boldsymbol{V} \right] \mathrm{d}\Omega \\
&= \int_\Omega \left[-\frac{1}{\Theta}\boldsymbol{Q}_E \cdot \nabla\Theta + \vartheta\dot{\eta} \right] \mathrm{d}\Omega \\
&= \int_\Omega \left[-\frac{1}{\Theta}\boldsymbol{Q}_E \cdot \nabla\Theta + \left(1 - \frac{\Theta_0}{\Theta}\right)\Theta\dot{\eta} \right] \mathrm{d}\Omega \\
&= \int_\Omega \left[-\frac{1}{\Theta}\boldsymbol{Q}_E \cdot \nabla\Theta + \left(1 - \frac{\Theta_0}{\Theta}\right)\left(-\mathrm{Div}\boldsymbol{Q} + \frac{1}{\Theta}\boldsymbol{Q}_E \cdot \nabla\Theta \right) \right] \mathrm{d}\Omega \\
&= \int_\Omega \left[-\frac{1}{\Theta}\boldsymbol{Q}_E \cdot \nabla\Theta + \frac{\Theta_0}{\Theta^2}\boldsymbol{Q} \cdot \nabla\Theta + \left(1 - \frac{\Theta_0}{\Theta}\right)\frac{1}{\Theta}\boldsymbol{Q}_E \cdot \nabla\Theta \right] \mathrm{d}\Omega \\
&= \int_\Omega \left[-\frac{\Theta_0}{\Theta^2}\boldsymbol{Q}_E \cdot \nabla\Theta + \frac{\Theta_0}{\Theta^2}\boldsymbol{Q}_E \cdot \nabla\Theta + \frac{\Theta_0}{\Theta^2}\boldsymbol{Q}_D \cdot \nabla\Theta \right] \mathrm{d}\Omega \\
&= \int_\Omega \frac{\Theta_0}{\Theta^2}\boldsymbol{Q}_D \cdot \nabla\Theta \, \mathrm{d}\Omega \\
&\leq 0.
\end{aligned} \tag{6.32}
$$

In the calculation leading to (6.32) we make use of the following: the time derivative of the free energy (6.22), the linear momentum balance (6.5) together with integration by parts, and then the energy balance in conservation form (6.24) with integration by parts, and homogeneity of the boundary with respect to the thermal and mechanical fields.

Equation (6.32) implies that the positive-definite functional V is monotonically decreasing along the flow defined by the IBVP, which proves the nonlinear stability of the continuous problem for the specific case outlined above. A similar result for the case of more general boundary conditions is not known, even in the classical case (see also [6]).

6.6 The linearized theory

The purpose of this section is to show that the generalized thermoelasticity problem formulated in this chapter is consistent, in the sense that its linearization is essentially the same as the linear theory discussed in Chapter 2.

The IBVP (6.27) is linearized about the state of reference configuration for which $\boldsymbol{u} = \boldsymbol{0}$, $\boldsymbol{V} = \boldsymbol{0}$, $\alpha = 0$, and $\Theta = \Theta_0$ (or $\vartheta = 0$) are assumed to be natural for the

configuration. As a consequence, the linearized version of IBVP (6.27) is given by

$$\begin{aligned} \dot{\boldsymbol{u}} &= \boldsymbol{V}, \\ \rho \boldsymbol{v} &= \mathrm{div}\boldsymbol{\sigma} + \rho \boldsymbol{b}, \\ \dot{\alpha} &= \Theta, \\ \Theta_0 \dot{\eta} &= -\mathrm{div}\boldsymbol{q} + r, \end{aligned} \tag{6.33}$$

with constitutive equations

$$\boldsymbol{\sigma} = \frac{\partial \psi}{\partial \boldsymbol{\varepsilon}}, \quad \eta = -\frac{\partial \psi}{\partial \Theta}, \quad \boldsymbol{q} = \boldsymbol{q}_e + \boldsymbol{q}_d, \quad \boldsymbol{q}_e = -\Theta_0 \frac{\partial \psi}{\partial \Lambda}, \quad \text{and} \quad \boldsymbol{q}_d = -\mathbf{K}_2 \nabla \Theta, \tag{6.34}$$

where ψ is the quadratic free energy function defined by

$$\psi = \frac{1}{2}\boldsymbol{\varepsilon} : \mathbb{C}\boldsymbol{\varepsilon} - \vartheta \mathbf{m} : \boldsymbol{\varepsilon} - \frac{\rho c}{2\Theta_0}\vartheta^2 + \frac{1}{2}\mathbf{K}_1 \nabla \alpha \cdot \nabla \alpha. \tag{6.35}$$

Then, by (6.34) and (6.35), we obtain

$$\boldsymbol{\sigma} = \mathbb{C}\boldsymbol{\varepsilon} - \vartheta \mathbf{m}, \quad \eta = \frac{\rho c}{\Theta_0}\vartheta + \mathbf{m} : \boldsymbol{\varepsilon}, \quad \text{and} \quad \boldsymbol{q} = -\Theta_0 \mathbf{K}_1 \nabla \alpha - \mathbf{K}_2 \nabla \Theta.$$

Here, $\boldsymbol{\sigma}$, $\boldsymbol{q}$, $\boldsymbol{\varepsilon}$, $\mathbf{m}$ are the stress tensor, the heat flux, the infinitesimal (symmetric) strain, and thermomechanical coupling tensor, respectively. Under the assumption of isotropy, the fourth-order elasticity tensor $\mathbb{C}$, and the non-classical conductivity tensor $\mathbf{K}_1$ are both symmetric and positive-definite, while the classical heat conduction tensor $\mathbf{K}_2$ is symmetric and positive-semidefinite.

Note the similarity between this linearized model and the type III model by Green and Naghdi as discussed in Chapter 2. The only difference is that the non-classical conductivity tensor $\mathbf{K}_1$ is replaced by $\Theta_0 \mathbf{K}_1$.

7

Space-time Galerkin finite element formulations for the nonlinear, generalized thermoelasticity problems

The free energy function (2.8) for the linear case is quadratic and convex. Consequently, the stability of the time-discontinuous formulation for the linear sub-problem in Chapter 3 can be conveniently analyzed in terms of the convexity of the free energy. The convexity property of the elastic energy is particularly important in relating the jumps of the displacement field to that of the elastic potential energy along the interface of any pair of space-time slabs. As a result of this, it can be shown that the same stability estimate as in Chapter 4 can be obtained.

However, in the finite deformation case such convexity assumption leads to nonphysical properties, for example, it is incompatible to the property that as the Jacobian of the deformation tends to zero, the elastic stored energy approaches to infinity. As the consequence of lack of convexity of the stored elastic energy in the finite strain case, the stability of time-discontinuous formulation is more challenging than the linear regime. A weaker type of convexity in which many useful material models are shown to satisfy, and which leads to a well-posed problem is called polyconvexity [7]. However, polyconvexity of the elastic potential is not used to establish stability of the time-discontinuous formulations.

In this chapter, we present various space-time finite element formulations for the generalized thermoelasticity in both monolithic and staggered approaches. In Section 7.1, space-time Galerkin formulations of two monolithic schemes are presented. The first one is referred to as *continuous Galerkin formulation*, in which all the unknown fields are continuous everywhere in the space-time domain Ω. In the second, which we refer to as *mixed Galerkin formulation*, only the thermal unknowns (i.e. α and Θ) are allowed to be discontinuous across any interface of the space-time slabs. In Section 7.2,

staggered schemes based on a stable operator split are presented in both mixed and (fully) time-discontinuous Galerkin formulations.

7.1 Monolithic approach

The lack of convexity of the free energy function in the nonlinear regime complicates how the jumps in the unknown fields are related to the jump in the free energy function. This results a major difficulty in the stability analysis of numerical schemes based on a direct extension of the time-discontinuous Galerkin formulations for the linear problem to the nonlinear one. To circumvent this problem, we consider various space-time Galerkin finite element formulations which do not result in discontinuity jumps in the elastic potential.

In this section we present two space-time Galerkin weak formulations for the generalized thermoelasticity at finite strains using the monolithic approach. In the first formulation, which we refer to as *continuous Galerkin formulation*, it is assumed that all the unknown fields are continuous along any interface of the space-time slabs. In the second formulation the displacement $\boldsymbol{u}$ and the temperature ϑ are assumed to be continuous along the interface of any adjacent space-time slabs, while the velocity $\boldsymbol{V}$ and the thermal displacement α are allowed to be discontinuous along any space-time interfaces. Because of the different continuity assumptions imposed on the various unknown fields of the problem along space-time interfaces we refer to the later formulation as a *mixed Galerkin formulation*.

7.1.1 Continuous Galerkin formulation

Due to the recursive nature of time-stepping algorithms we focus our attention on a typical space-time slab $\mathbb{\Omega}_n = \Omega \times I_n$, which is referred to as the *current space-time slab*. We also refer to the part of the boundary $\Omega \times \{t_n\}$ and $\Omega \times \{t_{n+1}\}$ as the *beginning* and the *end of the space-time slab* $\mathbb{\Omega}_n$ respectively. In each space-time slab, the problem can be viewed as a space-time boundary value problem with the values at the end of the previous slab posed as a boundary condition at the lower end of the space-time boundary of the current slab. Since the problem is first-order in time, we need only one space-time boundary condition in the time direction. This is given by the values at the

end of the previous space-time slab prescribed at the beginning of the current space-time slab, while the the values on other end of the current space-time boundary will be uniquely determined. In this way, we obtain a time-stepping computational algorithm for the nonlinear, generalized thermoelasticity problem in the space-time finite element context.

Assume that (approximate) solutions of the problem (6.27) $\boldsymbol{u}(t_n^-)$, $\boldsymbol{V}(t_n^-)$, $\alpha(t_n^-)$, $\vartheta(t_n^-)$ at the end of the previous space-time slab Ω_{n-1} (that is $\Omega \times \{t_n\}$) are given. Here, for clarity of notation as we have done in the linear case, we omit the spatial dependence of the primary fields. The corresponding space-time Galerkin weak form of the nonlinear evolution problem (6.27) in the space-time domain Ω_n is formally defined as

$$
\begin{aligned}
(\dot{\boldsymbol{u}} - \boldsymbol{V},\ \bar{\boldsymbol{u}})_{\Omega_n} &= 0, \\
(\rho_0 \dot{\boldsymbol{V}},\ \bar{\boldsymbol{v}})_{\Omega_n} + (\boldsymbol{P},\ \nabla \bar{\boldsymbol{v}})_{\Omega_n} &= (\widehat{\mathbf{T}},\ \bar{\boldsymbol{v}})_{\Gamma^n_{\mathbf{T}}} + (\rho_0 \boldsymbol{b},\ \bar{\boldsymbol{v}})_{\Omega_n}, \\
(\dot{\alpha} - \Theta,\ \bar{\alpha})_{\Omega_n} &= 0, \\
(\Theta \dot{\eta} - \frac{1}{\Theta} \boldsymbol{Q}_E \cdot \nabla \Theta,\ \bar{\vartheta})_{\Omega_n} - (\boldsymbol{Q},\ \nabla \bar{\vartheta})_{\Omega_n} &= -(\widehat{Q},\ \bar{\vartheta})_{\Gamma^n_Q} + (R,\ \bar{\vartheta})_{\Omega_n},
\end{aligned}
\tag{7.1}
$$

for functions $\bar{\boldsymbol{u}}$, $\bar{\boldsymbol{v}}$, $\bar{\alpha}$, and $\bar{\vartheta}$ in the space of weighting functions $\mathbb{S}_{\boldsymbol{u}}$, $\mathbb{S}_{\boldsymbol{v}}$, $\mathbb{S}_{\alpha}$, and $\mathbb{S}_{\vartheta}$ respectively. Recall that, the symbol $(\cdot,\ \cdot)_{\square}$ represents the space-time L^2-inner product over the space-time domain or its boundary, the prescribed functions $\widehat{\mathbf{T}}$ and $\widehat{Q}$ are the mechanical and thermal Neumann boundary conditions defined on $\Gamma^n_{\mathbf{T}}$ and Γ^n_Q. The weak formulation (7.1) is supplemented by the space-time boundary conditions

$$
\begin{aligned}
\boldsymbol{u} &= \widehat{\boldsymbol{u}} \qquad && \text{on} \quad \Gamma^n_{\boldsymbol{u}} = \Gamma_{\boldsymbol{u}} \times I_n, \\
\vartheta &= \widehat{\vartheta} \qquad && \text{on} \quad \Gamma^n_{\vartheta} = \Gamma_{\vartheta} \times I_n,
\end{aligned}
\tag{7.2}
$$

and (continuity) space-time boundary conditions that are derived from the given solutions at the end of the previous space-time slab:

$$
\left.
\begin{aligned}
\boldsymbol{u}(t_n^+) &= \boldsymbol{u}(t_n^-) \\
\boldsymbol{V}(t_n^+) &= \boldsymbol{V}(t_n^-) \\
\alpha(t_n^+) &= \alpha(t_n^-) \\
\vartheta(t_n^+) &= \vartheta(t_n^-)
\end{aligned}
\right\} \qquad \text{on} \quad \Omega. \tag{7.3}
$$

Equations (7.1)–(7.3) define a space-time version of a coupled nonlinear boundary problem for a thermomechanical system in the generalized setting with the respective constitutive equations relating the heat flux vector $\boldsymbol{Q}$ and the first-Kirchhoff stress tensor $\boldsymbol{P}$ to the thermal fields (ϑ and/or α) and the displacement $\boldsymbol{u}$.

The weak problem (7.1) can be posed in a more formal way as follows: find $\mathcal{X} = (\boldsymbol{u},\ \boldsymbol{V},\ \alpha,\ \vartheta)$ in $\mathbb{V}_{\boldsymbol{u}} \times \mathbb{V}_{\boldsymbol{V}} \times \mathbb{V}_{\alpha} \times \mathbb{V}_{\vartheta}$ such that for each $\bar{\mathcal{X}} = (\bar{\boldsymbol{u}},\ \bar{\boldsymbol{v}},\ \bar{\alpha},\ \bar{\vartheta})$ in $\mathbb{S}_{\boldsymbol{u}} \times \mathbb{S}_{\boldsymbol{v}} \times \mathbb{S}_{\alpha} \times \mathbb{S}_{\vartheta}$

$$B^{\mathrm{MC}}(\mathcal{X},\ \bar{\mathcal{X}}) = l^{\mathrm{MC}}(\bar{\mathcal{X}}),$$

where the nonlinear functional B^{MC} and the right-hand-side l^{MC} are given by

$$\begin{aligned} B^{\mathrm{MC}}(\mathcal{X},\ \bar{\mathcal{X}}) &= (\dot{\boldsymbol{u}} - \boldsymbol{V},\ \bar{\boldsymbol{u}})_{\mathbb{\Omega}_n} + (\rho_0 \dot{\boldsymbol{V}},\ \bar{\boldsymbol{v}})_{\mathbb{\Omega}_n} + (\boldsymbol{P},\ \nabla \bar{\boldsymbol{v}})_{\mathbb{\Omega}_n} + (\dot{\alpha} - \Theta,\ \bar{\alpha})_{\mathbb{\Omega}_n} + \\ &\qquad (\Theta \dot{\eta} - \frac{1}{\Theta} \boldsymbol{Q}_E \nabla \Theta,\ \bar{\vartheta})_{\mathbb{\Omega}_n} - (\boldsymbol{Q},\ \nabla \bar{\vartheta})_{\mathbb{\Omega}_n}, \\ l^{\mathrm{MC}}(\bar{\mathcal{X}}) &= (\widehat{\mathbf{T}},\ \bar{\boldsymbol{v}})_{\mathbb{\Gamma}^n_{\mathbf{T}}} + (\rho_0 \boldsymbol{b},\ \bar{\boldsymbol{v}})_{\mathbb{\Omega}_n} - (\widehat{Q},\ \bar{\vartheta})_{\mathbb{\Gamma}^n_{Q}} + (R,\ \bar{\vartheta})_{\mathbb{\Omega}_n}. \end{aligned}$$

Here the superscript MC is used to represent the fact that the quantities are referred to the *monolithic* approach for the *continuous* space-time Galerkin formulation.

Conservation property

It is immediately apparent that the continuous Galerkin formulation (7.1) is consistent with the corresponding local form (6.27) over each space-time domain $\mathbb{\Omega}_n$, and hence over $\mathbb{\Omega} = \Omega \times \mathbb{I}$. Moreover, since the formulation (7.1) does not include special terms, such as, jumps and 'artificial viscosities', it can also be shown that the continuous Galerkin scheme conserves the total energy in the case of type II model, in which the dissipative heat flux $\boldsymbol{Q}_D$ vanishes.

The continuous Galerkin formulation described above restricted to the isothermal elastodynamics case comfortably falls under the category of energy-momentum conserving schemes for nonlinear problems in continuum mechanics. Energy-momentum conserving methods were first introduced in the literature in the pioneering work of Simo and co-workers [89] in the framework of the method-of-lines (MoL) approach (a numerical procedure for time dependent partial differential equations where finite element is applied spatially, followed by temporal discretization using finite difference).

Such conservative methods are obtained by replacing the elastic potential or free energy function (which is generally non-convex in the finite strain regime) with a second-order approximate convex approximation. Then the stress constitutive equations is derived numerically from this convex approximation. This effectively means that the problem solved by such schemes is just a modification of the actual problem, in which the non-convex elastic potential function is replaced by a second-order approximation of a convex function, limiting the consistency to that order.

In this respect, the current space-time finite element formulation (continuous Galerkin formulation) offers a better option for numerically solving nonlinear problems of elastodynamics in that conservation is attained without the need to modify the elastic potential function, implying an arbitrary order of consistency.

7.1.2 Mixed Galerkin formulation

As already noted, the numerical scheme corresponding to the continuous space-time Galerkin formulation is energy conservative in the case for which the dissipative component $\boldsymbol{Q}_D$ of the heat flux vanishes. Generally it represents an optimal amount of dissipation in the sense that it does not contribute additional numerical dissipation other than the dissipative nature of the partial differential equation itself.

However, there are various situations in which the solution involves sharp gradient or shock propagations. It is a well known fact that, in the nonlinear case, shock may arise in a finite time even with a sufficiently smooth initial solution. In such cases, the continuous Galerkin could fail to give an accurate approximation as it can not offer additional dissipation mechanism to damp and localize spurious numerical oscillations that may be numerically created in the vicinity of the shock or high gradients. To alleviate the issue of representing shocks in numerical solutions the mixed Galerkin formulation, in which only temperature and thermal displacement fields are allowed to be discontinuous across the interfaces of space-time slabs, can provide an important alternative. The jump terms with respect to the velocity and thermal displacement offer additional numerical viscosity giving the scheme a mechanism to faithfully capture discontinuities in the solution without degrading the accuracy. The added viscosity through the jump terms is technically not an 'artificial viscosity' as it scales down as the mesh size diminishes. This is a very important property in view of convergence to

the true (exact) solution, because adding an 'artificial viscosity' amounts modifying the numerical scheme so that the limiting solution as the mesh gets refined is no longer the solution of the original problem, which is a disadvantage.

In this case, we focus our attention on the generalized thermomechanical description of materials corresponding to the canonical free energy function of the form

$$V(\boldsymbol{\mathcal{X}}) = \int_{\Omega} [\Psi_c + \frac{1}{2}\mathbf{k}_1 \nabla\alpha \cdot \nabla\alpha + \vartheta\eta + \frac{1}{2}\rho_0 \boldsymbol{V} \cdot \boldsymbol{V}] \mathrm{d}\Omega,$$

where $\Psi(\boldsymbol{F}, \vartheta, \nabla\alpha) = \Psi_c(\boldsymbol{F}, \vartheta) + \frac{1}{2}\mathbf{k}_1 \nabla\alpha \cdot \nabla\alpha$ is the free energy in the generalized sense, while Ψ_c is its classical counterpart. Here it is important to note that the classical free energy Ψ_c is not generally convex in its arguments. However, we can see that V is quadratic in $\nabla\alpha$ and $\boldsymbol{V}$, and is convex with respect to these variables for each arbitrary but fixed choice of $\boldsymbol{u}$ and ϑ in their corresponding state spaces. The continuity assumptions on $\boldsymbol{u}$ and ϑ imply that the jumps of $\Theta\eta$ and $\boldsymbol{u}$ along the the space-time interface $\Omega \times \{t_n\}$ vanish, that is

$$[\![\Theta(t_n)\eta(t_n)]\!] = 0, \quad \text{and} \quad [\![\boldsymbol{u}(t_n)]\!] = \mathbf{0}.$$

On the other hand the jumps of $\boldsymbol{V}$ and α may not necessarily be zero across such space-time interfaces. The continuity of these unknowns across the interfaces is then weakly enforced using a spatial L^2-inner product.

Assume that the (approximate) solutions $\boldsymbol{u}(t_n^-)$, $\boldsymbol{V}(t_n^-)$, $\alpha(t_n^-)$, and $\vartheta(t_n^-)$, at the end of the previous space-time slab, are given. Note that, since $\boldsymbol{V}$ and α are allowed to be discontinuous across the interface $\Omega \times \{t_n\}$ they might take different values from the right (t_n^+) and left (t_n^-) of t_n. While $\boldsymbol{u}$ and ϑ take just one value at each point in the space-time domain. The continuity of $\boldsymbol{u}$ and ϑ will be enforced as space-time boundary conditions along the beginning of the current space-time slab. In this case, the known values $\boldsymbol{u}(t_n^-)$ and $\vartheta(t_n^-)$ at the end of the previous slab are prescribed as a space-time Dirichlet boundary condition at the beginning of the current slab for $\boldsymbol{u}(t_n^+)$ and $\vartheta(t_n^+)$ respectively. Formally these boundary conditions are mathematically described as

$$\left.\begin{aligned} \boldsymbol{u}(t_n^+) &= \boldsymbol{u}(t_n^-) \\ \vartheta(t_n^+) &= \vartheta(t_n^-) \end{aligned}\right\} \quad \text{on} \quad \Omega \tag{7.4}$$

The mixed Galerkin weak formulation for the nonlinear coupled problem of generalized thermoelasticity in the monolithic regime is as follows: find $\boldsymbol{\mathcal{X}} = (\boldsymbol{u}, \boldsymbol{V}, \alpha, \vartheta)^{\mathtt{T}} \in \mathbb{V}$ such that

$$\begin{aligned}
(\dot{\boldsymbol{u}} - \boldsymbol{V},\ \bar{\boldsymbol{u}})_{\Omega_n} &= 0,\\
(\rho_0 \dot{\boldsymbol{V}},\ \bar{\boldsymbol{v}})_{\Omega_n} + (\boldsymbol{P},\ \nabla \bar{\boldsymbol{v}})_{\Omega_n} + \langle [\![\rho_0 \boldsymbol{V}(t_n)]\!],\ \bar{\boldsymbol{v}}(t_n^+) \rangle &= (\widehat{\mathbf{T}},\ \bar{\boldsymbol{v}})_{\Gamma_{\mathbf{T}}^n} + (\rho_0 \boldsymbol{b},\ \bar{\boldsymbol{v}})_{\Omega_n},\\
(\dot{\alpha} - \boldsymbol{\Theta},\ \bar{\alpha})_{\Omega_n} + \langle [\![\alpha(t_n)]\!],\ \bar{\alpha}(t_n^+) \rangle &= 0,\\
(\Theta \dot{\eta} - \frac{1}{\Theta} \boldsymbol{Q}_E \nabla \Theta,\ \bar{\vartheta})_{\Omega_n} - (\boldsymbol{Q},\ \nabla \bar{\vartheta})_{\Omega_n} &= -(\widehat{Q},\ \bar{\vartheta})_{\Gamma_Q^n} + (R,\ \bar{\vartheta})_{\Omega_n},
\end{aligned} \tag{7.5}$$

for weight functions $\bar{\boldsymbol{u}}$, $\bar{\boldsymbol{v}}$, $\bar{\alpha}$, and $\bar{\vartheta}$. Recall that the symbol $\langle \cdot,\ \cdot \rangle$ denotes the L^2-inner product over the space of admissible functions defined on Ω, in other words it is the spatial integral of the pointwise product of two functions. The argument t_n^+ of the weight functions in the integrals involving the jump terms represents their values is taken at t_n^+.

In order to specify the weak formulation (7.5) completely, in addition to the space-time boundary condition (7.4), boundary conditions, of the form (7.2), along parts of Γ have to be supplemented for all time $t \in [t_n,\ t_{n+1}]$.

A sufficiently smooth solution of the strong form (6.27) also solves the weak problem (7.5), since the jump terms vanish at the continuous fields. The jump integrals offer enhanced stability behaviour that perform well in capturing solutions involving large gradients or shocks. The enhanced stability property is obtained without the necessity of adding 'artificial viscosity', which potentially results in solving a modified form of the problem. In addition the jump integrals get smaller as we increase the resolution by refining the space-time mesh. On the other hand, artificial viscosities are values which are added externally, independent of the refinement level (that is the amount of artificial viscosity stays the same no matter how refined the space-time mesh is).

7.2 Staggered approaches

Both of the above mentioned space-time formulations are monolithic, i.e., all the four unknown functions are solved for simultaneously in each space-time slab. This is particularly an issue in terms of efficiency in the time-discontinuous Galerkin framework,

in which the number of unknowns to be solved for are increased, because of the discontinuity assumptions along the interfaces. An alternative approach, for such coupled problems, that has better efficiency while maintaining the stability property of the monolithic scheme, can be to use a staggered method where the the unknowns are grouped in some particular way so that at each space-time slab each group is solved sequentially in predictor-corrector manner (or possibly independently) to obtain the solution of the original problem at the end of the current slab. Such staggered methods have been discussed in detail in Chapter 3 for the linear generalized thermoelastic problem under operator-splitting.

In this section we first present a stable operator-split of the nonlinear generalized thermoelastic problem into two stable sub-problems. We then present two space-time formulations, namely *mixed* and *fully time-discontinuous* Galerkin methods. The former is based on the same continuity assumptions as the mixed time-discontinuous Galerkin formulation (7.5) in the monolithic regime, but applied in a staggered approach. The latter is based on discontinuity assumptions of all the four unknowns $\boldsymbol{u}$, $\boldsymbol{V}$, α, and ϑ across any space-time interfaces of the form $\Omega \times \{t_n\}$.

7.2.1 Operator split for the nonlinear, generalized thermoelasticity

A stable staggered algorithm based on the operator-splitting approach was first introduced for classical nonlinear thermoelasticity in [6]. The idea is that the fully coupled nonlinear problem is split into two smaller sub-problems, each inheriting the same stability behaviour as the global (original) problem. In Chapter 3 this idea is extended to generalized thermoelasticity in the linear case. In the following an operator split is considered such that the entropy and the thermal displacement are held fixed during the first phase, followed by the non-classical thermal conduction at fixed configuration in the second phase. We then proceed to show that each of the sub-problems inherit the stability property of the global problem.

Here, we extend the operator split methodology in Chapter 3 to the fully coupled nonlinear IBVP (6.27) described in Section 6.3. For the sake of clarity of exposition,

let us redefine, for now, the state vector $\boldsymbol{\mathcal{X}}$ by replacing[1] the relative temperature ϑ by the entropy η; that is, $\boldsymbol{\mathcal{X}} = (\boldsymbol{u}, \boldsymbol{V}, \alpha, \eta)^{\mathrm{T}}$.

The governing equations of generalized thermoelasticity (6.27) can be formally written as a first-order nonlinear evolution problem of the form

$$\dot{\boldsymbol{\mathcal{X}}} = \mathbf{G}(\boldsymbol{\mathcal{X}}), \quad \text{with} \;\; \boldsymbol{\mathcal{X}}(t_0) = \boldsymbol{\mathcal{X}}_0,$$

where $\mathbf{G}$ is a nonlinear operator on some suitably defined space; specifically, it is defined as

$$\mathbf{G}(\boldsymbol{\mathcal{X}}) \coloneqq \begin{bmatrix} \boldsymbol{V} \\ \dfrac{1}{\rho_0}\mathrm{Div}\boldsymbol{P} + \mathbf{B} \\ \Theta \\ -\dfrac{1}{\Theta}\mathrm{Div}\boldsymbol{Q} + \dfrac{1}{\Theta^2}\boldsymbol{Q}_E \cdot \nabla\Theta + \dfrac{1}{\Theta}R \end{bmatrix}.$$

The nonlinear operator $\mathbf{G}$ can be additively split into two operators $\mathbf{G}_1$ and $\mathbf{G}_2$ such that

$$\mathbf{G}_1 = \begin{bmatrix} \boldsymbol{V} \\ \dfrac{1}{\rho_0}\mathrm{Div}\boldsymbol{P} + \mathbf{B} \\ 0 \\ 0 \end{bmatrix}, \quad \text{and} \;\; \mathbf{G}_2 = \begin{bmatrix} \mathbf{0} \\ \mathbf{0} \\ \Theta \\ -\dfrac{1}{\Theta}\mathrm{Div}\boldsymbol{Q} + \dfrac{1}{\Theta^2}\boldsymbol{Q}_E \cdot \nabla\Theta + \dfrac{1}{\Theta}R \end{bmatrix}. \tag{7.6}$$

Clearly $\mathbf{G} = \mathbf{G}_1 + \mathbf{G}_2$. Next, consider the evolution sub-problems

$$\dot{\boldsymbol{\mathcal{X}}} = \mathbf{G}_1(\boldsymbol{\mathcal{X}}), \quad \text{and} \; \dot{\boldsymbol{\mathcal{X}}} = \mathbf{G}_2(\boldsymbol{\mathcal{X}}). \tag{7.7}$$

Following the terminology coined in [6], we refer to the first problem the *mechanical phase*, and the second one the *thermal phase*.

It is known that the nonlinear elastodynamics problem is energy-conserving provided that the potential for external loadings is conservative. By fixing the entropy in time the energy conservative behaviour of mechanical phase is still maintained, even though there might be variations in temperature in the process. The thermal phase represents

[1] Since, for fixed configuration, η is a function of ϑ and vice-versa, both groups of state variables $(\boldsymbol{u}, \boldsymbol{V}, \alpha, \eta)^{\mathrm{T}}$ and $(\boldsymbol{u}, \boldsymbol{V}, \alpha, \vartheta)^{\mathrm{T}}$ can equivalently and fully represent any thermomechanical system.

a dissipative process provided that $\boldsymbol{Q}_D \neq \boldsymbol{0}$, otherwise it is energy conservative as well. This observation can be proved as follows: let $\boldsymbol{\mathcal{X}}^{\mathrm{M}}$ and $\boldsymbol{\mathcal{X}}^{\mathrm{T}}$ be two state vectors satisfying the mechanical and thermal problem (7.7). Then

$$\begin{aligned} \frac{\mathrm{d}}{\mathrm{d}t}V(\boldsymbol{\mathcal{X}}^{\mathrm{M}}) &= \int_{\Omega}[\boldsymbol{P} : \dot{\boldsymbol{F}} + \rho_0 \dot{\boldsymbol{V}} \cdot \boldsymbol{V}] \, \mathrm{d}\Omega + \frac{\mathrm{d}}{\mathrm{d}t}\Pi_{ext} = 0, \\ \frac{\mathrm{d}}{\mathrm{d}t}V(\boldsymbol{\mathcal{X}}^{\mathrm{T}}) &= \int_{\Omega}[-\frac{1}{\Theta}\boldsymbol{Q}_E \cdot \nabla\Theta + \vartheta\dot{\eta}] \, \mathrm{d}\Omega = \int_{\Omega} \frac{\Theta_0}{\Theta}\boldsymbol{Q}_D \cdot \nabla\Theta \, \mathrm{d}\Omega \leq 0. \end{aligned} \tag{7.8}$$

Hence, the estimates in (7.8) show that both of the sub-problems share the same stability property as the global problem, and the thermal phase becomes conservative like the mechanical phase if $\boldsymbol{Q}_D = \boldsymbol{0}$. This is a desirable property in the sense that if there are consistent and stable time-stepping algorithms for each of the sub-problems, then a consistent and stable algorithm for the global problem is formally constructed by way of the product formula.

In the following, we present a stable semi-discrete approximation scheme for the mechanical and thermal phases based on a space-time finite element methodology.

7.2.2 Mixed space-time FE formulation

In the following we discuss a staggered algorithm based on a mixed time-discontinuous Galerkin formulation for both the mechanical and thermal phases. In the mechanical phase, an iterative procedure based on Newton's method is used to obtain an *intermediate temperature*, denoted by $\tilde{\Theta}$, which corresponds to a constant entropy. Consequently, the mechanical phase is reduced to a classical problem of elastodynamics with the stress constitutive relation corresponding to the intermediate temperature. The mechanical phase amounts to a purely heat conduction problem in the generalized regime, posed in conservation form.

Mechanical phase

Let us go back to our original definition of the state vector $\boldsymbol{\mathcal{X}} = (\boldsymbol{u}, \boldsymbol{V}, \alpha, \vartheta)^{\mathrm{T}}$. Assume that the solution $\boldsymbol{\mathcal{X}}(t_n^-)$ at the end of the previous space-time slab is known. In the mechanical phase the energy equation (i.e. $\Theta\dot{\eta} = 0$) can be viewed as a constraint on the elastodynamics problem involving a time-varying intermediate temperature $\tilde{\Theta}$ in

the stress. Fixed entropy in the mechanical phase implies that

$$\eta(\boldsymbol{F}(t), \tilde{\Theta}(t)) = \eta(\boldsymbol{F}(t_n^-), \Theta(t_n^-)), \qquad (t \in I_n). \tag{7.9}$$

This expression is purely algebraic but nonlinearly implicit in the intermediate temperature $\tilde{\Theta}$. The sole purpose of the intermediate temperature is to restrict the entropy to be fixed at the state at the end of the previous slab and to contribute a thermal influence to the stress $\boldsymbol{P}$ in the mechanical phase. In most practical applications, the intermediate temperature $\tilde{\Theta}$ can be solved in closed form, see for example, [6]. In general, a local iterative procedure can be used to solve for $\tilde{\Theta}$ numerically. For example, an iterative Newton scheme can be applied as follows:

Dropping the argument t, let the residual be

$$h(\tilde{\Theta}) = \eta(\boldsymbol{F}, \tilde{\Theta}) - \eta(\boldsymbol{F}(t_n^-), \Theta(t_n^-)). \tag{7.10}$$

Observe that

$$\frac{\partial h}{\partial \tilde{\Theta}} = \frac{\partial \eta}{\partial \tilde{\Theta}} = -\frac{\partial^2 \Psi}{\partial \tilde{\Theta}^2} = \frac{\rho_0 c_F}{\tilde{\Theta}}, \tag{7.11}$$

where $c_F > 0$ is the heat capacity, see (6.26). Now, by way of Newton's method, define recursively a sequence of approximate intermediate temperatures $\{\tilde{\Theta}_k\}_{k=0}^{\infty}$ (usually initialized at the value $\tilde{\Theta}_0 = \Theta(t_n^-)$ of the temperature at the end of the previous space-time slab) such that

$$\tilde{\Theta}_0 = \Theta(t_n^-), \quad \tilde{\Theta}_{k+1} = \tilde{\Theta}_k \left[1 - \frac{1}{\rho_0 c_F} h(\tilde{\Theta}_k) \right]. \tag{7.12}$$

Since in most practical situations the exact solution $\tilde{\Theta}$ is close to $\Theta(t_n^-)$, usually up to four iteration steps are enough to get to a desirable level of convergence. Note that the local iteration (7.12) is explicit (which doesn't involve inverting a matrix), and the numerical cost associated to it is almost negligible relative to the cost of the solving the mechanical problem as a whole.

After evaluating the stress at $\boldsymbol{F} = \boldsymbol{F}(t)$, $\Theta = \tilde{\Theta}$, and $\alpha = \alpha(t_n^-)$ from the constitutive relation $(6.20)_1$ as

$$\boldsymbol{P} = \left. \frac{\partial \Psi}{\partial \boldsymbol{F}} \right|_{\boldsymbol{F}(t),\ \tilde{\Theta},\ \alpha(t_n^-)}, \tag{7.13}$$

the problem in the mechanical phase reduces to a nonlinear elastodynamics problem

$$\begin{aligned} \dot{\boldsymbol{u}} &= \boldsymbol{V} \\ \rho_0 \dot{\boldsymbol{V}} &= \mathrm{Div}\boldsymbol{P} + \rho_0 \boldsymbol{b}, \end{aligned} \tag{7.14}$$

subject to appropriate initial and boundary conditions derived from that of the coupled IBVP (6.27).

Next, we construct a mixed-type space-time Galerkin formulation of the mechanical problem. For the sake of minimizing the number and complexity of symbols, we use the notation for the state vectors $\boldsymbol{\mathcal{X}}$ for $(\boldsymbol{u}, \boldsymbol{V})^{\mathrm{T}}$, the space of admissible $\mathbb{V}$ and weighting $\mathbb{S}$ spaces as in the case of the fully-coupled thermoelasticity problem. To this end we adopt the notation

$$\boldsymbol{\mathcal{X}} = (\boldsymbol{u}, \boldsymbol{V})^{\mathrm{T}} \in \mathbb{V} = \mathbb{V}_{\boldsymbol{u}} \times \mathbb{V}_{\boldsymbol{V}}, \quad \text{and} \quad \bar{\boldsymbol{\mathcal{X}}} = (\bar{\boldsymbol{u}}, \bar{\boldsymbol{v}})^{\mathrm{T}} \in \mathbb{S} = \mathbb{S}_{\boldsymbol{u}} \times \mathbb{S}_{\boldsymbol{V}}.$$

Next, we define the mixed time-discontinuous weak formulation for the problem (7.14) in the mechanical phase as follows. We seek a solution $\boldsymbol{\mathcal{X}}(t) \in \mathbb{V}$ defined in the current space-time slab $\mathbb{\Omega}_n$, such that for each $\bar{\mathcal{X}} \in \mathbb{S}$

$$B^M_{MG}[\boldsymbol{\mathcal{X}}, \bar{\boldsymbol{\mathcal{X}}}] = L^M_{MG}(\bar{\boldsymbol{\mathcal{X}}}), \tag{7.15}$$

where

$$B^M_{MG}[\boldsymbol{\mathcal{X}}, \bar{\boldsymbol{\mathcal{X}}}] = (\dot{\boldsymbol{u}} - \boldsymbol{V},\ \bar{\boldsymbol{u}})_{\mathbb{\Omega}_n} + (\rho_0 \dot{\boldsymbol{V}},\ \bar{\boldsymbol{v}})_{\mathbb{\Omega}_n} + (\boldsymbol{P},\ \nabla \bar{\boldsymbol{v}})_{\mathbb{\Omega}_n} + \langle \rho_0 \boldsymbol{V}(t_n^+),\ \bar{\boldsymbol{v}}(t_n^+) \rangle,$$

$$L^M_{MG}(\bar{\boldsymbol{\mathcal{X}}}) = (\widehat{\mathbf{T}},\ \bar{\boldsymbol{v}})_{\mathbb{\Gamma}^{\mathbf{T}}_n} + (\rho_0 \boldsymbol{b},\ \bar{\boldsymbol{v}})_{\mathbb{\Omega}_n} + \langle \rho_0 \boldsymbol{V}(t_n^-),\ \bar{\boldsymbol{v}}(t_n^+) \rangle.$$

The superscript M refers to the mechanical problem, whereas, the subscript $_{MG}$ refers to mixed time-discontinuous Galerkin formulation. Equation (7.15) is supplemented with the space-time initial-boundary conditions

$$\boldsymbol{u} = \widehat{\boldsymbol{u}} \qquad \text{on} \quad \mathbb{\Gamma}_{\boldsymbol{u}}^n = \Gamma_{\boldsymbol{u}} \times I_n, \tag{7.16}$$

$$\boldsymbol{V}(t_n^+) = \boldsymbol{V}(t_n^-) \qquad \text{on} \quad \Omega. \tag{7.17}$$

Hence, equation (7.15) along with the space-time boundary conditions (7.16) and (7.17) defines a space-time boundary value problem for nonlinear elastodynamics with constitutive equation for the stress given by (7.13). The corresponding Euler-Lagrange forms to (7.15) are written as

$$\begin{aligned} 0 &= (\dot{\boldsymbol{u}} - \boldsymbol{V},\ \bar{\boldsymbol{u}})_{\mathbb{\Omega}_n}, \\ 0 &= (\rho_0 \dot{\boldsymbol{V}} - \mathrm{Div}\boldsymbol{P} - \rho_0 \boldsymbol{b},\ \bar{\boldsymbol{V}})_{\mathbb{\Omega}_n} + \langle [\![\rho_0 \boldsymbol{V}(t_n)]\!],\ \bar{\boldsymbol{v}}(t_n^+) \rangle, \end{aligned} \tag{7.18}$$

for each $\bar{\boldsymbol{u}} \in \mathbb{S}_{\boldsymbol{u}}$ and $\bar{\boldsymbol{V}} \in \mathbb{S}_{\boldsymbol{V}}$. Since a sufficiently smooth exact solution of the local (strong) form (7.14) satisfies the Euler-Lagrange forms (7.18) and vice-versa, the time-discontinuous weak formulation (7.15) is consistent with the local form (7.14).

Following the standard procedure of the finite element method, we replace the trial and weighting function spaces by the finite dimensional spaces $\mathbb{V}^h$ and $\mathbb{S}^h$ in the space-time weak form (7.15) and apply the space-time boundary conditions (7.16) and (7.17) to get a system of nonlinear algebraic equations. Usually such system of nonlinear equations is solved using iterative (incremental) approaches such as Newton's method to obtain approximate solutions for $\boldsymbol{u}$ and $\boldsymbol{V}$ in the current space-time slab $\mathbb{\Omega}_n$. From a time-stepping point of view, we are particularly interested in the part of these solutions at the end of the slab, that is, $\boldsymbol{u}(t_{n+1}^-)$ and $\boldsymbol{V}(t_{n+1}^-)$. These constitute the approximate solution to the global coupled problem corresponding to the mechanical fields.

What is then remaining is to approximate the solution for the thermal field. This is pursued in the following, in the context of the time-discontinuous Galerkin formulation.

Thermal phase

The outputs of interest from the mechanical phase are approximate solutions $\boldsymbol{u}(t_{n+1}^-)$ and $\boldsymbol{V}(t_{n+1}^-)$ at the end of the current space-time slab. To complete the solution for the fully coupled problem, we need to solve the problem of the thermal phase, which represents a purely nonlinear generalized heat conduction problem under fixed configuration, that is,

$$\left.\begin{aligned} \dot{\alpha} &= \Theta \\ \Theta\dot{\eta} &= -\frac{1}{\Theta}\mathrm{Div}\boldsymbol{Q} + \frac{1}{\Theta^2}\boldsymbol{Q}_E\cdot\nabla\Theta + \frac{1}{\Theta}R \end{aligned}\right\} \quad \text{in} \quad \mathbb{\Omega}_n \tag{7.19}$$

subject to appropriate space-time boundary conditions which will be discussed as we present the mixed-type space-time Galerkin formulation. After solving for α and ϑ in the space-time domain $\mathbb{\Omega}_n$, a complete solution of interest for the nonlinear coupled problem consists of the values of the solutions of the mechanical and thermal phases at the end of the current time step, that is, $\boldsymbol{u}(t_{n+1}^-)$, $\boldsymbol{V}(t_{n+1}^-)$, $\alpha(t_{n+1}^-)$, and $\vartheta(t_{n+1}^-)$.

Because only α and η have first-order derivative in time and they are constant in the mechanical phase, with respect to the current space-time slab $\mathbb{\Omega}_n$ their initial condition is the values at the end of the previous slab $\mathbb{\Omega}_{n-1}$.

The time-discontinuous Galerkin formulation for the thermal phase in the space-time domain $\mathbb{\Omega}_n$ is defined as: find $\boldsymbol{\mathcal{X}}^T = (\alpha,\ \vartheta)^{\mathtt{T}} \in \mathbb{V}_\alpha \times \mathbb{V}_\vartheta$, for each $\bar{\boldsymbol{\mathcal{X}}}^T = (\bar{\alpha}, \bar{\vartheta})$ such that

$$B_{MG}^T[\boldsymbol{\mathcal{X}}^{\boldsymbol{T}}, \bar{\boldsymbol{\mathcal{X}}}^T] = L_{MG}^T(\bar{\boldsymbol{\mathcal{X}}}^T), \tag{7.20}$$

where

$$B_{MG}^T[\boldsymbol{\mathcal{X}}^T, \bar{\boldsymbol{\mathcal{X}}}^T] = (\dot{\alpha} - \Theta,\ \bar{\alpha})_{\mathbb{\Omega}_n} + (\Theta\dot{\eta} - \frac{1}{\Theta}\boldsymbol{Q}_E\cdot\nabla\Theta,\ \bar{\vartheta})_{\mathbb{\Omega}_n} - (\boldsymbol{Q},\ \nabla\bar{\vartheta})_{\mathbb{\Omega}_n} + \langle\alpha(t_n^+),\ \bar{\alpha}(t_n^+)\rangle$$

$$L_{MG}^T(\bar{\boldsymbol{\mathcal{X}}}^T) = -(\widehat{Q},\ \bar{\vartheta})_{\mathbb{\Gamma}_Q^n} + (R,\ \bar{\vartheta})_{\mathbb{\Omega}_n} + \langle\alpha(t_n^-),\ \bar{\alpha}(t_n^+)\rangle.$$

Here the only non-vanishing jump term is

$$[\![\alpha(t_n)]\!] = \alpha(t_n^+) - \alpha(t_n^-).$$

The space-time Galerkin formulation (7.20) supplemented by the corresponding thermal constitutive relation for $\boldsymbol{Q},\ \boldsymbol{Q}_E,$ and η in terms of α, Θ and the space-time boundary conditions of the form

$$\vartheta = \widehat{\vartheta} \qquad \text{on} \quad \mathbb{\Gamma}_\vartheta^n = \Gamma_\vartheta \times I_n, \tag{7.21}$$

$$\eta(t_n^+) = \eta(t_n^-) \qquad \text{on} \quad \Omega, \tag{7.22}$$

defines a space-time boundary value problem.

In a similar way as in the previous formulations, it can be shown that the time-discontinuous formulation (7.20) is consistent with the IBVP (7.19). Following the standard finite element procedure on the space-time domain $\mathbb{\Omega}_n$, we replace the trial and weighting functions spaces by their finite dimensional counterparts to obtain a system of nonlinear algebraic equation, which will be solved using Newton's method for the thermal solution on the current space-time domain.

7.2.3 Fully time-discontinuous FE formulation

In this section we present a staggered approach consisting of algorithms based on a time-discontinuous Galerkin formulation for both the mechanical and thermal phase (7.14) and (7.19), respectively.

Suppose we have the approximate solutions $\boldsymbol{u}(t_n^-)$, $\boldsymbol{V}(t_n^-)$, $\alpha(t_n^-)$, and $\vartheta(t_n^-)$ at the end of the previous space-time slab. Our aim is to find the corresponding solutions in the current slab $\mathbb{\Omega}_n$, particularly the solutions at the end of the slab. As noted previously, the operator-split (7.6) is characterized by the entropy controlling mechanism in which at each time-step both the mechanical and thermal phases are solved simultaneously.

Mechanical phase

Applying the entropy constraint $\Theta\dot{\eta} = 0$ and following the same argument leading to (7.13), we find the stress constitutive relation in terms of the intermediate temperature. Here we present a fully time-discontinuous Galerkin formulation for the IBVP (7.14) of the mechanical phase.

The fully time-discontinuous Galerkin formulation for the problem in the mechanical phase is defined as follows: We seek a solution $\boldsymbol{\mathcal{X}}(t) \in \mathbb{V}_{\boldsymbol{u}} \times \mathbb{V}_{\boldsymbol{V}}$ defined in the current space-time slab $\mathbb{\Omega}_n$, such that for each test state $\bar{\boldsymbol{\mathcal{X}}} \in \mathbb{S}_{\boldsymbol{u}} \times \mathbb{S}_{\boldsymbol{V}}$

$$B_{DG}^{M}[\boldsymbol{\mathcal{X}}, \bar{\boldsymbol{\mathcal{X}}}] = L_{DG}^{M}(\bar{\boldsymbol{\mathcal{X}}}), \tag{7.23}$$

where

$$B^M_{DG}[\boldsymbol{\mathcal{X}}, \bar{\boldsymbol{\mathcal{X}}}] = (\dot{\boldsymbol{u}} - \boldsymbol{V},\ \bar{\boldsymbol{u}})_{\Omega_n} + (\rho_0 \dot{\boldsymbol{V}},\ \bar{\boldsymbol{v}})_{\Omega_n} + (\boldsymbol{P},\ \nabla \bar{\boldsymbol{v}})_{\Omega_n} + \langle \boldsymbol{u}(t_n^+),\ \bar{\boldsymbol{u}}(t_n^+)\rangle + \langle \rho_0 \boldsymbol{V}(t_n^+),\ \bar{\boldsymbol{v}}(t_n^+)\rangle,$$

$$L^M_{DG}(\bar{\boldsymbol{\mathcal{X}}}) = (\widehat{\mathbf{T}},\ \bar{\boldsymbol{v}})_{\mathbb{\Gamma}^{\mathtt{T}}_n} + (\rho_0 \boldsymbol{b},\ \bar{\boldsymbol{v}})_{\Omega_n} + \langle \boldsymbol{u}(t_n^-),\ \bar{\boldsymbol{u}}(t_n^+)\rangle + \langle \rho_0 \boldsymbol{V}(t_n^-),\ \bar{\boldsymbol{v}}(t_n^+)\rangle.$$

Equation (7.23) subject to the appropriate space-time boundary condition derived from the mechanical Dirichlet boundary conditions and the constitutive equation of the form (7.13) gives the weak form of the space-time boundary value problem. Note that the solutions for the mechanical fields at the end of the previous space-time slab are incorporated into the weak formulation (7.23) through the L^2-inner product to enforce the continuity of the mechanical fields weakly across the space-time interface.

Following similar arguments leading to the consistency of the space-time Galerkin formulation in the monolithic case, it can be easily shown that the formulation (7.23) is consistent with the strong initial-boundary value problem (7.14).

Thermal phase

Here we present a fully time-discontinuous Galerkin formulation for the IBVP (7.19) in the thermal phase. The mechanical fields in this case are fixed at the values $\boldsymbol{u}(t^-_{n+1})$ and $\boldsymbol{V}(t^-_{n+1})$ at the end of the mechanical phase within the current space-time slab. Since entropy η and α were fixed during the mechanical phase at their values at the end of the previous slab, the continuity of entropy and thermal displacement in the thermal phase are enforced weakly through the jumps between their values at t_n^+ of the thermal phase and at (t_n^-) of the previous solution.

Formally, the fully time-discontinuous Galerkin formulation of the IBVP (7.19) of the thermal phase is defined as follows. We seek a solution $\boldsymbol{\mathcal{X}} = (\alpha, \vartheta)^{\mathtt{T}} \in \mathbb{V}_\alpha \times \mathbb{V}_\vartheta$ such that for each $\bar{\boldsymbol{\mathcal{X}}} \in (\bar{\alpha}, \bar{\vartheta})^{\mathtt{T}} \in \mathbb{S}_\alpha \times \mathbb{S}_\vartheta$

$$B^T_{DG}[\boldsymbol{\mathcal{X}}^{\boldsymbol{T}}, \bar{\boldsymbol{\mathcal{X}}}^T] = L^T_{DG}(\bar{\boldsymbol{\mathcal{X}}}^T), \tag{7.24}$$

where

$$B^T_{DG}[\boldsymbol{\mathcal{X}}^T, \bar{\boldsymbol{\mathcal{X}}}^T] = (\dot{\alpha} - \Theta,\ \bar{\alpha})_{\mathbb{\Omega}_n} + (\Theta\dot{\eta} - \frac{1}{\Theta}\boldsymbol{Q}_E \cdot \nabla\Theta,\ \bar{\vartheta})_{\mathbb{\Omega}_n} - (\boldsymbol{Q},\ \nabla\bar{\vartheta})_{\mathbb{\Omega}_n} + \langle \alpha(t_n^+),\ \bar{\alpha}(t_n^+)\rangle +$$
$$\langle \Theta(t_n^+)\eta(t_n^+),\ \bar{\vartheta}(t_n^-)\rangle \tag{7.25}$$

$$L^T_{DG}(\bar{\boldsymbol{\mathcal{X}}}^T) = -(\widehat{Q},\ \bar{\vartheta})_{\mathbb{\Gamma}^n_Q} + (R,\ \bar{\vartheta})_{\mathbb{\Omega}_n} + \langle \alpha(t_n^-),\ \bar{\alpha}(t_n^+)\rangle + \langle \Theta(t_n^-)\eta(t_n^-),\ \bar{\vartheta}(t_n^-)\rangle.$$

The weak formulation (7.24) along with the space-time boundary condition (7.21) and constitutive equations for $\boldsymbol{Q}_D$, $\boldsymbol{Q}_E$, and η in terms of the α and ϑ defines a space-time BVP over the domain $\mathbb{\Omega}_n$.

It can also easily be shown that the fully time-discontinuous Galerkin formulation (7.24) is consistent with the strong form of the IBVP (7.19).

8

Algorithmic stability

The objective of this chapter is to establish the stability of the various monolithic and staggered schemes formulated in Chapter 7. The basic difference between the time-discontinuous formulations for the linear IBVP presented Chapter 3 and the space-time Galerkin finite element formulations of the preceding chapter is the absence of jumps of the displacement field (or related quantities such as the deformation gradient and the stress tensor) from the latter. This facilitates the stability analysis of the space-time formulations for the nonlinear IBVP formulated in Chapter 6.

The structure of the rest of the chapter is as follows. In Section 8.1 the notion of energy method applied to the stability analysis of nonlinear time-stepping algorithms is briefly discussed. An important result that establish links between the space-time weak forms involving the primary fields to integral equations involving the derived quantities is presented. In Section 8.2 and 8.3 the stability of the monolithic and staggered schemes, respectively, are presented. Finally, a staggered time-stepping algorithm based on a modified Newton iterative method for the time-discontinuous Galerkin approach that includes displacement jumps is presented, and its stability analyzed.

8.1 Stability of the semi-discrete schemes

The energy method is especially suited for analyzing stability of time-stepping algorithms for nonlinear problems. It is similar to the stability analysis of the strong form of the IBVP in that it involves finding a positive-definite functional defined on the discrete state space that decays along the flow. However, the energy functional for the

discrete case and the Lyapunov function of the continuous problem may not be the same.

Recall that an algorithm that generates a sequence of solutions $\{\boldsymbol{\mathcal{X}}(t_n^-)\}_0^N$ at discrete time levels is said to be (nonlinearly) stable if there exists a positive-definite function $\mathbb{E}$ defined on the space of admissible discrete states such that

$$\mathbb{E}(\boldsymbol{\mathcal{X}}(t_{n+1}^-)) \leq \mathbb{E}(\boldsymbol{\mathcal{X}}(t_n^-)), \qquad \text{for each } n = 0, 1, \cdots, N-1. \tag{8.1}$$

In fact, in the context of schemes based on space-time Galerkin finite element methods, the discrete energy function $\mathbb{E}$ is chosen to coincide with the continuous Lyapunov function V as defined in (6.31), that is, on the time interval $(t_n,\ t_{n+1})$;

$$\mathbb{E}(\boldsymbol{\mathcal{X}}) = \int_\Omega \left[\Psi + \vartheta\eta + \frac{1}{2}\rho_0 \boldsymbol{V}\cdot\boldsymbol{V}\right] \mathrm{d}\Omega. \tag{8.2}$$

Through the constitutive relations (6.20), its time derivative will have the form

$$\frac{\mathrm{d}}{\mathrm{d}t}\mathbb{E}(\boldsymbol{\mathcal{X}}) = \int_\Omega [\boldsymbol{P} : \dot{\boldsymbol{F}} - \Theta^{-1}\boldsymbol{Q}_E\cdot\boldsymbol{\Lambda} + \vartheta\dot{\eta} + \rho_0\dot{\boldsymbol{V}}\cdot\boldsymbol{V}]\ \mathrm{d}\Omega. \tag{8.3}$$

The stability definition can be based on any sequence of approximate solutions of the semi-discrete algorithm developed in the preceding chapter with time subdivision which is not necessarily uniform. The discrete values are then evaluated from the left of each time step t_n^-.

For the sake of simplicity, we base our analysis of algorithmic stability on the following assumptions:

i. The body force and heat source are assumed to be homogeneous ($\boldsymbol{b} = \boldsymbol{0}$, and $R = 0$).

ii. No Neumann boundary conditions, that is, $\Gamma_{\mathbf{T}} = \Gamma_Q = \emptyset$.

iii. Homogeneous Dirichlet boundary conditions, that is, the prescribed boundary data are $\widehat{\boldsymbol{u}} = \boldsymbol{0}$ and $\widehat{\vartheta} = 0$.

The following lemma is crucial for proofs of the various results on the stability of semi-discrete schemes based on the space-time Galerkin formulations.

Lemma 8.1. *Let $\boldsymbol{\mathcal{X}} = (\boldsymbol{u}, \boldsymbol{V}, \alpha, \vartheta)^T$ be an admissible state vector in the space of weighting functions $\mathbb{V}$, with some value $\boldsymbol{\mathcal{X}}(t_n^-)$ at end of the previous slab Ω_{n-1}, and satisfying the following:*

(a) $(\dot{\boldsymbol{u}} - \boldsymbol{V},\ \bar{\boldsymbol{u}})_{\Omega_n} + \langle [\![\boldsymbol{u}(t_n)]\!],\ \bar{\boldsymbol{u}}(t_n^+)\rangle = 0,$

(b) $(\dot{\alpha} - \Theta,\ \bar{\alpha})_{\Omega_n} + \langle [\![\alpha(t_n)]\!],\ \bar{\alpha}(t_n^+)\rangle = 0,$

for each $\bar{\boldsymbol{u}} \in \mathbb{S}_{\boldsymbol{u}}$, $\bar{\alpha} \in \mathbb{S}_\alpha$ and $\Theta = \vartheta + \Theta_0$. Let $\boldsymbol{P}$ and $\boldsymbol{Q}_E$ be the corresponding stress tensor and energetic heat flux vector, respectively. Moreover, assume that $\mathrm{Div}\boldsymbol{P} \in [L^2(\Omega_n)]^d$ *and* $\mathrm{Div}[\Theta^{-1}\boldsymbol{Q}_E] \in L^2(\Omega_n)$*. Then we have the following:*

(1) $(\dot{\boldsymbol{F}} - \nabla \boldsymbol{V},\ \boldsymbol{P})_{\Omega_n} + \langle [\![\boldsymbol{F}(t_n)]\!],\ \boldsymbol{P}(t_n^+)\rangle = 0,$

(2) $(\dot{\boldsymbol{\Lambda}} - \nabla\Theta,\ \dfrac{1}{\Theta}\boldsymbol{Q}_E)_{\Omega_n} + \langle [\![\boldsymbol{\Lambda}(t_n)]\!],\ \dfrac{1}{\Theta(t_n^+)}\boldsymbol{Q}_E(t_n^+)\rangle = 0.$

Recall that $\boldsymbol{\Lambda} = \nabla\alpha$.

Proof. Let $\boldsymbol{\Pi}$ and $\widetilde{\boldsymbol{\Pi}}$ be the L^2-projections

$$\boldsymbol{\Pi} : [L^2(\Omega_n)]^d \to \mathbb{S}_{\boldsymbol{u}} \quad \text{and} \quad \widetilde{\boldsymbol{\Pi}} : L^2(\Omega_n) \to \mathbb{S}_\alpha,$$

defined, for $\boldsymbol{g} \in [L^2(\Omega_n)]^d$ and $f \in L^2(\Omega_n)$, by

$$(\bar{\boldsymbol{u}},\ \boldsymbol{\Pi}\,\boldsymbol{g})_{\Omega_n} = (\bar{\boldsymbol{u}},\ \boldsymbol{g})_{\Omega_n} \quad \forall \bar{\boldsymbol{u}} \in \mathbb{S}_{\boldsymbol{u}}, \tag{8.4}$$

$$(\bar{\alpha},\ \widetilde{\boldsymbol{\Pi}}\, f)_{\Omega_n} = (\bar{\alpha},\ f)_{\Omega_n} \quad \forall \bar{\alpha} \in \mathbb{S}_\alpha. \tag{8.5}$$

By hypothesis, we can choose $\bar{\boldsymbol{u}} = \boldsymbol{\Pi}\,\mathrm{Div}\boldsymbol{P}$ in *(a)* such that

$$(\dot{\boldsymbol{u}} - \boldsymbol{V},\ \boldsymbol{\Pi}\,\mathrm{Div}\boldsymbol{P})_{\Omega_n} + \langle [\![\boldsymbol{u}(t_n)]\!],\ \boldsymbol{\Pi}\,\mathrm{Div}\boldsymbol{P}(t_n^+)\rangle = 0. \tag{8.6}$$

Under the conditions (i-iii) listed above we observe that both $\mathbb{V}_{\boldsymbol{u}}$ and $\mathbb{V}_{\boldsymbol{V}}$ coincide with $\mathbb{S}_{\boldsymbol{u}}$. Since the functions in $\mathbb{V}_{\boldsymbol{u}}$ are essentially polynomials in time, then $\dot{\boldsymbol{u}} \in \mathbb{S}_{\boldsymbol{u}}$, and hence $\dot{\boldsymbol{u}} - \boldsymbol{V} \in \mathbb{S}_{\boldsymbol{u}}$. Thus, by (8.4) , we can remove the projection from (8.6) and obtain

$$(\dot{\boldsymbol{u}} - \boldsymbol{V}, \mathrm{Div}\boldsymbol{P})_{\Omega_n} + \langle [\![\boldsymbol{u}(t_n)]\!],\ \mathrm{Div}\boldsymbol{P}(t_n^+)\rangle = 0. \tag{8.7}$$

Consequently, by applying integration by parts and considering the boundary conditions listed in (ii) and (iii) above, equation (8.7) implies the result *(1)*.

Similarly, choosing $\bar{\alpha} = \widetilde{\mathbf{\Pi}}\,\mathrm{Div}[\Theta^{-1}\boldsymbol{Q}_E]$ in *(b)* and following similar argument leading to (8.7), we obtain

$$(\dot{\alpha} - \Theta, \mathrm{Div}[\Theta^{-1}\boldsymbol{Q}_E])_{\mathbb{\Omega}_n} + \langle [\![\alpha(t_n)]\!],\ \mathrm{Div}[\Theta^{-1}\boldsymbol{Q}_E](t_n^+)\rangle = 0. \tag{8.8}$$

Again, by applying integration by parts and using the boundary condition considered in here, equation (8.8) also leads to the result *(2)*. □

We observe that, Lemma 8.1 is valid in both the continuous and discontinuous cases. Since, in the continuous case, the left and right values are the same at the interface of the space-time slab $\mathbb{\Omega}_n$, the spatial integrals of the jump terms vanish.

8.2 The monolithic schemes

In this section we present stability results for the semi-discrete algorithms corresponding to the monolithic Galerkin approaches in both continuous and mixed frameworks which were developed in Chapter 7.

8.2.1 Continuous Galerkin formulation

The weak formulation (7.1) can be viewed in this case as the standard Galerkin weak statement in space-time $\mathbb{\Omega}_n$ with the associated initial condition assuming Dirichlet space-time boundary conditions at the beginning of the space-time boundary $\Omega \times \{t_n\}$, that is,

$$\boldsymbol{\mathcal{X}}(\boldsymbol{X}, t_n^+) = \boldsymbol{\mathcal{X}}(\boldsymbol{X}, t_n^-), \quad \text{on} \quad \Omega. \tag{8.9}$$

Here the argument $\boldsymbol{X}$ is used to emphasize that the boundary condition is prescribed at each point $\boldsymbol{X}$ of the reference domain Ω at the time t_n. Note that with regard to the current space-time domain $\mathbb{\Omega}_n$, the solution $\boldsymbol{\mathcal{X}}(t_n^-)$ is considered as externally prescribed data.

The following result states the stability of the semi-discrete scheme of the continuous Galerkin formulation (7.1).

Proposition 8.1. *The semi-discrete algorithm* (7.1) *corresponding to the continuous Galerkin formulation is (nonlinearly) stable. Moreover, if* $\boldsymbol{Q}_D = \boldsymbol{0}$*, then the scheme is conservative.*

Proof. Let $\boldsymbol{\mathcal{X}} = (\boldsymbol{u}, \boldsymbol{V}, \alpha, \vartheta)^{\mathtt{T}}$ be a solution of the time discrete scheme (7.1), and $\{\boldsymbol{\mathcal{X}}(t_n)\}_{n=0}^N$ be a sequence of its values[1] at the time steps $\{t_n\}_{n=0}^N$. Our objective is to show that the inequality (8.1) holds, and that it becomes an equality in the case for which $\boldsymbol{Q}_D = \boldsymbol{0}$.

In the weak formulation (7.1), choosing $\bar{\boldsymbol{v}} = \boldsymbol{V}$ and $\bar{\vartheta} = \vartheta/\Theta$ and applying Lemma 8.1, we obtain

$$\begin{aligned}
(\dot{\boldsymbol{F}},\ \boldsymbol{P})_{\Omega_n} - (\nabla \boldsymbol{V},\ \boldsymbol{P})_{\Omega_n} &= 0,\\
(\rho_0 \dot{\boldsymbol{V}},\ \boldsymbol{V})_{\Omega_n} + (\boldsymbol{P},\ \nabla \boldsymbol{V})_{\Omega_n} &= 0,\\
(\dot{\boldsymbol{\Lambda}},\ \frac{1}{\Theta}\boldsymbol{Q}_E)_{\Omega_n} - (\nabla\Theta,\ \frac{1}{\Theta}\boldsymbol{Q}_E)_{\Omega_n} &= 0,\\
(\dot{\eta},\ \vartheta)_{\Omega_n} - (\boldsymbol{Q}_D,\ \frac{\Theta_0}{\Theta^2}\nabla\Theta)_{\Omega_n} - (\boldsymbol{Q}_E,\ \frac{1}{\Theta}\nabla\Theta)_{\Omega_n} &= 0.
\end{aligned} \tag{8.10}$$

Here we also apply the boundary conditions considered in this analysis. Multiplying equation $(8.10)_3$ by (-1) and summing all of the resulting equations of (8.10), we then deduce that

$$(\dot{\boldsymbol{F}},\ \boldsymbol{P})_{\Omega_n} + (\dot{\eta},\ \vartheta)_{\Omega_n} - (\dot{\boldsymbol{\Lambda}},\ \frac{1}{\Theta}\boldsymbol{Q}_E)_{\Omega_n} + (\rho_0\dot{\boldsymbol{V}},\ \boldsymbol{V})_{\Omega_n} = (\boldsymbol{Q}_D,\ \frac{\Theta_0}{\Theta}\nabla\Theta)_{\Omega_n}. \tag{8.11}$$

Observe that the left hand side of (8.11) is exactly the integral over the time interval $(t_n,\ t_{n+1})$ of the time derivative of the discrete energy function, that is, of equation (8.3). Thus we obtain

$$\int_{t_n}^{t_{n+1}} \frac{\mathrm{d}}{\mathrm{d}t}\mathbb{E}(\boldsymbol{\mathcal{X}}(t))\ \mathrm{d}t = \int_{t_n}^{t_{n+1}} \int_\Omega \frac{\Theta_0}{\Theta}\boldsymbol{Q}_D \cdot \nabla\Theta\ \mathrm{d}\Omega\mathrm{d}t. \tag{8.12}$$

From the constitutive constraint $\boldsymbol{Q}_D \cdot \nabla\Theta \leq 0$ on the dissipative component of the heat flux, we obtain

$$\mathbb{E}(\boldsymbol{\mathcal{X}}(t_{n+1})) - \mathbb{E}(\boldsymbol{\mathcal{X}}(t_n)) = \int_{t_n}^{t_{n+1}} \int_\Omega \frac{\Theta_0}{\Theta}\boldsymbol{Q}_D \cdot \nabla\Theta\ \mathrm{d}\Omega\mathrm{d}t \leq 0, \tag{8.13}$$

[1] Note that both the left and the right values along the space-time interface $\Omega \times \{t_n\}$ are equal in the case of the continuous formulation.

since $\Theta > 0$, and equality holds if $\boldsymbol{Q}_D = \boldsymbol{0}$. $\square$

8.2.2 Mixed Galerkin formulation

In this case, since $\boldsymbol{u}$ and ϑ (and hence η) are continuous, space-time boundary conditions of Dirchlet-type of the form (7.4) are prescribed at the beginning of the current slab. On the other hand, continuity of $\boldsymbol{V}$ and α along space-time interfaces are enforced using the spatial L^2-inner product.

The following result furnishes the stability of the semi-discrete scheme associated with the mixed space-time Galerkin formulation.

Proposition 8.2. *The monolithic semi-discrete scheme for the mixed formulation characterized by the free energy function of the form*

$$\Psi = \Psi_c + \frac{1}{2}\mathbf{K}_1\boldsymbol{\Lambda}\cdot\boldsymbol{\Lambda}, \tag{8.14}$$

where Ψ_c is the free energy corresponding to the classical thermoelasticity, is (nonlinearly) stable. Moreover, it is associated with numerical dissipation per time-step

$$D = \frac{1}{2}\langle[\![\rho_0\boldsymbol{V}(t_n)]\!],\ [\![\boldsymbol{V}(t_n)]\!]\rangle + \frac{1}{2}\langle[\![\mathbf{K}_1\boldsymbol{\Lambda}(t_n)]\!],\ [\![\boldsymbol{\Lambda}(t_n)]\!]\rangle.$$

Proof. With respect to the free energy (8.14), the constitutive equation for $\boldsymbol{Q}_E$ becomes

$$\boldsymbol{Q}_E = -\Theta\frac{\partial\Psi}{\partial\boldsymbol{\Lambda}} = -\Theta\mathbf{K}_1\boldsymbol{\Lambda},$$

and the time derivative of the discrete energy will be

$$\frac{\mathrm{d}}{\mathrm{d}t}\mathbb{E}(\boldsymbol{\mathcal{X}}) = \int_\Omega [\boldsymbol{P} : \dot{\boldsymbol{F}} - \mathbf{K}_1\boldsymbol{\Lambda}\cdot\dot{\boldsymbol{\Lambda}} + \vartheta\dot{\eta} + \rho_0\dot{\boldsymbol{V}}\cdot\boldsymbol{V}]\ \mathrm{d}\Omega. \tag{8.15}$$

Following similar line of argument to that leading to (8.11) corresponding to the mixed formulation, we obtain

$$\begin{aligned}(\dot{\boldsymbol{F}},\ \boldsymbol{P})_{\Omega_n} + (\dot{\eta},\ \vartheta)_{\Omega_n} - (\dot{\boldsymbol{\Lambda}},\ \mathbf{K}_1\boldsymbol{\Lambda})_{\Omega_n} + (\rho_0\dot{\boldsymbol{V}},\ \boldsymbol{V})_{\Omega_n} + \\ \langle[\![\rho_0\boldsymbol{V}(t_n)]\!],\ \boldsymbol{V}(t_n^+)\rangle + \langle[\![\mathbf{K}_1\boldsymbol{\Lambda}(t_n)]\!],\ \boldsymbol{\Lambda}(t_n^-)\rangle = (\boldsymbol{Q}_D,\ \frac{\Theta_0}{\Theta}\nabla\Theta)_{\Omega_n}.\end{aligned} \tag{8.16}$$

By equation (8.15), we obtain

$$\int_{t_n}^{t_{n+1}} \frac{\mathrm{d}}{\mathrm{d}t}\mathbb{E}(\boldsymbol{\mathcal{X}}(t))\ \mathrm{d}t + \langle[\![\rho_0 \boldsymbol{V}(t_n)]\!],\ \boldsymbol{V}(t_n^+)\rangle + \langle[\![\mathbf{K}_1 \boldsymbol{\Lambda}(t_n)]\!],\ \boldsymbol{\Lambda}(t_n^-)\rangle = \int_{t_n}^{t_{n+1}} \int_\Omega \frac{\Theta_0}{\Theta} \boldsymbol{Q}_D \cdot \nabla\Theta\ \mathrm{d}\Omega\mathrm{d}t, \tag{8.17}$$

which is equivalent to

$$\mathbb{E}(\boldsymbol{\mathcal{X}}(t_{n+1}^-)) - \mathbb{E}(\boldsymbol{\mathcal{X}}(t_n^+)) + \langle[\![\rho_0 \boldsymbol{V}(t_n)]\!],\ \boldsymbol{V}(t_n^+)\rangle + \langle[\![\mathbf{K}_1 \boldsymbol{\Lambda}(t_n)]\!],\ \boldsymbol{\Lambda}(t_n^-)\rangle = \int_{t_n}^{t_{n+1}} \int_\Omega \frac{\Theta_0}{\Theta} \boldsymbol{Q}_D \cdot \nabla\Theta\ \mathrm{d}\Omega\mathrm{d}t. \tag{8.18}$$

We apply the identity

$$-\frac{1}{2}(a^+)^2 + (a^+ - a^-)a^+ = \frac{1}{2}(a^+ - a^-)^2 - \frac{1}{2}(a^-)^2, \qquad (a^+,\ a^- \in \mathbb{R}), \tag{8.19}$$

on equation (8.18) to obtain

$$\mathbb{E}(\boldsymbol{\mathcal{X}}(t_{n+1}^-)) + \underbrace{\frac{1}{2}\langle[\![\rho_0 \boldsymbol{V}(t_n)]\!],\ [\![\boldsymbol{V}(t_n)]\!]\rangle + \frac{1}{2}\langle[\![\mathbf{K}_1 \nabla\alpha(t_n)]\!],\ [\![\nabla\alpha(t_n)]\!]\rangle}_{D} = \mathbb{E}(\boldsymbol{\mathcal{X}}(t_n^-)) + \int_{t_n}^{t_{n+1}} \int_\Omega \frac{\Theta_0}{\Theta} \boldsymbol{Q}_D \cdot \nabla\Theta\ \mathrm{d}\Omega\mathrm{d}t. \tag{8.20}$$

Here we employ the fact that the discrete energy is continuous with respect to the displacement $\boldsymbol{u}$ and the relative temperature ϑ. Therefore, equation (8.20) implies the energy estimate (8.1), since the quadratic quantity D is non-negative. Hence the monolithic time-discrete scheme of the mixed space-time Galerkin formulation is unconditionally stable.

Note also that, from equation (8.20), the numerical dissipation in the scheme is exactly D. The total energy dissipated from the system D_T is the sum of the numerical dissipation D and the characteristic dissipation arising the thermodynamics consistency of the system, that is,

$$D_T = D - \int_{t_n}^{t_{n+1}} \int_\Omega \frac{\Theta_0}{\Theta} \boldsymbol{Q}_D \cdot \nabla\Theta\ \mathrm{d}\Omega\mathrm{d}t. \tag{8.21}$$

For the case that the dissipative component of heat vanishes identically, that is, $Q_D = 0$, the total dissipation is only the numerical one, $D_T = D$. $\square$

8.3 Staggered approaches

In this section we present conditions for the stability of the staggered semi-discrete schemes in both mixed and fully time-discontinuous Galerkin formulations. The stability of the staggered scheme of the mixed formulation follows essentially the same line of argument as the monolithic scheme of the mixed formulation, except that the two phases are now treated separately and each shown to be stable on its own.

However, as noted before, the stability analysis of the fully time-discontinuous formulation is complicated due to the fact that the associated free energy functions corresponding to generalized thermoelasticity at finite strains are not convex (or quadratic in particular). Here, we present a particular iterative algorithm, which will be discussed in detail later in this section, for solving the nonlinear problem of the fully time-discontinuous formulation, which has the desired stability features.

8.3.1 Mixed scheme

The mixed scheme in the staggered framework involves algorithms for the mechanical and thermal phases based on a mixed-type space-time finite element approach. In the mechanical phase, the displacement is continuous, while the velocity is allowed to be discontinuous across any space-time interface. Meanwhile, in the thermal phase, the thermal displacement is assumed to be discontinuous across space-time interfaces, whereas the temperature (and hence the entropy) is continuous. The mixed scheme includes the same amount of numerical dissipation, and has the same stability property as the mixed monolithic scheme.

If the mixed algorithm for each phase is stable, then by Lemma 3.1 the single-pass algorithms for the global coupled problem is also stable. The following proposition gives conditions for the stability of the algorithm for the global coupled problem.

Proposition 8.3. *The single-pass staggered scheme composed of the mixed-space-time formulations* (7.15) *and* (7.20) *for the mechanical and thermal phases, characterized*

by the free energy function given in equation (8.14)*, is nonlinearly stable. Moreover, each of the sub-algorithms is associated with numerical dissipations given by*

$$D^M = \frac{1}{2}\langle [\![\rho_0 \boldsymbol{V}(t_n)]\!],\ [\![\boldsymbol{V}(t_n)]\!]\rangle, \qquad \textit{(Mechanical phase)}$$
$$D^T = \frac{1}{2}\langle [\![\mathbf{K}_1 \nabla\alpha(t_n)]\!],\ [\![\nabla\alpha(t_n)]\!]\rangle, \qquad \textit{(Thermal phase)}$$

and hence the numerical dissipation D equals the sum of that of the individual sub-algorithms, that is, $D = D^M + D^T$.

Proof. The proof of this proposition follows along similar lines to the monolithic algorithm except that here the mechanical and thermal phases are treated separately, showing each of them are stable on their own. Then we apply Lemma 3.1 to conclude that the single-pass staggered algorithm for the global problem is stable as well. It can be apparent from the energy estimates for both algorithms that the results in this proposition hold for the numerical dissipation of each of the algorithms and hence for the overall staggered global one. □

8.3.2 Fully time-discontinuous scheme

Due to the lack of convexity of the free energy in the finite strain case, a direct extension of the fully time-discontinuous Galerkin formulation for the linear problem, as discussed in Chapter 3 and 4, to the finite strain case, is more complicated. To circumvent this problem, here we develop a particular staggered algorithm based on the fully time-discontinuous Galerkin formulations (7.23) and (7.20) for both the mechanical and thermal phases so that the resulting algorithm has the same stability property as the linear case. The algorithm is based on framing the formulations (7.23) and (7.20) in incremental settings with a particular initialization by which the first increment problems are solved with some known algorithm with its stability already established. This can be used as a predictor step to compute the jump while maintaining the stability feature. Then the rest of the incremental problems correspond to the continuous formulation, which is shown to be stable, in the staggered sense. Consequently, it is immediately clear that algorithms based on such an incremental setting are also stable.

Incremental problems

Here our objective is to set up the vehicle for a stable algorithm for solving the non-linear problem (7.23) and (7.20) in a modified Newton iterative procedure. We first present incremental problems associated with the mechanical and thermal phases in the strong sense by deriving them carefully from a Taylor expansion. We then discuss the corresponding time-Discontinuous Galerkin formulation for the incremental problems.

Recall that the problem in the mechanical phase is

$$\begin{aligned} \dot{\boldsymbol{u}} &= \boldsymbol{V} \\ \rho_0 \dot{\boldsymbol{V}} &= \mathrm{Div}\boldsymbol{P} + \rho_0 \boldsymbol{b} \\ \textbf{subject to:} \quad \dot{\alpha} &= \Theta\dot{\eta} = 0; \end{aligned} \tag{8.22}$$

while the problem in the thermal phase is

$$\begin{aligned} \dot{\alpha} &= \boldsymbol{\Theta} \\ \Theta\dot{\eta} &= -\mathrm{Div}\boldsymbol{Q} + \frac{1}{\Theta}\boldsymbol{Q}_E \cdot \nabla\Theta + R \\ \textbf{subject to:} \quad \dot{\boldsymbol{u}} &= \dot{\boldsymbol{V}} = \boldsymbol{0}, \end{aligned} \tag{8.23}$$

each with their respective initial and boundary conditions. These problems can also be posed as a problem of finding the root in some space of admissible states of some functionals as follows: find admissible state vector $\boldsymbol{\mathcal{X}}$ which satisfies the corresponding constraints including the initial and boundary conditions and the equation

$$\boldsymbol{\mathcal{R}}_a(\boldsymbol{\mathcal{X}}) = \boldsymbol{0}, \qquad a \in \{M, T\}, \tag{8.24}$$

where

$$\boldsymbol{\mathcal{R}}_M(\boldsymbol{\mathcal{X}}) = \begin{bmatrix} \dot{\boldsymbol{u}} - \boldsymbol{V} \\ \rho_0 \dot{\boldsymbol{V}} - \mathrm{Div}\boldsymbol{P} - \rho_0 \boldsymbol{b} \end{bmatrix}, \text{ and } \boldsymbol{\mathcal{R}}_T(\boldsymbol{\mathcal{X}}) = \begin{bmatrix} \dot{\alpha} - \Theta \\ \Theta\dot{\eta} + \mathrm{Div}\boldsymbol{Q} - \frac{1}{\Theta}\boldsymbol{Q}_E \cdot \nabla\Theta - R \end{bmatrix}.$$

In fact, $\boldsymbol{\mathcal{R}}_a$, $a \in \{M, T\}$ are simply the residuals of the corresponding differential equations.

Now by Taylor's theorem, the series expansion of $\boldsymbol{\mathcal{R}}_a$ at $\boldsymbol{\mathcal{X}} + \delta\boldsymbol{\mathcal{X}}$, with $\delta\boldsymbol{\mathcal{X}}$ a small perturbation, about $\boldsymbol{\mathcal{X}}$ is given by

$$\boldsymbol{\mathcal{R}}_a(\boldsymbol{\mathcal{X}} + \delta\boldsymbol{\mathcal{X}}) = \boldsymbol{\mathcal{R}}_a(\boldsymbol{\mathcal{X}}) + \boldsymbol{\mathcal{R}}'_a(\boldsymbol{\mathcal{X}};\ \delta\boldsymbol{\mathcal{X}}) + \cdots , \tag{8.25}$$

where $\boldsymbol{\mathcal{R}}'_a(\boldsymbol{\mathcal{X}};\ \delta\boldsymbol{\mathcal{X}})$ is the Gâteaux (directional) derivative of $\boldsymbol{\mathcal{R}}_a$ at $\boldsymbol{\mathcal{X}}$ in the direction of an increment (or perturbation) $\delta\boldsymbol{\mathcal{X}}$, and is given by

$$\begin{aligned}\boldsymbol{\mathcal{R}}'_a(\boldsymbol{\mathcal{X}};\ \delta\boldsymbol{\mathcal{X}}) &= \lim_{\epsilon\to 0} \frac{\boldsymbol{\mathcal{R}}_a(\boldsymbol{\mathcal{X}} + \epsilon\delta\boldsymbol{\mathcal{X}}) - \boldsymbol{\mathcal{R}}_a(\boldsymbol{\mathcal{X}})}{\epsilon} \\ &= \frac{\mathrm{d}}{\mathrm{d}\epsilon}\boldsymbol{\mathcal{R}}_a(\boldsymbol{\mathcal{X}} + \epsilon\delta\boldsymbol{\mathcal{X}})\bigg|_{\epsilon=0}.\end{aligned}$$

By analogy with functions of several real variables, we also denote the directional derivative in terms of the tangent by $\partial\boldsymbol{\mathcal{R}}_a/\partial\boldsymbol{\mathcal{X}}$ so that

$$\frac{\mathrm{d}}{\mathrm{d}\epsilon}\boldsymbol{\mathcal{R}}_a(\boldsymbol{\mathcal{X}} + \epsilon\delta\boldsymbol{\mathcal{X}})\bigg|_{\epsilon=0} = \frac{\partial\boldsymbol{\mathcal{R}}_a}{\partial\boldsymbol{\mathcal{X}}} \cdot \delta\boldsymbol{\mathcal{X}}. \tag{8.26}$$

In general, the tangent is understood as an operator acting on the space of admissible state vectors.

Thus the first-order approximation of $\boldsymbol{\mathcal{R}}_a(\boldsymbol{\mathcal{X}} + \delta\boldsymbol{\mathcal{X}})$ is given by

$$\boldsymbol{\mathcal{R}}'_a(\boldsymbol{\mathcal{X}};\ \delta\boldsymbol{\mathcal{X}}) \approx \boldsymbol{\mathcal{R}}_a(\boldsymbol{\mathcal{X}}) + \frac{\partial\boldsymbol{\mathcal{R}}_a}{\partial\boldsymbol{\mathcal{X}}} \cdot \delta\boldsymbol{\mathcal{X}}. \tag{8.27}$$

Suppose, for some non-negative integer k, an approximate solution of (8.24) $\boldsymbol{\mathcal{X}}_k$ is known. A Newton–type iterative scheme for solving the increment $\delta\boldsymbol{\mathcal{X}}_k$ is obtained by setting the left hand side of (8.27) to zero, and evaluating both the tangent $\partial\boldsymbol{\mathcal{R}}_a/\partial\boldsymbol{\mathcal{X}}$ and the residual $\boldsymbol{\mathcal{R}}_a$ at the known value $\boldsymbol{\mathcal{X}}_k$, and hence the corresponding incremental problem is given by

$$\frac{\partial\boldsymbol{\mathcal{R}}_a}{\partial\boldsymbol{\mathcal{X}}}\bigg|_{\boldsymbol{\mathcal{X}}_k} \cdot \delta\boldsymbol{\mathcal{X}}_k = -\boldsymbol{\mathcal{R}}_a(\boldsymbol{\mathcal{X}}_k). \tag{8.28}$$

Solving the linear incremental problem (8.28) for the update $\delta\boldsymbol{\mathcal{X}}_k$ results in the next approximate solution $\boldsymbol{\mathcal{X}}_{k+1} = \boldsymbol{\mathcal{X}}_k + \delta\boldsymbol{\mathcal{X}}_k$. From now onwards we denote the directional derivative of a quantity $\square$ at a $\boldsymbol{\mathcal{X}}_k$ in the direction of $\delta\boldsymbol{\mathcal{X}}_k$ by $\mathrm{d}[\square]_k$. Thus, for example, the directional derivative $\mathrm{d}[\boldsymbol{P}]_k$ of the stress $\boldsymbol{P}$ becomes

$$
\begin{aligned}
\mathrm{d}[\boldsymbol{P}]_k &= \frac{\mathrm{d}}{\mathrm{d}\epsilon}\boldsymbol{P}(\boldsymbol{\mathcal{X}}_k;\ \delta\boldsymbol{\mathcal{X}}_k)\bigg|_{\epsilon=0} \\
&= \underbrace{\frac{\partial \boldsymbol{P}}{\partial \boldsymbol{F}}\bigg|_{\boldsymbol{F}_k}}_{\mathbb{B}_k} : \delta\boldsymbol{F} + \underbrace{\frac{\partial \boldsymbol{P}}{\partial \Theta}\bigg|_{\Theta^I}}_{-\mathbf{M}^I}\delta\vartheta^I \\
&= \mathbb{B}_k : \delta\boldsymbol{F}_k - \mathbf{M}^I\delta\vartheta^I \\
&=: \boldsymbol{\Sigma}_k
\end{aligned}
$$

where ϑ^I (resp. Θ^I) are the intermediate relative (resp. absolute) temperature which accounts for the constraint that during the mechanical phase the entropy is fixed, that is, $\dot{\eta} = 0$, $\mathbb{B}_k$ is the elastic tangent fourth-order symmetric tensor with respect to the k^{th} approximate solution, and $\mathbf{M}^I$ the coupling symmetric second-order tensor corresponding to the intermediate temperature and the k^{th} approximate solution.

Consequently, the k^{th} incremental linear problem reads as follows: Find the increment $(\delta\boldsymbol{u}_k,\ \delta\boldsymbol{V}_k)$ satisfying

$$
\begin{aligned}
\delta\dot{\boldsymbol{u}}_k &= \delta\boldsymbol{V}_k - (\dot{\boldsymbol{u}}_k - \boldsymbol{V}_k), \\
\rho_0\delta\dot{\boldsymbol{V}}_k &= \mathrm{Div}[\boldsymbol{\Sigma}_k] - (\rho_0\dot{\boldsymbol{V}}_k - \mathrm{Div}\boldsymbol{P}_k - \rho_0\boldsymbol{b}),
\end{aligned}
\tag{8.29}
$$

subject to some incremental initial and boundary conditions derived from the full problem (8.22).

The time-discontinuous Galerkin formulation for the linear incremental problem (8.29) in the mechanical phase reads: find $\delta\boldsymbol{\mathcal{X}}_k = (\delta\boldsymbol{u}_k,\ \delta\boldsymbol{V}_k)^{\mathsf{T}}$ for each $\bar{\boldsymbol{\mathcal{X}}} = (\bar{\boldsymbol{u}},\ \bar{\boldsymbol{v}})$ such that

$$
\begin{aligned}
(\delta\dot{\boldsymbol{u}}_k - \delta\bar{\boldsymbol{v}}_k,\ \bar{\boldsymbol{u}})_{\Omega_n} + \langle[\delta\boldsymbol{u}_k(t_n^+) - \boldsymbol{u}(t_n^-)],\ \bar{\boldsymbol{u}}(t_n^+)\rangle &= -R_k^{\boldsymbol{u}}, \\
(\rho_0\delta\dot{\boldsymbol{V}}_k,\ \bar{\boldsymbol{v}})_{\Omega_n} + (\boldsymbol{\Sigma}_k,\ \nabla\bar{\boldsymbol{v}})_{\Omega_n} + \langle\rho_0[\delta\boldsymbol{V}_k(t_n^+) - \boldsymbol{V}(t_n^-)],\ \bar{\boldsymbol{v}}\rangle &= -R_k^{\boldsymbol{v}},
\end{aligned}
\tag{8.30}
$$

where

$$
\begin{aligned}
R_k^{\boldsymbol{u}} &= (\dot{\boldsymbol{u}}_k - \boldsymbol{V}_k,\ \bar{\boldsymbol{u}})_{\Omega_n} - \langle\boldsymbol{u}_k(t_n^+),\ \bar{\boldsymbol{u}}(t_n^+)\rangle, \\
R_k^{\boldsymbol{V}} &= (\rho_0\dot{\boldsymbol{V}}_k,\ \bar{\boldsymbol{v}})_{\Omega_n} - (\boldsymbol{P}_k,\ \nabla\bar{\boldsymbol{v}})_{\Omega_n} + (\rho_0\boldsymbol{b},\ \bar{\boldsymbol{v}})_{\Omega_n} - \langle\rho_0\boldsymbol{V}_k(t_n^+),\ \bar{\boldsymbol{v}}(t_n^+)\rangle.
\end{aligned}
$$

Here $\boldsymbol{P}_k$ represents the stress at the k^{th} approximate deformation gradient $\boldsymbol{F}_k$ and the intermediate temperature ϑ^I.

The formulation of the incremental problem associated with the the thermal phase requires the directional derivative of the entropy, that is,

$$\begin{aligned}\frac{\mathrm{d}}{\mathrm{d}\epsilon}\eta(\boldsymbol{\mathcal{X}}+\epsilon\delta\boldsymbol{\mathcal{X}})\Big|_{\epsilon=0} &= \frac{\partial\eta}{\partial\boldsymbol{F}}:\delta\boldsymbol{F}+\frac{\partial\eta}{\partial\Theta}\delta\vartheta_k\\ &= -\frac{\partial\boldsymbol{P}}{\partial\Theta}:\delta\boldsymbol{F}+\frac{\partial\eta}{\partial\Theta}\delta\vartheta\\ &= \mathbf{M}:\delta\boldsymbol{F}-\frac{1}{\Theta}\rho_0 c_F\delta\vartheta.\end{aligned}$$

Here we use the conjugacy relation $\partial\boldsymbol{P}/\partial\Theta=-\partial\eta/\partial\boldsymbol{F}$ between the stress $\boldsymbol{P}$ and the entropy η and the definition of the heat capacity c_F in terms of the partial derivative of the entropy. Recall the constitutive relations for the heat flux vectors, that is,

$$\boldsymbol{Q}_D=-\mathbf{K}_2\nabla\Theta,\quad \boldsymbol{Q}_E=-\Theta\mathbf{K}_1\nabla\alpha,\qquad\text{and}\quad \boldsymbol{Q}=\boldsymbol{Q}_E+\boldsymbol{Q}_E. \tag{8.31}$$

The directional derivatives $\mathrm{d}[\Theta\dot{\eta}]_k$, $\mathrm{d}[\boldsymbol{Q}]_k$, and $\mathrm{d}[\Theta^{-1}\boldsymbol{Q}_E\cdot\nabla\Theta]_k$ which are of particular interest in formulating the incremental problem associated to the thermal phase. Simple calculations reveal that

$$\mathrm{d}[\Theta\dot{\eta}]_k=\dot{\eta}_k\delta\Theta_k+\Theta_k\mathbf{M}_k:\delta\nabla\boldsymbol{V}_k+\rho_0 c_F\delta\dot{\vartheta}_k, \tag{8.32}$$

$$\mathrm{d}[\boldsymbol{Q}]_k=\underbrace{-\Theta_k\mathbf{K}_1\nabla\delta\alpha_k-\delta\vartheta_k\mathbf{K}_1\nabla\alpha_k}_{\mathrm{d}[\boldsymbol{Q}_E]_k}\underbrace{-\mathbf{K}_2\nabla\Theta_k}_{\mathrm{d}[\boldsymbol{Q}_D]_k}, \tag{8.33}$$

$$\mathrm{d}[\Theta^{-1}\boldsymbol{Q}_E\cdot\nabla\Theta]_k=-\Theta_k^{-2}\boldsymbol{Q}_E^k\cdot\nabla\Theta_k+\Theta_k^{-1}\mathrm{d}[\boldsymbol{Q}_E]_k\cdot\nabla\Theta_k+\Theta_k^{-1}\boldsymbol{Q}_E^k\cdot\nabla\delta\Theta_k. \tag{8.34}$$

Here $\boldsymbol{Q}_E^k$ is the energetic heat flux vector at the k^{th} solution of the thermal phase, $\Theta_k=\Theta_0+\vartheta_k$ is the k^{th} approximate absolute temperature, $\delta\Theta_k$ is the corresponding increment relative to the reference temperature Θ_0.

Next, from the directional derivatives (8.32)–(8.34), the incremental problem associated with the thermal phase reads: find an increment $(\delta\alpha_k,\ \delta\vartheta_k)$ satisfying

$$\begin{aligned}\delta\dot{\alpha}_k &= \delta\Theta_k-(\dot{\alpha}_k-\Theta_k),\\ \mathrm{d}[\Theta\dot{\eta}]_k &= -\mathrm{Div}\mathrm{d}[\boldsymbol{Q}]_k+\mathrm{d}[\Theta\boldsymbol{Q}_E\cdot\nabla\Theta]_k-(\Theta_k\dot{\eta}_k+\mathrm{Div}\mathbf{Q}_k-\Theta_k^{-1}\cdot\nabla\Theta_k-R),\end{aligned} \tag{8.35}$$

subject to appropriate incremental initial and boundary conditions derived from the the full problem (8.23) of the thermal phase. The mechanical constraints $\dot{\boldsymbol{u}} = \dot{\boldsymbol{V}} = \boldsymbol{0}$ are also implied here. Moreover, the time-discontinuous Galerkin formulation for the incremental problem (8.35) associated with the thermal phase is defined as follows: We seek an increment $\delta\boldsymbol{\mathcal{X}}_k = (\delta\alpha_k,\ \delta\vartheta_k)^{\intercal}$ such that

$$\begin{aligned}
(\delta\dot{\alpha}_k - \delta\dot{\Theta}_k,\ \bar{\alpha})_{\Omega_n} &= \langle[\delta\alpha_k(t_n^+) - \alpha(t_n^-)],\ \bar{\alpha}(t_n^+)\rangle - R_k^{\alpha},\\
(\mathrm{d}[\Theta\dot{\eta}]_k,\ \bar{\vartheta})_{\Omega_n} - (\mathrm{d}[\boldsymbol{Q}]_k,\ \nabla\bar{\vartheta})_{\Omega_n} &= (\mathrm{d}[\Theta^{-1}\boldsymbol{Q}_E\cdot\nabla\Theta]_k,\ \bar{\vartheta})_{\Omega_n} - R_k^{\alpha},\\
&\quad + \langle[\mathrm{d}[\Theta\eta]_k(t_n^+) - \Theta(t_n^-)\eta(t_n^-)],\ \bar{\vartheta}(t_n^+)\rangle,
\end{aligned} \tag{8.36}$$

for each associated weighting vector function $\bar{\boldsymbol{\mathcal{X}}} = (\bar{\alpha}, \bar{\vartheta})^{\intercal}$. Here the residuals R_k^{α} and R_k^{ϑ} are defined by

$$\begin{aligned}
R_k^{\alpha} &= (\dot{\alpha}_k - \Theta_k,\ \bar{\alpha})_{\Omega_n} + \langle\alpha_k(t_n^+),\ \bar{\alpha}(t_n^+)\rangle,\\
R_k^{\vartheta} &= (\Theta_k\dot{\eta}_k,\ \bar{\vartheta})_{\Omega_n} - (\boldsymbol{Q}_k,\ \nabla\bar{\vartheta})_{\Omega_n} - (\Theta_k^{-1}\boldsymbol{Q}_E^k\cdot\nabla\Theta_k,\ \bar{\vartheta})_{\Omega_n} + \langle\Theta_k(t_n^+)\eta_k(t_n^+),\ \bar{\vartheta}(t_n^+)\rangle.
\end{aligned}$$

The standard Newton procedure for solving the nonlinear problems of the fully time-DG formulation in staggered case, which was discussed in Chapter 8, involves choosing a suitable initialization for $\boldsymbol{\mathcal{X}}_0$, then for each $k = 0, 1, 2, \ldots$ solving the linear incremental problems (8.30) and (8.36) for increments (updates), denoted by $\delta\boldsymbol{\mathcal{X}}_k$. The next approximate solution is then $\boldsymbol{\mathcal{X}}_{k+1} = \boldsymbol{\mathcal{X}}_k + \delta\boldsymbol{\mathcal{X}}_k$. The process continues until a desired level of accuracy is reached, where accuracy is measured in terms of either the norm of updates $\delta\boldsymbol{\mathcal{X}}_k$ or the norm of the residuals (that is, of R_k^{α} and R_k^{ϑ}) or both.

Here we develop a modified form of the Newton method in such a way that a particular initial solution is used to turn the first iterate problems (8.30) and (8.36), for $k = 0$, into known problems (particularly, the linear time-discontinuous Galerkin formulations for the linear problems whose stability is proved in Chapter 4) whose solution has been shown to be stable. Next, all the later updates will be constrained at the beginning the space-time slab Ω_n so that they represent iterative problems corresponding to the continuous space-time Galerkin formulation which is also known to be stable. The modified algorithm for solving the fully time-Discontinuous Galerkin formulation in the staggered approach is thus as follows.

Algorithm

1. First incremental problem, $k = 0$

The first step involves choosing a special initialization $\boldsymbol{\mathcal{X}}_k$ for $k = 0$ so that the corresponding incremental problems (8.30) and (8.36) take a known form, that is, the time-discontinuous Galerkin formulation for the linear problem.

To this end, let $\boldsymbol{\mathcal{X}}_0 = \mathbf{0}$, that is, $\boldsymbol{u}_0 = \mathbf{0}$, $\boldsymbol{v}_0 = \mathbf{0}$, $\alpha_k = 0$, and $\vartheta_k = 0$. As a consequence of this choice of initialization, we obtain the following:

$$\mathbb{B}_0 : \delta\boldsymbol{F}_0 =: \mathbb{C} : \boldsymbol{\varepsilon}_0, \qquad \boldsymbol{\Sigma}_0 \coloneqq \boldsymbol{\sigma}_0, \qquad \mathbf{M}_0 =: \mathbf{m}, \qquad \boldsymbol{P}_0 = \mathbf{0}, \qquad \eta_0 = 0,$$

$$\mathrm{d}[\Theta\eta]_0 = \Theta_0\mathbf{m} : \nabla\delta\boldsymbol{V}_0 + \rho_0 c_F \delta\dot{\vartheta}_0 \coloneqq \Theta\delta\dot{\eta}_0,$$

$$\mathrm{d}[\boldsymbol{Q}]_0 = -\Theta_0\mathbf{K}_1\nabla\delta\alpha_0 - \mathbf{K}_2\nabla\Theta_0 =: \boldsymbol{q}_0,$$

$$\mathrm{d}[\Theta^{-1}\boldsymbol{Q}_E \cdot \nabla\Theta]_0 = 0,$$

where $\mathbb{C}$ and $\mathbf{m}$ are the classical elasticity fourth-order tensor and the coupling second-order tensor with respect to the infinitesimal strain theory, $\boldsymbol{\varepsilon}_0$ and $\boldsymbol{\sigma}_0$ are the infinitesimal strain and stress tensors with respect to the first increment $\delta\boldsymbol{u}_0$.

Hence the first problem of the increments corresponding to (8.30) and (8.36), respectively, become

$$\underbrace{\begin{aligned}\delta\dot{\boldsymbol{u}}_0 &= \delta\boldsymbol{V}_0\\ \rho_0\delta\dot{\boldsymbol{V}}_0 &= \mathrm{Div}[\boldsymbol{\sigma}_0] + \rho_0\boldsymbol{b},\end{aligned}}_{\text{Mechanical phase}} \quad \text{and} \quad \underbrace{\begin{aligned}\delta\dot{\alpha}_0 &= \delta\Theta_0\\ \Theta_0\dot{\eta}_0 &= -\mathrm{Div}[\boldsymbol{q}_0] + R,\end{aligned}}_{\text{Thermal phase}} \tag{8.37}$$

which are exactly the split problems of linear thermoelasticity into mechanical and thermal phases, where in the former case the constraint $\dot{\eta} = 0$ is already enforced in its nonlinear form before linearization, giving an intermediate temperature from which the stress $\boldsymbol{P}$ is evaluated.

The time-discontinuous Galerkin formulation corresponding to the linear problems (8.37) are the same as those of the linear case in the operator-splitting sense as discussed in Chapter 3 & 4.

2. Incremental problems, $k \geq 1$

The first step can be considered as a predictor step for an initial guess for the next iterations by calculating the jumps in a stable manner. Then the remaining iterations conform to the continuous formulation with initial condition prescribed at the value of the solution from first step at the beginning of the current space-time slab, that is, for each $k \geq 1$, the space-time boundary condition at $\Omega \times \{t_n\}$ is taken to be

$$\boldsymbol{\mathcal{X}}_k(t_n^+) = \boldsymbol{\mathcal{X}}_0(t_n^+). \tag{8.38}$$

To achieve this, we first impose a Dirichlet-type constraint on the increments that, for each $k \geq 1$, $\delta\boldsymbol{\mathcal{X}}_k(t_n^+) = \mathbf{0}$ at the beginning of the current slab $\mathbb{\Omega}_n$. This leads to the requirement that, following the standard Galerkin approach in space-time, the weighting functions $\bar{\boldsymbol{\mathcal{X}}}$ should satisfy the same constraint, that is,

$$\bar{\boldsymbol{\mathcal{X}}}(t_n^+) = \mathbf{0}.$$

Consequently, the space-time Galerkin formulations (8.30) and (8.36) take the forms

$$\begin{aligned} (\delta\dot{\boldsymbol{u}}_k - \delta\bar{\boldsymbol{v}}_k,\ \bar{\boldsymbol{u}})_{\mathbb{\Omega}_n} &= -(\dot{\boldsymbol{u}}_k - \boldsymbol{V}_k,\ \bar{\boldsymbol{u}})_{\mathbb{\Omega}_n}, \\ (\rho_0\delta\dot{\boldsymbol{V}}_k,\ \bar{\boldsymbol{v}})_{\mathbb{\Omega}_n} + (\boldsymbol{\Sigma}_k,\ \nabla\bar{\boldsymbol{v}})_{\mathbb{\Omega}_n} &= -(\rho_0\dot{\boldsymbol{V}}_k,\ \bar{\boldsymbol{v}})_{\mathbb{\Omega}_n} + (\boldsymbol{P}_k,\ \nabla\bar{\boldsymbol{v}})_{\mathbb{\Omega}_n} - (\rho_0\boldsymbol{b},\ \bar{\boldsymbol{v}})_{\mathbb{\Omega}_n}, \end{aligned} \tag{8.39}$$

and

$$\begin{aligned} (\delta\dot{\alpha}_k - \delta\Theta_k,\ \bar{\alpha})_{\mathbb{\Omega}_n} &= -R_k^{\alpha}, \\ (\mathrm{d}[\Theta\dot{\eta}]_k,\ \bar{\vartheta})_{\mathbb{\Omega}_n} - (\mathrm{d}[\boldsymbol{Q}]_k,\ \nabla\bar{\vartheta})_{\mathbb{\Omega}_n} &= (\mathrm{d}[\Theta^{-1}\boldsymbol{Q}_E\cdot\nabla\Theta]_k,\ \bar{\vartheta})_{\mathbb{\Omega}_n} - R_k^{\alpha}, \end{aligned} \tag{8.40}$$

where the residuals for the thermal phase become

$$\begin{aligned} R_k^{\alpha} &= (\dot{\alpha}_k - \Theta_k,\ \bar{\alpha})_{\mathbb{\Omega}_n}, \\ R_k^{\vartheta} &= (\Theta_k\dot{\eta}_k,\ \bar{\vartheta})_{\mathbb{\Omega}_n} - (\boldsymbol{Q}_k,\ \nabla\bar{\vartheta})_{\mathbb{\Omega}_n} - (\Theta_k^{-1}\boldsymbol{Q}_E^k\cdot\nabla\Theta_k,\ \bar{\vartheta})_{\mathbb{\Omega}_n}. \end{aligned}$$

Equations (8.39) and (8.40) correspond exactly to the continuous space-time Galerkin in the operator-splitting framework, which also can easily be shown to be unconditionally stable by analogy with the analysis for the monolithic algorithm. These equations are solved iteratively until convergence is achieved within the space-time slab $\mathbb{\Omega}_n$. The resulting solution can be interpreted as follows: it is the solution of the continuous formulation of the nonlinear problem which admits a jump discontinuity equal to that of the solution from the first step.

We conclude the analysis of the modified staggered algorithm for the fully time-discontinuous Galerkin scheme with the following proposition.

Proposition 8.4. *The staggered algorithm based on the above two steps in an incremental setting of the fully time-discontinuous Galerkin finite element formulation for the nonlinear generalized thermoelasticity under the class of constitutive equations of the form* (6.28) *along with* (8.31) *is unconditionally stable.*

Proof. Since the incremental algorithm consists of two stable incremental steps, it is also stable.

9

Numerical examples: the nonlinear generalized thermoelasticity

In the preceding two chapters various schemes based on the space-time Galerkin formulation for generalized thermoelasticity at finite strains were presented, and the stability of each scheme analysed. In this chapter we present simulations of two set of example problems designed to demonstrate various features of the generalized theory of thermoelastictiy using the fully time-discontinuous Galerkin finite element method. Such methods are characterized by the discontinuity assumptions imposed on each of the involved unknown fields across a space-time interface.

The first set of problems deal with purely nonlinear heat conduction in a rigid body. Both type II and III theories of heat conduction are considered. The non-dimensional form of the problems are solved to illustrate the qualitative aspects of the transmission of thermal disturbances induced by a pulsing laser heat source. The problem of the transmission of thermal disturbances is considered in two types of domains to examine the influence of geometry of the medium on the propagation of nonlinear thermal waves. The first problem domain is a simple rectangular region, and the second one is a more complex domain consisting of a converging-diverging channel. As the thermal wave propagates through the medium the nonlinearity becomes apparent as the front of the wave becomes sharper. This nonlinear feature of the thermal wave and its interaction with boundaries are well represented by the time-discontinuous Galerkin scheme.

The second set of problems involve the application of the generalized theory of thermoelasticity to biothermomechanics of skin. The skin is approximated by four layers which have significantly varying material and thermal properties. Two cases are considered: the first is concerned with the thermomechanical response of the skin specimen under the classical theory of thermoelasticity at finite strains. The surface of the skin

is contacted with a hot metal indenter which compresses the skin to some prescribed depth. The second case is concerned with the thermomechanical behaviour of the skin specimen under type III thermoelasticity in which the wave mechanism transport of thermal energy is incorporated together with the usual diffusion. In this case we examine the thermomechanical response of the skin as thermal load is applied quickly in an increasing manner starting from the reference temperature to some prescribed value, and no mechanical loading is applied. All the four layers are assumed to have the same non-classical thermal conduction property in which the characteristic speed of thermal wave propagation is the same in all layers. Quasi-static behaviour is assumed in both cases.

9.1 Two-dimensional laser-pulsing in rigid body

In this set of example problems we consider the propagation of thermal waves induced by a pulsing laser heat source in a rigid body. This set of problems has been investigated by several other researchers including [3, 4, 68] analyzed using the linear hyperbolic heat conduction model of Cattaneo. Thermal conduction is governed by the nonlinear generalized thermal conduction problem formulated in Chapter 7, and is given by

$$\begin{cases} \dot{\alpha} = \Theta, \\ \rho c \dot{\vartheta} = \operatorname{Div} \boldsymbol{Q} - \dfrac{1}{\Theta} \boldsymbol{Q}_E \cdot \nabla \Theta + Q, \end{cases} \tag{9.1}$$

with constitutive relations for the heat flux vectors defined by

$$\boldsymbol{Q} = \boldsymbol{Q}_E + \boldsymbol{Q}_D, \quad \boldsymbol{Q}_E = -\Theta \mathbf{k}_1 \nabla \alpha, \quad \text{and} \quad \boldsymbol{Q}_D = -\mathbf{k}_2 \nabla \Theta. \tag{9.2}$$

Here, recall that $\boldsymbol{Q}_E$ and $\boldsymbol{Q}_D$ are the energetic and dissipative components of the heat flux vector $\boldsymbol{Q}$. We considered spatially isotropic materials, that is, $\mathbf{k}_i = k_i \mathbf{1}$, $i = 1, 2$. Recall also that ϑ is the relative temperature with respect to the reference temperature Θ_0 such that the absolute temperature is $\Theta = \vartheta + \Theta_0$. All the results presented in this section correspond to the non-dimensional form of the equations in (9.1) where the non-dimensional material parameters such as ρ, c, Θ_0 are set to unity. The nonlinearity of the governing partial differential equations lies in the constitutive relations (9.2)

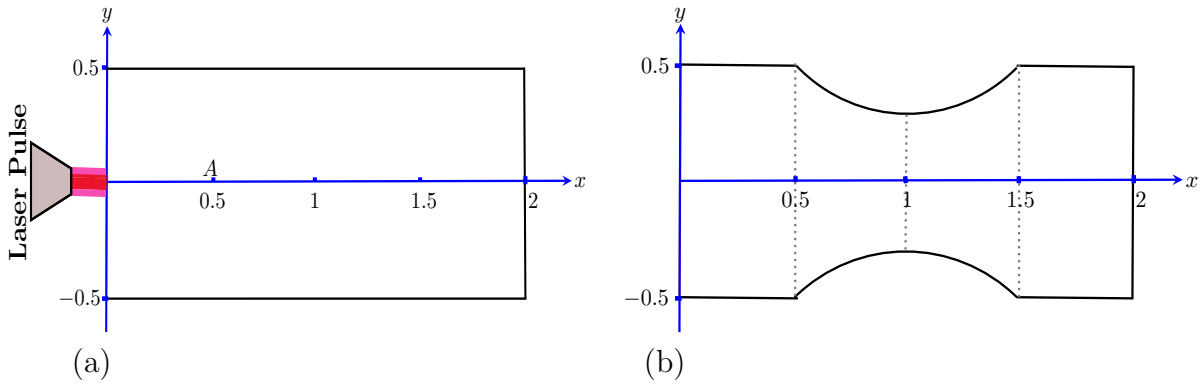

Fig. 9.1: Pulsing laser study: schematic of two dimensional domains of a rectangular (a) and a converging-diverging (b) channel.

through the terms $\mathrm{Div}\,\boldsymbol{Q}$ and $\Theta^{-1}\boldsymbol{Q}_E \cdot \nabla\Theta$. Particularly, performing differentiation on the former produces, among other linear and nonlinear factors, a quasilinear term $\Theta\mathrm{Div}[\mathbf{k}_1\nabla\alpha]$. This represents the typical nonlinear behaviour that is present in the well-known *inviscid Burger's equation*, in which the characteristic speed is proportional to the value of the temperature Θ. This is equivalent to stating that a point at a higher temperature moves faster than those at lower temperatures. This characteristic of the propagation of thermal waves is manifested by the sharpness of the wave front as it travels in a medium. Here we emphasize that the nonlinearity present in the current model is not a mathematical artefact, rather it is naturally present as a consequence of the laws of thermodynamics.

9.1.1 Rectangular channel problem

The first problem considered here involves the two-dimensional propagation of non-linear thermal waves generated by a pulsing laser heat source in a regular domain. The rectangular channel domain, as depicted in Fig. 9.1(a), occupies the planar region $\Omega = [0,\ 2]\times[-0.5,\ 0.5]$. The laser pulse incident on the left of the domain is represented as a Gaussian-type heat source given by

$$Q(x,y,t) = \frac{1}{2Dt_p}\exp\left[-\frac{1+x}{D} - \frac{y^2}{\Delta_r} - \left(\frac{t}{t_p}\right)^2\right], \tag{9.3}$$

where D is the penetration depth in the horizontal direction, Δ_r is the width of the pulse (the radius in the vertical direction), and t_p is the characteristic duration of the laser pulse. In the analysis, $D = 0.05$, $\Delta_r = 0.10$, and $t_p = 0.10$.

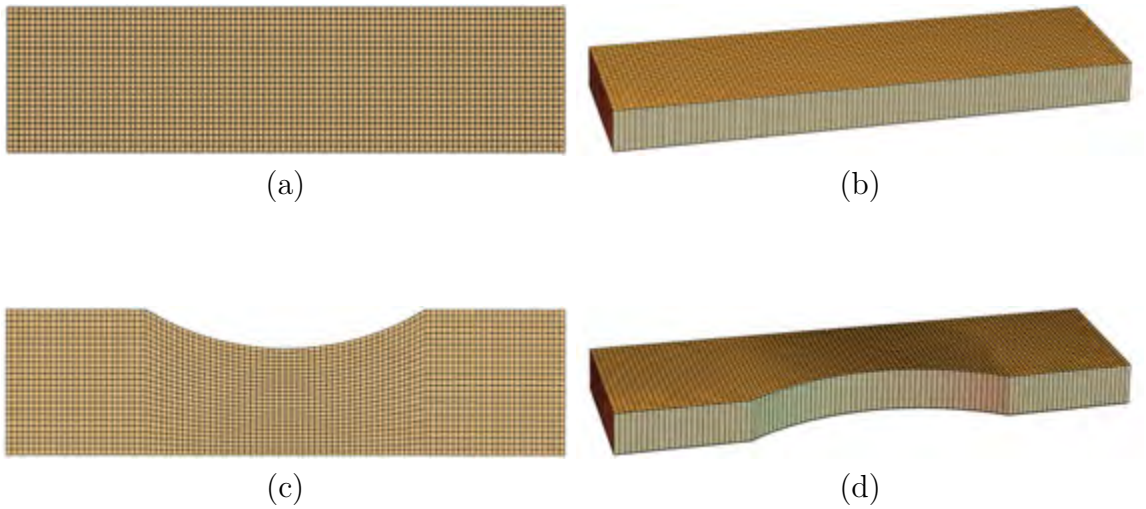

Fig. 9.2: Spatial, (a) and (c), and space-time, (b) and (d), meshes of the computational domains of rectangular, (a) and (b), and converging-diverging, (c) and (d), channels. Note that the actual spatial mesh density used in the simulation was higher than displayed here, and the temporal thickness is magnified for viewing.

The results presented here consider two models of thermal transmission. The first, type II thermal conduction, corresponds to $k_1 = 1$ and $k_2 = 0$, while the other, type III thermal conduction mode, corresponds to $k_1 = 0.5$ and $k_2 = 0.2$. A situation is chosen in which the system is driven by the pulsing laser heat source only, that is, the initial conditions with respect to α and ϑ are chosen to be homogeneous. Moreover, the boundaries of the channel in each case are assumed to be insulated throughout the simulation.

We exploit the symmetry of the problem by taking as the analysis domain the upper-half of Ω, that is, $[0,\ 2] \times [0,\ 0.5]$. For the simulation, we used 100×50 quadrilateral elements spatially as shown in the Fig. 9.2(a). In the temporal direction each space-time slab consists of one element of thickness $\Delta t = 0.01$, resulting in 100×50 trilinear space-time elements, in which the space-time mesh is shown in the Fig. 9.2(b), are used at each time step.

Fig. 9.3 shows a time sequence of snapshots of the evolution of temperature distribution, according to type II (left) and type III (right) models of heat conduction, within the rectangular channel domain Ω. The numerical solutions obtained from the simulations using the fully-time-discontinuous scheme are reflected about the x-axis in the visualization to give the complete problem domain.

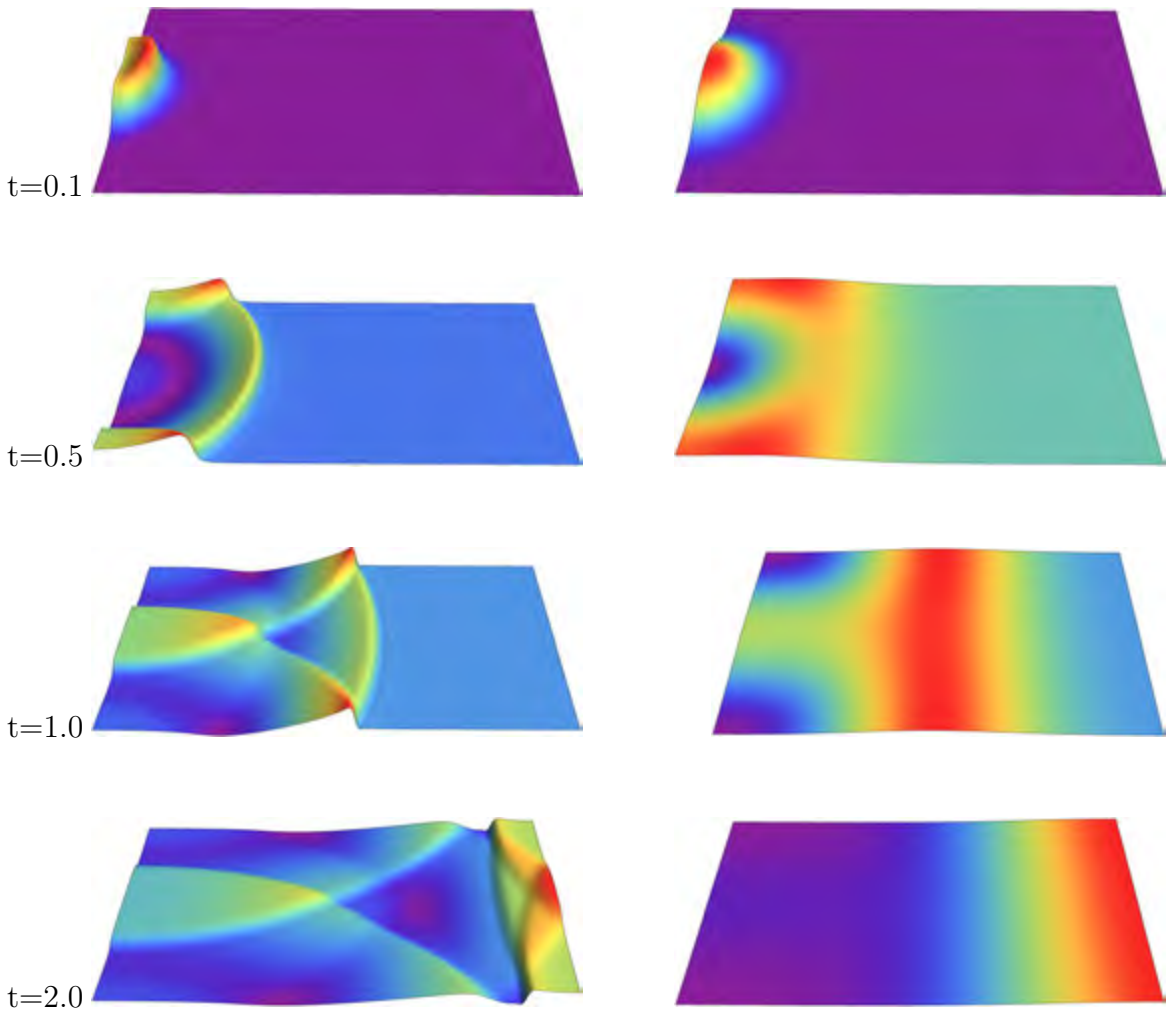

Fig. 9.3: Temperature evolution, according to type II (left column) and type III (right column) non-classical heat conduction, in the rectangular channel domain heated by a Gaussian-type laser pulse

Fig. 9.3 show a time sequence of snapshots of the evolution of temperature according to the nonlinear type II (left) and type III (right) heat conduction models. At $t = 0.10$ it is

shown that the Gaussian-type laser pulse generates a thermal distribution whose shape reflects its source with a somewhat sharper front. The wave reached the boundary at $t = 0.50$ and reflected back into the channel. At $t = 1.00$ the reflected thermal waves are seen to interact nonlinearly, resulting a nearly uniform temperature distribution in the region between their peaks, while the non-reflected part of the wave is at about half way into the channel. Finally, at $t = 2.00$ the wave reaches the other end of the channel and reflects backwards. The other important nonlinear feature of the thermal wave is demonstrated through its appearance. As the wave propagates forward its front gets sharper and it also appears to be extended from behind, i.e., the well known nonlinear feature known as *rarefaction*. On the other hand the plots to the right of Fig. 9.3 show the thermal energy transmission in the type III model. It is shown in these plots that the wave mechanism of thermal energy still exists in this case with more attenuation.

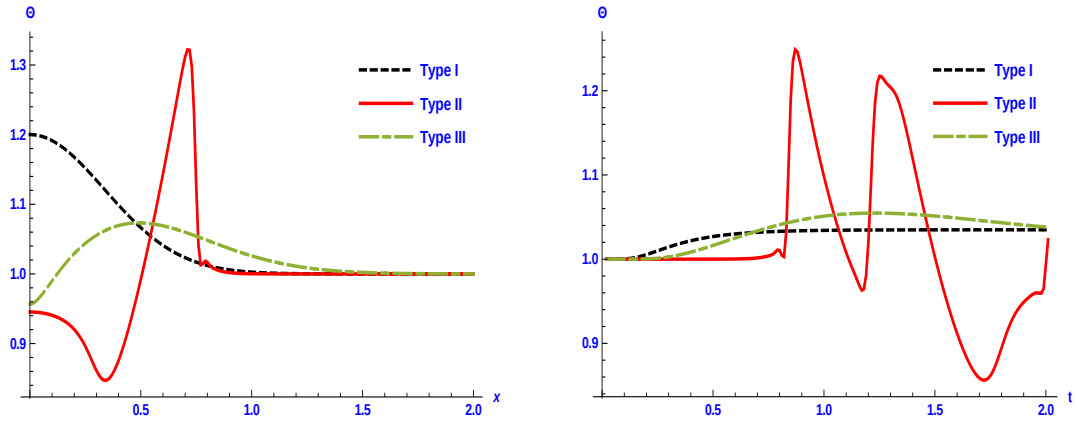

(a) (b)

Fig. 9.4: Temperature profiles according to the various heat conduction models in the rectangular channel domain (a) across the mid-horizontal axis $y = 0$ at time $t = 0.6$, and (b) at the point $A(0.5,\ 0)$ over the duration $t \in [0,\ 2]$

Fig. 9.4(a) presents the temperature profile along the mid-line $y = 0$ at time $t = 0.6$. The temperature curve corresponding to the classical theory, type I is superimposed to serve as a reference for the non-classical ones. Notice that the peaks of both curves corresponding to type II and III have been shifted to the right compared to the one with type I. This is an indication that both type II and III support wave propagation of thermal energy. We also notice that the peak of the type II curve is accompanied

by a sharp front but this is not observed in the case of type III, for which case the dissipation is higher and the profile appears to be smoother. Apart from the small over- and under-shoot at the foot of the wave peak, the fully-time-discontinuous Galerkin scheme captures the sharp wave front quite well. It generally resolves a number of fine scale solution features which are particularly important in the nonlinear dynamics of thermal waves. Fig. 9.4(b) shows the temperature profile of a point in the channel domain at (0.5, 0) over the whole duration of the simulation. In case of type II, it is clearly seen that the thermal disturbances reach the point at about $t = 0.8$. Later the thermal waves which were reflected by the boundary reach the point at about $t = 1.3$. In the case of type I, it is clearly shown that the temperature increases almost immediately after the laser pulse is applied, which demonstrates the fact that Fourier's or type I heat conduction permits an instantaneous transmission of thermal energy. The temperature profile of type III is characterized by its dissipative feature and wave mechanism of transmission of thermal energy. Unlike the case of type I, the temperature rise does not happen immediately after the thermal disturbance has been induced in the form of the pulsing laser heat source.

9.1.2 Converging-diverging channel problem

The objective of this problem is to demonstrate the ability of the fully-time-discontinuous Galerkin method to model and capture complex solution features of heat conduction problems involving thermal wave propagations through a more complicated region. As shown in Fig. 9.1(b), the domain consists of a uniform inlet followed by a converging-diverging region, and then a uniform outlet. This problem has also been investigated in [68] with the linear hyperbolic heat conduction model of Cattaneo. A pulsing laser modelled as a Gaussian-type heat source Q given by equation (9.3) is applied to the left of the channel domain. The pulse is of $D = 0.05$ penetration depth, $\Delta_r = 0.10$ width, and $t_p = 0.10$ characteristic duration.

Two cases are considered: the first, type II, corresponds to $k_1 = 1$ and $k_2 = 0$, and the second, type III, corresponds to $k_1 = 0.5$, and $k_2 = 0.2$. Homogeneous initial conditions with respect to α and ϑ are considered, and the boundaries of the domain are insulated throughout the simulation.

The problem is symmetrical with respect to the x-axis, and only the upper-half of the domain is analysed. An optimal spatial mesh, as shown in Fig.9.2(c), with each element having aspect ratio as close to one as possible is considered, and consists of 115×50 quadrilateral elements. In the temporal direction each space-time slab is of one element of thickness $\Delta t = 0.01$. In total 115×50 trilinear space-time elements were used for each space-time slab. In the visualization, the numerical solution obtained from the simulations using the fully-time-discontinuous Galerkin method are reflected about the x-axis to give the complete problem domain. The images shown in the Fig. 9.5 are 3D scatter plots such that for each node within the domain a point is shown with its color and height corresponding to the temperature value at that point.

Fig. 9.5 shows the temporal sequence of the evolution of temperature according to the nonlinear heat conduction models. The plots at the right side of Fig. 9.5 show the evolution of temperature according to the type II model. The plot at $t = 0.1$ shows the early stages of the temperature distribution reflecting the Gaussian-type thermal pulse with a sharper front. At $t = 0.5$ the wave is about to enter the converging region, while some boundary interaction patterns are also evident. As the wave passes through the compression region, it is expected that the amplitude of the waves will increase. This results in a layered thermal distribution as shown at $t = 2$, created by the waves reflected by the boundaries. This pattern is clearly different from the one obtained for the regular channel domain shown in Fig. 9.3. On the other hand, the thermal distribution patterns according to the type III model do not seem to be affected by the complexity of the geometry, and are similar to those obtained for the regular channel domain.

9.2 Space-time finite elements in 3D

In the previous 2D examples, the space-time discretization of slabs consists of a 3D mesh of one element thickness in the temporal direction. In these problems, space-time finite element spaces can be constructed in the same way as in the standard Galerkin finite element in 3D spatial domains for equilibrium problems. The time-discontinuous finite element implementation for problems in 3D such as the problems considered in the following section requires a 4D space-time mesh. An abstraction of a 4D mesh based on

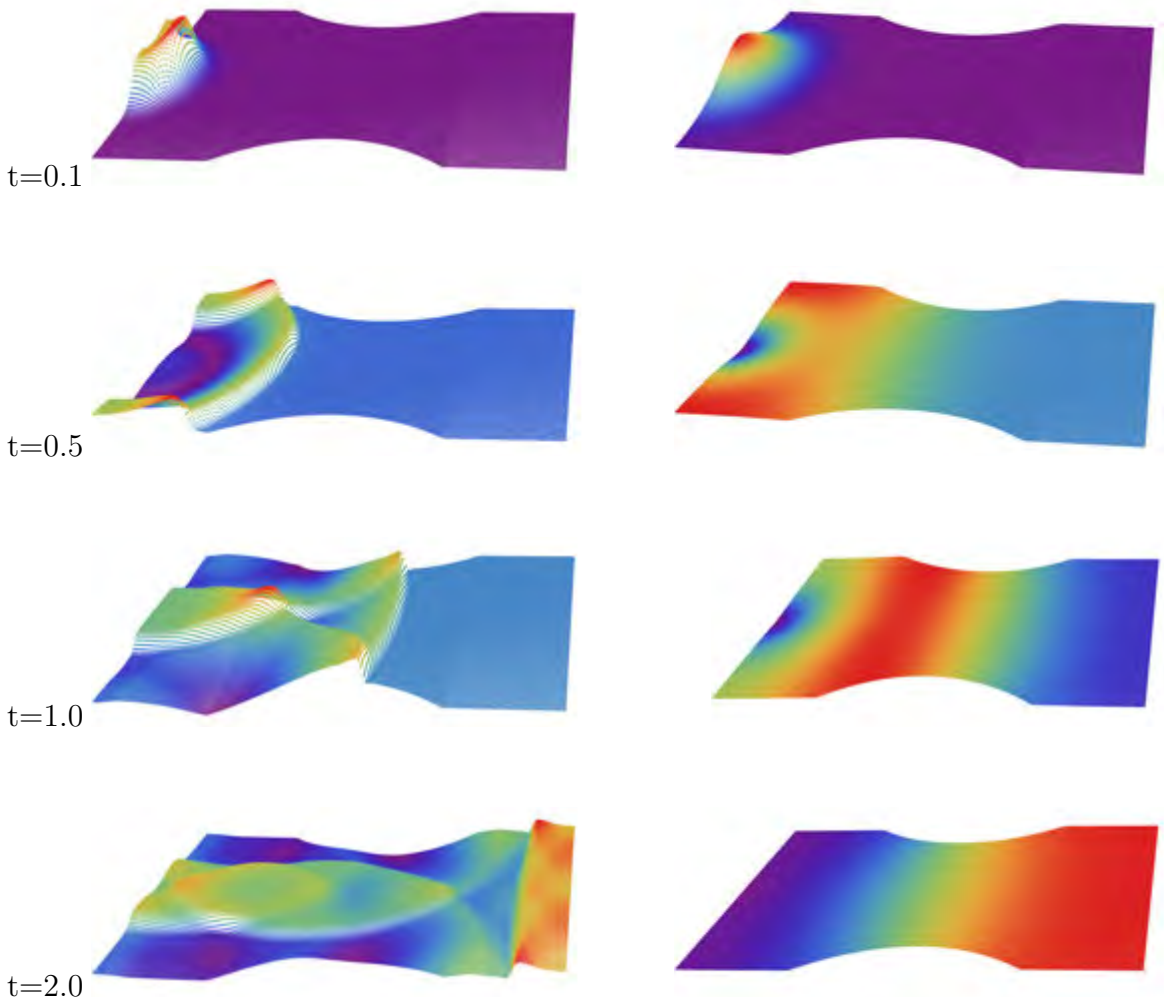

Fig. 9.5: Temperature evolution, according to type II (Left) and type III (right) theory of non-classical theory of nonlinear heat conduction, in the converging-diverging channel domain heated by a Gaussian-type laser pulse

an underlying 3D mesh in space, and of one element thickness in the temporal direction can be achieved. In the following we present the construction of 4D scalar finite element functions by considering the spatial 3D mesh and the sub-interval $I_n = [t_n,\ t_{n+1}]$.

Consider a typical spatial mesh element Ω^e defined by the location of its nodes $\boldsymbol{X}_A^e$, where $A = 1, \ldots, \mathrm{nd}_{\mathrm{el}}$ and the number of nodes per element is denoted by $\mathrm{nd}_{\mathrm{el}}$. We denote by N^A and L^a the local spatial and temporal shape functions defined in terms of the natural coordinates $\boldsymbol{\xi} \in \square := [-1,\ 1]^3$ and $\tau \in [-1,\ 1]$, respectively. The functions $\boldsymbol{\xi} \mapsto \boldsymbol{X}$ and $\tau \mapsto t$ defined by using the isoparametric concept

$$\boldsymbol{X} = \boldsymbol{X}(\boldsymbol{\xi}) = \sum_{A=1}^{\mathrm{nd_{el}}} N^A(\boldsymbol{\xi})\boldsymbol{X}_A^e, \text{ and } \ t = t(\tau) = \sum_{a=1}^{n_t} L^a(\tau)t_a, \tag{9.4}$$

map the parent domains $\square$ and $[-1,\ 1]$ to the actual elements Ω^e and I_n, respectively. Here $t_a \in I_n$ denotes a temporal node. The maps (9.4) being bijective, associate $\boldsymbol{\xi}_A \in \square$ and $\tau_a \in [-1,\ 1]$ to each node $\boldsymbol{X}_A^e \in \Omega^e$ and $t_a \in I_n$, respectively. We note that the shape functions satisfy the (completeness) condition that $N^A(\boldsymbol{\xi}_B) = \delta_B^A$ and $L^a(\tau_b) = \delta_b^a$. Having the spatial and temporal shape function defined, we are in a position to construct the space-time shape functions corresponding to space-time element $\mathbb{\Omega}^e = \Omega^e \times I_n$. The space-time shape function corresponding to the node $(\boldsymbol{X}_A^e, t_a)$ is denoted by F^{Aa} defined in terms of the natural coordinate $(\boldsymbol{\xi}, \tau) \in \square \times [-1,\ 1]$ as

$$F^{Aa}(\boldsymbol{\xi}, \tau) = N^A(\xi)L^a(\tau). \tag{9.5}$$

Note that the space-time shape function (9.5) also satisfies the completeness condition expressed as $F^{Aa}(\boldsymbol{\xi}_B, \tau_b) = \delta_B^A\delta_b^a$. The Galerkin projection of the trial space $\mathbb{V}$ onto a finite dimensional trial subspace $\mathbb{V}^h \subset \mathbb{V}$ is defined as follows: for each $(\boldsymbol{X}, t) = (\boldsymbol{X}(\boldsymbol{\xi}), t(\tau)) \in \mathbb{\Omega}^e$, the trial displacement $\boldsymbol{u}^h$, velocity $\boldsymbol{V}^h$, thermal displacement α^h, and temperature ϑ^h, are given by

$$\begin{aligned}
\boldsymbol{u}^h(\boldsymbol{\xi}, \tau) &= \sum_{A=1}^{\mathrm{nd_{el}}} \sum_{a=1}^{\mathrm{n_t}} F^{Aa}(\boldsymbol{\xi}, \tau)\boldsymbol{u}_a^A, \\
\boldsymbol{V}^h(\boldsymbol{\xi}, \tau) &= \sum_{A=1}^{\mathrm{nd_{el}}} \sum_{a=1}^{\mathrm{n_t}} F^{Aa}(\boldsymbol{\xi}, \tau)\boldsymbol{V}_a^A, \\
\alpha^h(\boldsymbol{\xi}, \tau) &= \sum_{A=1}^{\mathrm{nd_{el}}} \sum_{a=1}^{\mathrm{n_t}} F^{Aa}(\boldsymbol{\xi}, \tau)\alpha_a^A, \\
\vartheta^h(\boldsymbol{\xi}, \tau) &= \sum_{A=1}^{\mathrm{nd_{el}}} \sum_{a=1}^{\mathrm{n_t}} F^{Aa}(\boldsymbol{\xi}, \tau)\vartheta_a^A,
\end{aligned} \tag{9.6}$$

where the symbol $\{\cdot\}_a^A$ represents the value of $\{\cdot\}$ at the node point $(\boldsymbol{X}_A, t_a)$. The corresponding finite-dimensional subspace $\mathbb{S}^h \subset \mathbb{S}$ consists of state vectors of the same form as that of the trial functions (9.6) up to their respective homogeneous Dirichlet boundary conditions.

9.3 Biothermomechanics of skin

The skin is the largest single organ of the body and acts as an interface to the outside world. With its multi-layered structure, as shown in Fig. 9.6, the skin plays important roles including thermal regulation, host defense, maintaining water equilibrium, sensory system, etc. Biothemomechanical properties of skin are of great importance as they contribute to or are responsible for skin health and disease, structural integrity, cosmesis, and ageing. Major advances involving thermal methods, such as laser, microwave, radio-frequency have been achieved in treatment of injured/diseased skin tissue. Accurate quantitative and qualitative prediction of thermal, mechanical, biological and neural responses of the affected skin tissue under various thermal and mechanical loading are essential for the effectiveness of such treatment methods.

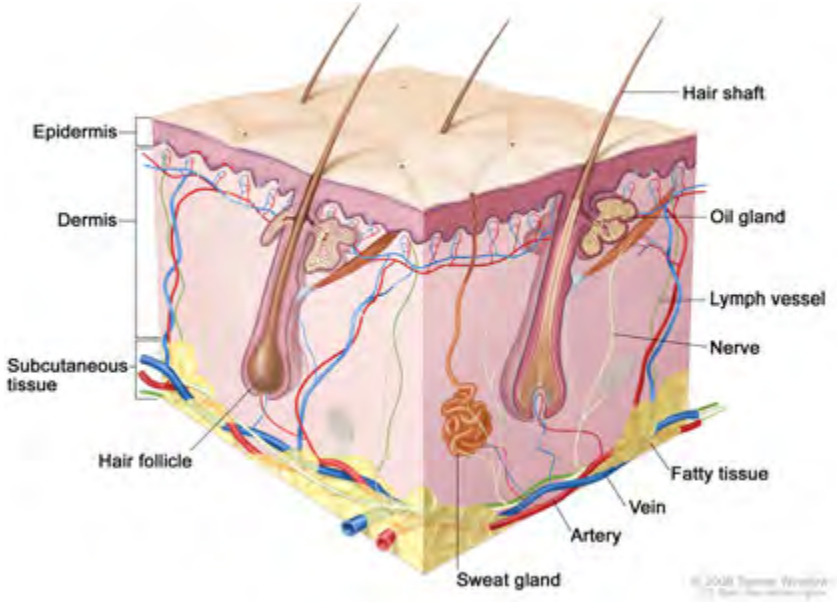

Fig. 9.6: Anatomy of the skin (© 2008 Terese Winslow, Medical and Scientific Illustration)

Thermal transfer in biological tissue has been modelled using the Pennes equation [78] which is primarily based on Fourier's law, along with other components which account for blood perfusion, sweating and surface cooling. However, the wave mechanism of heat conduction has been observed experimentally in materials with non-homogeneous inner structure, which are similar in heterogeneity to biological tissue [17, 30, 80]. Experimen-

tal results on biological tissue, for example [8, 48, 61, 62, 69], coupled with mathematical analysis have also shown that the temperature oscillation is better explained with the thermal wave analyses than the classical diffusion mechanism of thermal conduction by Fourier's law. The non-homogeneous inner structure together with the temperature oscillation commonly observed in biological tissue suggests the existence of a wave mechanism of thermal conduction in biological tissue. A more comprehensive review of literature on the non-Fourier heat transfer process in biological tissues can be found in [105].

The objective of this set of computational examples is to apply the models to the underlying biothemomechanical mechanisms in skin tissue. A great deal of research has been done focusing on thermal and/or thermomechanical skin tissue mainly based on the classical Fourier law of heat conduction supplemented by some quantities describing bioheat transfer in the skin tissue, see for example, [104, 105]. In this section, we consider a 3D skin specimen consist of four layers, as shown Fig. 9.7, having significantly differing mechanical and thermal properties, summarized in Table 9.1.

Table 9.1: Parameters for the four layer skin thermomechanical model [104]

		Stratum corneum	Epidermis	Dermis	Subcutaneous Fat
Thickness	[mm]	0.02	0.08	1.5	4.4
Young's modulus (E)	[N/mm^2]	1998	102	10.2	0.0102
Poisson ratio (ν)	[–]	0.48	0.48	0.48	0.48
Conductivity ($\mathbf{K}_2$)	[N/sK]	0.235	0.235	0.445	0.185
Density (ρ_0)	[$10^{-9}\times$ Kg/mm^3]	1500	1190	1116	976
Heat capacity (c_F)	[$10^3\times$ Nmm/KgK]	3600	3600	3300	2700
Thermal expansion (ω)	[$10^{-4}\times$1/K]	1.000	1.000	1.000	1.000

The thermomechanical coupling in the skin specimen is investigated using two distinct models: the first is the classical thermoelasticity using Fourier's law of heat conduction at finite strains, and the second is the nonlinear generalized thermoelasticity of type III. The fully-time-discontinuous Galerkin method is employed to simulate such highly-coupled, multi-scale, and nonlinear problems involving very fine solution features on a relatively coarse mesh. The results show very good agreement with the literature in the case of the the classical model at finite strains. In the second case, responses of a highly-complicated nature are obtained which are derived from the fact that the

thermal conduction model supports nonlinear wave transport mechanism of thermal energy coupled with the mechanical deformation at finite strains. Such fine features of solutions of the generalized model are well represented by using the fully-time-discontinuous scheme.

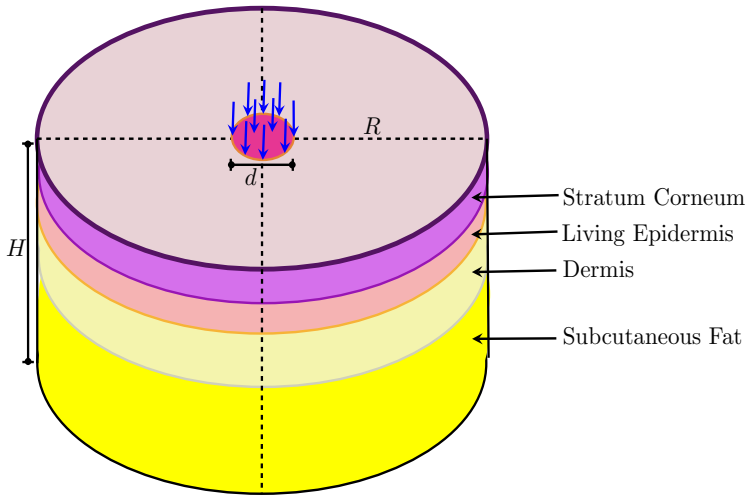

Fig. 9.7: Biothermomechanics of skin: schematic of three dimensional skin specimen

The thermomechanical response of a cylindrical skin specimen of radius R and height H, as shown in the Fig. 9.7, consisting of four layers is investigated under the classical and generalized model of quasi-static thermoelasticity at finite strains. The layers have significantly varying thermal and mechanical properties listed in the Table 9.1 [104]. The dimension of the skin specimen including the depth of each layer is listed in Table 9.1. Except for some radially symmetric variations in each case, the problems basically involve the thermomechanical response of the specimen under thermal loading applied as a hot plate (at 90 ^0C) with radius d coming into contact with the skin surface at the center. We exploit the symmetry of the problem by taking as the analysis domain the quarter of the cylinder in the first octant. Fig. 9.8 (b) shows the spatial mesh used for the analysis. Due to the presence of strong coupling, the temperature discontinuity from the thermal boundary at the edge of the contact (around the center of the specimen at radius d), causes a stress singularity. The mesh is refined around this region through the bottom of the last layer (subcutaneous fat), and since the layers near the surface are stiffer and thinner, the mesh is also refined in these regions too.

Fig. 9.1 (b) illustrates the relative thickness of the skin layers investigated. We assume that the thermomechanical response of the skin is characterized by the free energy function of the form

$$\begin{aligned}\Psi(\boldsymbol{F},\Theta,\boldsymbol{\Lambda}) = \frac{1}{2}\lambda(\ln J)^2 + \frac{1}{2}\mu(\boldsymbol{F}:\boldsymbol{F} - 3 - 2\ln J) - 3\omega\kappa\vartheta\frac{\ln J}{J} \\ + c_F\left(\vartheta - \Theta\ln\left[\frac{\Theta}{\Theta_0}\right]\right) + \frac{1}{2}\mathbf{K}_1\boldsymbol{\Lambda}\cdot\boldsymbol{\Lambda} - \Xi_0\vartheta.\end{aligned} \tag{9.7}$$

The term $\frac{1}{2}\lambda(\ln J)^2 + \frac{1}{2}\mu(\boldsymbol{F} : \boldsymbol{F} - 3 - 2\ln J)$ is the classical, compressible neo-Hookean free energy function characterized by the two Lamé constants λ and μ. The thermomechanical coupling is captured through the temperature Θ and Jacobian J of the deformation gradient $\boldsymbol{F}$ by the term $-3\omega\kappa\vartheta(\ln J)/J$, in which ω denotes the thermal expansion coefficient, and $\kappa = \lambda + \frac{2}{3}\mu$ the bulk modulus. The term $c_F[\vartheta - \Theta\ln(\Theta/\Theta_0)] + \frac{1}{2}\mathbf{K}_1\boldsymbol{\Lambda}\cdot\boldsymbol{\Lambda}$ accounts for the purely thermal response in terms of the specific heat capacity c_F and the non-classical thermal contribution of the free energy in terms of the gradient $\boldsymbol{\Lambda}$ of the thermal displacement α, and $\mathbf{K}_1$ denotes the non-classical thermal conductivity tensor. The last term $\Xi_0\vartheta$ represents the material specific absolute entropy.

The constitutive equation for the dissipative component $\boldsymbol{Q}_D$ of the heat flux vector $\boldsymbol{Q}$ is assumed to be of the form

$$\boldsymbol{Q}_D = -\mathbf{K}_2\nabla\Theta, \tag{9.8}$$

where $\mathbf{K}_2$ is the classical thermal conductivity tensor. Each layer is assumed to be thermally and mechanically isotropic, in which case the thermal conductivity tensors take the form

$$\mathbf{K}_1 = k_1\mathbf{1}, \qquad \text{and} \qquad \mathbf{K}_2 = k_2\mathbf{1}, \tag{9.9}$$

As a consequence of the constitutive relations (6.20) the stress, entropy, and the energetic heat flux become

$$\begin{aligned}\boldsymbol{P} &\coloneqq \frac{\partial\Psi}{\partial\boldsymbol{F}} = (\lambda\ln J - \mu)\boldsymbol{F}^{-\mathrm{T}} + \mu\boldsymbol{F} - \frac{3\omega\kappa}{J}\vartheta(1-\ln J)\boldsymbol{F}^{-\mathrm{T}}, \\ \eta &\coloneqq -\frac{\partial\Psi}{\partial\Theta} = 3\omega\kappa\frac{\ln J}{J} + c_F\ln\left[\frac{\Theta}{\Theta_0}\right] + \Xi_0, \\ \boldsymbol{Q}_E &\coloneqq -\Theta\frac{\partial\Psi}{\partial\boldsymbol{\Lambda}} = -\Theta\mathbf{K}_1\boldsymbol{\Lambda}.\end{aligned}$$

We refer to the model as the classical thermoelastic model or type I if the thermal conduction tensor responsible for the non-classical heat conduction is assumed zero, that is when $\mathbf{K}_1 = \mathbf{0}$. In this case, the heat flux consists of only the dissipative component whose constitutive equation (9.8) is the classical Fourier's law. If both $\mathbf{K}_1$ and $\mathbf{K}_2$ are active (non-vanishing), we refer to the model as generalized, non-classical, or type III thermoelastic model. In this case the model supports wave mechanisms of thermal conduction as well as diffusion.

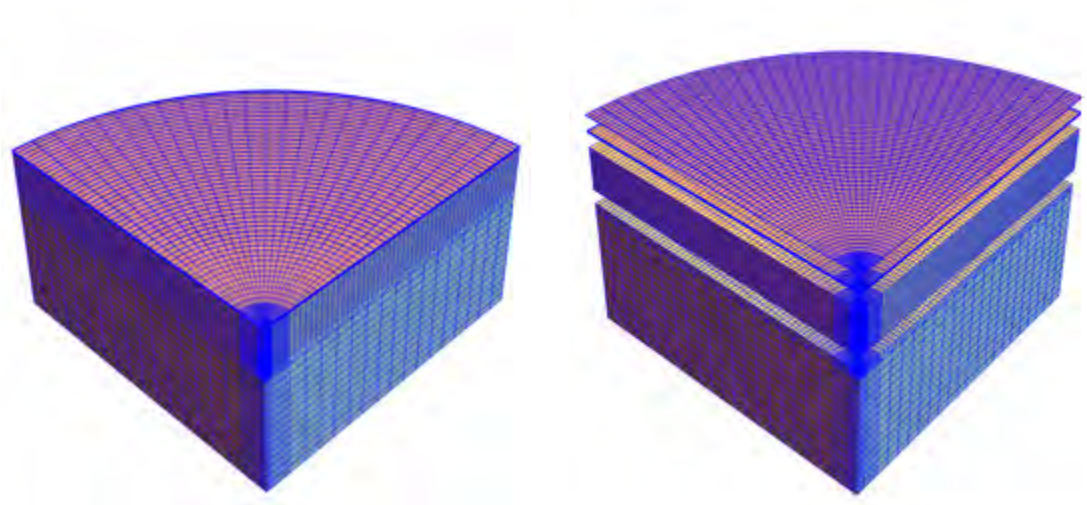

(a) (b)

Fig. 9.8: Biothermomechanics of skin: the computational domain (a), and (b) showing the relative thickness of the layers of the skin specimen

9.3.1 Biothermomechanics via classical thermoelasticity

The skin specimen is subject to a hot plate (at $\Theta_{\text{ext}} = 90\ ^oC$) acting as a frictionless indenter as shown in the Fig. 9.7. The indentation is applied at a constant rate and the final indentation depth is 25% of the height H of the specimen in the reference configuration (at a rate of 15 mm/s) resulting in significant deformation. Due to symmetry of the problem, only a quarter of the domain is analyzed.

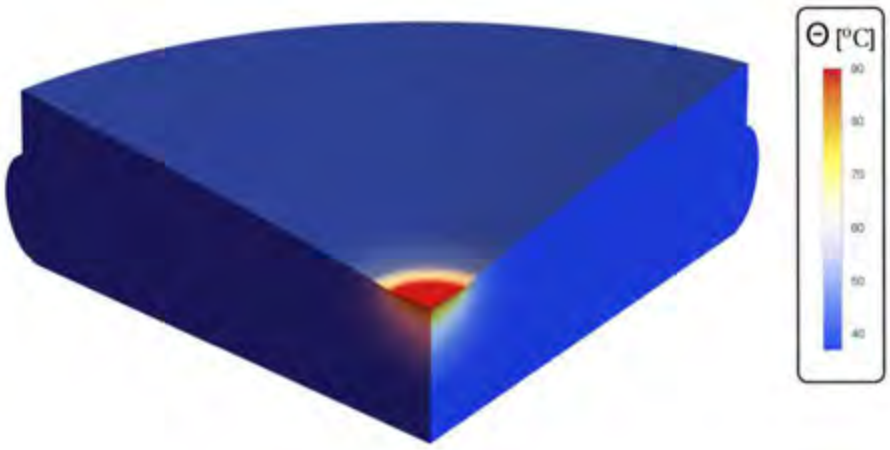

Fig. 9.9: Biothermomechanics of skin: temperature distribution over the skin specimen at the final time

The skin is initially undeformed and at the reference body temperature $\Theta_{\text{body}} = 37\,^{o}C$. With respect to the boundary conditions, the base of the skin is attached with the core of the body (hence the displacement is zero on this surface) and kept at the body temperature Θ_{body}. The boundary conditions around the circumference of the skin specimen (along the lateral side) are: traction-free (homogenous Nuemann) and Dirichlet thermal with $\Theta = \Theta_{\text{body}}$. The surface, excluding the region occupied by the indenter, is insulated. The symmetric boundary conditions are: displacements in the direction perpendicular to the vertical planar surfaces is zero, and thermal flow across these surfaces is also zero.

Fig. 9.9 shows the temperature distribution over the deformed domain at the final time. Despite the large variation in the thermal and mechanical properties across the layers, the temperature distribution is quite smooth, reflecting the dissipation property as a result of the diffusion mechanism of thermal conduction in the classical model.

Fig. 9.10 displays the distribution of the magnitude of stress over the deformed domain at the final time. Remarkably, much of the stress is concentrated in the outermost layer, the Strutum Corneum. This shows that this layer of the skin is responsible for resisting and protecting the inner soft tissues from extreme external mechanical and thermal fluctuations.

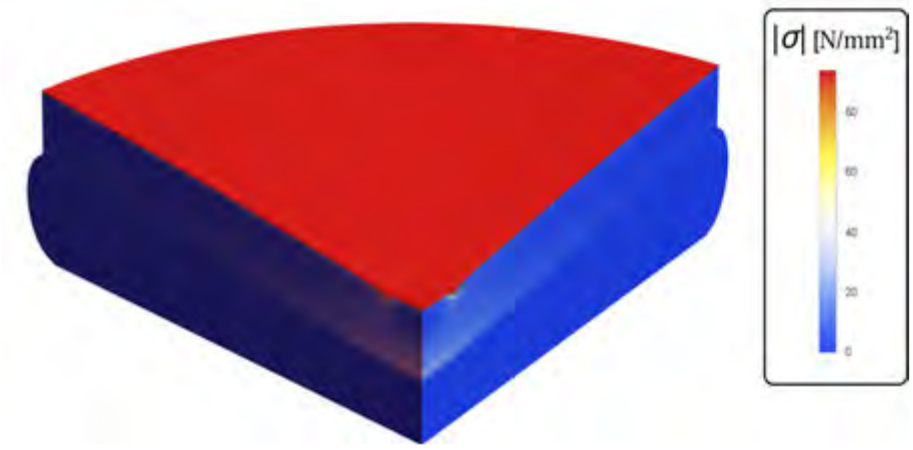

Fig. 9.10: Biothermomechanics of skin: stress distribution over the skin specimen at the final time

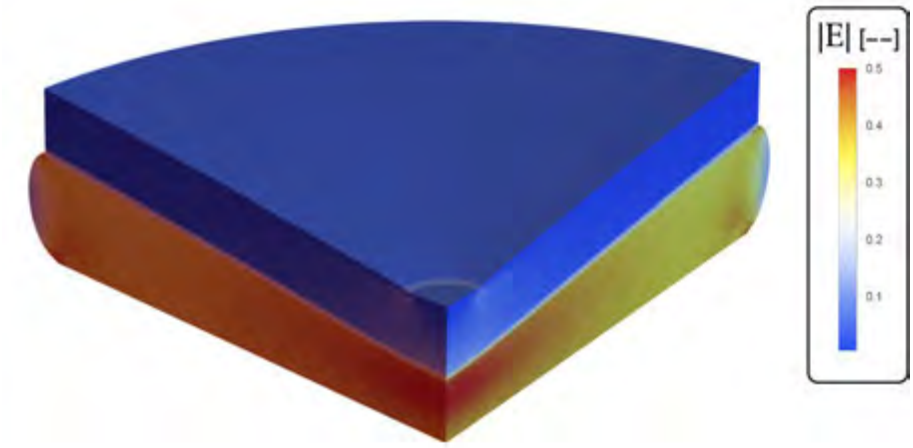

Fig. 9.11: Biothermomechanics of skin: strain distribution over the skin specimen at the final time

The strain magnitude distribution over the deformed domain at the final time is depicted in Fig. 9.11. It is seen here that most of the mechanical deformation take place in the innermost layer, the subcutaneous fat, reflecting the softness of the layer, whose Young's modulus is about 0.01 MPa which is in stark contrast to 2 GPa for the strutum

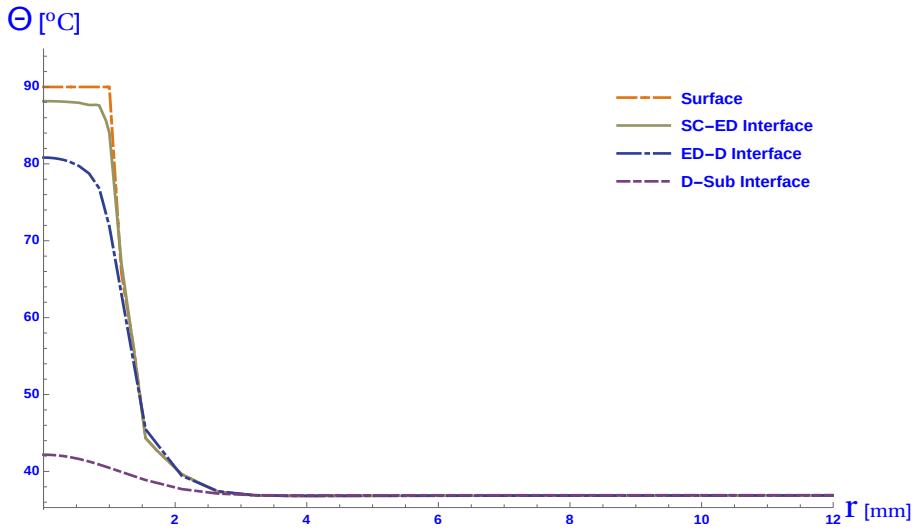

Fig. 9.12: Biothermomechanics of skin: final radial temperature distribution at the various interfaces

corneum layer. It is also shown that there is a stronger jump discontinuity in strain across the interface between the dermis and subcutaneous fat layers.

Fig. 9.12 shows the temperature profile of each interface including the surface along a radial direction from the centre to the edge of the domain. The result obtained here is in good agreement with [104] that considered similar problems in a more simplistic situation involving two dimensional analysis. The role of the strutum corneum in resisting the conduction of extreme external thermal loading into the softer parts is also in display. The temperature variation in the other layers, especially in the subcutaneous fat, is relatively low. This is also evident in Fig. 9.13 that displays the temperature drop along the centre axis from the surface down to the body core.

The temperature profile of points at the middle of each layer is tracked throughout the duration of the simulation as shown in Fig. 9.14. This result is also in good agreement with [104]. Here, it is shown that the temperature reaches equilibrium quite fast in the strutum corneum and epidermis, while in the dermis the temperature increases slowly, and almost no variation in temperature is observed in the subcutaneous fat layer.

Finally, the stress magnitude at the middle of each layer is also tracked over the duration of the simulation as depicted in Fig. 9.15. While, consistent with the result displayed

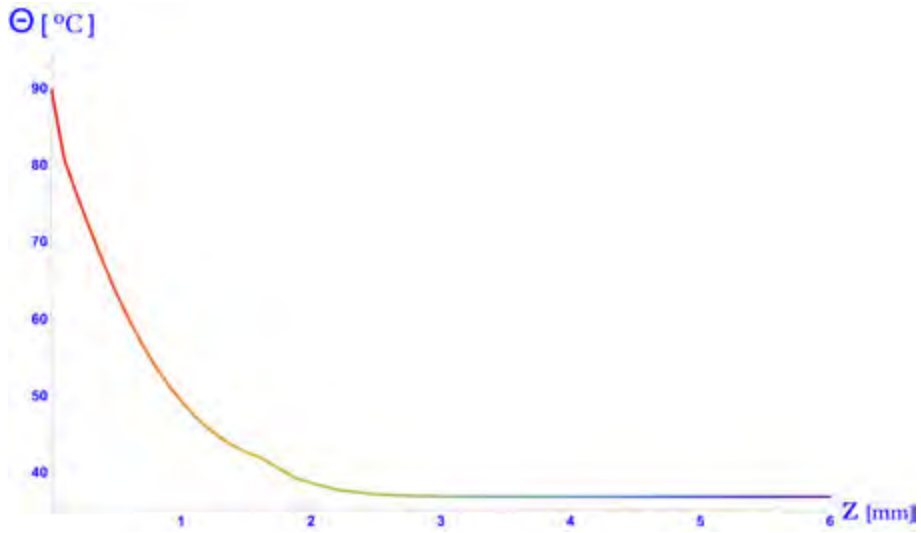

Fig. 9.13: Biothermomechanics of skin: final temperature profile across the centre along the axis of the cylindrical the skin specimen

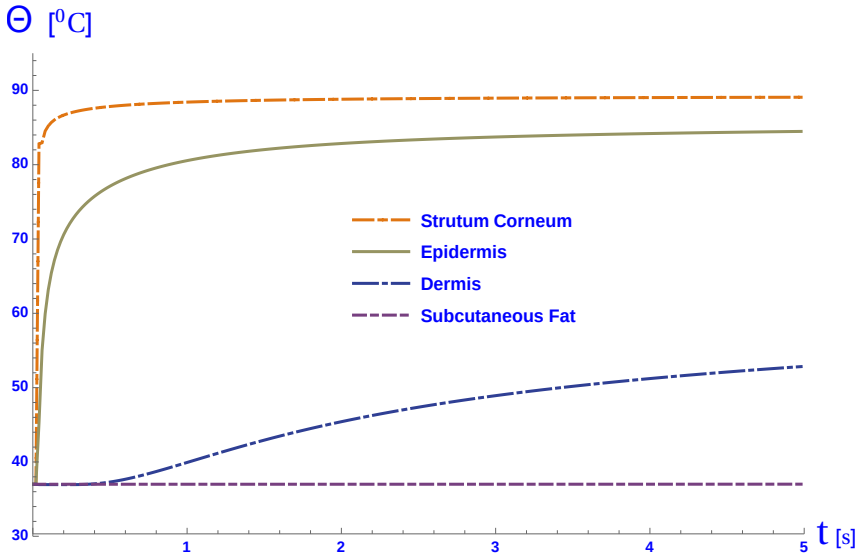

Fig. 9.14: Biothermomechanics of skin: Temperature profile in the skin over time

in Fig. 9.10, the stress level in the epidermis, dermis and subcutaneous fat layers is quite small, but an interesting scenario has developed in the strutum corneum layer. Due to the strong coupling in the outermost layer, the temperature discontinuity as the hot plate came into contact with the skin surface, generates a stress singularity around the region where the thermal load is applied. As shown from the plot, the stress singularity which was induced initially drops very rapidly, which is due to the

dissipation mechanism of the classical model. Again because of the strong coupling,

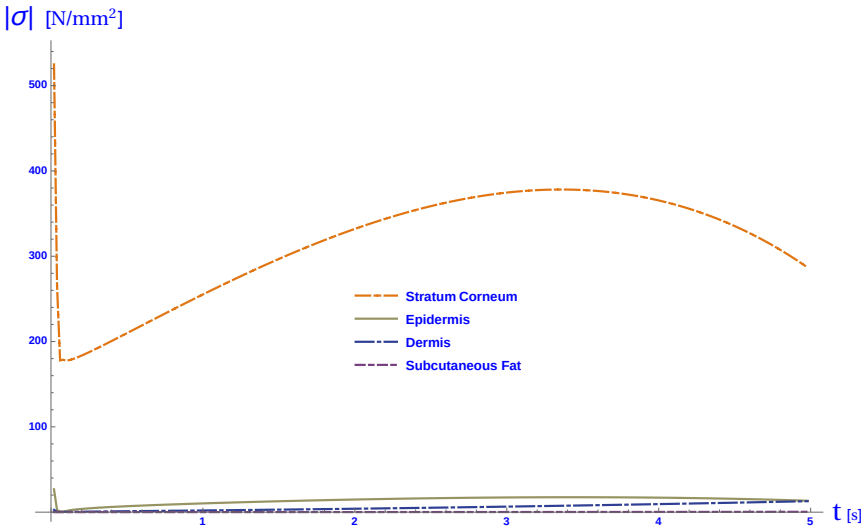

Fig. 9.15: Biothermomechanics of skin: stress profile at the various points in the skin over time

the stress starts to rise immediately after the drop. After the final indentation depth has been reached the mechanical loading was stopped and around that time the stress reached a maximum and started to relax thereafter.

9.3.2 Biothermomechanics via the generalized theory

One of the most widely used models to explain thermal propagation at finite speed is Cattaneo's equation [18]. It is a linear model, and is mainly based on the idea of incorporating the thermal relaxation time τ_q which characterizes the time delay between the heat flux and the gradient of the temperature.

The generalized thermal model discussed in this thesis, being nonlinear and thermodynamically consistent, supports thermal wave phenomenon which is represented through the non-classical heat conduction parameter k_1. Motivated by this and dimensional analysis, it suggests that the non-classical thermal conduction k_1 is related to the characteristic speed v of thermal wave in a medium via

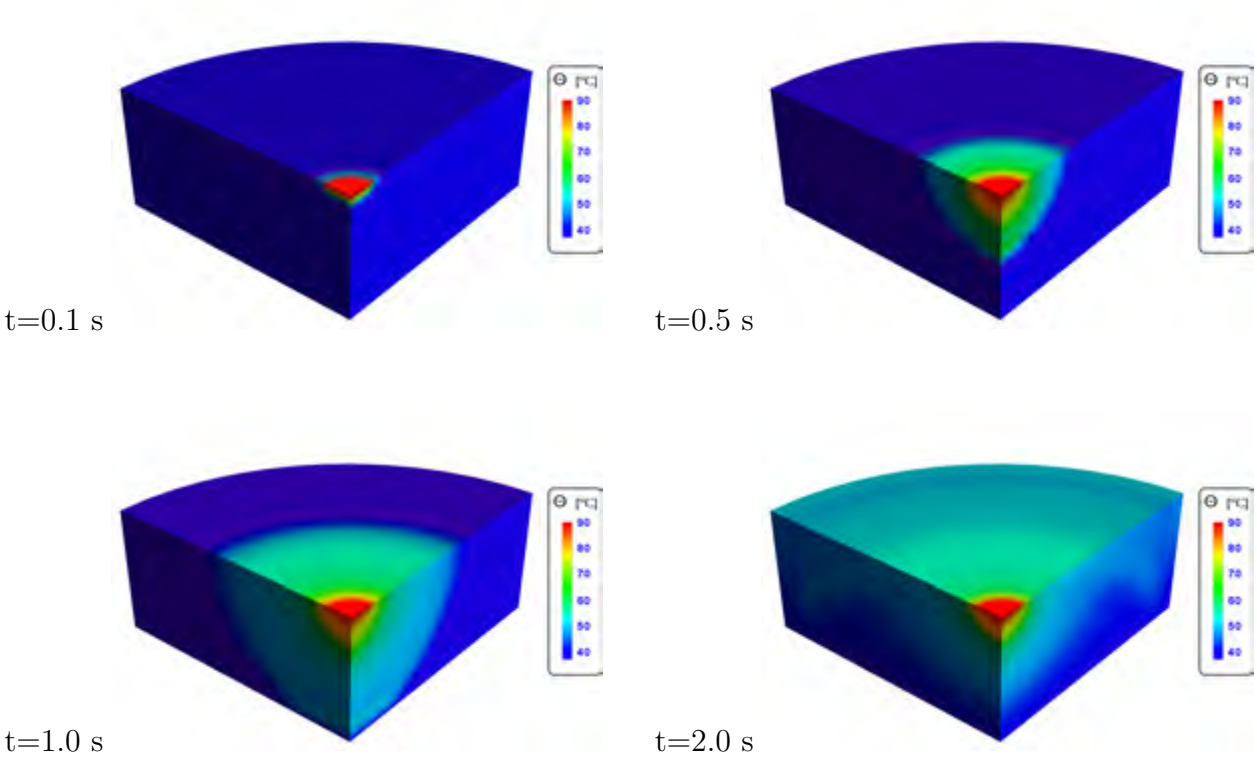

Fig. 9.16: Biothermomechanics of skin: temperature evolution in the skin according to type III thermoelasticity

$$k_1 = \frac{\rho_0 c_0}{\Theta_0} v^2. \tag{9.10}$$

In attempts to fit experimental data with Cattaneo's hyperbolic model, it was found that the thermal relaxation time τ_q in biological tissue is in the range of 10 to 20 seconds, see [69, 105] and the references therein. According to these values, we estimate the characteristic speed v of thermal wave in biological tissue to be 5.48 m/s.

In this problem, the thermomechanical response of skin tissue is analysed based on the generalized thermoelastic model at finite strains. The main aim of this simulation is to demonstrate the capability of the generalized model in capturing the temperature oscillation and thermal wave propagation phenomena observed experimentally in biological tissue. The problem set-up, here, is almost the same as the previous problem except for some changes in the boundary loadings. The plate, now, is heated linearly from the body reference temperature $\Theta_{\text{body}} = 37\ ^oC$ to $\Theta_{\text{ext}} = 90\ ^oC$ during the first 0.1 s, and thereafter it remains constant at the maximum value. The boundary condi-

tions around the circumference is the same as the previous problem that free-traction and Dirichlet boundary temperature $\Theta = \Theta_0$ are prescribed. Since the main focus of this example problem is to examine the role of the non-classical model on the thermal transfer mechanism in heterogeneous medium such as the skin tissue, we remove the mechanical loading (indentation). All the rest of material parameters, computational domain, and the mesh density are as in the previous problem.

Fig. 9.16 displays a time sequence of snapshots of the evolution of temperature distribution in the skin. Thermal wave propagation is clearly evident in this plot, and at $t = 0.1\ s$ temperature oscillation is observed as the thermal wave crosses the various layers of the skin. At $t = 1.0\ s$, the thermal oscillations are attenuated as a result of the smoothing effect of the dissipative component of the heat flux. At $t = 2.0\ s$ the thermal disturbance initiated at the surface reaches almost every part of the domain with non-uniform distribution. This is a unique feature of the generalized model that is absent in the classical theory.

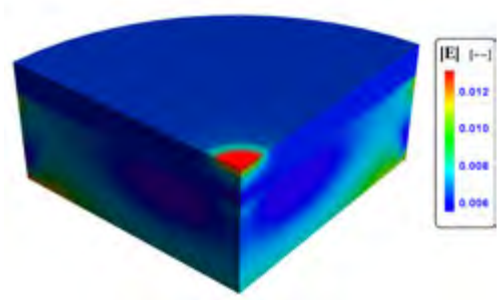

t=0.1 s

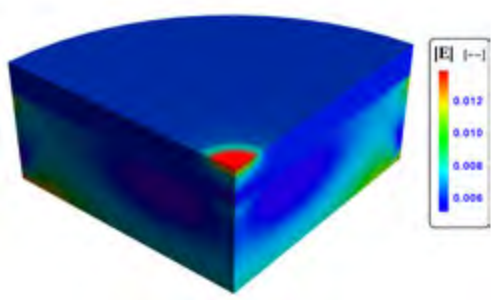

t=0.5 s

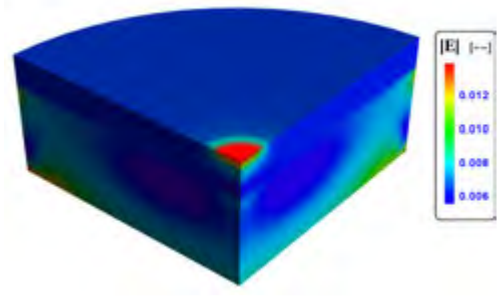

t=1.0 s

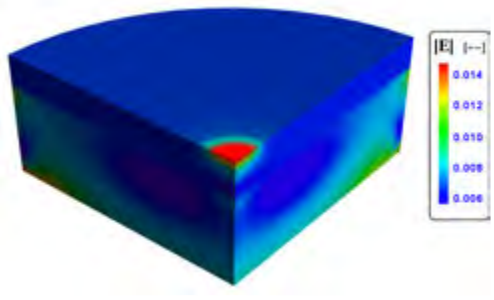

t=2.0 s

Fig. 9.17: Biothermomechanics of skin: strain evolution in the skin according to type III thermoelasticity

Fig. 9.17 displays snapshots of the evolution of the strain distribution in the skin. The distribution pattern of the magnitude of strain in the skin is the same over the duration of the simulation. The reason for this is that the thermoelastic model we used here is quasi-static. Moreover, a higher magnitude of deformation was observed in the regions of contact with the hot plate and in the regions of the soft subcutaneous fat layer.

The temperature profiles of points at the mid of each layer along the axis of the domain were tracked over the duration of the simulation as shown in Fig. 9.18. As expected, due to the small thickness and higher stiffness of the stratum corneum layer, the temperature profile in this layer follows that of the plate. The finite speed of thermal propagation was remarkably demonstrated as the thermal disturbance was delayed for some time, according to how far each point is from the source, before it reaches the point. As shown complex thermal oscillation was exhibited in all the layers except the stratum corneum.

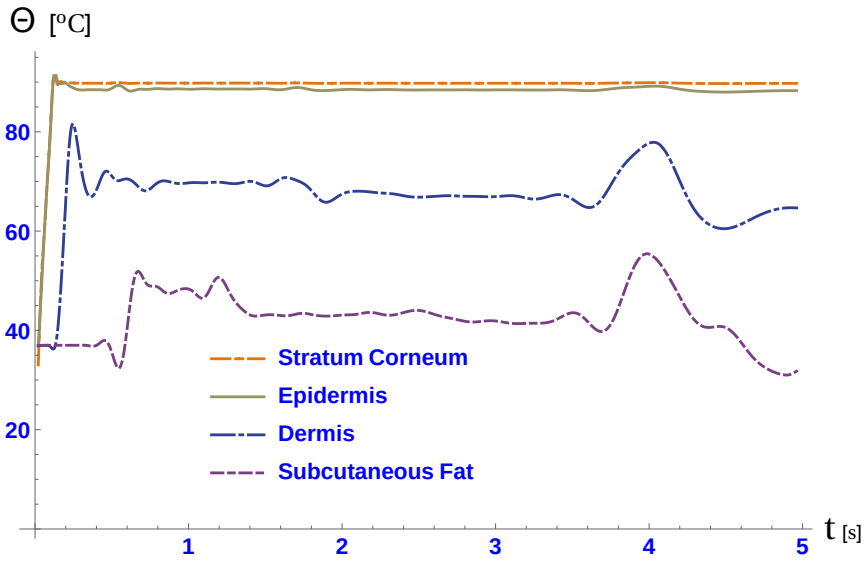

Fig. 9.18: Biothermomechanics of skin: temperature profile, according to type III thermoelasticity, at the various points in the skin over the time time period

The strong mechanical coupling induced a significantly higher stress in the skin as shown in the Fig. 9.19. Here, snapshots of stress distribution in the the skin are shown at various points of time. As in the classical case, here we also observe that most of the stress was accumulated in the stratum corneum layer, exhibiting its resistance in

withstanding externally induced disturbances from affecting the inner soft tissue. It is also shown that the stress distribution follows the pattern of that of the temperature at the surface of the skin.

Finally, Fig. 9.20 shows the temperature profile of the axis of the domain across all four layers. Each curve represents the temperature distribution at a particular time. The curves from left to right are obtained at an increasing sequence of times, showing the wave nature of thermal propagation in the skin.

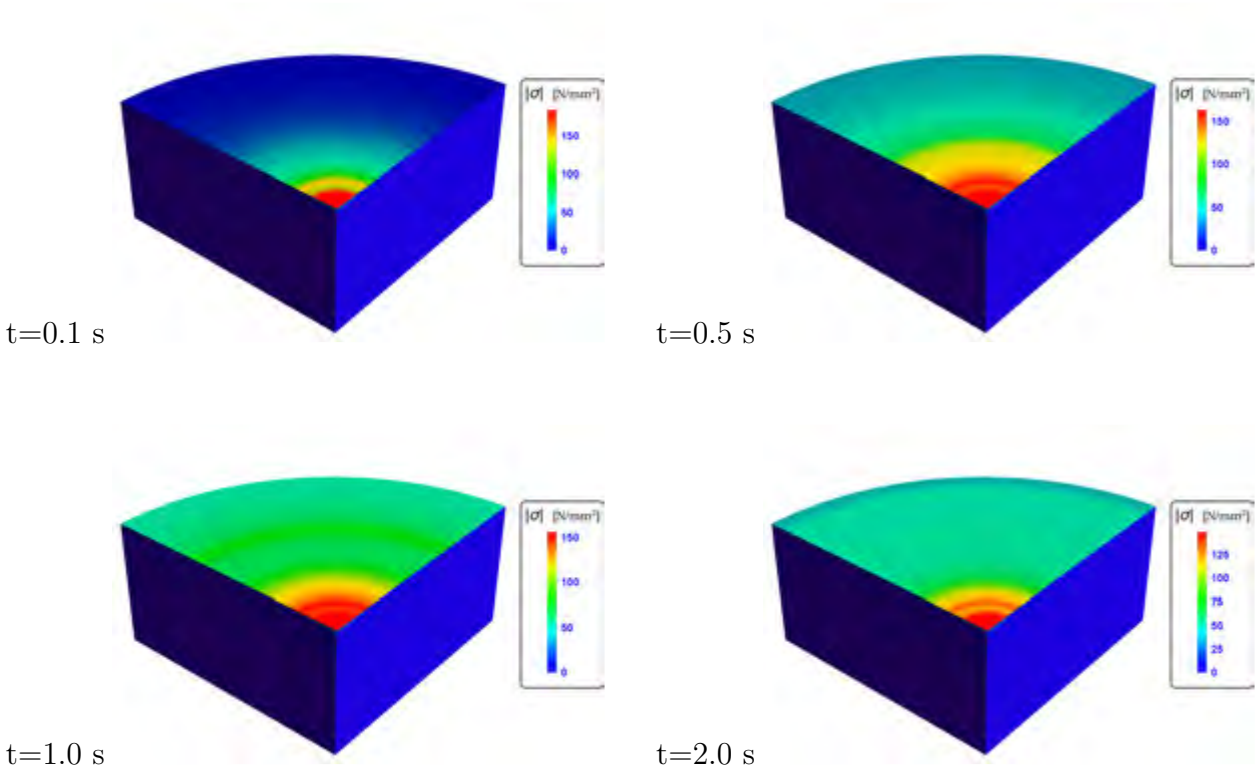

Fig. 9.19: Biothermomechanics of skin: stress evolution in the skin according to type III thermoelasticity

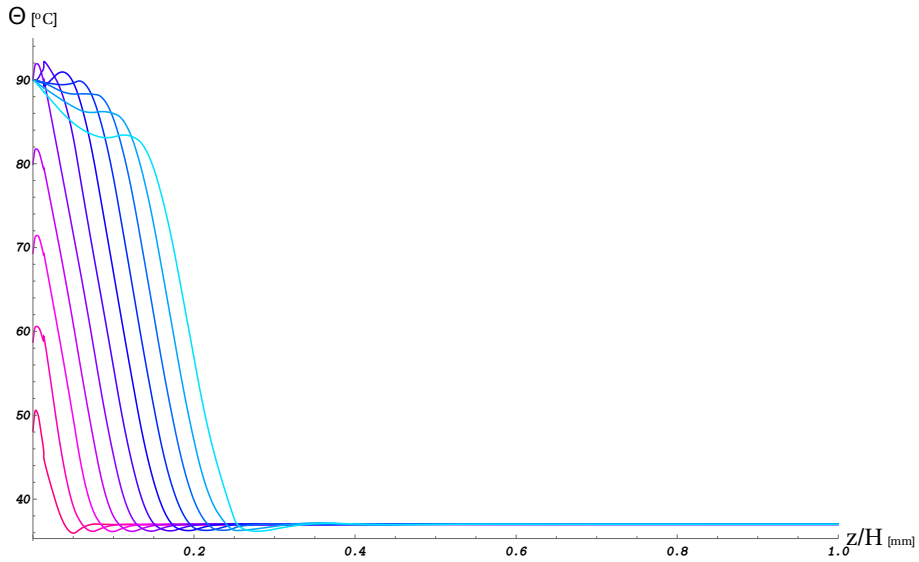

Fig. 9.20: Biothermomechanics of skin: temperature profile across the axial direction through the centre. Looking from left to right, each line corresponds to an increasing value of time, where the time increment is 0.2 sec.

10

Conclusion and future work

A new unconditionally stable, staggered time-stepping algorithm based on operator-splitting and the time-discontinuous Galerkin methods for the linear, non-classical thermoelastic problem has been proposed. The thermoelastic model is a two-way coupling between the non-classical heat conduction model of Green and Naghdi, which is of hyperbolic-type, and classical linear elastodynamics. Well-posedness and contractivity of the full coupled problem has been proved in a general context. A stable operator-split, which extends the work of Armero and Simo [6] to the non-classical coupled problems, has been proposed. The time-discontinuous Galerkin formulation is an extension of the formulation introduced by Hulbert and Hughes [52] and Hughes and Hulbert [51] for the linear elastodynamics problem. In their work, the two-field (displacement and velocity) equations are weakly enforced using the energy-inner product. The novelty of the present formulation lies particularly in the use of the more general L_2-inner product to weakly enforce the two-field equations. Hence, it makes the extension of the time-discontinuous formulation to a general class of time-dependent partial differential equations quite straightforward and natural. Remarkably, the stability analysis of the discrete problem also revealed that the two formulations are equivalent. New numerical results have also been presented which demonstrated the performance of the numerical scheme and the capability of the non-classical model of thermoelasticity in capturing various interesting phenomena of the non-Fourier thermal behaviour.

The other major contribution of this work concerns the extension of the linear, non-classical thermoelastic theory to the finite-deformation framework. A thermodynamically consistent formulation of generalized thermoelasticity at finite strains has been realized through two fundamental assumptions which are motivated by existing non-

Fourier models and theoretical and experimental evidences that heat conduction in solids is caused by phonon vibrations. The new model formally is shown to generalize the linear theory of Green and Naghdi in that the latter is a linearization of the general model about a natural configuration (state). A direct extension of the operator-split proposed for linear problems to the finite strain case is shown to be stable, inheriting the same stability property of the fully–coupled problem. It is known that the elastic-potential energy lacks the convexity property under finite strain conditions. Thus, the lack of this convexity property prevents a direct extension of the time-discontinuous method for the mechanical phase. This is because it is not clear how a jump in the displacement would be related to a jump in elastic-potential energy, when it is not convex (in the finite strain regime). To circumvent this situation, we proposed various monolithic and staggered schemes within the framework of space-time Galerkin methods. The stability analysis, particularly, of the continuous space-time Galerkin formulation for the nonlinear elastodynamics part of the problem revealed an interesting property, that is, the continuous formulation is a higher-order method that falls comfortably in the class of energy-momentum conserving methods [16, 37, 38, 88, 89]. Such conserving schemes are based on replacing the elastic-potential by a second-order convex approximation prior to the full discretization as a means of achieving a stable energy conserving scheme. In [67] a conservative scheme is obtained for nonlinear elastodynamics by utilizing finite elements in time on a discrete system of ordinary differential equation which are derived from a discrete counterpart of momentum conservation, resulting in the so-called *N–body problem*. The continuous space-time Galerkin formulation proposed in this thesis is fully consistent and higher-order as it does not not rely on a numerical approximation of elastic-potential prior to discretization. The rest of the proposed methods for generalized thermoelasticity have different degrees of stability features depending on the number of fields which are allowed to be discontinuous across any space-time interface. Furthermore, a fully-discontinuous method formulated based on an Newton-type iterative scheme, which combines the features of the time-discontinuous formulation for the linear problem and the continuous formulation for the nonlinear problem in a step-wise process, has been proposed in the staggered approach. It offers a better stability property than any of the rest of the space-time schemes for the nonlinear, generalized thermoelastic problem.

Two numerical examples were presented to demonstrate the performance of the numerical scheme and the capability of the new model in capturing non-Fourier thermal propagation properties. The first problem involves a rigid body heat conduction problem in two space dimensions. The model used is a thermal conduction equation resulting from the generalized model of thermoelasticity by neglecting mechanical effects. The second example was an application in three space dimensions which involves the thermomechanical response of skin tissue under external thermal and mechanical loadings. The response is analysed in terms of both the classical and generalized models of thermoelasticity. The result corresponding to the classical model qualitatively agrees with the literature [105] that considered a similar analysis in two space dimensions. The result for the generalized model demonstrates very interesting features of heat propagation which are observed in materials with heterogeneous inner–structure such as the skin tissue (see [105] and the references therein).

Possible areas of extension and suggestions for future work arising out of this research project include the following.

- It has been demonstrated in the numerical results that the generalized thermoelastic model gave qualitatively accurate descriptions of the various non-Fourier features of thermoelastic responses in materials; moreover, the well-known linear thermoelastic theory of Green and Naghdi is recovered from the generalized model as a linearization about a natural configuration (state). However, for the new generalized model to be useful in applications, it is essential to devise a theoretical and experimental method for specifying and measuring the energetic thermal conductivity tensor $\mathbf{K}_1$ of a given medium. For example, for a thermally isotropic material, one way of determining $\mathbf{K}_1$ would be through Eq. (9.10), which requires measuring a characteristic speed v of the thermal wave in the medium at low ranges of temperature.
- The time-discontinuous Galerkin formulation proposed in this work has been shown to perform very well in problems involving propagation of high gradients. However, it is well known that a discontinuous Galerkin scheme alone cannot provide enough viscosity to localize numerical oscillation in the vicinity of strong shocks. As a result, shock-capturing higher-order schemes have been increasingly important in problems involving shock propagation, such as transient fluid flow problems, and generalized thermoelastic problems where the classical conductivity tensor $\mathbf{K}_2$ is nearly vanish-

ing. In the area of spatial discontinuous Galerkin methods utilizing shock capturing, the notable works include [14, 15, 79]. In these works, a PDE-based artificial viscosity which follows the solution feature is added to resolve shocks within very few spatial elements. The current time-discontinuous Galerkin formulation provides a natural framework for shock sensing and adding tunable artificial viscosity through the previous time step solution. We have implemented this method for several simple linear models with some success. It would be interesting to investigate the possibility of extending the time-discontinuous formulation to a more complete shock-capturing scheme.

- The proposed fully-continuous Galerkin space-time finite element scheme has been shown to have an energy-momentum conservation property. Since this method is fully consistent and results in a symmetric formulation for nonlinear elastodynamics, its potential has to be investigated in more detail.
- We presented an application problem involving the thermomechanical response of skin tissue. But we did not incorporate those biological factors, such as sweating, surface heating/cooling, blood perfusion, which affect the biothermomechanical responses of skin tissue. A more realistic biothermomechanical model could be an interesting area of investigation.
- The current formulation only allows discontinuity of the primary unknowns across any space-time slab, yet it offers good stabilization properties. Therefore, one would like to consider an extension of the current formulation which allows for discontinuity across any space inter-element interfaces to enhance the stabilization property.
- Mesh adaptation techniques have been used for efficient simulation of various physical phenomena including boundary and interior layers, shocks, and moving interfaces. Local mesh refinement (*h–adaptivity*) has been the standard practice in most numerical software. The other less popular adaptive method is moving mesh adaptation, for example, see the works [93, 101–103]. This is due to the difficulty of deriving a partial differential equation governing the adaptive mapping. However, its implementation is very simple and it is indispensable for numerical simulation of time-dependent problems of dominantly hyperbolic nature, such as generalized thermoelastic problem. Therefore, the time-discontinuous Galerkin formulation provides a suitable framework for such an extension.

- The time-discontinuous Galerkin formulation results in a large system of nonlinear algebraic equations. Newton's method has been the most commonly used strategy in solid mechanics for solving such system of equations. It requires evaluating and storing the entries of the true tangent matrix at each iteration step. This is expensive and requires significant computer memory. Formulation of efficient nonlinear solvers remains active area in research. One of the relatively newer techniques in this area is the Jacobian-free Newton–Krylov (JFNK) method. An excellent overview of the method can be found in [57]. Implementation of the JFNK method for problems in solid mechanics has been reported in [47]. The JFNK method is the combination of Newton-type methods and Krylov subspace methods for solving the Newton updates. It only involves approximation of Jacobian-vector product without forming and storing the elements of the true Jacobian. This makes it attractive in the computational communities. Issues like preconditioning and globalization plays an important role in efficiency of the method. We have implemented the JFNK method (not reported in this work) for the numerical solution of highly nonlinear system of ordinary differential equations in an implicit discretization method with success.
- In this work, direct solvers in conjunction with Newton–Raphson method has been used. Combining the numerical approaches discussed in this work with more efficient iterative solvers and preconditioners such as multigrid methods is an interesting area for future investigation.

References

[1] C.C. Ackerman, B. Bertman, H.A. Fairbank, and R.A. Guyer. Second sound in solid Helium. *Physical Review Letters*, 16(18):789, 1966.

[2] C.C. Ackerman and W.C. Overton Jr. Second sound in solid helium-3. *Physical Review Letters*, 22(15):764, 1969.

[3] X. Ai and B.Q. Li. A discontinuous finite element method for hyperbolic thermal wave problems. *Engineering Computations*, 21(6):577–597, 2004.

[4] X. Ai and B.Q. Li. Numerical simulation of thermal wave propagation during laser processing of thin films. *Journal of Electronic Materials*, 34(5):583–591, 2005.

[5] J.H. Argyris, J. St Doltsinis, P.M. Pimenta, and H. Wüstenberg. Thermomechanical response of solids at high strains–natural approach. *Computer Methods in Applied Mechanics and Engineering*, 32(1):3–57, 1982.

[6] F. Armero and J.C. Simo. A new unconditionally stable fractional step method for non-linear coupled thermomechanical problems. *International Journal for Numerical Methods in Engineering*, 35:737–766, 1992.

[7] J.M. Ball. Convexity conditions and existence theorems in nonlinear elasticity. *Archive for Rational Mechanics and Analysis*, 63(4):337–403, 1977.

[8] A.A. Banerjee, C.D. Ogale, and K.M.C. Subramanian. Temperature distribution in different materials due to short pulse laser irradiation. *Heat Transfer Engineering*, 26(8):41–49, 2005.

[9] S. Bargmann, A. Favata, and P. Podio-Guidugli. A revised exposition of the Green-Naghdi theory of heat propagation. *Journal of Elasticity*, 114(2):143–154, 2014.

[10] S. Bargmann, A.T. McBride, and P. Steinmann. Models of solvent penetration in glassy polymers with an emphasis on case II diffusion. A comparative review. *Applied Mechanics Reviews*, 64(1):010803, 2011.

[11] S. Bargmann and P. Steinmann. Theoretical and computational aspects of non-classical thermoelasticity. *Computer Methods in Applied Mechanics and Engineering*, 196:516–527, 2006.

[12] S. Bargmann and P. Steinmann. Classical results for a non-classical theory: remarks on thermodynamic relations in Green–Naghdi thermo-hyperelasticity. *Continuum Mechanics and Thermodynamics*, 19(1-2):59–66, 2007.

[13] S. Bargmann and P. Steinmann. Modeling and simulation of first and second sound in solids. *International Journal of Solids and Structures*, 45(24):6067–6073, 2008.

[14] G.E. Barter. Shock capturing with PDE-based artificial viscosity for an adaptive, higher-order discontinuous Galerkin finite element method. Technical report, Massachusetts Institute of Technology, Cambridge Department of Aeronautics and Astronautics, 2008.

[15] G.E. Barter and D.L. Darmofal. Shock capturing with PDE-based artificial viscosity for DGFEM: Part I. Formulation. *Journal of Computational Physics*, 229(5):1810–1827, 2010.

[16] P. Betsch and C. Hesch. Energy-momentum conserving schemes for frictionless dynamic contact problems. In *IUTAM Symposium on Computational Methods in Contact Mechanics*, 2007.

[17] J.B. Brown, D.Y. Chung, and P.W. Matthews. Heat pulses at low temperatures. *Physics Letters*, 21(3):241–243, 1966.

[18] C. Cattaneo. Sur une forme de l'équation de la chaleur liminant le paradoxe d'une propagation instantane. *Comptes Rendus*, 247(4):431, 1958.

[19] D.S. Chandrasekharaiah. Thermoelasticity with second sound: a review. *Applied Mechanics Reviews*, 39(3):355–376, 1996.

[20] D.S. Chandrasekharaiah. Hyperbolic thermoelasticity: A review of recent literature. *Applied Mechanics Reviews*, 51:705–729, 1998.

[21] A.J. Chorin, T.J.R. Hughes, M.F. McCracken, and J.E. Marsden. Product formulas and numerical algorithms. *Communications on Pure and Applied Mathematics*, 31(2):205–256, 1978.

[22] B. Cockburn. Discontinuous Galerkin methods. *ZAMM-Journal of Applied Mathematics and Mechanics/Zeitschrift für Angewandte Mathematik und Mechanik*, 83(11):731–754, 2003.

[23] B. Cockburn and C.-W. Shu. TVB Runge-Kutta local projection discontinuous Galerkin finite element method for conservation laws. II. General framework. *Mathematics of computation*, 52(186):411–435, 1989.

[24] B. Cockburn and C.-W. Shu. Runge–Kutta discontinuous Galerkin methods for convection-dominated problems. *Journal of scientific computing*, 16(3):173–261, 2001.

[25] B.D. Coleman, M. Fabrizio, and D.R. Owen. II secondo suono nei cristalli: termodinamica ed equazioni costitutive. *Rendiconti del Seminario Matematico della Università di Padova*, 68:207–227, 1982.

[26] B.D. Coleman, M. Fabrizio, and D.R. Owen. On the thermodynamics of second sound in dielectric crystals. *Archive for Rational Mechanics and Analysis*, 80(2):135–158, 1982.

[27] B.D. Coleman and W. Noll. The thermodynamics of elastic materials with heat conduction and viscosity. *Archive for Rational Mechanics and Analysis*, 13(1):167–178, 1963.

[28] C. Dascalu and V.K. Kalpakides. Configurational thermomechanics and crack driving forces. In *Mechanics of Material Forces*. Springer, 2005.

[29] R.J. Donnelly. The two-fluid theory and second sound in liquid helium. *Physics Today*, 62(10):34–39, 2009.

[30] W. Dreyer and H. Struchtrup. Heat pulse experiments revisited. *Continuum Mechanics and Thermodynamics*, 5(1):3–50, 1993.

[31] D. Dureisseix and H. Bavestrello. Information transfer between incompatible finite element meshes: application to coupled thermo-viscoelasticity. *Computer Methods in Applied Mechanics and Engineering*, 195(44):6523–6541, 2006.

[32] C.A. Felippa and K.C. Park. Staggered transient analysis procedures for coupled mechanical systems: formulation. *Computer Methods in Applied Mechanics and Engineering*, 24(1):61–111, 1980.

[33] C.A. Felippa, K.C. Park, and C. Farhat. Partitioned analysis of coupled mechanical systems. *Computer Methods in Applied Mechanics and Engineering*, 190(24):3247–3270, 2001.

[34] J. Fourier. *Théorie analytique de la chaleur*. Paris: Firmin Didot Pére et Fils, 1822.

[35] N. Fox. Generalised thermoelasticity. *International Journal of Engineering Science*, 7(4):437–445, 1969.

[36] M.J. Fryer and H. Struchtrup. Moment model and boundary conditions for energy transport in the phonon gas. *Continuum Mechanics and Thermodynamics*, 26(5):593–618, 2014.

[37] O. Gonzalez. Exact energy and momentum conserving algorithms for general models in nonlinear elasticity. *Computer Methods in Applied Mechanics and Engineering*, 190(13):1763–1783, 2000.

[38] O. Gonzalez and J.C. Simo. On the stability of symplectic and energy-momentum algorithms for non-linear hamiltonian systems with symmetry. *Computer methods in applied mechanics and engineering*, 134(3):197–222, 1996.

[39] S. Govindjee and J.C. Simo. Coupled stress-diffusion: Case II. *Journal of the Mechanics and Physics of Solids*, 41(5):863–887, 1993.

[40] A.E. Green and K.A. Lindsay. Thermoelasticity. *Journal of Elasticity*, 2(1):1–7, 1972.

[41] A.E. Green and P.M. Naghdi. A re-examination of the postulates of thermomechanics. *Proceedings of the Royal Society of London Series A*, 423:171–194, 1991.

[42] A.E. Green and P.M. Naghdi. On undamped heat waves in an elastic solid. *Journal of Thermal Stresses*, 15:253–264, 1992.

[43] A.E. Green and P.M. Naghdi. Thermoelasticity without energy dissipation. *Journal of Elasticity*, 31:189–208, 1993.

[44] A.E. Green and P.M. Naghdi. A new thermoviscous theory of fluids. *Journal of Non-Newtonian Fluid Mechanics*, 56:289–306, 1995.

[45] M.E. Gurtin, E. Fried, and L. Anand. *The Mechanics and Thermodynamics of Continua*. Cambridge University Press, 2010.

[46] M.E. Gurtin and A.C. Pipkin. A general theory of heat conduction with finite wave speeds. *Archive for Rational Mechanics and Analysis*, 31(2):113–126, 1968.

[47] J.D. Hales, S.R. Novascone, R.L. Williamson, D.R. Gaston, and M.R. Tonks. Solving nonlinear solid mechanics problems with the Jacobian-free Newton–

Krylov method. *Computer Modeling in Engineering & Sciences (CMES)*, 84(2):123–153, 2012.

[48] H. Herwig and K. Beckert. Experimental evidence about the controversy concerning Fourier or non-Fourier heat conduction in materials with a nonhomogeneous inner structure. *Heat and Mass Transfer*, 36(5):387–392, 2000.

[49] R.B. Hetnarski and J. Ignacza. Generalized Thermoelasticity. *Journal of Thermal Stresses*, 22(4-5):451–476, 1999.

[50] H. Holden. *Splitting Methods for Partial Differential Equations with Rough Solutions: Analysis and MATLAB Programs*. European Mathematical Society, 2010.

[51] T.J.R. Hughes and G.M. Hulbert. Space-time finite element methods for elastodynamics: formulation and error estimates. *Computer Methods in Applied Mechanics and Engineering*, 66:339–363, 1988.

[52] G. Hulbert and T.J.R. Hughes. Space-time finite element methods for second-order hyperbolic equations. *Comuter Methods in Applied Mechanics and Engineering*, 84:327–348, 1990.

[53] H.E. Jackson, C.T. Walker, and T.F. McNelly. Second sound in NaF. *Physical Review Letters*, 25(1):26, 1970.

[54] C. Johnson. Discontinuous Galerkin finite element methods for second order hyperbolic problems. *Computer Methods in Applied Mechanics and Engineering*, 107(1-2):117–129, 1993.

[55] D.K. Khalmanova and F. Costanzo. A space-time discontinuous Galerkin finite element method for fully coupled linear thermo-elasto-dynamic problems with strain and heat flux discontinuities. *Computer Methods Applied Mechanics and Engineering*, 197(13-16):1323–1342, 2008.

[56] C. Kittel. *Introduction to Solid State Physics*. Wiley, 2005.

[57] D.A. Knoll and D.E. Keyes. Jacobian-free Newton–Krylov methods: a survey of approaches and applications. *Journal of Computational Physics*, 193(2):357–397, 2004.

[58] J. Korelc. Multi-language and multi-environment generation of nonlinear finite element codes. *Engineering with Computers*, 18(4):312–327, 2002.

[59] A. Kuzmin, M. Luisier, and O. Schenk. Fast methods for computing selected elements of the Greens function in massively parallel nanoelectronic device sim-

ulations. In F. Wolf, B. Mohor, and D. Mey, editors, *Euro-Par 2013 Parallel Processing*. Springer Berlin Heidelberg, 2013.

[60] L. Landau. Theory of the Superfluidity of Helium II. *Physical Review*, 60(4):356–358, 1941.

[61] J. Liu, Z.P. Ren, and C.C. Wang. Simulating experimental study on the mechanisms of temperature oscillation in living tissue. *Journal of Basic Science and Engineering*, 4(2):173–182, 1996.

[62] J. Liu, C. Wang, and Z. Ren. Theory and experiments on temperature oscillations effects in living tissues. *Journal-Tsinghua University*, 37:91–95, 1997.

[63] H.W. Lord and Y. Shulman. A generalized dynamical theory of thermoelasticity. *Journal of the Mechanics and Physics of Solids*, 15(5):299–309, 1967.

[64] B. Markert. *Weak or strong: on coupled problems in continuum mechanics*. D93 – Habilitation, Universität Stuttgart, Institut für Mechanik (Bauwesen), Universiät Stuttgart, 2010.

[65] Mathematica. Wolfram Research Inc., Version 10.1s. *Wolfram Research, Inc., Champaign, Illinois*, 2015.

[66] Matlab. The MathWorks Inc., Version 8.01.0.604 (R2013a). *The MathWorks Inc., Natick, Massachusetts*, 2013.

[67] G. Michael. *Conserving time integrators for nonlinear elastodynamics*. PhD thesis, Fachbereich Maschinenbau und Verfahrenstechnik, Technischen Universität Kaiserslautern, 2004.

[68] S.T. Miller and R.B. Haber. A spacetime discontinuous Galerkin method for hyperbolic heat conduction. *Computer Methods in Applied Mechanics and Engineering*, 198(2):194–209, 2008.

[69] K. Mitra, S. Kumar, A. Vedevarz, and M.K. Moallemi. Experimental evidence of hyperbolic heat conduction in processed meat. *Journal of Heat Transfer*, 117(3):568–573, 1995.

[70] I. Müller. Die Kältefunktion, eine universelle Funktion in der Thermodynamik viskoser wärmeleitender Füssigkeiten. *Archive for Rational Mechanics and Analysis*, 40(1):1–36, 1971.

[71] V. Narayanamurti and R.C. Dynes. Observation of second sound in Bismuth. *Physical Review Letters*, 28(22):1461, 1972.

[72] W. Nernst. *Die Theoretischen und Experimentellen Grundlagen des Neuen Wärmesatzes*. Halle, 1918.

[73] T. Öncü and T. Moodie. On the constitutive relations for second sound in elastic solids. *Archive for rational mechanics and analysis*, 121:87–99, 1992.

[74] K.C. Park. Partitioned transient analysis procedures for coupled-field problems: stability analysis. *Journal of Applied Mechanics*, 47(2):370–376, 1980.

[75] K.C. Park and C.A. Felippa. A variational framework for solution method developments in structural mechanics. *Journal of Applied Mechanics*, 65(1):242–249, 1998.

[76] K.C. Park and C.A. Felippa. A variational principle for the formulation of partitioned structural systems. *International Journal for Numerical Methods in Engineering*, 47(1-3):395–418, 2000.

[77] K.C. Park, C.A. Felippa, and J.A. DeRuntz. Stabilization of staggered solution procedures for fluid-structure interaction analysis. *Computational Methods for Fluid-Structure Interaction Problems*, 1:95–124, 1977.

[78] H.H. Pennes. Analysis of tissue and arterial blood temperatures in the resting human forearm. *Journal of applied physiology*, 1(2):93–122, 1948.

[79] P.O. Persson. Shock capturing for high-order discontinuous Galerkin simulation of transient flow problems. In *21st AIAA Computational Fluid Dynamics Conference*, 2013.

[80] V. Peshkov. The second sound in Helium II. *J. Phys.*, 8:381, 1944.

[81] P. Podio-Guidugli. A virtual power format for thermomechanics. *Continuum Mechanics and Thermodynamics*, 20:479–487, 2009.

[82] R. Quintanilla. Existence in thermoelasticity without energy dissipation. *Journal of Thermal Stresses*, 25:195–202, 2002.

[83] R. Quintanilla. Thermoelasticity without energy dissipation of materials with microstructure. *Applied Mathematical Modelling*, 26(12):1125–1137, 2002.

[84] R. Racke. Thermoelasticity with second sound-exponential stability in linear and non-linear 1-d. *Mathematical Methods in the Applied Sciences*, 25(5):409–441, 2002.

[85] M.R. Ross, C.A. Felippa, K.C. Park, and M.A. Sprague. Treatment of acoustic fluid–structure interaction by localized Lagrange multipliers: Formulation. *Computer Methods in Applied Mechanics and Engineering*, 197(33):3057–3079, 2008.

[86] A.V. Saetta and R.V. Vitaliani. Unconditionally convergent partitioned solution procedure for dynamic coupled mechanical systems. *International journal for numerical methods in engineering*, 33(9):1975–1996, 1992.

[87] O. Schenk and K. Gärtner. Solving unsymmetric sparse systems of linear equations with PARDISO. *Journal of Future Generation Computer Systems*, 20(3):475–487, 2004.

[88] J.C. Simo and N. Tarnow. The discrete energy-momentum method. conserving algorithms for nonlinear elastodynamics. *Zeitschrift für angewandte Mathematik und Physik ZAMP*, 43(5):757–792, 1992.

[89] J.C. Simo, N. Tarnow, and K.K. Wong. Exact energy-momentum conserving algorithms and symplectic schemes for nonlinear dynamics. *Computer Methods in Applied Mechanics and Engineering*, 100(1):63–116, 1992.

[90] L. Simoni and B.A. Schrefler. A staggered finite-element solution for water and gas flow in deforming porous media. *Communications in Applied Numerical Methods*, 7(3):213–223, 1991.

[91] D.W. Snoke. *Solid State Physics: Essential Concepts*. Addison-Wesley, 2009.

[92] L. Stainier and M. Ortiz. Study and validation of a variational theory of thermo-mechanical coupling in finite visco-plasticity. *International Journal of Solids and Structures*, 47(5):705–715, 2010.

[93] J.B. Timothy. Mesh adaptation strategies for problems in fluid dynamics . *Finite Elements in Analysis and Design*, 25(3-4):243–273, 1997.

[94] L. Tisza. Sur la supraconductibilité thérmique de l'hélium II liquide et la statistique de Bose-Einstein. *CR Acad. Sci.*, 207:1035–1037, 1938.

[95] E. Turska and B.A. Schrefler. On convergence conditions of partitioned solution procedures for consolidation problems. *Computer Methods in Applied Mechanics and Engineering*, 106(1):51–63, 1993.

[96] P.K. Vijalapura and S. Govindjee. Numerical simulation of coupled-stress case II diffusion in one dimension. *Journal of Polymer Science Part B: Polymer Physics*, 41(18):2091–2108, 2003.

[97] P.K. Vijalapura and S. Govindjee. An adaptive hybrid time-stepping scheme for highly non-linear strongly coupled problems. *International Journal for Numerical Methods in Engineering*, 64(6):819–848, 2005.

[98] P.K. Vijalapura, J. Strain, and S. Govindjee. Fractional step methods for index-1 differential-algebraic equations. *Journal of Computational Physics*, 203(1):305–320, 2005.

[99] M.F. Wakeni, B.D. Reddy, and A.T. McBride. A thermodynamically consistent formulation of generalized thermoelasticity at finite deformations. *International Journal of Engineering and Science (in review).*

[100] M.F. Wakeni, B.D. Reddy, and A.T. McBride. An unconditionally stable algorithm for generalized thermoelasticity based on operator-splitting and time-discontinuous Galerkin finite element methods. *Computer Methods in Applied Mechanics and Engineering*, 306:425–451, 2016.

[101] H. Weizhang. Practical aspects of formulation and solution of moving mesh partial differential equations. *Journal of Computational Physics*, 171(2):753–775, 2001.

[102] H. Weizhang and D.R. Robert. Adaptive mesh movement—the MMPDE approach and its applications. *Journal of Computational and Applied Mathematics*, 128(12):383–398, 2001.

[103] H. Weizhang and R.D. Russell. *Adaptive moving mesh methods*, volume 174. Springer Science & Business Media, 2010.

[104] F. Xu, T.J. Lu, and K.A. Seffen. Biothermomechanics of skin tissues. *Journal of the Mechanics and Physics of Solids*, 56(5):1852–1884, 2008.

[105] F. Xu, K.A. Seffen, and T.J. Lu. Non-Fourier analysis of skin biothermomechanics. *International Journal of Heat and Mass Transfer*, 51(9):2237–2259, 2008.

[106] Q. Yang, L. Stainier, and M. Ortiz. A variational formulation of the coupled thermo-mechanical boundary-value problem for general dissipative solids. *Journal of the Mechanics and Physics of Solids*, 54(2):401–424, 2006.

[107] O.C. Zienkiewicz, D.K. Paul, and A.H.C. Chan. Unconditionally stable staggered solution procedure for soil-pore fluid interaction problems. *International Journal for Numerical Methods in Engineering*, 26(5):1039–1055, 1988.